THE HIGH FREQUENCY ELECTROMAGNETIC PROPERTIES OF CONDUCTING POLYMERS

Mijan Miah

A thesis submitted in partial fulfilment of Kingston University
for the degree of Doctor of Philosophy

This research programme was carried out in collaboration with

Defence Evaluation and Research Agency

MARCH 2000

Faculty of Science

Department of Applied Chemistry

Kingston University

Penrhyn Road

Kingston upon Thames

Surrey

KT1 2EE

This thesis is dedicated to my family: the late Mr Mohammed Obaidullah Miah, Mehatb Miah, Mrs Sitera Miah, my wonderful and supportive wife Zeema, and to my little angel Yazmeen without whose dedicated encouragement and support would not be where I am today – I owe it all to you.

Abstract

Organic semiconductors such as polypyrrole, polyalkylthiophenes and polyanilines are being used as alternatives to current materials for electromagnetic interference (EMI) technology. Their production, processability, lightweight construction and cost compare very favourably with those of materials in more established technologies. The project involves the synthesis and purification of the conducting polymers, and the selective use of dopant additives to alter the local structure of the polymer chain, termed as 'doping' in order to produce desired interactions with electromagnetic radiation. Conducting polymers are effectively a new class of microwave absorbing material, and in order to optimise the use of such materials, correlations have been made between the structural variables (e.g. molecular weight, crystal structure, counter-ion size, side-group functionality), the electrical properties (σ_{dc}, ε^*) and the magnetic properties (μ^*)

Polythiophenes and polypyrroles were synthesised using both chemical and electrochemical methods; however, it was found that the chemical methods were more effective, as more processable, soluble and therefore lower molecular weight materials were produced as opposed to the brittle insoluble high molecular weight materials. This allows the manipulation of subtle properties of the conducting polymer such as ε', ε'', μ' or μ'' in order to enhance the lossy behaviour. These materials were doped to a wide range of conductivities, ranging from the undoped insulating state usually associated with polymers, through a semiconducting up to a metallic state, with conductivities comparable to that of copper. As the conductivity changed, it was found that the electromagnetic radiation could either be transmitted through the polymer material in the insulating state, or be reflected from the material in the conducting state. The intermediate semiconducting form had a maximum absorption of the electromagnetic radiation. The real and imaginary dielectric and magnetic constants of the conducting polymer were measured at microwave frequencies, using a vector network analyser.

These conducting polymers were also arranged in a sandwich structure, together with other components with the aim of providing a lightweight, durable and portable device that may be switched 'on' or 'off' under the potentiostatic control, providing a method of controlling the radiation throughput of the device at optical and microwave frequencies. The rate of switching the reflective and transmissive states more conventionally known as the doped and undoped states respectively was controlled by the ionic volume of the dopant ions. The ionic volume of dopant ions was determined to be $< 1.8 \times 10^{-27} m^3$ based on using a variety of dopant

ion volumes and measuring the diffusion coefficients. This device was constructed using a variety of techniques to determine which arrangement would confer the fastest switching time and give the best 'radiation absorbing characteristics'. A variety of conducting polymers, electrode and electrolyte combinations were used in order to fabricate a lightweight and portable device that could be made to interact with the incident electromagnetic radiation.

This project investigates the effect of electromagnetic absorption with paramagnetic metal ion complexation to conducting polymers. Current electromagnetic absorption technology addresses either the electric component or the magnetic component of the electromagnetic wave. It has been established that an oscillating electromagnetic field is absorbed to some extent by conducting polymers by the excitation of the mid-gap states at intermediate doping levels. However, this addresses only the electric component of the electromagnetic wave. By complexing paramagnetic ions within the polymer chain, it is expected that this will provide additional electromagnetic absorption. With the electrochromic properties of conducting polymers being well understood, it is also the aim of this project to use the complexed conducting polymer to switch between the conducting and insulating state under the user's control. It is therefore of interest to find the limiting factors affecting the rate of switching.

It was found that the complexation of magnetic ions into the polymer contributed to electromagnetic absorption by providing additional loss mechanisms for the incident radiation. Low conductivity materials that were doped to 3-5 mol% and were governed by DC conduction processes were the best absorbers of the electromagnetic radiation.

CONTENTS

LIST OF ABBREVIATIONS

AC	alternating current
BF_4^-	tetrafluoroborate ion
BPh_4^-	tetraphenylborate ion
CE	counter electrode
$CHCl_3$	tricholoromethane
ClO_4^-	perchlorate ion
CSA	camphor sulphonic acid
DC	direct current
DERA	Defence Evaluation and Research Agency
dm^{-3}	per deci metres cubed
ECD	electrochromic display
EM	electromagnetic
GCMS	coupled gas chromatography and mass spectrometry
HCl	hydrochloric acid
HOMO	highest occupied molecular orbital
ICP-AES	Inductively coupled plasma atomic emission spectroscopy
IMS	industrially methylated spirits
ITO	indium-tin oxide glass
Fe	iron
$FeCl_3$	iron (III) chloride
LCD	liquid crystal display
LUMO	lowest occupied molecular orbital
mA	milli amps
P3MT	poly(3-methylthiophene)
PANI	polyaniline
PEO	polyethylene oxide
Polyamps	Poly(acrylamidomethylpropanesulphonic acid)
PPy	polypyrrole
PTFE	polytetrafluoroethylene
SSCE	Saturated sodium calomel electrode
TBATPB	tetrabutylammonium tetraphenylborate
TEATFB	tetraethylammonium tetrafluoroborate
TEM	transverse electromagnetic wave
TMAP	tetramethylammonium perchlorate
TTF	Tetrathiafulvene

LIST OF SYMBOLS

Å	angstroms
a	distance
A	geometric surface area
A_1	rate of trapping
A_2	rate of detrapping
b	interchain separation
$\bar{B}$	magnetic field vector
B	energy band width
β	phase constant
C_3	a constant
C_o	original bulk concentration of dopant ions
Co	cobalt
ΔH_β	activation energy for the tan δ near T_g
D	diffusion coefficient
E	measured potential
E_A	energy at the conduction band edge
E_0	equilibrium potential (measured)
e^-	electron
e	electronic charge
ε^*	complex dielectric constant
ε_0	vacuum dielectric constant
ε'	real part of the complex dielectric constant
ε''	imaginary part of the complex dielectric constant
E	measured potential
E_0	equilibrium potential
E_a	Energy at the conduction band edge
E_c	Energy at the mobility edge
E_F	Fermi level
$\bar{E}$	electric field vector
eV	electron volts
F	Faraday's constant
f	Fermi distribution
G(E)	density of states with a single spin
i	$\sqrt{-1}$

k	eigenvalue
k	Maxwell-Boltzmann constant
K_2CO_3	potassium carbonate
L	1-D localisation length
me	methyl
ml	millilitres
M_m	molar mass
mM	milli moles
mmHg	millimetres of mercury
m_e	electron rest mass
M_n	Number average molecular weight
mol	mole
mol%	percentage doping level of the bulk polymer film
$moldm^{-3}$	moles per deci metres cubed
m_s	magnetic spin quantum number
n	free electron concentration
n(E)	density of states
$N(E_F)$	density of states at the Fermi level
$NaClO_4$	sodium perchlorate
N_c	density of states for the conduction band
Ni	nickel
Nt	occupied trap concentration
n_t	concentration of filled traps
°C	degrees celcius
$\bar{P}$	polarisation vector
P	polarisation
$\bar{P}_{eq}$	equilibrium polarisation vector
R	resistance
ρ	resistivity
R	ideal gas constant
S11	reflection coefficient (port 1 to port 1)
S12	transmission coefficient (port 1 to port 2)
S21	transmission coefficient (port 2 to port 1)
S22	reflection coefficient (port 2 to port 2)
Scm^{-1}	Siemens per cm
t	duration of pulse

T	Temperature (Kelvin)
T_g	glass transition temperature
U	Coulombic energy
UV	ultraviolet
W	potential
W_2	activation energy
W_b	barrier width
W_h	barrier height
WE	working electrode
x-t	x-axis vs time plotter
Y	admittance
Y	propagation constant
z	number of nearest chains
Z	impedance

LIST OF GREEK SYMBOLS

ΔH_m	potential energy barrier height
α	attenuation constant
α	radius of the localised carrier wave
β	phase constant
γ	original number of dopants per monomer
δ	loss angle
δE	barrier height for quantum tunnelling
ε^*	complex dielectric constant
ε'	real permeability
ε''	imaginary permeability
ε_0	vacuum permeability
ε_a	gain in energy of the charge carrier under an electric field
ε_s	permittivity at high frequency
ε_{mw}	microwave dielectric constant
ε_s	permittivity at zero frequency
γ	propagation constant
Γ	impurity wave function
λ	wavelength
λ_c	cut-off wavelength
λ_o	free-space wavelength
μ	magnetic permeability
μ_r	relative magnetic permeability
ν_{ph}	phonon frequency
π	pi
π^*	asymmetric wavefunction
ρ	density
σ	conductivity
σ_{AC}	AC conductivity
σ_{DC}	DC conductivity
σ_{mw}	microwave conductivity
τ	mean free path of the charge carrier
ω	angular Frequency ($2\pi f$)
ω_p	plasma frequency

ξ	localisation length
ψ	Absolute wave function
ψ_m	bonding molecular orbital
ψ_m^*	anti–bonding molecular orbital
Ξ	degree of overlap between adjacent wavefunctions

LIST OF FIGURES

LIST OF TABLES

ACKNOWLEDGEMENTS

CHAPTER ONE

INTRODUCTION TO CONDUCTING POLYMERS

1.1   INTRODUCTION

The range of electrical conductivities found within the area of polymers covers some 25 orders of magnitude - the largest range in any material properties. Although polymers are generally thought of as insulating, advances within the last 25 years have proved otherwise. Persons within the field have discovered the simplest form of conducting polymer – polyacetylene [1], may be made to exhibit near-metallic conductivity as well as n-type and p-type semiconductivity. (Figure 1.1)
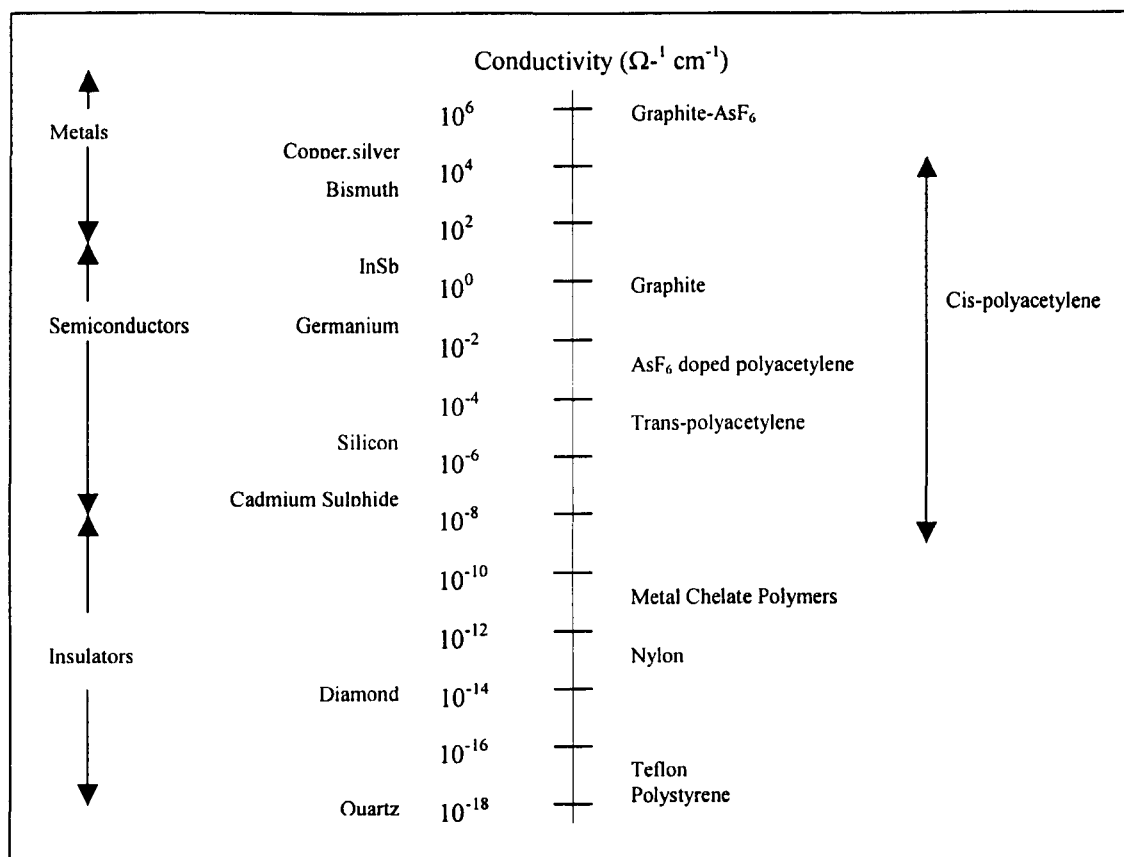
FIGURE 1.1
THE GENERAL SCALE OF CONDUCTIVITY

Conducting polymers are unique in the range of structures that may be formed, and the manner in which these alterations may manifest themselves as local or general changes. These materials may exist as highly crystalline or amorphous materials, or a mixture of the two. Each polymer chain has its own individual identity, based on its previous history from polymerisation through chemical reactions and purification processes to manufacture. Polymer chains may take different orientations with respect to other polymer chains, generally resulting in weak inter-chain interactions. These numerous parameters and relationships provide a varied and unique field of study. These properties are in contrast to

those of inorganic semiconductor counterparts, which are highly ordered covalent or ionically bonded materials. These differences have profound effects on most of the properties of polymers. They are generally heat insulators, which are soft and easily moulded with limited electrical conductivity.

1.2   ELECTRONIC PROPERTIES OF MATERIALS

Consider a simple case in which every atom has the same energy level diagram (Figure 1.2)
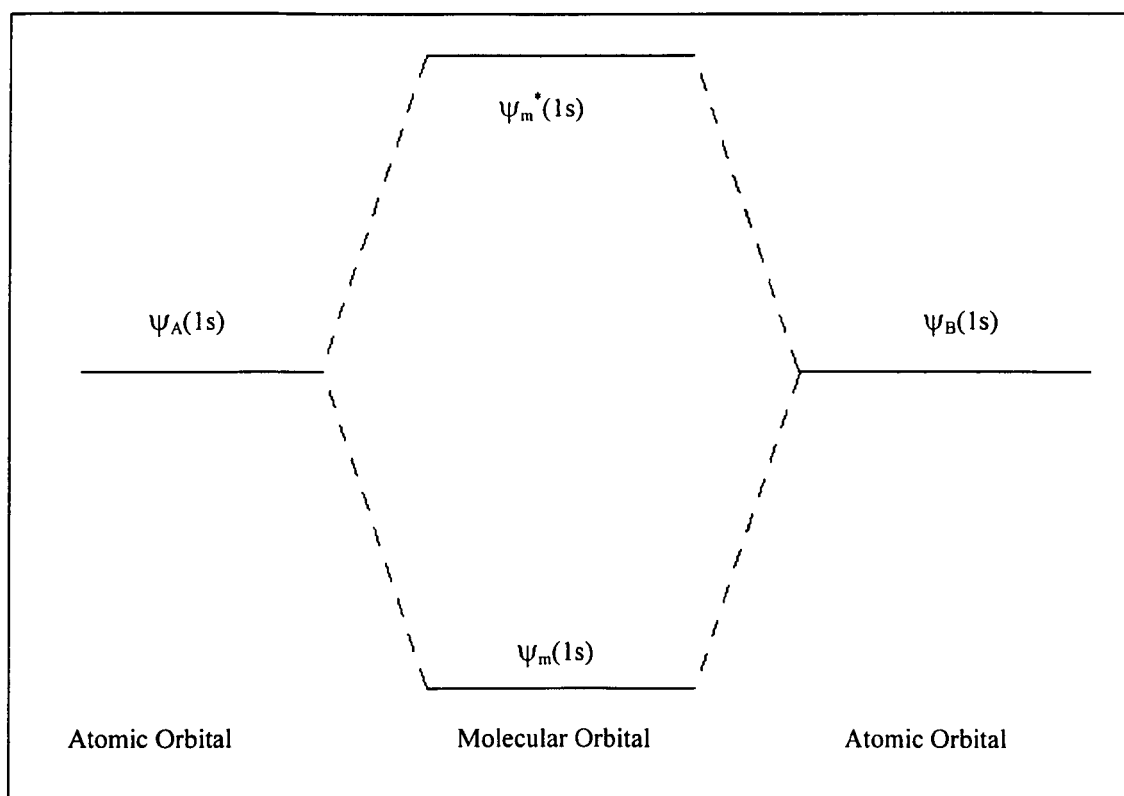
FIGURE 1.2

ENERGY LEVEL DIAGRAM FOR MOLECULAR ORBITALS AND THEIR RESULTING ATOMIC ORBITALS FOR H_2

The molecular wave functions ψ_m and ψ_m^* are bonding and antibonding molecular orbitals, joined by a line representing the symmetry axis for the electron distribution. When the two 1s orbitals (or wave functions) are added, they reinforce one another in the region between the two nuclei; the build-up of electron density reduces the intermolecular repulsion and a bond results. When one of the two 1s wave functions is subtracted from the other, they exactly cancel within the plane midway between the two nuclei. This lack of electron density raises the intermolecular repulsion, and the total energy becomes higher than that of the two separate nuclei. Hence an anti-bonding orbital results.

 If we push n identical atoms closer together, the electronic interactions cause the orbitals to distort, especially those containing the outer or valence electrons. The corresponding energies also shift upwards and downwards by varying amounts and the valence electron wave functions become less localised and extend over more atoms. Therefore valence states that formerly gave a sharp energy level now give rise to a continuous band containing N electrons within N levels. The value of N is near the order of Avogadro's number. Between the adjacent energy bands is a region where no energy band exists; therefore, no electron may exist for any duration of time − it is known as the forbidden region (figure 1.3). The configuration of the energy bands dictates the electronic, and to some extent physical characteristics of the material. In insulators and semiconductors, the valence band is completely filled at absolute zero, and the conduction band is completely empty.
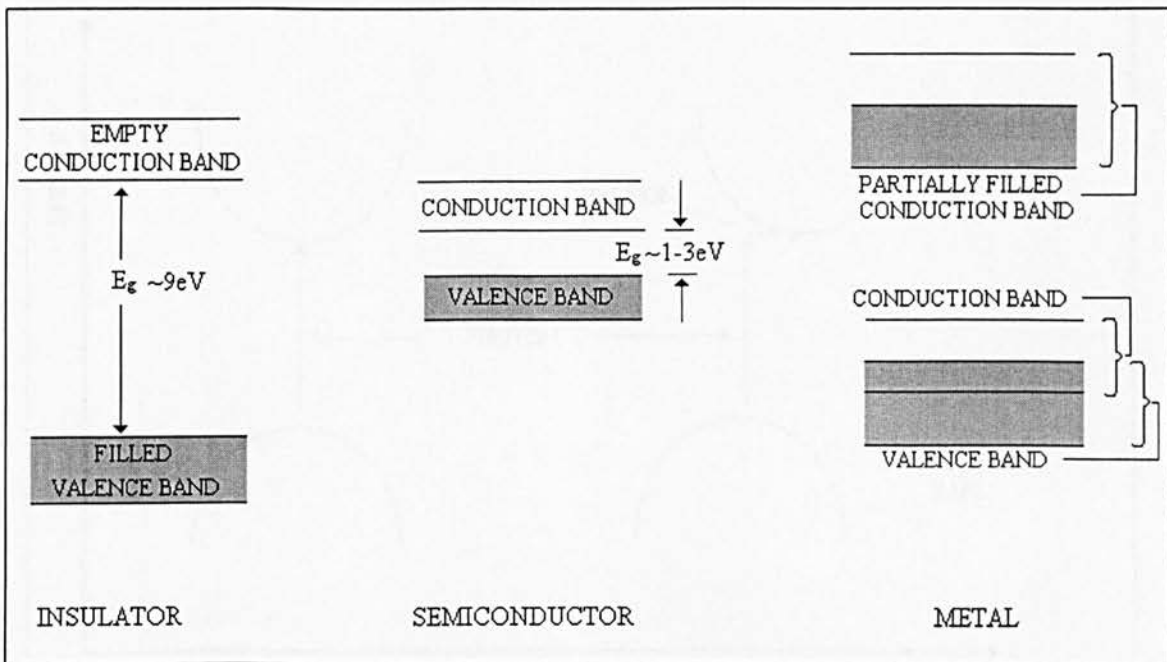
FIGURE 1.3

SIMPLIFIED BAND STRUCTURE CLASSIFICATION OF MATERIALS

The energy gap separating the valence band from the conduction band is of the order of 1-5eV. Above absolute zero, there is a finite probability that an electron is able to gain some energy to jump to the conduction band. Once in the conduction band, the electron is then able to move in response to an applied electric field. As the temperature increases more electrons have a greater probability of moving into the conduction band.

A distinguishing feature of many conductors, including all metals, is that the valence band is only partially filled. Electrons in states near the top of the filled portion of the band may have adjacent unoccupied states available, and may be able to gain or lose small amounts of energy in response to an external (such as an optical or thermal) energy source. These electrons are therefore mobile and may contribute to electrical conductivity. There are two types of excitation transitions in intrinsic semiconductors that are dependent on the momentum properties of the valence and conduction bands (figure 1.4). If the bottom of the conduction band lies directly above the valence band (the same position in momentum space), then an electron requires only a photon of energy to be promoted to an excited state. If there is an offset between the valence band and the conduction band, then a photon and a phonon are necessary for an electron transition.
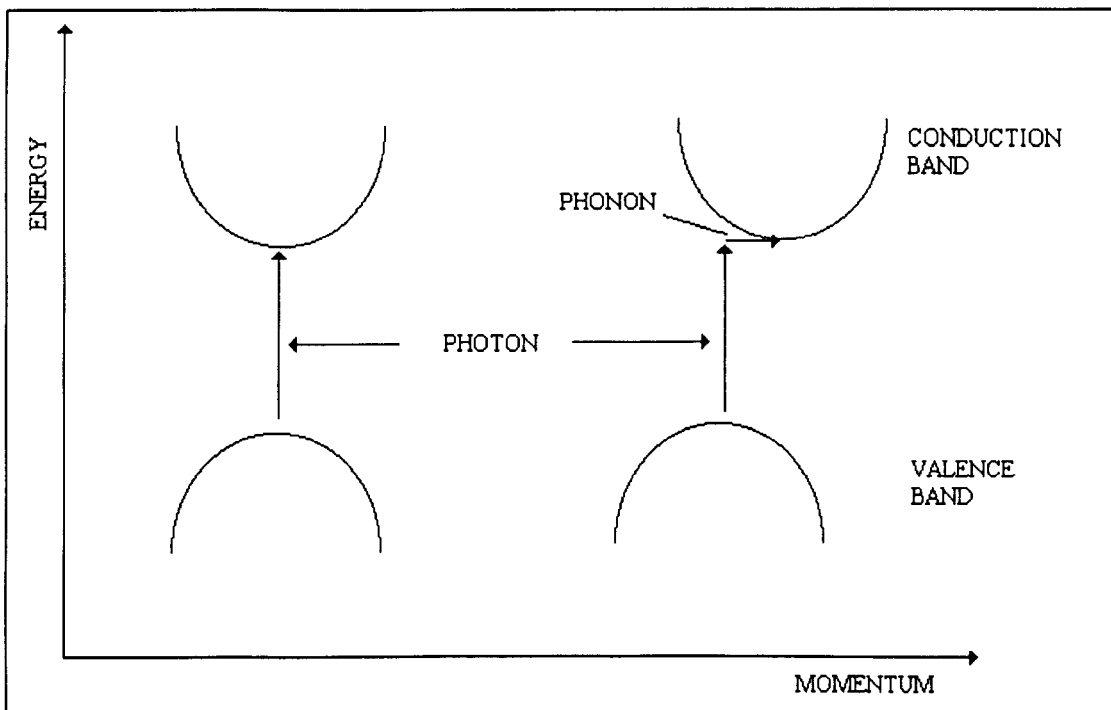
FIGURE 1.4

THE EXCITATION TRANSITIONS IN DIRECT AND INDIRECT BAND-GAP
SEMICONDUCTORS

Two common examples of intrinsic semiconductors are GaAs and Si, which have direct and indirect band gaps of 1.42 and 1.12eV at 300K respectively [2].

1.2.1   THE DENSITY OF STATES

Within a crystalline material, we may define the density of states, $N(E).dE$, which denotes the number of states per unit volume available for an electron with a known spin and energy in

the range of E and E+dE. As observed in the band theory of solids, these states may be occupied or empty. Gubanov and Banyai [3-4] suggested that the states at the edges of the valence band and conduction band would be localised in most amorphous materials.

The density of states for a crystalline material is shown in Figure 1.5a.
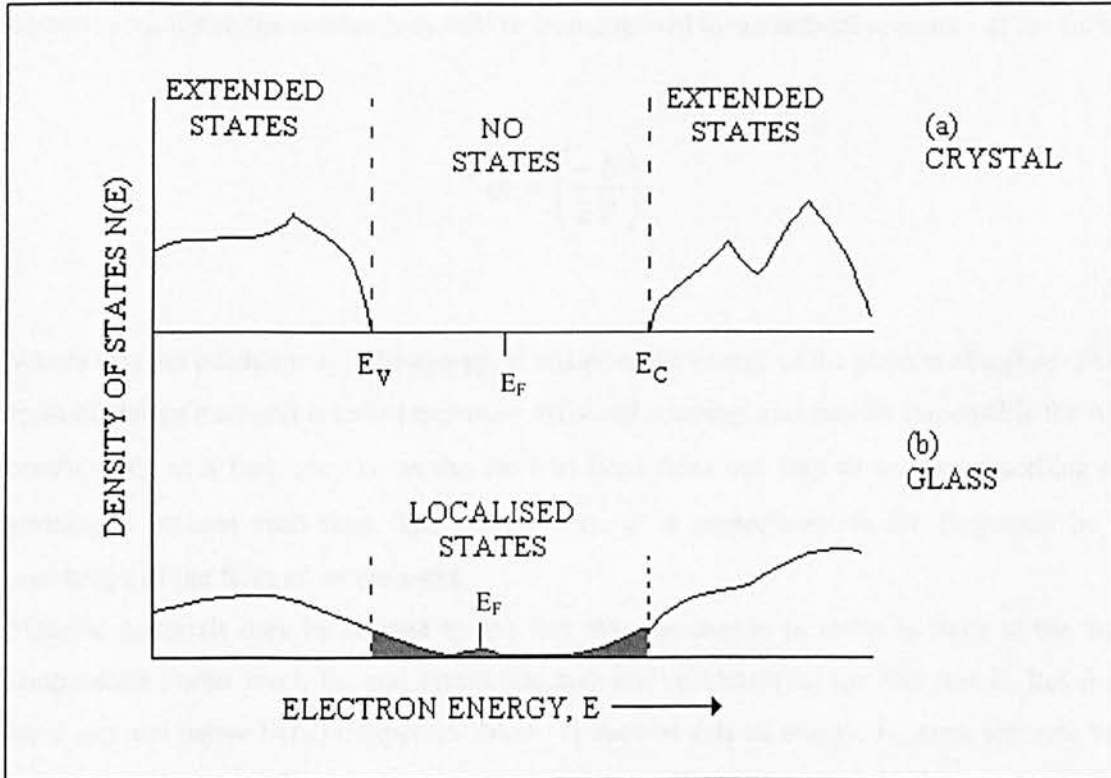
FIGURE 1.5

THE IDEAL DENSITY OF STATES FOR AN IDEAL (a) CRYSTAL AND (b)
AMORPHOUS MATERIAL

In amorphous materials, where there is no long range order, the sharp contours of $N(E)$ are not present. If the degree of disorder is sufficient to comply with Anderson's model (see Figure 1.8), then all the states in the valence band are localised. Even if there is a slight degree of disorder, Mott suggested that the electron tails in the valence band and conduction band are localised [5]. Figure 1.5 shows a density of states map for a crystalline (Figure 1.5a) and an amorphous material (Figure 1.5b). The major difference between the amorphous and crystalline materials is that there are band gaps present within the band structure of amorphous materials, where $N(E) > 0$ whereas, it is highly unlikely to find an electron between E_V and E_C within the forbidden region of a crystalline material.

The term localisation would therefore be indicative of a 'trap' region that can exist for a range of energies where the states are all localised even though the wave functions overlap. These states must also exist at the bottom of the conduction band or at the top of the valence band. The term 'localisation' implies [6] that phonon absorption or emission occurs when an electron moves from one state to another in the vicinity. The absorption of a phonon is rate determining, hence the conductivity will be characterised by an activation energy of the form:

$$\sigma \propto \left(\frac{-E}{kT} \right)$$

Where σ is the conductivity. The energy, E relates to the energy of the phonon absorbed. This form of charge transport is called thermally activated hopping, and may be responsible for AC conductivity at a frequency ω, as the electron hops from one trap to another absorbing or emitting a phonon each time. The conductivity, σ is proportional to the frequency by a constant, s of the form ω^s where s~0.8.

Metallic materials may be defined by the fact that the density of states is finite at the low temperature Fermi level, E_F, and semiconductors and insulators by the fact that E_F lies in a band gap and hence $N(E_F)$ disappears. Mott [7] showed that an energy, E_C must separate the localised and non-localised states near the band edge. The energy state is also known as the mobility edge [8].

1.2.2 ELECTRONIC BAND THEORY

The Bloch model is basic to the understanding of band theory, and is linked to the Schrödinger equation. The situation is more involved than the simple band theory and the valence and conduction bands may be divided into sub-bands. An insulator is characterised by having one band completely full and one completely empty of electrons, and a metal by having a large number of vacant holes in its valence band available for the conducting electrons.

Gubanov [9] and Banyai [10] suggested that in most non-crystalline materials the edges of the conduction and valence bands contained localised states. Figure 1.6 shows the comparison between these localised (Fig 1.6a) states and extended (Fig 1.6b) states.
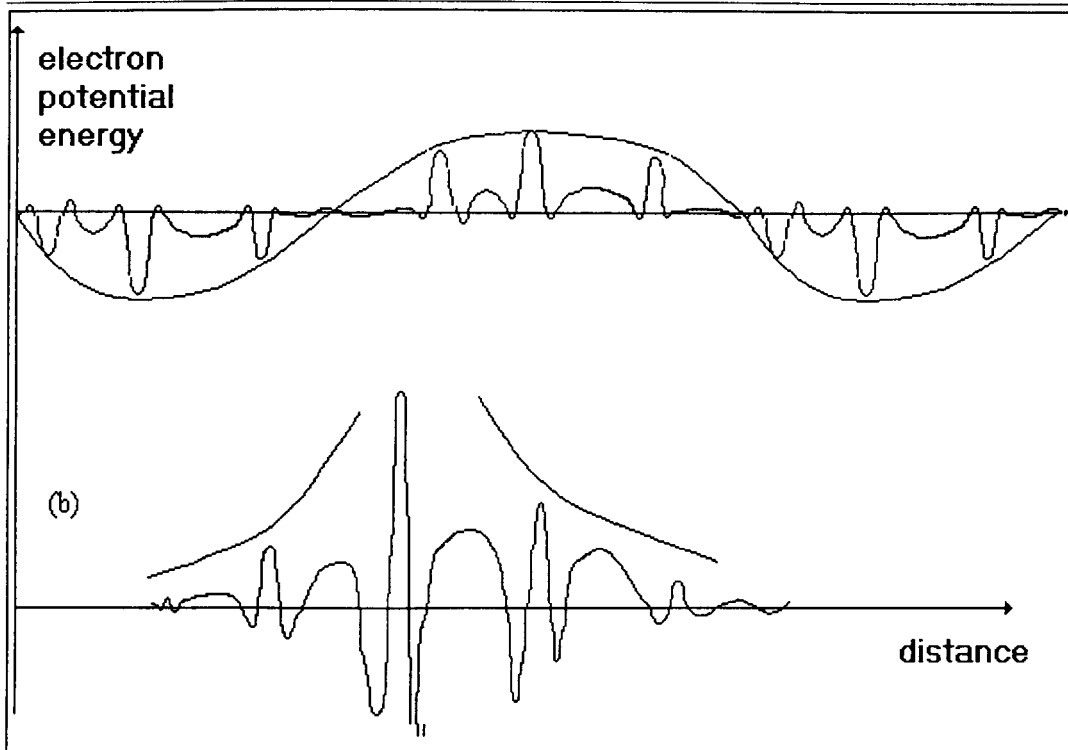
FIGURE 1.6

A COMPARISON BETWEEN (a) EXTENDED STATES AND (b) LOCALISED STATES

The term localisation is derived from the work of Anderson [11]. The Bloch theory is a single electron theory, and when multiple electrons and their interactions are taken into account, it breaks down. Mott accounted for these phenomena by suggesting that the Bloch theory does not consider the electron correlation energy, as shown in Figure 1.7.
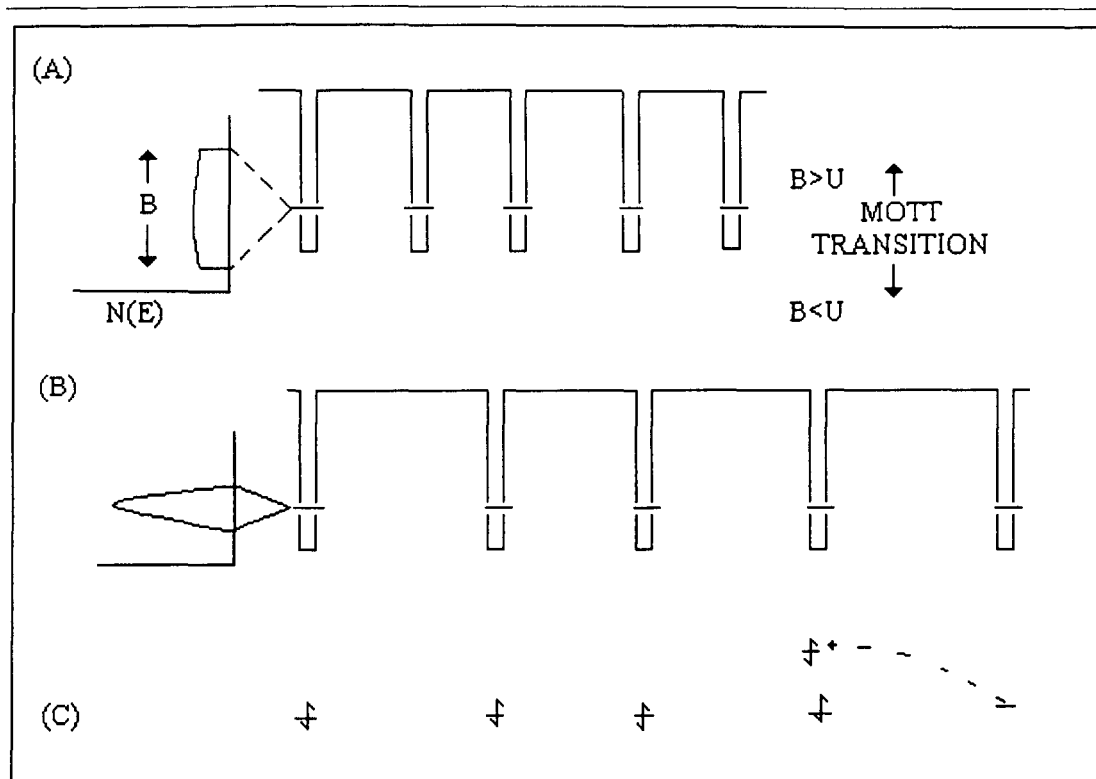
FIGURE 1.7

A SCHEMATIC REPRESENTATION FOR THE MOTT TRANSITION

The Mott model describes a material as a series of potential energy wells, occupied by a single electron at a particular energy state (Figure 1.7a). In an ordered material such as a crystal, these energy states interact and are defined as an energy band of width B. This energy band extends from −B/2 to +B/2 energy units of the orbital energy of the free atom. For a crystalline metallic material, the band is typically only half filled, and hence the average energy of the valence electron is ~B/4. The energy decrease from B to −B/4 is due to a reduction in the kinetic energy resulting from the delocalisation of the electron into the extended states (Figure 1.6a).

However, when there is an increase in the atomic spacings between the individual atoms, the reduction in energy is not as effective, and hence delocalisation does not occur (Figure 1.7b). This leads to the presence of localised states in which the wave function is concentrated near a centre composed of a few atoms, and has little presence elsewhere (Figure 1.6b).

Figure 1.7c shows an atom with a pair of valence electrons of opposite spin occupying the same orbital. In this situation, the crowding energy is equal to the coulombic energy (U). The electrons are not able to avoid repelling each other, and this introduces an average potential

energy gain per electron of U/4. Previously, the average kinetic energy for band formation was B/4, and if U/4 > B/4 then localisation occurs. The condition for a 'Mott insulator' (correlation –induced localisation) is therefore:

$$U > B$$

The most important transition for amorphous materials is the Anderson transition, which is similar to the Mott transition in that it is a delocalisation-to-localisation transition. The metal side of the Anderson transition is identical to that detailed in the Mott theory (Figure 1.8a)[12-13].
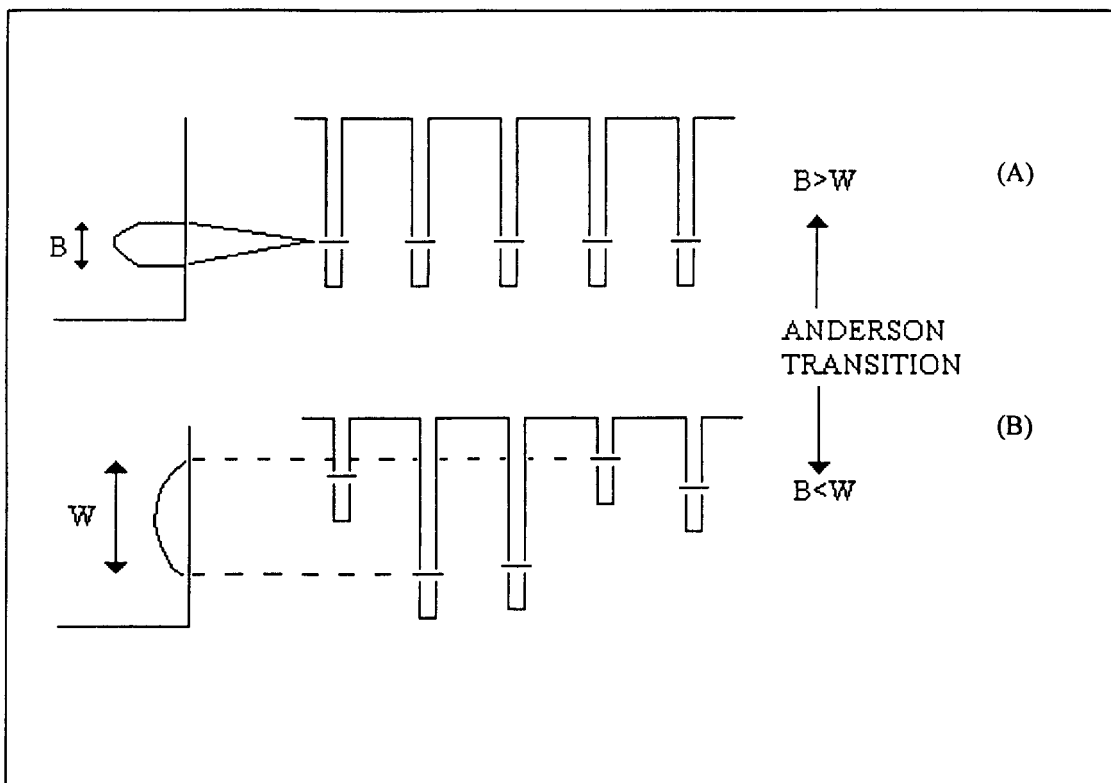
FIGURE 1.8

A SCHEMATIC REPRESENTATION OF THE ANDERSON TRANSITION

The classical representation of the electronic states of an amorphous material is described by a disorder-induced potential fluctuation shown in Figure 1.8b. The atoms are again represented by a potential energy well, which varies randomly. When the variation of the potential (W) is greater than the bandwidth (B), an Anderson transition may occur. However, when W/B >>1, then all the states in the valence band are localised [14].

1.3   ELECTRONIC PROPERTIES OF CONDUCTING POLYMERS

1.3.1   POLYACETYLENE

A major breakthrough in the field of conducting polymers came in 1977 with the intrinsically insulating organic polymer polyacetylene. By exposing the polymer to oxidising (or reducing) agents the conductivity was raised from $10^{-8}Scm^{-1}$ to 10^3 Scm^{-1}. This process was often referred to, in analogy to its inorganic counterpart, as doping; whereas the process is really more analogous to a redox reaction. The insulating and neutral polymer chain is converted into an ionic complex consisting of a polymeric cation (or anion if using a reducing agent), and a counterion, which is the reduced form of the oxidising agent. The use of oxidising agents is termed p-type doping, and reducing agents n-type doping. This process has been successfully applied to a rapidly expanding number of conducting polymer systems [15]. In some cases, oxidation or reduction may be achieved electrochemically by subjecting the polymer to an oxidising or a reducing potential in an electrochemical cell. The charge that appears on the polymer backbone is neutralised by importing the counter ion from the electrolyte solution.

1.3.2   DOPING IN CONDUCTING POLYMERS

Figure 1.9 shows that it is energetically favourable to have a geometry relaxation in the ionised state, when E_0-E_2 (=$\Delta\varepsilon$) is greater than E_1; or when the increase in the ionisation energy on distortion due to doping is greater than the elastic restoring forces required to make the distortion.
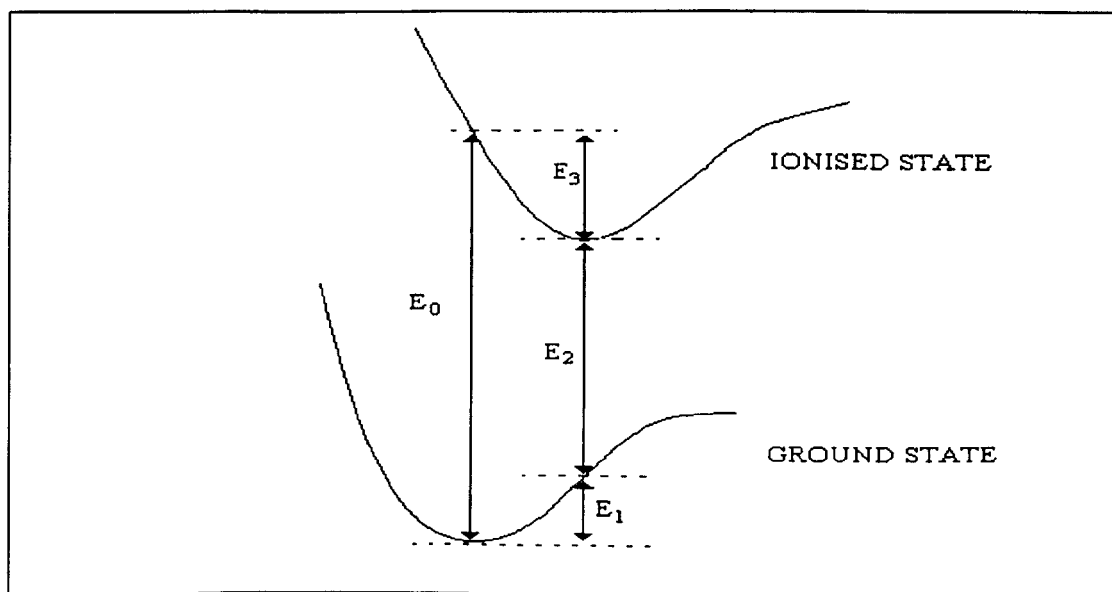
FIGURE 1.9

DIAGRAM SHOWING THE FAVOURABILITY OF DOPING IN THE IONISIED STATE
IN COMPARISON TO THE GROUND STATE

If we consider the single electron energy levels of the molecule, this distortion leads to an upward shift $\Delta\varepsilon$ of the HOMO and a downward shift of the LUMO (Figure 1.10).
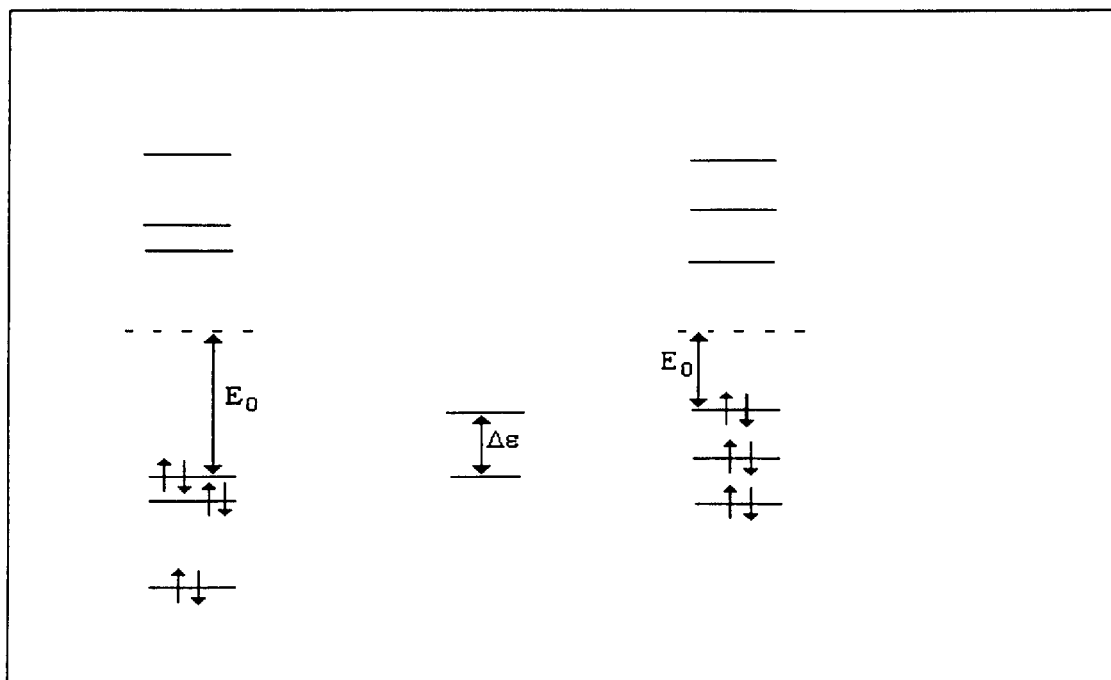
FIGURE 1.10

THE UPWARD SHIFT OF THE HOMO AND DOWNWARD SHIFT OF THE LUMO AS A CONSEQUENCE OF DOPING

A vertical excitation process results in putting an electron into the conduction band (and a hole in the valence band). This additional charge is delocalised over the whole chain (or more realistically over several monomer units), whilst little distortion of the surrounding lattice occurs.

It is also energetically favourable to localise the charge on the chain and to have a localised lattice distortion. This process allows the formation of a localised energy state within the band gap, due to a local upward shift of the HOMO level (Figure 1.10). If an electron is removed from the polymer chain, an energy $\Delta\varepsilon$ is gained in the ionisation energy. If $\Delta\varepsilon > E_1$ (E_1 may be seen as the energy required to locally distort the lattice), then this charge localisation is favoured and a polaron is formed. A polaron can be seen as a radical ion of spin $\pm 1/2$ associated with a localised lattice distortion, and localised mid gap energy state [16-18].
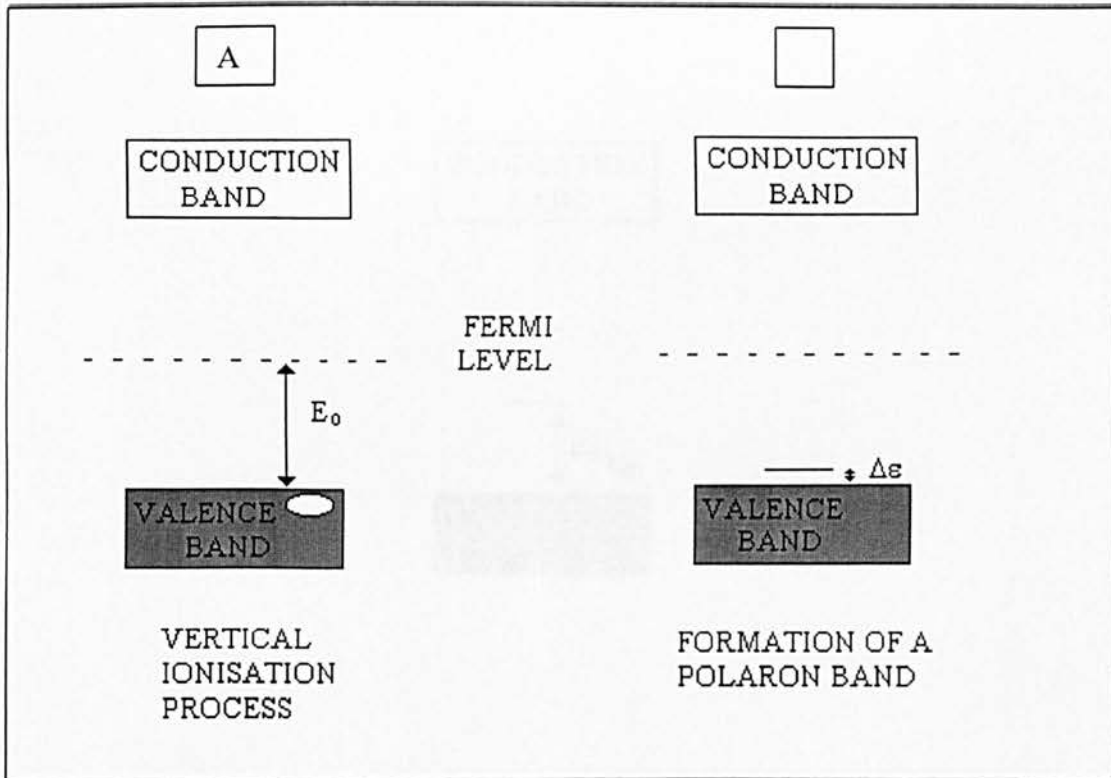
FIGURE 1.11

THE FORMATION OF A POLARON BAND AS A CONSEQUENCE OF DOPING

The quantity $\Delta\varepsilon-E_3$ corresponds to the polaron binding energy (Figure 1.9) that is of the order of 0.05eV in polyacetylene [19-20], 0.03eV in polyparaphenylene [20] and 0.12eV in polypyrrole [21]. In the case of polaron formation, the valence band remains full and the conduction band empty, and there is no metallic character as the half-occupied level is localised in the mid gap (Figure 1.11b).

The removal of a second electron is more favourable, in which case we have the formation of a bipolaron that may be defined as a pair of like charges (or a dication) associated with a very strong lattice distortion. The formation of a bipolaron indicates that the energy gained by the interaction with the lattice is larger than the Coulombic repulsion forces between the charges [22].

The band structure associated with the formation of a bipolaron is shown in Figure 1.12. As the lattice distortion is greater around two charges, E_1, the distortion energy for the bipolaron is greater than E_1 for a polaron and the electronic states appearing in the gap for a polaron. The bipolaron is more thermodynamically stable than two polarons, despite the repulsion between the two like charges [21].
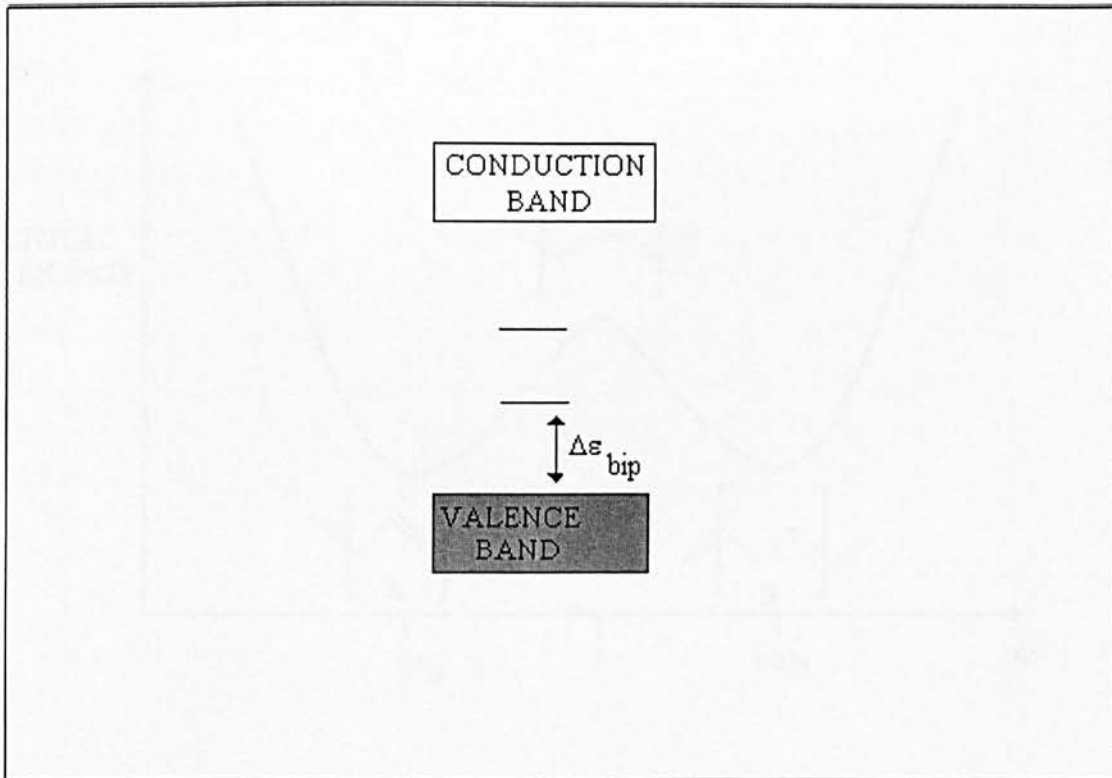
FIGURE 1.12

BIPOLARON FORMATION IN A CONDUCTING POLYMER

Additionally, the presence of dopant counter-ions neutralises the presence of the polarons. In the case of p-type doping, the bipolaron levels are empty (or fully occupied in n-type doping), and are therefore spinless. The presence of bipolarons allows a further two possible inter-gap transitions:

1.   From the valence band to the lower polaron level and,
2.   From the valence band to the upper polaron level.

For polarons, a third transition between the polaron levels is feasible.

Trans-polyacetylene possesses a degenerate ground state [23] (Figure 1.13).
Usually, the degree of bond length alternation (the difference between the length of a single band and a double bond) is 0.08Å [24], and consequently the two charges forming in polyacetylene (figure 1.14b) would be a bipolaron and would easily separate (Figure 1.14c).
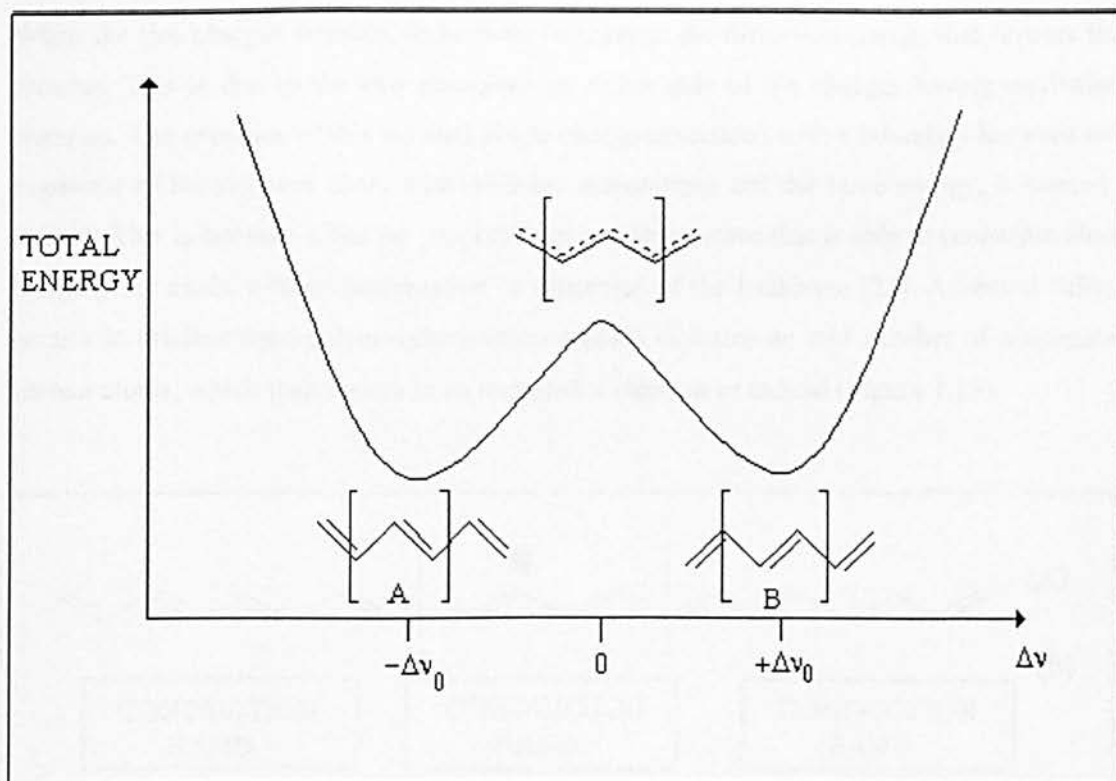
FIGURE 1.13

THE TOTAL ENERGY CURVE FOR A TRANS-POLYACETYLENE POLYMER CHAIN
AS A FUNCTION OF THE DEGREE OF BOND LENGTH ALTERNATION, Δr
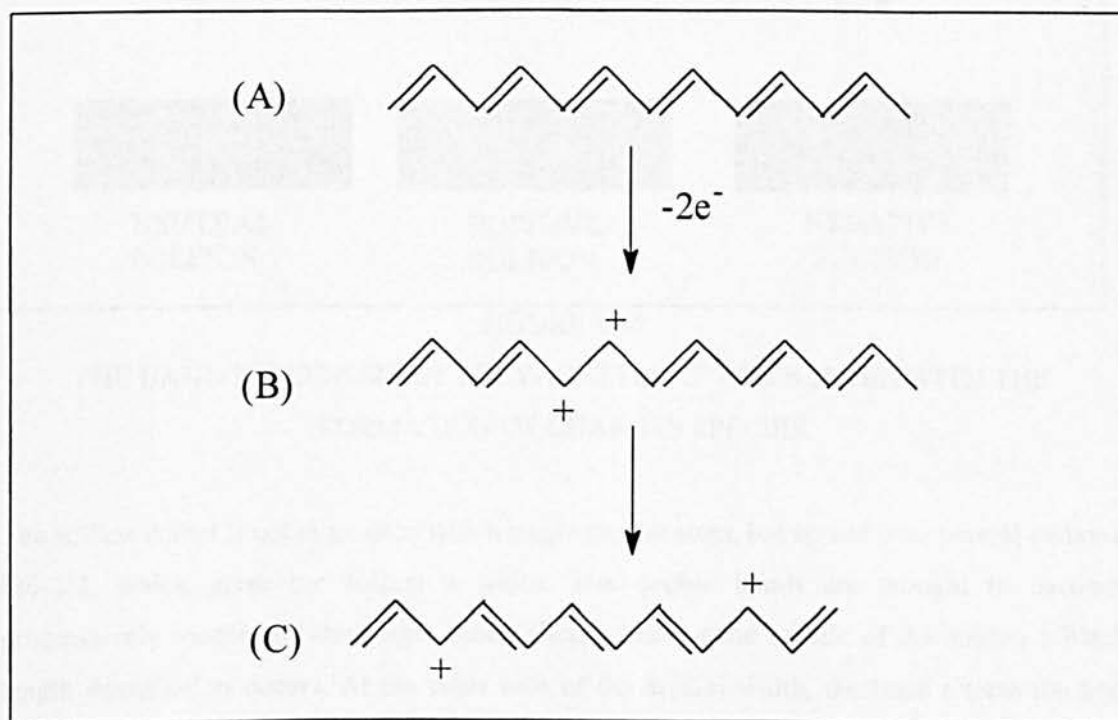
FIGURE 1.14

(a) POLYACETYLENE DOPED TO FORM A BIPOLARON (b) SEPARATING TO FORM
2 POLARONS

When the two charges separate, there is no increase in the distortion energy that favours this process. This is due to the two structures on either side of the charges having equivalent energies. The presence of this isolated single charge associated with a boundary between two segments of the polymer chain with different orientations but the same energy, is termed a soliton. This is because it has the properties of a solitary wave that is able to propagate along the polymer chain without deformation or distortion of the backbone [25]. A neutral soliton occurs in pristine trans-polyacetylene when a chain contains an odd number of conjugated carbon atoms, which then results in an unpaired π electron or radical (Figure 1.15).
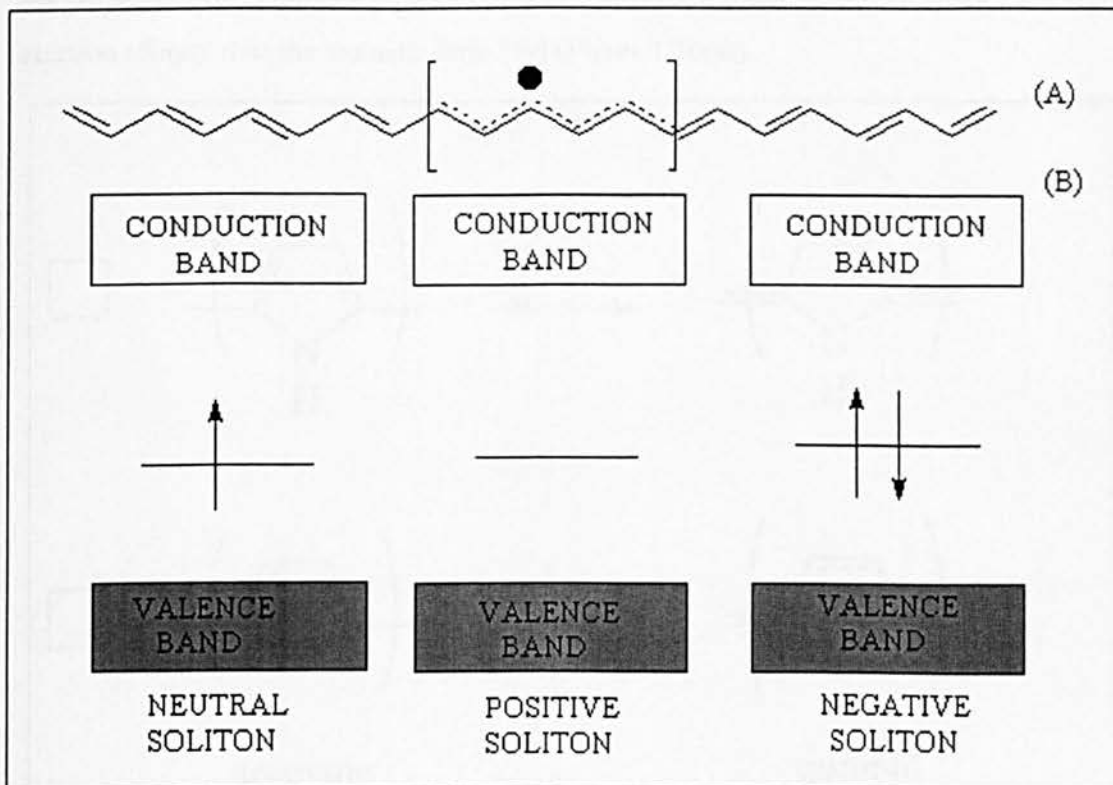
FIGURE 1.15

THE BAND STRUCTURE OF POLYACETYLENE ASSOCIATED WITH THE
FORMATION OF CHARGES SPECIES

The soliton defect is not associated with a single carbon atom, but spread over several carbons [26-28], which gives the soliton a width. The double bonds are thought to become progressively longer and the single bonds shorter until at the middle of the soliton a bond length equalisation occurs. At the other side of the soliton width, the bond alternation has completely reversed itself. The presence of a soliton leads to the formation of a localised electronic mid-gap level. Unlike trans-polyacetylene, polypyrrole, polythiophene and

polyparaphenylene possess a non-degenerate ground state, since their ground state corresponds to a single structure.

1.3.3   ELECTRONIC TRANSPORT AT HIGH DOPING LEVELS

Experimental and theoretical investigations on the electronic transport properties of conducting polymers in relation to their doping levels have been carried out on polyacetylene [29-32], polypyrrole [33-37] and polythiophene [38-39].

When polythiophene is undoped, the band gap is about 2eV. By removing an electron from the polymer chain, a quinoid structure may be formed of a lower ionisation energy and higher electron affinity than the aromatic form [39] (Figure 1.16(a)).

aromatic   quinoid
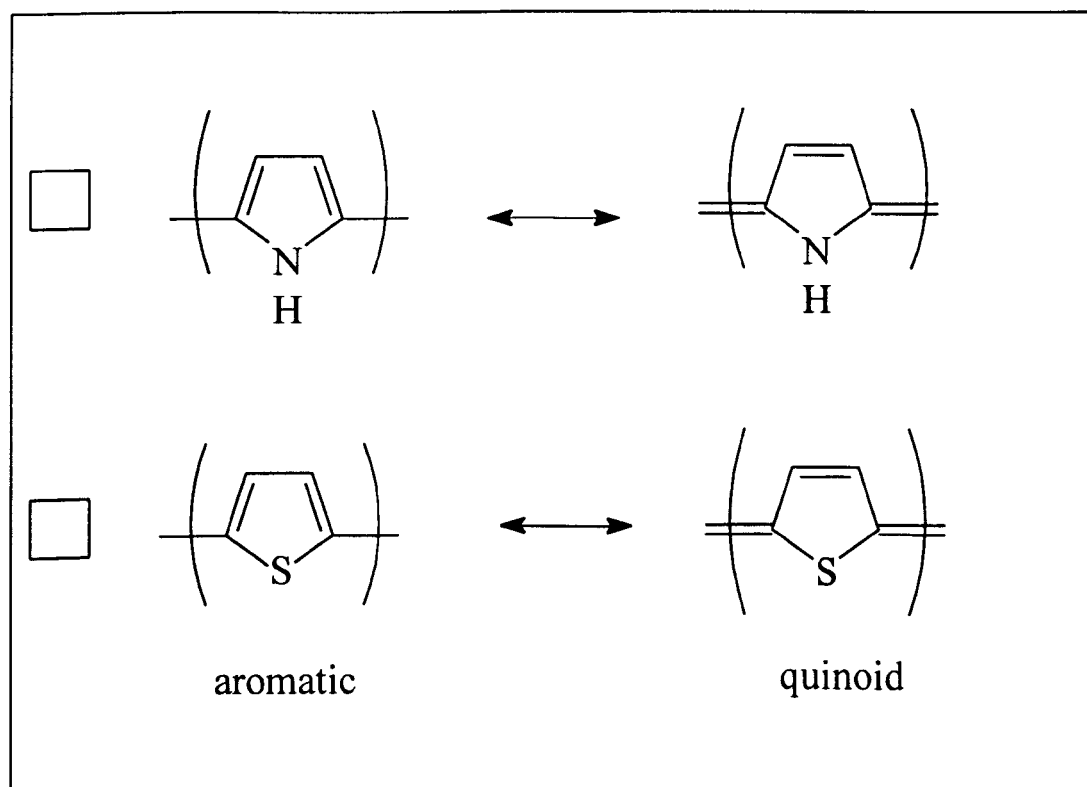
FIGURE 1.16

THE RESONANCE STRUCTURES ASSOCIATED WITH (a) POLYANILINE AND (b) POLYTHIOPHENE

The quinoid geometry extends over ~2 thiophene rings. The polaron levels are 0.5eV above the valence band (Figure 1.17).

When a second electron is removed from the polymer chain, the most stable species to be formed is a bipolaron, which also extends over ~2 monomer units. The geometry within the

bipolaron is more quinoid-like than in the case of a polaron, and hence the bipolaron level is 0.7-1.2eV away from the band edge (Figure 1.17b).
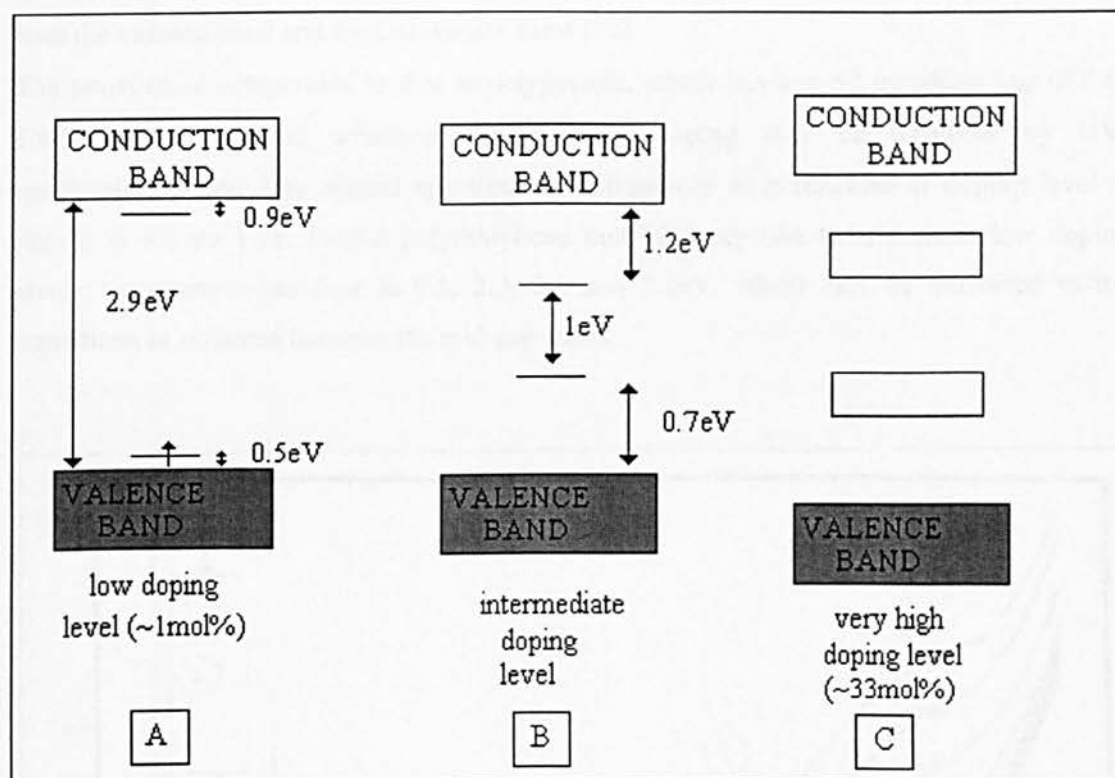
FIGURE 1.17

THE DOPING PROCESS IN CONDUCTING POLYMERS

The band structure for a doping level of 33mol%, which is usually only achieved by electrochemical means is shown in Figure 1.17(c). The band-gap has widened by 0.69eV and are due to the bipolaron states entering the gap from the valence and conduction band edges.

Chung *et al* have proposed that the transport properties of organic semiconductors may become comparable to those of a metal at very high doping level [38]. This may be understood by an increase in the width of the bipolaronic states within the band gap eventually leading to the mergence of the lower and upper bipolaronic levels with the valence and conduction bands respectively [36]. For p-type polythiophene, this would result in a new unfilled valence band and the possibility of metallic conduction.

The transport properties of trans-polyacetylene are comparable to that of polythiophene. At low doping levels, charged solitons in polyacetylene rather than polarons are formed from neutral solitons that are either already present, or by the decomposition of polarons. As the doping level is increased, the individual solitonic states within the $\pi-\pi^*$ transition overlap to

form a soliton band. When the doping level is in the range of 0.1-7mol%, a high conductivity is observed. Above 7 mol%, a metallic-like conduction is seen as the soliton band merges with the valence band and the conduction band [39].

The situation is comparable to that in polypyrrole, which has a π–π^* transition gap of 3.0-3.4eV, and the band structure evolution on doping may be observed by UV-spectrophotometry. The optical spectrum of polypyrrole as a function of doping level is shown in Figure 1.18. Unlike polythiophene that has only two transitions at low doping levels, polypyrrole has four at 0.5, 2.3, 2.8 and 3.4eV, which may be attributed to the transitions of polarons between the mid-gap states.
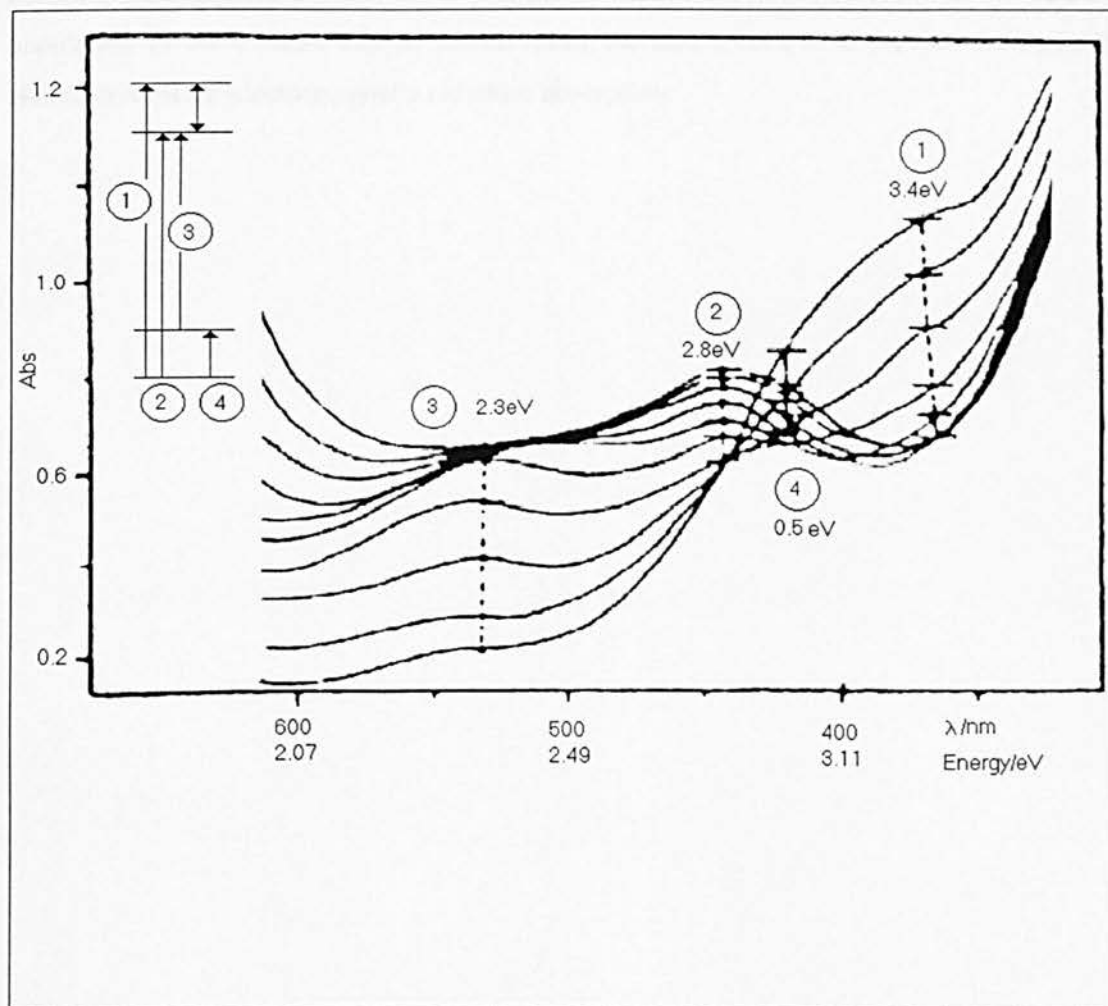
FIGURE 1.18
UV-VIS SPECTROPHOTOMETRY OF POLYPYRROLE

At intermediate doping levels, the transition between the polaron levels at 1.4eV disappears. At very high doping levels, two broad absorption peaks at 1.0 and 2.7eV are present below the gap, which agrees with the presence of bipolaronic bands [40] which is analogous to the

UV-visible spectrometry characteristics of undoped and uncomplexed poly(3-methylthiophene).

1.4 SUMMARY OF THE ELECTRONIC PROPERTIES OF CONDUCTING POLYMERS

Conducting polymers are unusual materials that combine the electrical conductivity of metals and semiconductors with the mechanical properties and processability of traditional polymers. However, the conduction mechanisms are completely different to that of metals and the more traditional inorganic semiconductors, and these characteristics must be thoroughly understood if they are to be used to our advantage. The presence of mid-gap states that may be used to absorb electromagnetic radiation is of paramount importance to this project, and the type and population of these states can be placed under the user's control to provide the optimum characteristics for electromagnetic radiation absorption.

CHAPTER TWO

ELECTROCHROMIC PROPERTIES OF CONDUCTING POLYMERS

2.1   INTRODUCTION

Conducting polymers are amongst a small group of materials that exhibit an electrically induced colour change (greek: *electros*: electrical and *chromos*: colour). The colour change or electrochromic effect is accompanied by a change in the electrical conductivity of the polymer film. An understanding of the factors involved in the electrochromic effect will give a better understanding in the construction of a display device that can change colour under active control of the user.

2.2   ELECTROCHROMISM

Many different materials including liquid crystals and electroluminescent materials have been used successfully in display technology. Conducting polymer research provides promising alternatives which overcome some deficiencies of liquid crystal displays (LCDs). In particular, both active and passive polymeric devices may have angle-independent viewing, high contrast ratio, continuously variable intensity of coloration, information storage without power consumption, adequate coloration and bleaching rate (switching speed), UV stability and a large operational temperature range. However, an undesired and potentially limiting side effect of some electrochromic devices is the occurrence of irreversible reactions at high potentials resulting in polymer degradation.

Electrochromic display (ECD) device structures (Figure 2.1) may be broken down into several components: an active electrochromic layer or *working electrode* that provides coloration and bleaching by the injection and ejection of charged species into/from the polymer layer; a *counter electrode* provides a source (or sink) of electrons and combines with the working electrode to form a cell; and an *electrolyte* placed between the working and counter electrodes providing an ion-conducting but electron insulating layer. For visual clarity, both electrodes and the electrolytes must be transparent, and generally indium-tin oxide (ITO)-coated glass is used since it offers the combination of a good electrical conductivity and high transparency. For this application, low surface resistance is necessary, particularly in large-scale ECD construction where the potential drop across the visible area of the device must be minimised.
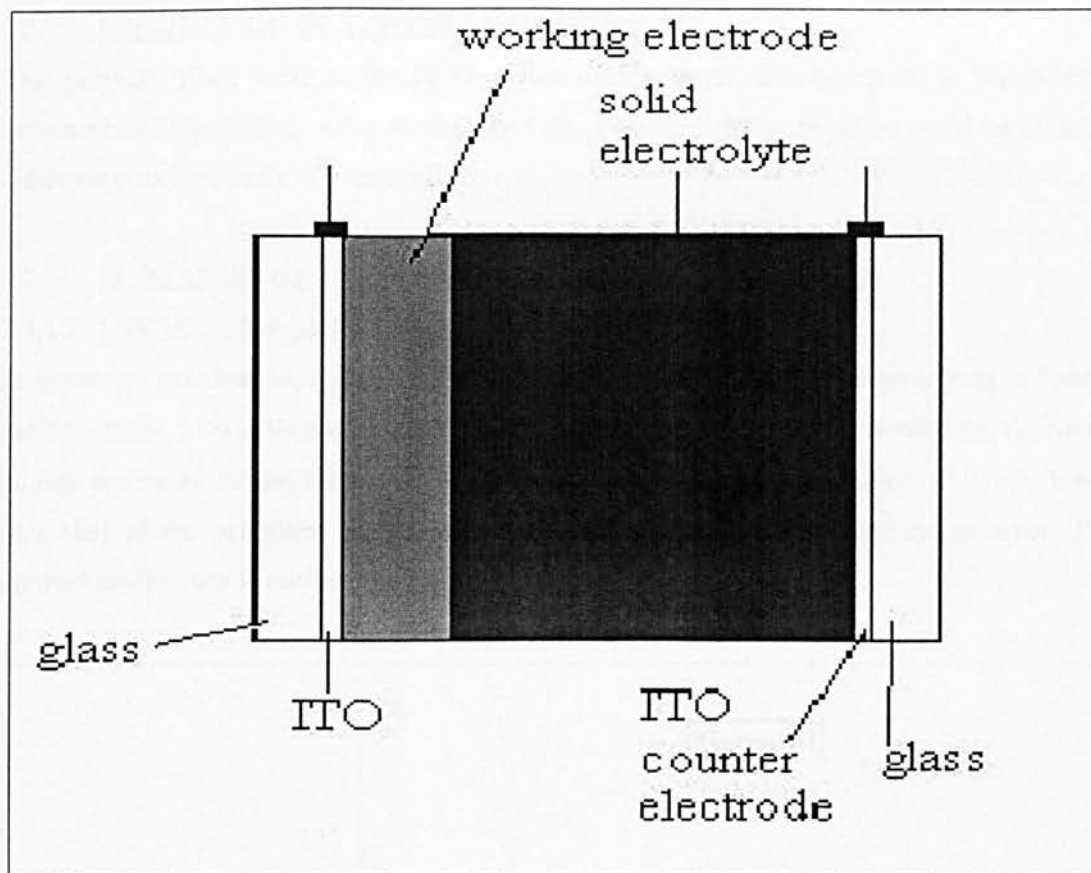
FIGURE 2.1

A SCHEMATIC DIAGRAM OF AN ELECTROCHROMIC DEVICE

The choice of electrolyte has an important influence on the properties of the ECD, as this directly controls the ease of movement of the ions through the medium and thus may determine the switching speed. Many ECD devices using conducting polymers have been reported. However, there exists no definitive study of the effects of each component of the typical cell, particularly at high frequencies. In this work we attempted to look at the effect on device efficiency by changing systematically the polymer coatings on the working electrode and the electrolyte separating the electrodes. Liquid and polymeric electrolytes were used to determine changes in the device characteristics due to variability in the electrolyte viscosity and ion concentration. In this study, three dopant salts were used for a comparison of the effect of the charge density and molecular volume of the anion on the diffusion coefficient of the dopant ions and switching time.

2.3   PRODUCTION OF THE POLYMER FILMS

The polymer films used in the ECD device design were each based on a 5-membered heterocyclic ring system. After synthesis of the monomer, polymerisation could be effected either electrochemically or chemically.

2.3.1   PRINCIPLES OF THE POLYMERISATION METHODS USED

2.3.1.1   MECHANISM OF POLYMERISATION

In electropolymerisation, the anode removes an electron from the heterocyclic ring to form a radical cation. This is then attacked by another heterocycle. After further oxidation, the dimer attains neutrality by the loss of $2H^+$. The oxidation potential of the dimer is slightly lower than that of the monomer, and the process therefore continues to form the polymer. The general mechanism is outlined in Figure 2.2.
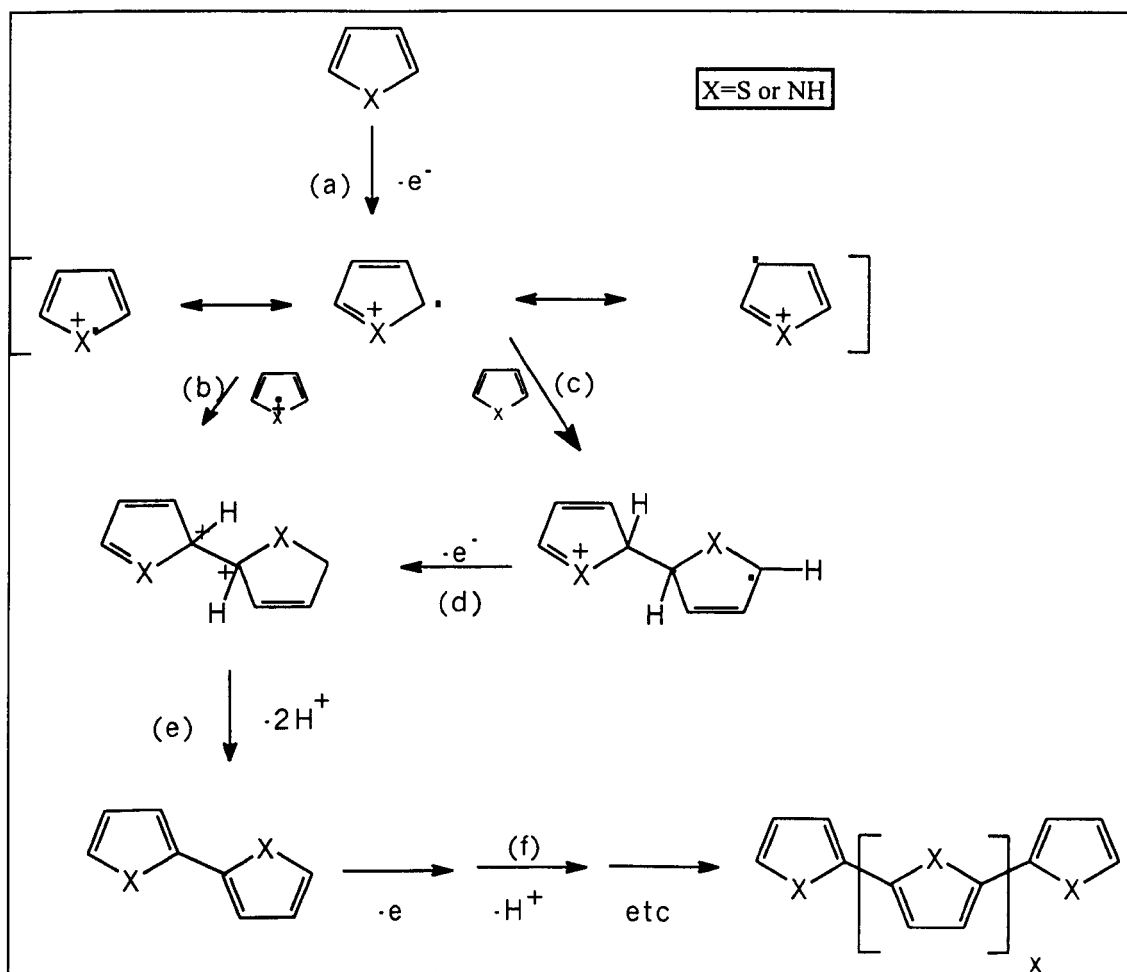
FIGURE 2.2

(A) OXIDATION OF MONOMER. (B) RADICAL-RADICAL COUPLING. (C) RADICAL-MONOMER. (D) OXIDATION OF DIMER RADICAL. (E) AROMATIZATION. (F) PROPAGATION TO FORM POLYMER. SYNTHETIC PATHWAY FOR THE ELECTROPOLYMERISATION OF A HETEROCYCLIC MONOMER

2.3.1.2 <u>CONSTRUCTION OF ELECTROPOLYMERISATION EQUIPMENT</u>

The cell assembled according to Figure 2.3, had the counter electrode (CE) and working electrode (WE) arranged parallel to each other in order to give an even current density and hence uniform polymer film on the working electrode. A saturated sodium calomel reference electrode (SSCE) was used to give a measure of the potential applied by the potentiostat.
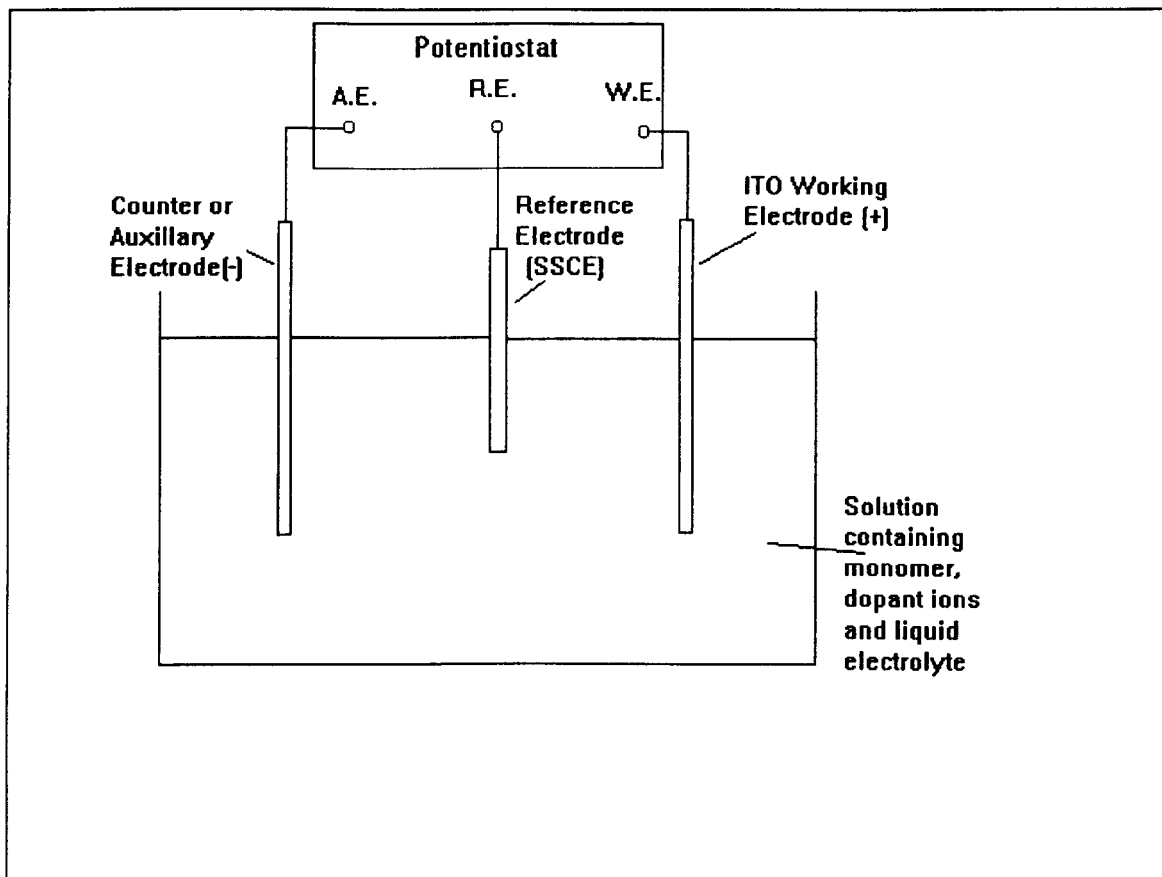
FIGURE 2.3

SETUP OF CELL USED FOR ELECTROPOLYMERISATION OF MONOMERS INTO CONDUCTING POLYMERS

In order to assemble an ECD, a layer of polymer must be deposited onto the ITO glass anode, where the film thicknesses may be controlled to a high degree by adjustment of the current density (rate of polymerisation) and duration of application. Also, the electrical conductivity of the resulting films may be tailored for the application by controlling the concentration of dopant ions in solution.

The morphology and thickness of polymer films may be determined by controlling by the current density and duration of current application. By selecting dopant ions of varying sizes, and synthesising polymer films of varying thicknesses, the effect on the rate of electrochromic switching may be investigated.

2.4 MEASUREMENT OF POLYMER ELECTROCHROMIC ACTIVITY

Electrochromic switching between the opaque doped state and the undoped transparent state can be induced using an electrical current. The rate of the electrochromic optical response (switching time) may then be monitored using a monochromatic light source and a photodiode detector, and recorded using an X-T plotter or computer data capture (Figure 2.4).
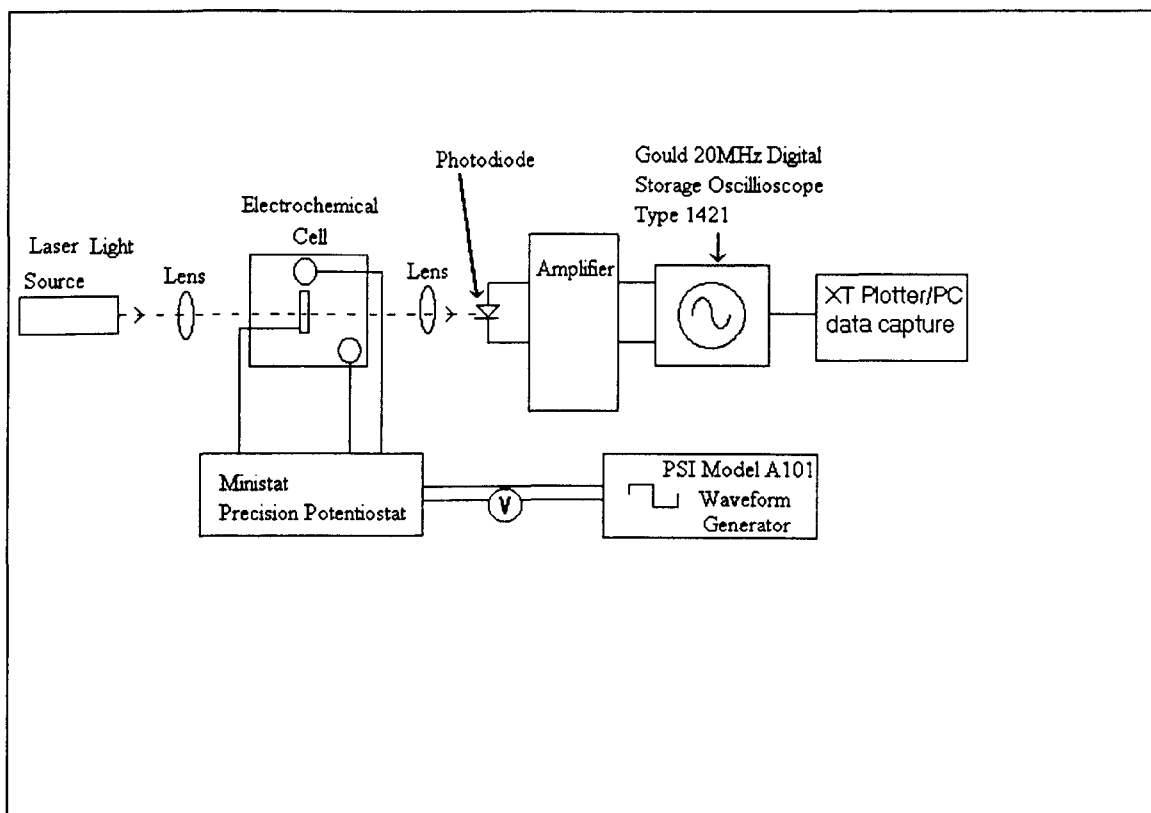
FIGURE 2.4

SETUP OF EQUIPMENT USED TO OBSERVE THE ELECTROCHROMIC RESPONSE

The square-wave potential was applied to the sample, and the electrochromic response was measured in comparison to transmitted light without any attenuation. The switching time ($\tau_{0.5}$) was defined as the time at which the transmitted light intensity changed reached 50% of the final values of (I_u-I_d) (Figure 2.5). The semiconductor laser used was an ALGaInP source at 780nm. It should be emphasised that the switching time of the undoping phase is strongly dependent on the previously doped state.
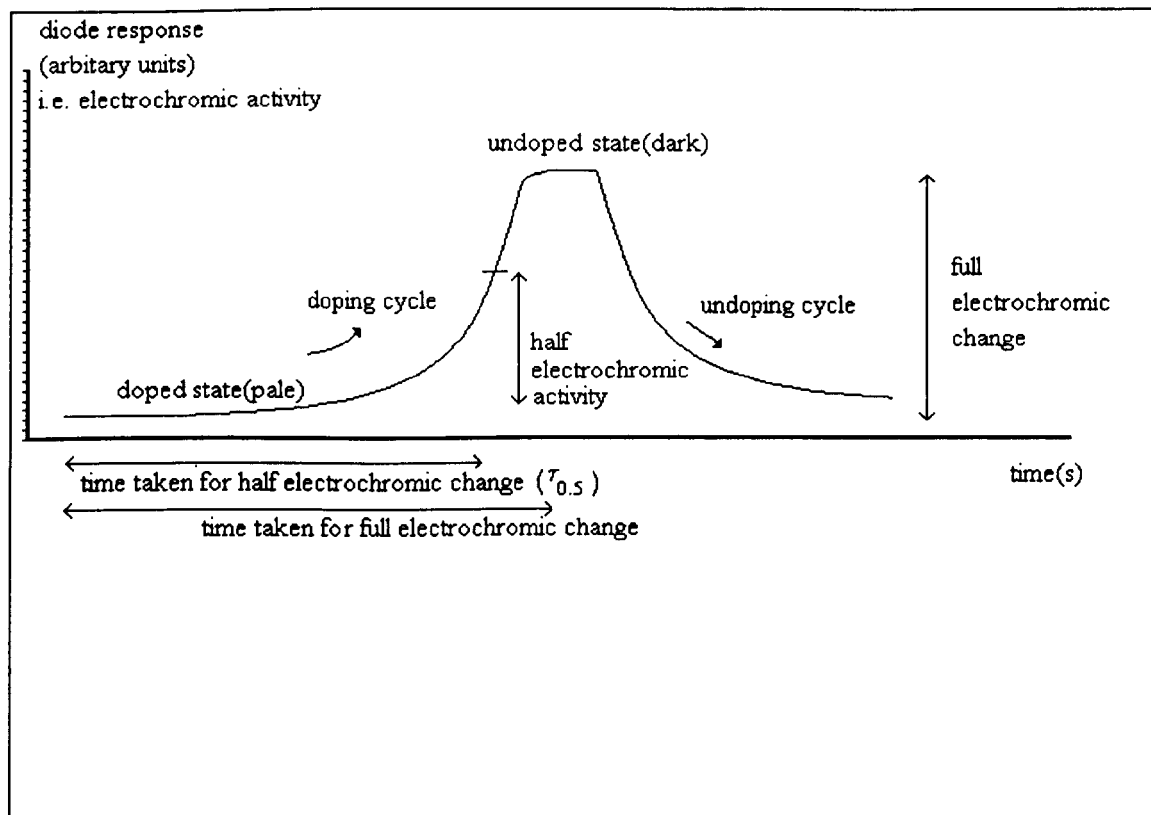
FIGURE 2.5

DIAGRAM DEPICTING A TYPICAL PHOTODIODE RESPONSE TO AN
ELECTROCHROMIC EFFECT

2.5 MEASUREMENT OF DIFFUSION COEFFICIENT OF DOPANT IONS

As-prepared poly(3-methylthiophene) and polypyrrole films were undoped in an electrochemical cell containing the appropriate electrolyte solution by applying a limited current of a few micro-amperes at room temperature. A Keithley 617 Programmable Electrometer and Keithley 224 Programmable Current Source recorded the current versus an aluminium pseudo-reference electrode at regular intervals.

Diffusion measurements were made using the galvanostatic pulse technique [41]. This involves passing a short current pulse through the cell after equilibration at the required and known doping level. A known molar excess of ions is thus applied to the electrode surface, causing a small change in the electrode voltage versus the reference electrode. This is proportional to the concentration of ions deposited on the electrode; if the voltage step is much less than the total voltage change during the fully doping process, and if the number of ions deposited is much less than that in the doped electrode. The recovering voltage (as ions diffuse away from the electrode surface and into its interior) is a function of the ion's diffusion coefficient.

The time dependence of the electrode potential is given by [42]:

$$\exp\left\{\frac{(E-E_0)F}{RT}\right\} - 1 = \frac{I\tau}{FAC_0(\pi Dt)^{0.5}}$$

EQUATION 2.1

F=Faraday constant (96486Cmol^{-1})   t=duration of pulse (s)

I=current pulse (mA)   E=measured potential (V)

A=geometric surface area (cm^2)   R=ideal gas constant (8.314Jmol^{-1}K^{-1})

T=absolute temperature (K)   D=diffusion coefficient (cm^{2}s^{-1})

E$_0$=Initial equilibrium potential (V)

The term C_0 is the original bulk concentration of dopant present, and is defined as:

$$C_0 = \frac{\rho y}{M_m}$$

EQUATION 2.2

where,

ρ=density of polymer (g cm^{-3})

M_m=molar mass of polymer repeat unit

y=original number of dopants per monomer unit, i.e. the stoichiometry (for a doping level of 50%, y=0.5)

For small values of voltage perturbation (i.e. E-E$_0$<=50mV), this relationship simplifies to:

$$E - E_0 = \frac{I\tau RT}{F^2 AC_0(\pi Dt)^{0.5}}$$

EQUATION 2.3

where the slope, S of a plot of the change in potential, ΔE against $t^{1/2}$ (Figure 2.6) is given by equation 2.4:

$$S = \frac{IPRT}{(1-y)^2 F^2 AC_0\sqrt{\pi D}}$$

EQUATION 2.4

where P is the duration of the voltage pulse in seconds.

Hence the diffusion coefficient, D can be given by equation 2.5:

$$D = \frac{I^2 t^2 R^2 T^2}{(1-y)^2 F^4 A^2 C_0^2 S^2 \pi}$$

EQUATION 2.5

By plotting ΔE against $t^{\frac{1}{2}}$, a straight line graph should be obtained if the diffusion behaviour is governed by Fick's Law as shown in figure 2.6.
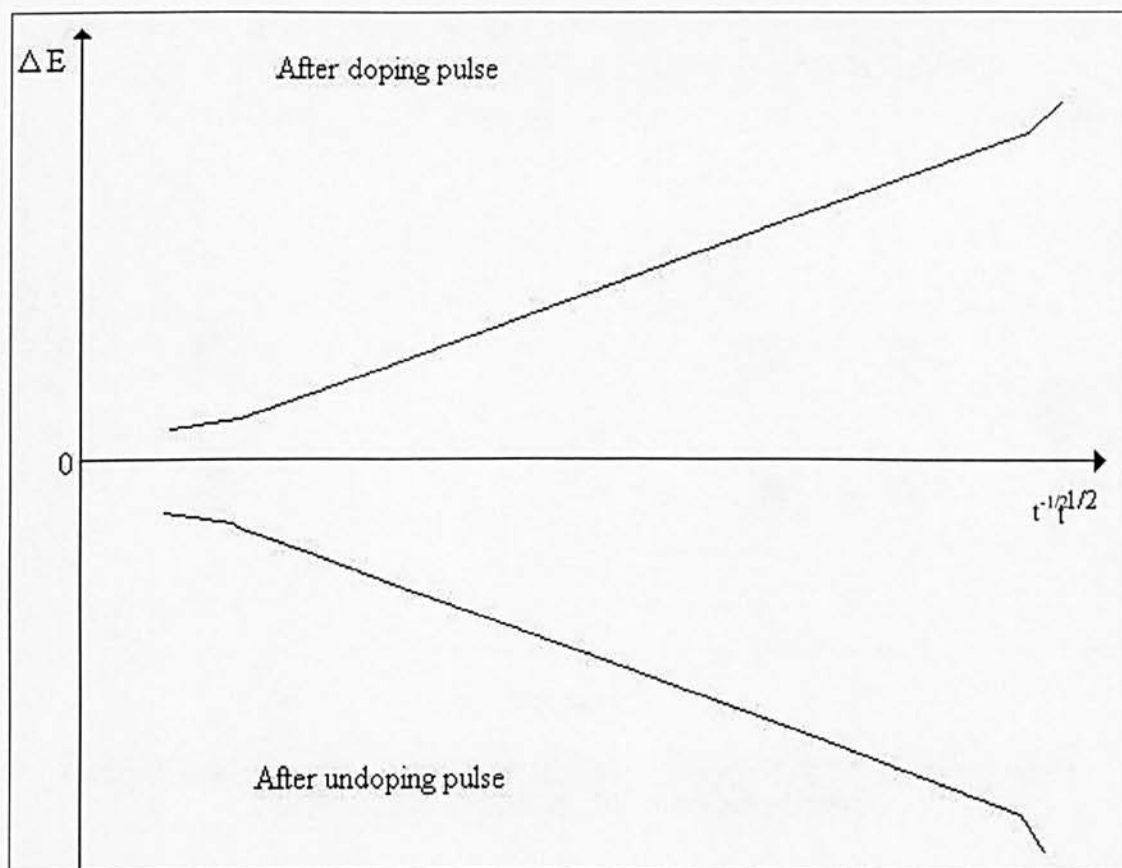
FIGURE 2.6

SCHEMATIC PLOT OF ΔE VERSUS $t^{1/2}$ SHOWING A LINEAR RELATIONSHIP AS EXPECTED FOR FICKIAN DIFFUSION

ΔE denotes the change in the electrode potential.

It is essential to know the initial concentration of dopant in the polymer for the estimation of the diffusion coefficient, and this was determined coulometrically for as-prepared films by fully undoping the polymer film in the appropriate electrolyte solution. In some cases, this was also done before and after diffusion measurements in order to establish that there was no

loss of dopant by any other reaction. The voltage against an aluminium "pseudo-reference" electrode was recorded at regular intervals.

2.6 MEASUREMENT OF THE DC ELECTRICAL CONDUCTIVITY OF POLYMER FILMS

Van der Pauw's four-probe method [42] was used to measure the electrical conductivities of the polymers produced. Current was passed through one pair of electrodes and the voltage recorded under computer control between another pair of electrodes. The contacts were made of silver paint and applied in the laboratory atmosphere in the shortest possible time. Figure 2.7 shows the circuit diagram and contact arrangement for the four-probe method.
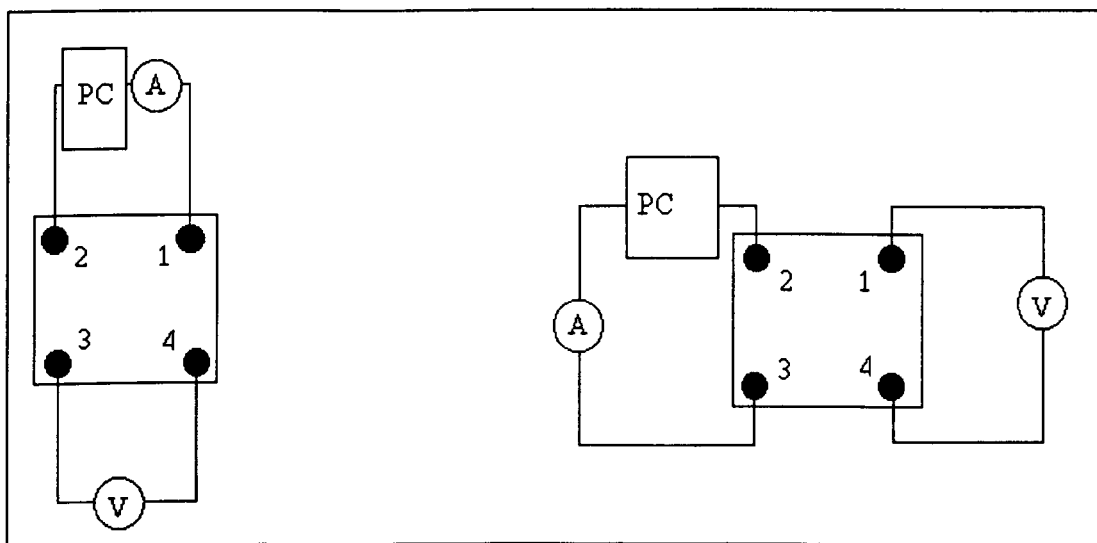
FIGURE 2.7

DIAGRAM SHOWING THE CONNECTIONS MADE FOR A VAN DER PAUW
ELECTRICAL CONDUCTIVITY MEASUREMENT

The current through the sample was increased under computer control via a Keithley 224 multimeter using limits set by the user. The voltage was measured using a Keithley 617 electrometer. The data was captured using a computer program, and the slope of the graph of potential difference against current was used to calculate the resistance.

The electrical conductivity was calculated using the following equation:

$$\rho = \frac{t R \pi}{\ln 2}$$

EQUATION 2.6

and,
$$\sigma = \frac{1}{\rho}$$

EQUATION 2.7

where, σ = conductivity(S cm^{-1})   t = thickness of film (cm)

ρ = resistivity (Ω^{-1})   R = resistance (ohm)

2.7 ELECTROCHROMIC DEVICE CONSTRUCTION

Polymer films were synthesised either chemically or electrochemically to make electrochromic devices of the structure:

ITO glass / polymer coating / high viscosity or solid electrolyte / ITO glass

The ITO glass served as both a counter electrode and as a pseudo reference electrode, having been calibrated against standard reference electrodes.

2.7.1   POLYPYRROLE-BASED ELECTROCHROMIC DEVICE CONSTRUCTION

These electrochromic devices used polyethylene oxide as the high viscosity electrolyte. A minimum of electrolyte was used to maintain complete contact between the two ITO electrodes, and its thickness was of the order of 0.2µm. The electrolyte appeared to solidify in contact with air and was therefore self-sealing at the edges of the electrochromic device.

2.7.2   POLYANILINE-BASED ELECTROCHROMIC DEVICE CONSTRUCTION

Poly(acrylamidomethylpropanesulphonic acid) (POLYAMPS) was used as the solid electrolyte for polyaniline-based electrochromic devices, which were of the structure:

ITO glass / polyaniline-based polymer / polyAMPS / ITO glass

2.8 UV-VISIBLE SPECTROPHOTOMETRY

The optical spectrophotometric properties of a wide range of conducting polymers has been established [43]; yielding information on the electronic transitions, the nature of the charge carriers and the effectiveness of conjugation in the backbone of the polymer chain. However, a study of an 'in-situ' electrochromic device has not been investigated to-date. Significant structural deformations during the doping and undoping of electrochromic materials are apt to shorten their cyclability [44]. The observation and comparison of the UV-visible spectra of the polymers at various stages of doping and undoping were used to determine the safe

voltage range (and consequent current density) to permit rapid degradation-free switching and therefore improve the long-term reversibility.

2.9 SUMMARY OF THE ELECTROCHROMIC PROPERTIES OF CONDUCTING POLYMERS

The electrochromic effect is the result of the optical transitions available to the charge carriers as the mid-gap states become available for optical transitions. When these electrochromic effects are applied in the presence of a suitable electrolyte and either oxidising or reducing ions, a time dependent current and a source of electrons, the result is a change in the conductivity of the polymer associated with the ions entering the polymer films (doping) and leaving the polymer film (undoping). These factors were studied to develop a 'switchable' device to either reflect, transmit or absorb incident electromagnetic radiation.

CHAPTER THREE

ELECTRONIC PROPERTIES OF CONDUCTING
POLYMERS

3.1   ELECTRICAL CONDUCTIVITY OF POLY-(3-HEXYLTHIOPHENE)

Several theories describe the mechanisms by which amorphous semiconductors are able to participate in electrical conduction [45]. The primary mechanism of conduction is dictated by the band structure, the type, and distribution of the majority charge carrier and the distribution of traps and defects within the material. The path of the charge carriers may be interrupted by physical defects, impurity atoms or many other possible inconsistencies in the material, thereby contributing to a reduction in the bulk conductivity of the material.

Metals are understood to have free-flowing electrons, and the conductivity decreases with increasing temperature according to equation 3.1.

$$\sigma \propto \frac{N e^2 \tau}{(m_e \, k \, T)^{0.5}}$$

EQUATION 3.1

Where τ represents the mean free time of the charge carrier, e the electron charge, k is the Boltzmann constant and m_e the mass of the electron. Typical electron velocities are in the range of $10^6 ms^{-1}$ at room temperature and the density of free carriers is of the order of $10^{22} cm^{-3}$.

Unlike the electrons in metals, charge carriers in semiconductors are not free flowing, and the conduction mechanism(s) are dependent on the number of electrons that are thermally excited into the conduction band. The temperature dependence of semiconductors vary exponentially with $1/T$ and hence, the electrical conductivity of a semiconductor consequently increases rapidly with temperature. The velocity of the charge carrier is typically $10^5 ms^{-1}$ in a wide band-gap semiconductor, while the occupied trap concentration, may be as high as $10^{17} cm^{-3}$ [46], which corresponds to about 1 trap per 1000 monomer units. The charge carrier density is independent of temperature; hence any temperature dependence is from the mean free path, which decreases with increasing temperature. By the use of Fermi statistics, the rate of detrapping (A_2) is (Equation 3.2):

$$A_2 = A_1 \exp \left[\frac{-(E_c - E_t)}{kT} \right]$$

EQUATION 3.2

The term A_1 is used to describe the rate of trapping and (E_C-E_t) gives the trap depth.

Equation 3.2 describes the Shockley-Read model of detrapping [46], which may be visualised in Figure 3.1:
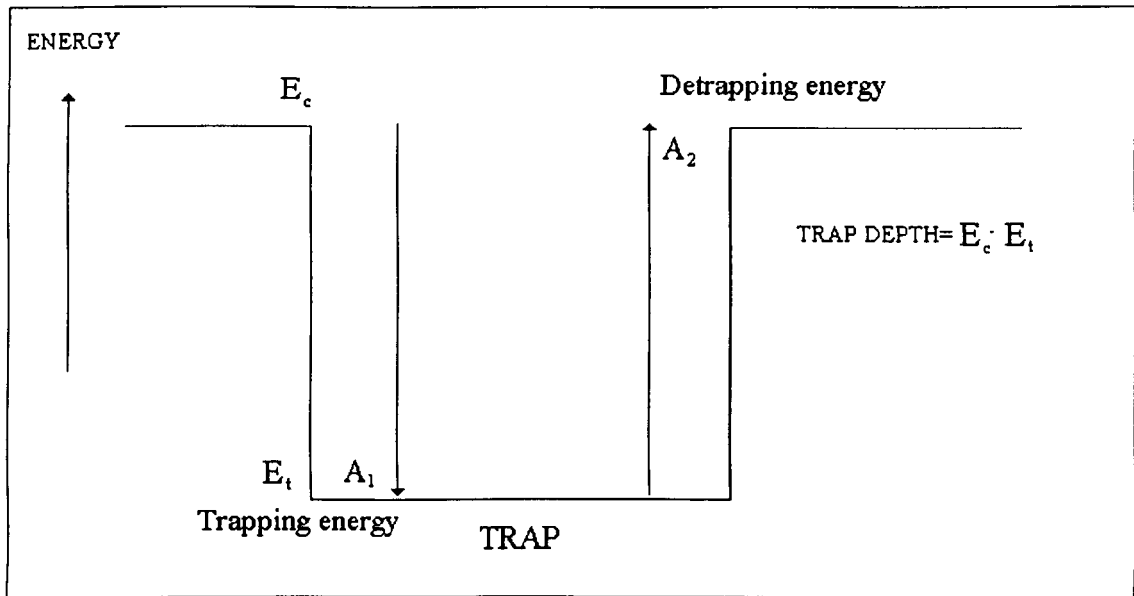
FIGURE 3.1

SHOCKLEY-READ MODEL OF DETRAPPING

The material may be represented as a series of potential energy walls, of depth ΔH_m, separated by a distance a. The probability α that the charge carrier will 'jump' over the potential energy barrier indicated by the relationship:

$$\alpha \propto \exp\left(\frac{-\Delta H_m}{kT}\right)$$
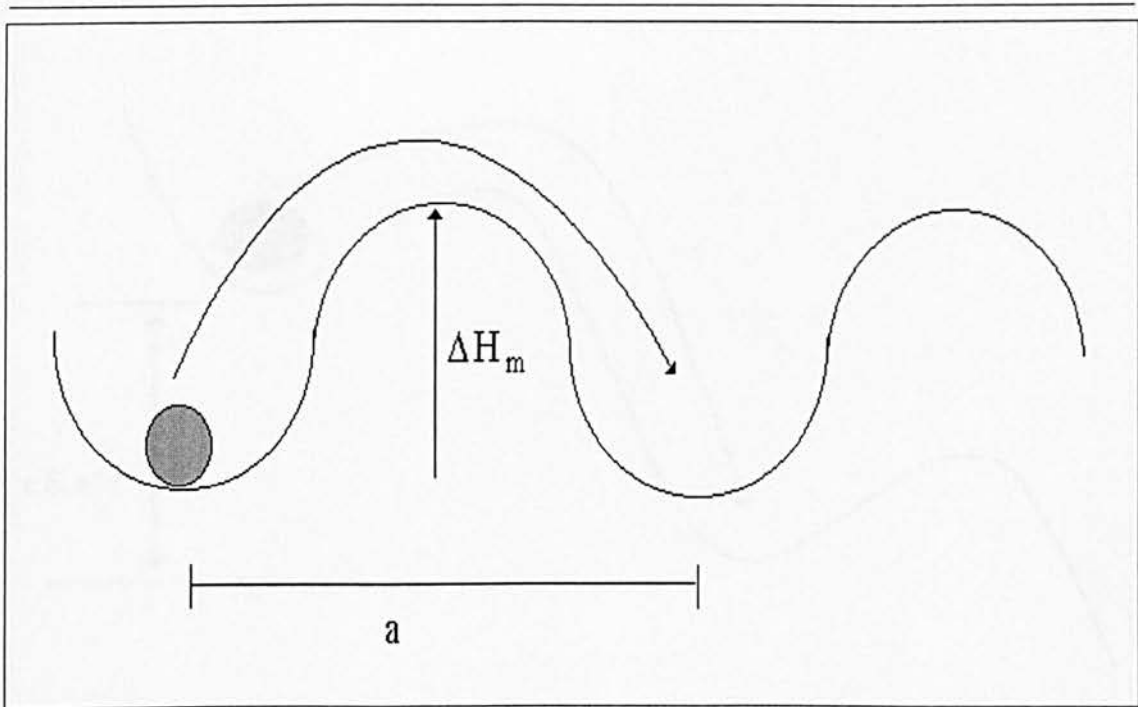
FIGURE 3.2

DIAGRAM TO SHOW THE POTENTIAL ENERGY BARRIERS TO A CHARGE CARRIER
FOR AN OHMIC-TYPE RESPONSE

Under the influence of an electric field, the carrier has an additional energy $e\bar{E}a/2$, thereby increasing the overall probability of overcoming the barrier height ΔH_m, and reducing the Boltzmann factor. There is also the possibility of the charge carrier jumping to the left; however, the presence of the electric field reduces this chance. This reduction of the barrier height may be represented by tilting the potential energy barrier curve downwards, indicating a more favourable movement in the direction of the electric field (Figure 3.3).
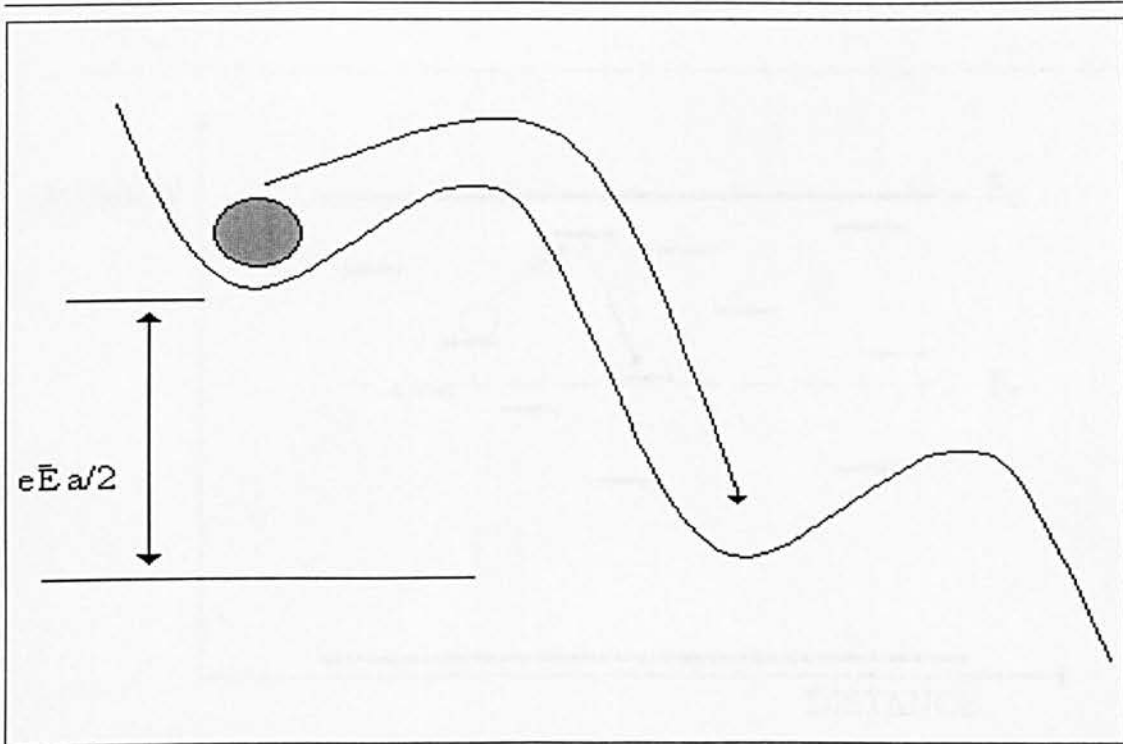
FIGURE 3.3

DECREASE IN POTENTIAL ENERGY BARRIER HEIGHT IN THE PRESENCE OF AN
ELECTRIC FIELD, INDICATED BY A MORE FAVOURABLE MOVEMENT TO THE
RIGHT BY THE CHARGE CARRIER

Once the carrier has sufficient energy to overcome the initial energy well, it may then migrate
from trap to trap with essentially no barrier in its path.

Another response mechanism may be described by polaron motion or hopping between
neighbouring localised states. Polarons within amorphous materials tend to be small, of the order
of atomic or molecular dimensions. The polaron is able to hop between sites by an energy W.
This is described generally by the relationship:

$$\sigma \propto \exp\left(\frac{-W}{kT}\right)$$

The hopping between localised states is shown below in Figure 3.4.
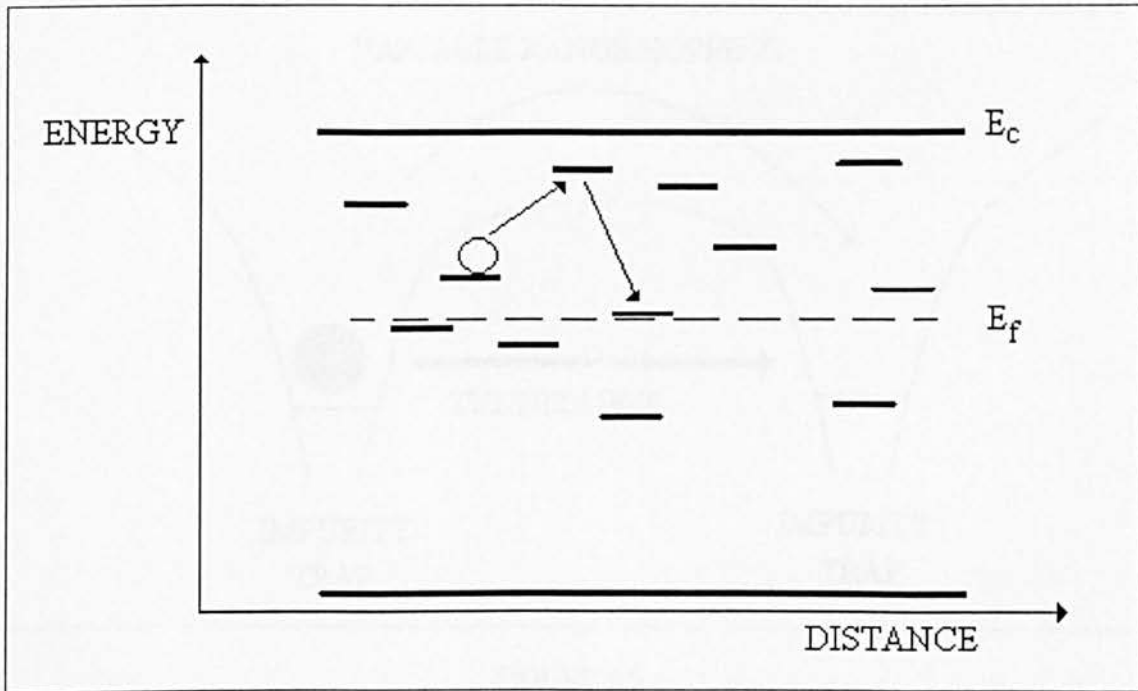
FIGURE 3.4

SOME POSSIBLE DESTINATIONS OF A CHARGE CARRIER IN VARIABLE RANGE
HOPPING

Disordered materials tend to have a broad distribution of the position and energy of the energy
levels. The broad distribution may be due to the presence of imperfections such as impurities or
levels associated with physical disorder (defects, dislocations etc), band tails (due to smearing of
the band edges by the irregular nature of the molecular arrangement within the bulk material).
The distinction between barrier hopping and variable range hopping is that the wave functions of
the localised sites may overlap, allowing the possibility of tunnelling (Figure 3.5).

VARIABLE RANGE HOPPING

TUNNELLING

IMPURITY
TRAP
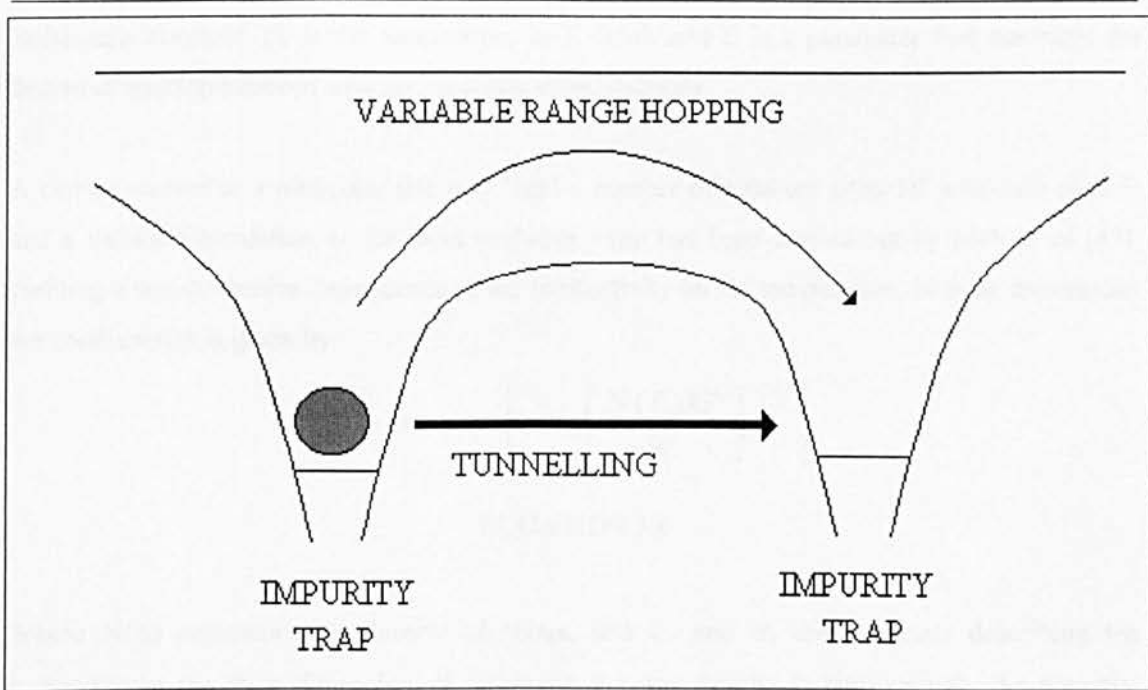
IMPURITY
TRAP

FIGURE 3.5

THE DIFFERENCES BETWEEN TUNNELLING AND VARIABLE RANGE HOPPING
MODELS OF CONDUCTION. THE HIGH CONCENTRATION OF IMPURITY
WAVEFUNCTIONS CAUSES AN OVERLAP BETWEEN THEIR WAVEFUNCTIONS.

The probability that the carrier will jump between the impurity wavefunctions, Γ is given by the equation:

$$\Gamma = \upsilon_{ph} \; \exp\left[-\frac{W_0 \pm eRF}{kT} - 2\, \Xi\, \overline{E}\right]$$

EQUATION 3.3

where $\Xi = \dfrac{\left(2\,m_e\,W_0\right)^{1/2}}{\hbar}$

where υ_{ph} is the phonon frequency, and W_0 is the energy difference between the two impurity energy states. If the localisation is very strong, the electron will jump to the nearest state, since the term $\exp(-2\,\Xi R)$ decreases with distance, R. $\overline{E}$ is the field strength, m_e is the mass of an electron and W_0 is the energy level for the electron in a single potential energy well. k is the

Boltzmann constant, (T is the temperature in Kelvin), and Ξ is a parameter that describes the degree of overlap between adjacent impurity wavefunctions.

A carrier located at a particular site may 'see' a number of adjacent sites, all with their own E_t and a values. Calculation of the most probable jump has been carried out by Mott *et al* [47], yielding a non-Arrhenius dependence of the conductivity on the temperature. In three dimensions the conductivity is given by:

$$\sigma = \sigma_3 \exp \left\{ - C_3 \left[\frac{N(E)kT}{\Xi^3} \right]^{-1/4} \right\}$$

EQUATION 3.4

Where N(E) represents the density of states, and C_3 and σ_3 are constants describing the movement in the third dimension. If, however, the trap density is high enough, the potential energy walls will overlap (Figure 3.5), and the barrier height between successive traps, ΔH is less than the ionisation energy, W_1. The barrier height is now given by equation 3.5, where e is the electronic charge, ε' is the real part of the dielectric constant, ε_0 is the vacuum dielectric permittivity and a is the separation between the potential energy walls of the impurity traps:

$$\Delta H = W_1 - \frac{e^2}{\pi \, \varepsilon' \varepsilon_0 \, a}$$

EQUATION 3.5

In the limit of high concentrations, this system may go into a tunnelling arrangement or into an impurity level if $\Delta H \rightarrow 0$. Marchant [48] described these models and carried out both temperature and frequency dependant conductivity studies on poly-3-(hexylthiophene). The data appeared to fit the variable-range hopping model at temperature below 150K. On increasing the temperature, the dependence appeared to fit an activated process where the charge carrier was required to overcome a barrier height of 0.5eV, resulting from a potential energy barrier due to the presence of (bi)polarons. The bi(polarons) are due to the excitation of the π-band electrons to the (bi)polaron states to form a new band during the doping process. At room temperatures, the activation energy is reduced to 0.27eV and reduces further to 0.003eV on strong doping.

3.2 DC CONDUCTIVITY

The DC conductivity of amorphous semiconductors is governed by four main mechanisms of charge transport :

3.2.1 THERMAL ACTIVATION TO EXTENDED STATES (E_C-E_F) [49]

Transport by carriers excited beyond the mobility edge into non-localised (or extended) states at E_C or E_V. The electron flow can be described by:

$$\sigma_{DC} = \sigma_1 \exp\left(-\frac{E_C - E_F}{kT}\right)$$

EQUATION 3.6

The activation energy of the process may be calculated by plotting $\log_e \sigma$ against $1/T$.

3.2.2 THERMALLY ACTIVATED HOPPING IN BAND TAILS (E_A-E_F+W_1) [50]

Transport by charge carriers into localised states at the band edges and hopping energies close to localised states at the band edges. If we again assume that the charge carriers are electrons then:

$$\sigma_{DC} = \sigma_1 \exp\left(-\frac{E_C - E_F + W_1}{kT}\right)$$

EQUATION 3.7

where W_1 is the hopping activation energy and E_A is the energy at the conduction band edge. Once again a straight line graph is obtained when plotting $\log_e \sigma$ against $1/T$.

3.2.3 POLARON HOPPING [51]

This conduction process is due to the contribution from charge carriers between localised states with energies near the Fermi level, and is analogous to impurity conduction in heavily doped crystalline semiconductors. These carriers can then hop between localised states, and may be described by:

$$\sigma_{DC} = \sigma_2 \exp\left(-\frac{\omega_2}{kT}\right)$$

where $\sigma_2 \leq \sigma_1$ and ω_2 is the hopping energy of the order of half the band width. When $\log_e \sigma$ is plotted against $1/T$, a straight-line graph is obtained only when hopping occurs between nearest neighbours.

3.2.4 HOPPING IN STATES NEAR THE FERMI LEVEL [52]

As the temperature decreases, there is less energy available for hopping i.e. the energy barrier for the hopping process increases, and tunnelling between the potential wells becomes more favourable, hence ω_2 decreases such that:

$$\sigma_{DC} = \sigma'_2 \exp\left(-\frac{B}{T^{\frac{1}{4}}}\right)$$

EQUATION 3.9

where

$$B = 2\left\{\frac{\alpha^3}{k\,N(E_F)}\right\}$$

α represents the radius of the localised carrier wave and is of the order of 10^{-10}m for amorphous materials. Figure 3.6 shows pictorially how the various temperature dependent DC conductivities contrast against each other when plotted on a graph of $\log_e \sigma$ against $1/T$.
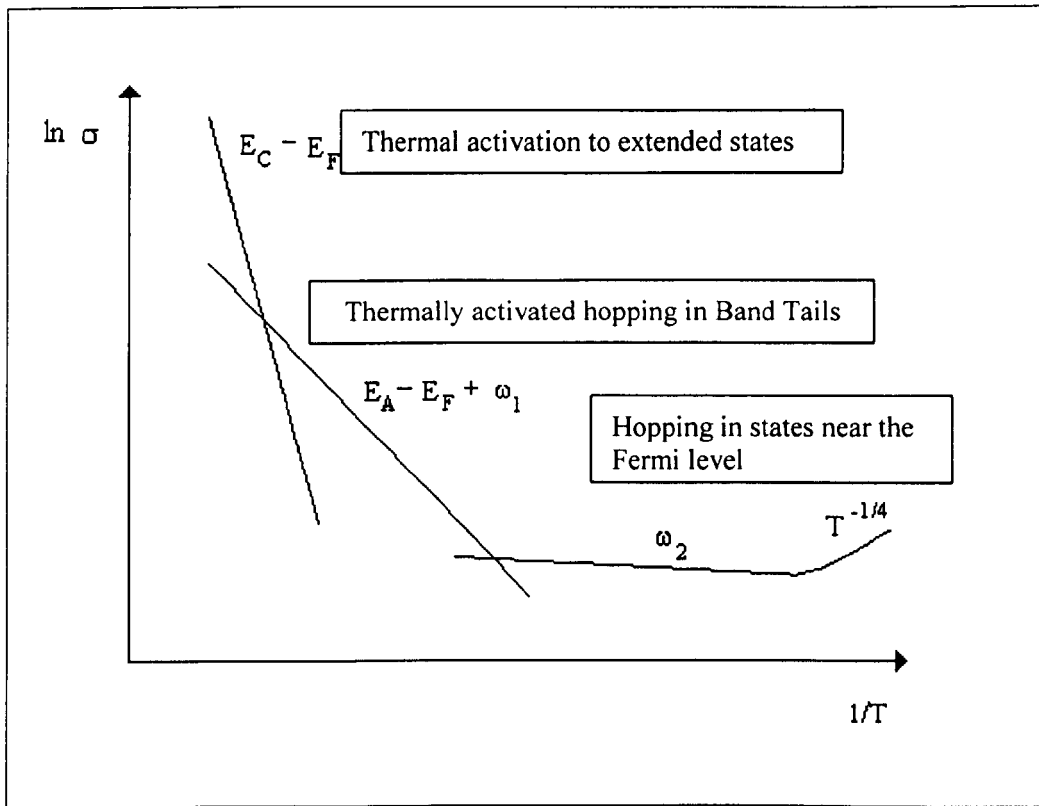
FIGURE 3.6

IDEALISED REPRESENTATION OF THE TEMPERATURE DEPENDENCE OF DC
CONDUCTIVITY IN AN AMORPHOUS SEMICONDUCTOR

3.3   A.C. CONDUCTIVITY

The presence of an alternating electric field produces microscopic displacements about the nucleus of the semiconductor atoms, resulting in shifts of electron density. This polarisation gives rise to a dipole moment that may be detected electrically. There are several main types of polarisation (Figure 3.7):

Electronic Polarisation: The nucleus is displaced relative to the electron cloud in the presence of an electric field. This type has the fastest response time.

Atomic Polarisation: The presence of an electric field distorts the arrangement of the atomic nuclei within a molecule. Atomic polarisation is not observed above

infra-red frequencies due to the relatively large inertia of the atomic nucleus. From vibrational spectroscopy, bond bending is generally the greatest contributor to atomic polarisation.

Dipole or Orientational	If the molecule already possesses a permanent dipole moment due to the presence of polar groups, there will be a tendency of that molecule to align
Polarisation:	in the direction of an applied electric field, giving a net polarisation in that direction. This polarisation process is usually slow to develop, but may make a large contribution to the total polarisation of that material within an electric field.
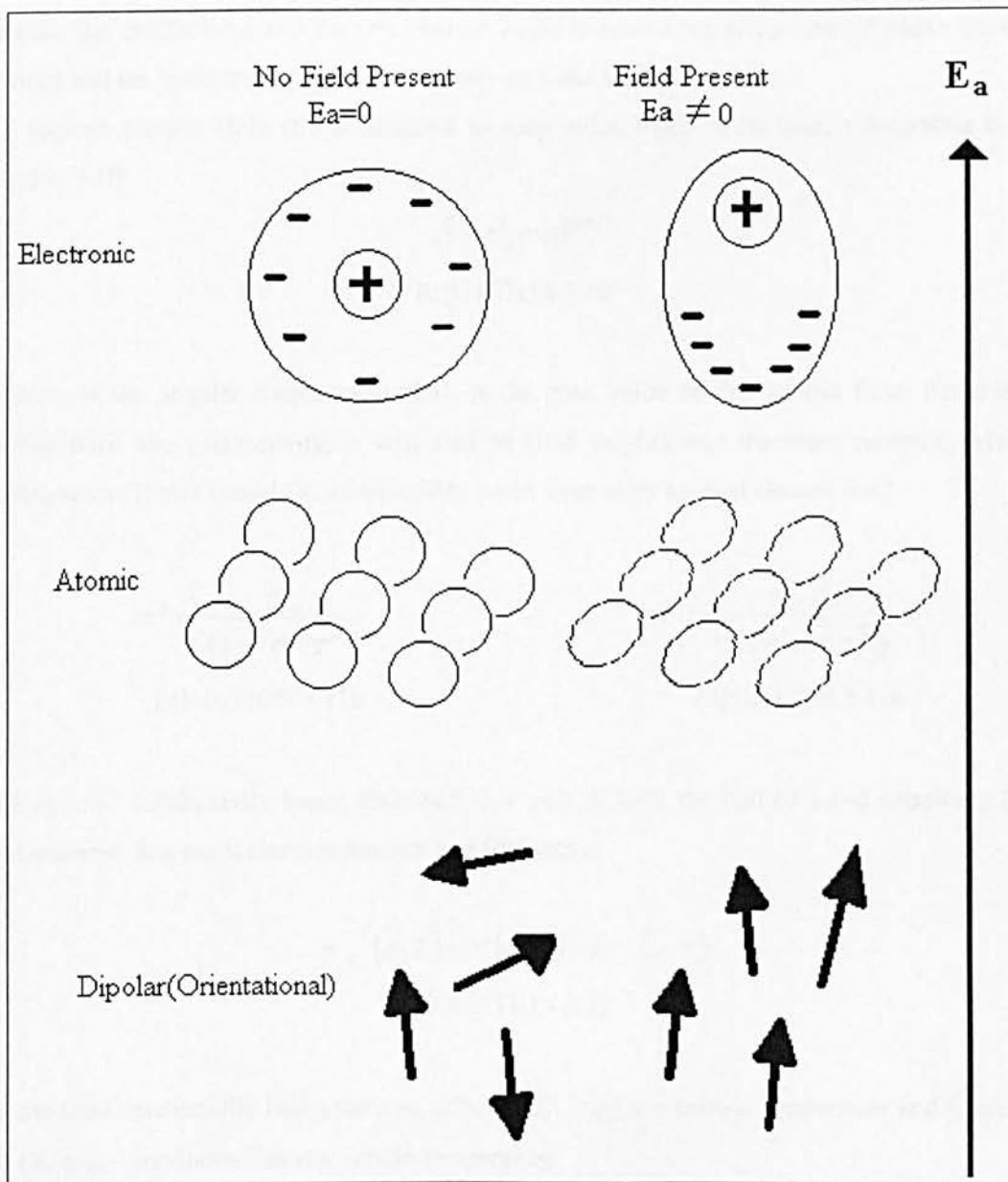
FIGURE 3.7

Diagrammatic representation of the various types of polarisation processes

In the presence of an alternating field, the charges oscillate back and forth. If the frequency is sufficiently low $\omega \ll 1/\tau_R$, any free charges will respond in phase with the field (ie $\sigma(\omega)$ will be predominantly real), whereas any bond charges will respond out of phase with the field (ie $\varepsilon(\omega)$ will be predominantly real). As the frequency increases, the charges will no longer be able to

maintain the oscillations, and the free charges begin to have a significant out of phase response for $\sigma(\omega)$ and the bond charges give an in phase response for $\varepsilon(\omega)$.

The applied electric field (E) is assumed to vary sinusoidally with time, t according to the equation 3.10:

$$\bar{E} = \bar{E}_0 \exp^{-i\omega t}$$

EQUATION 3.10

where ω is the angular frequency, and E_0 is the peak value of the electric field. For a time-varying field, the conductivity, σ will also be time varying and therefore complex, with σ_0 relating to the Drude model DC conductivity when there is no applied electric field:

$$\sigma' = \frac{\sigma_0}{(1 + \omega^2 \tau^2)} \qquad\qquad \sigma'' = \frac{\sigma_0 \omega \tau}{(1 + \omega^2 \tau^2)}$$

EQUATION 3.11a   EQUATION 3.11b

With the AC conductivity being described as a sum of both the real (σ') and imaginary (σ'') conductivities at a particular temperature and frequency:

$$\sigma_{AC}(\omega, T) = \sigma'(\omega, T) + i\sigma''(\omega, T)$$

EQUATION 3.12

and the total conductivity being the sum of both AC (σ_{AC}) at a certain temperature and frequency and DC (σ_{DC}) conductivities at a certain temperature:

$$\sigma_{TOT}(\omega, T) = \sigma_{DC}(T) + \sigma_{AC}(\omega, T)$$

EQUATION 3.13

The temperature dependence of the AC conductivity in semiconducting materials is described by the Austin-Mott theory [47], where the charge carriers are thought to tunnel between the individual localised states close to the Fermi level:

$$\sigma_{AC} = \frac{ne^2 kT}{3[N(E_F)]^2 \alpha^{-5} \omega \left[\ln\left(\frac{\upsilon_{ph}}{\omega}\right)\right]^4}$$

EQUATION 3.14

Where α denotes the radius of the localised carrier wavefunction ($\sim 1\times10^9$m for amorphous materials), $N(E_F)$ is the density of states at the Fermi level, υ_{ph} is the phonon assisted attempt frequency ($\sim 10^{12}$Hz), n is the number of electrons per unit volume, e is the electronic charge, k is the Boltzmann constant, and T the temperature, with ω being the angular frequency. The relationship between the complex dielectric constant ($\varepsilon^* = \varepsilon' + i\varepsilon''$) and the frequency shows that at low frequencies, the numerous polarisation processes will all contribute to a high value of the permittivity. As the frequency increases, the individual mechanisms of polarisation create a resonance or a relaxation with ε' decreasing, and a maximum occurring with ε''(Figure 3.8).
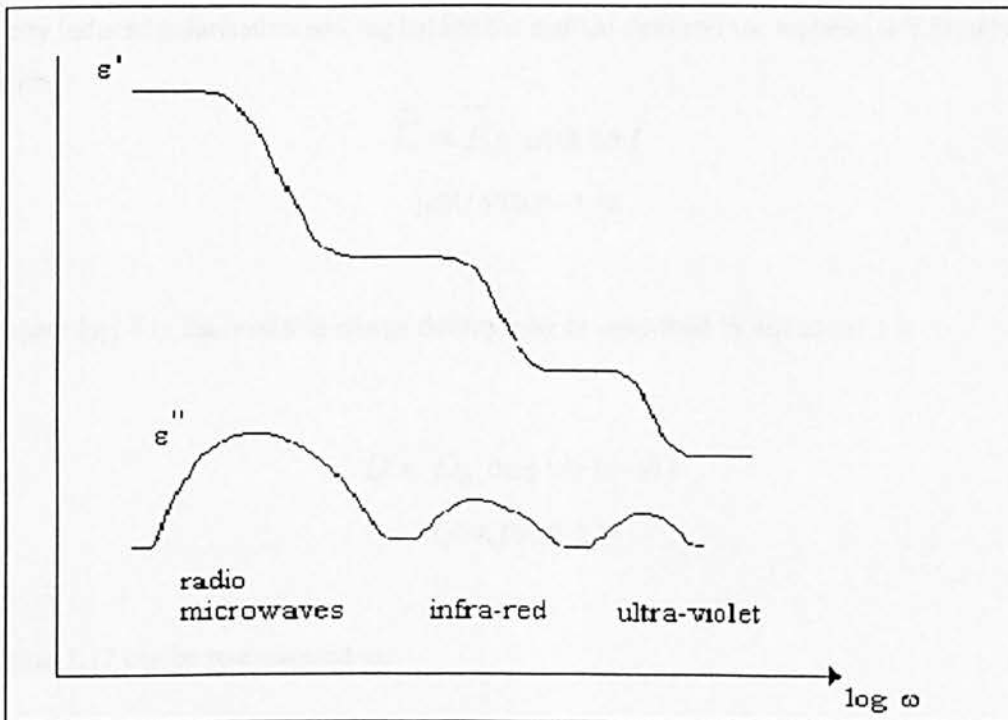
FIGURE 3.8

VARIATIONS IN THE DIELECTRIC CONSTANT AS A FUNCTION OF FREQUENCY FOR A TYPICAL DIELECTRIC MATERIAL. A RESONANCE IS PRODUCED FOR ε'' WHEN ε' DECREASES IN RELATION TO THE FREQUENCY

The dielectric response of a material is the result of polarisation mechanisms occurring within the material due to an external stimulus from an applied electric or magnetic field. Typical mechanisms that give rise to polarisabilitv are the distortion of electron clouds or atomic dipoles or the rearrangement of permanent dipoles. The polarisation induced by the applied field is given by:

$$P = D - \overline{E}\, \varepsilon_0\, \varepsilon_r$$

EQUATION 3.15

where D is the dielectric displacement, $\overline{E}$ is the applied electric field and ε_0 the electric permittivity of a vacuum [53].

When an alternating electric field E of amplitude E_0 (equation 3.16) is applied to the material, then any induced polarisation will lag behind the applied field and the material will behave like a capacitor

$$\overline{E} = \overline{E}_0\, \cos \omega\, t$$

EQUATION 3.16

The phase lag, δ in the resulting charge density may be described by equation3.17:

$$D = D_0\, \cos\left(\omega\, t - \delta\right)$$

EQUATION 3.17

Equation 3.17 can be re-expressed as:

$$D = D_1\, \cos \omega\, t + D_2\, \sin \omega\, t$$

EQUATION 3.18

where $D_1 = D_0 \cos \delta$ and $D_2 = D_0 \sin \delta$

The measured dielectric constants, ε' and ε'' may then be related to the applied electric field and charge density by:

$$\varepsilon' = \frac{D_1}{\varepsilon_0 \, E_0} \qquad\qquad \varepsilon'' = \frac{D_2}{\varepsilon_0 \, E_0}$$

EQUATION 3.19A   EQUATION 3.19B

The imaginary (lossy) part of the dielectric constant can be related to the AC conductivity [54] by equation 3.20.

$$\sigma_{AC}(\omega) = \varepsilon_0 \, \omega \, \varepsilon''(\omega)$$

EQUATION 3.20

One main characteristic of the dielectric properties of conducting polymers compared to insulating polymers is that the AC conductivity is not dependent on dipolar orientations that have very temperature dependent relaxation times. For dopant levels greater than 1%, the conductivity is dependent on the temperature over a wide temperature range from -170K to 293K [55]. Feldblum *et al* [56] carried out measurements of DC conductivity and high frequency AC conductivity on polyacetylene foams doped up to 3% with iodine. Their results indicated that conductivity measurements carried out on foam-based materials are the same whether they are made using a DC or high frequency electric field within experimental error.

3.3.1   CLASSICAL RELAXATION MODELS

3.3.1.1   Drude Model

This model uses delocalised electronic states to describe charge transport, as in metals, and would therefore only be used for very highly doped or aligned conducting polymers.

3.3.1.2   Diffusive Transport

This mechanism tends to be used with ionic conductors. Jonscher [57] predicted that an increase in the concentration of ionic species yields a $1/\sqrt{\omega}$ for both ε' and ε''.

$$\varepsilon'(\omega) \propto \omega^{-1/2} \qquad\qquad and \qquad\qquad \varepsilon''(\omega) \propto \omega^{-1/2}$$

3.3.1.3 Debye Model

Debye established this model for use with polar molecules in a dilute solution [58]. A dipole with several possible orientations, which then returns back to an equilibrium position, with a relaxation time τ after displacement. Therefore, P is the polarisation vector and P_{eq} is the equilibrium polarisation vector:

$$\frac{d\vec{P}}{dt} = \frac{\vec{P} - \vec{P}_{eq}}{\tau}$$

EQUATION 3.21

If $\vec{P} = \vec{P}_{eq}$ then $\dfrac{d\vec{P}}{dt} = 0$

If $\vec{P} \neq \vec{P}_{eq}$ then $\vec{P}$ returns to $\vec{P}_{eq}$

The complex dielectric constant ε^* may be related to the polarisation vector, P by:

$$\vec{P} = \frac{\varepsilon_s - \varepsilon_\infty}{\varepsilon_0 \, \varepsilon} \overline{E}_0 \, \exp\left(i\omega t\right)$$

EQUATION 3.22

When equation 3.22 is substituted into equation 3.21 then:

$$\frac{d\vec{P}}{dt} = \frac{1}{\tau}\left[\frac{\varepsilon_s - \varepsilon_\infty}{\varepsilon_0 \, \varepsilon} E_0 \exp\left(i\omega t\right) - \vec{P}_{eq} \right]$$

EQUATION 3.23

the solution of which yields expressions for both the real and imaginary parts of the dielectric constant:

$$\varepsilon\,'\!\left(\omega\right) = \varepsilon_{\infty} + \frac{\varepsilon_{s} - \varepsilon_{\infty}}{1 + \omega^{2}\tau^{2}}$$

EQUATION 3.24

$$\varepsilon\,''\!\left(\omega\right) = \left(\varepsilon_{s} - \varepsilon_{\infty}\right)\!\left(\frac{\omega\tau}{1 + \omega^{2}\tau^{2}}\right)$$

EQUATION 3.25

Where ε_{∞} is the permittivity at high frequency, ε_{s} is the permittivity at zero frequency; ω is the angular frequency, τ the relaxation time and E_0 represents the amplitude of the electric field.
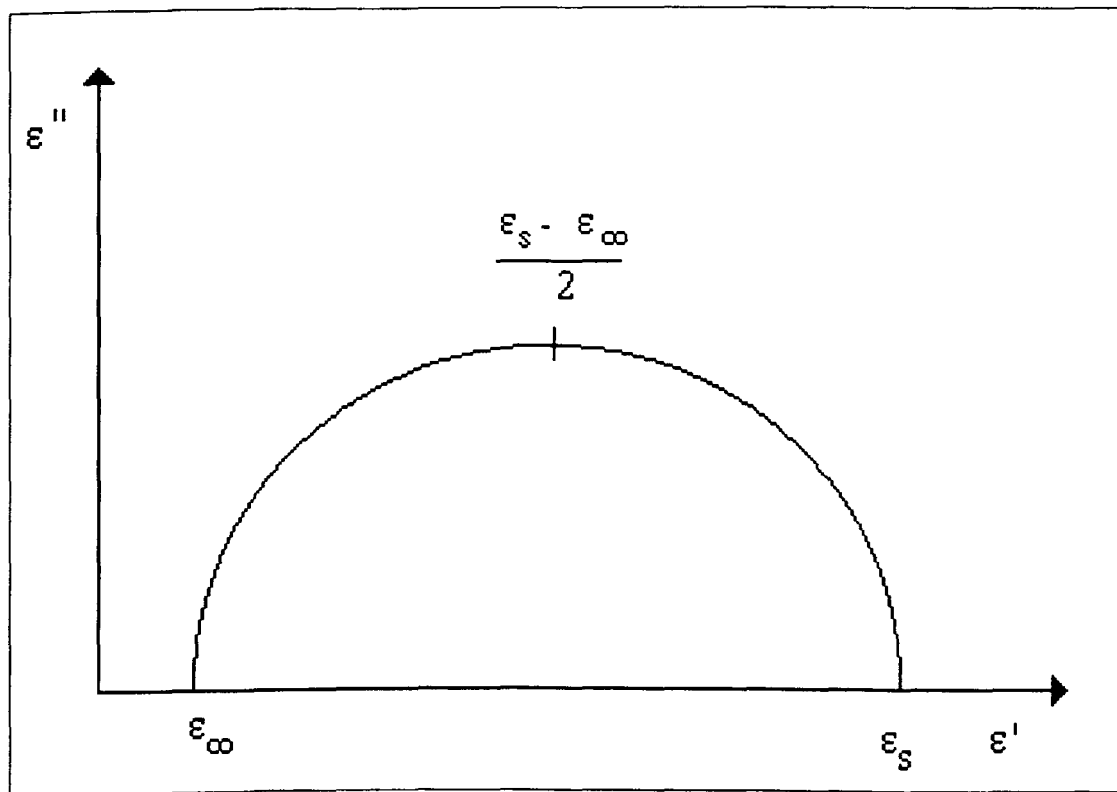
FIGURE 3.9

SCHEMATIC REPRESENTATION OF A COLE-COLE PLOT

This may be represented by a diagram known as the Cole-Cole diagram [59], where ε' is plotted against ε''. The plot is ideally a semi-circle where the highest point indicates the relaxation frequency.

Several models have been derived from the Debye model; these lead to the following kinds of frequency-dependence:

3.3.1.4 Cole-Cole

$$\varepsilon^*(\omega) = \varepsilon_\infty + \frac{\varepsilon_s - \varepsilon_\infty}{1 + (i\omega\tau)^{1-\alpha}}$$

EQUATION 3.26

3.3.1.5 Cole-Davidson

$$\varepsilon^*(\omega) = \varepsilon_\infty + \frac{\varepsilon_s - \varepsilon_\infty}{(1 + i\omega\tau)^{1-\beta}}$$

EQUATION 3.27

Where α is a constant

3.3.1.6 Havriliak-Negami

$$\varepsilon^*(\omega) = \varepsilon_\infty + \frac{\varepsilon_s - \varepsilon_\infty}{\left(1 + (i\omega\tau)^{1-\alpha}\right)^{1-\beta}}$$

EQUATION 3.28

where α and β are constants that relate to the Cole-Cole plot, and not directly to the material's dielectric properties. These frequency dependent models imply that there is a distribution of hopping charges and relaxation times. These (and other) factors cause deviations from the 'ideal' Cole-Cole plot. The constants α and β are used to solely describe these deviations from the empirical formulae and cannot be easily attributed to the intrinsic properties of the material.

These may then contribute to the AC conductivity by the following methods:

A: Transport by carriers in the extended states near Ec or Ev

This is analogous to a Drude-type process, where the frequency dependent conductivity σ(ω) is given by:

$$\sigma(\omega) = \frac{\sigma(0)}{1 + \omega^2 \tau^2}$$

EQUATION 3.29

However, this is more applicable to most liquid metals, and not to amorphous semiconductors.

B: Transport by charge carriers into localised states at the edges of the valence band or
      conduction bands

A similar trend may be expected to that of the hopping transport by electrons with energies near the Fermi level (see (c) below), and therefore according to $\omega\{\log_e(v_{ph}/\omega)\}^4$. This varies according to ω^s, if s<1 and $\omega<v_{ph}$.

C: Hopping transport by electrons with energies near the Fermi level

The phonon frequency may be derived using equation 3.14, with a plot of loge σ_{AC} versus $\log_e$ ω yielding a linear slope of value:

$$slope = \frac{d\left[\ln\left\{\omega \ \ln^{\ 4}\left(\frac{v_{ph}}{\omega}\right)\right\}\right]}{d\left(\ln \ \omega\right)}$$

EQUATION 3.30

Where v_{ph} represents the phonon frequency.

A Mott-Davis analysis to determine the AC conductivity for variable range hopping in non-crystalline semiconductors [60] has yielded the following relationship between the frequency and the AC conductivity:

$$\sigma(\omega) = \frac{1}{3} \pi e^2 \, k \, T\{N(E_F)\}^2 \, \alpha^{-5}\omega\left\{\ln\left(\frac{\upsilon_{ph}}{\omega}\right)\right\}^4$$

EQUATION 3.31

where α is the radius of the localised carrier wave and is approximately 10^{-10}m, and ν_{ph} is the phonon frequency which is of the order of 10^{-12}Hz. This is based on the assumption that hopping between multiple sites does not occur and that the hopping energy is not related to the hopping distance. Equation 3.31 may be summarised by the following relationship including the temperature dependence and frequency dependence parameters (n and s respectively):

$$\sigma(\omega) \propto T^n \, \omega^s$$

where s is a function of the frequency and $\omega \ll \nu_{ph}$. The three conduction mechanisms are shown graphically in Figure 3.10.
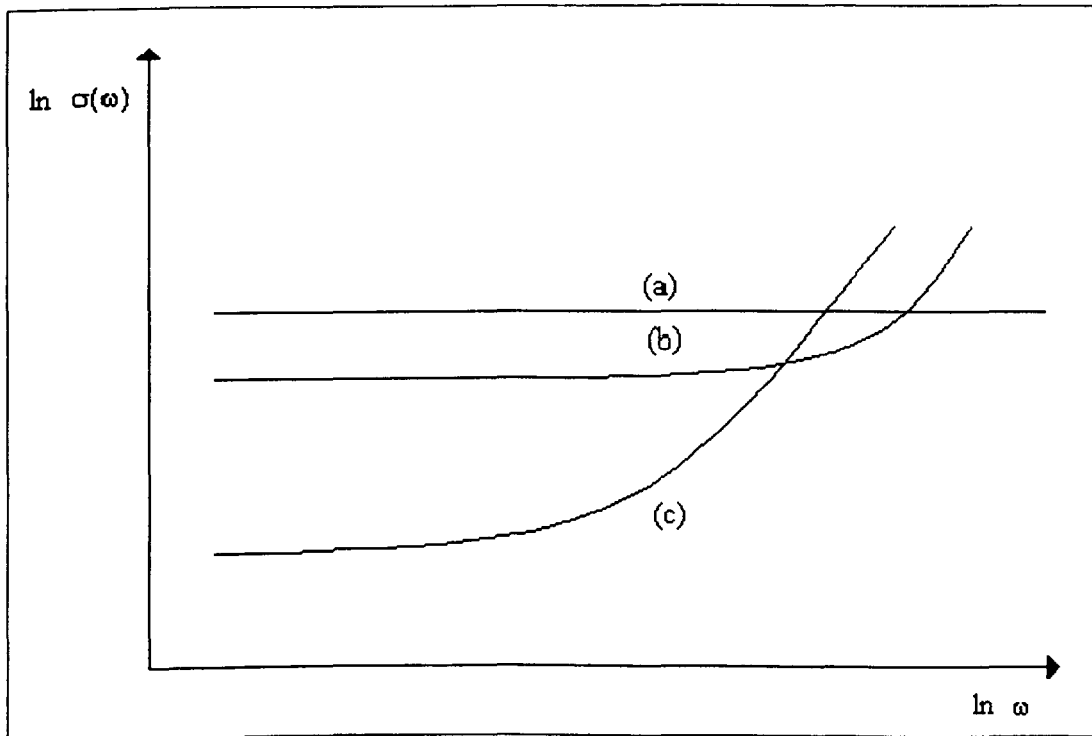
FIGURE 3.10

SCHEMATIC DIAGRAM FOR $\sigma(\omega)$ FOR THE THREE MACHANISMS OF AC CONDUCTION

For the two hopping processes (b) and (c), the total AC conductivity increases as a function of ω^s. From the relationship above, the dependency on the exponent s may be determined by plotting the double $\log_e$ of the total AC conductivity against the frequency:

$$\text{where} \quad s = 1 - \frac{4}{\ln\left(\dfrac{v_{ph}}{\omega}\right)}$$

the intercept of the plot is given by:

$$\text{intercept} = \ln \frac{\pi^2 \, e^2 \, k \, T \, \alpha^{-5} \, N(E_F)}{3}$$

3.4   CONDUCTING POLYMERS

3.4.1   POLYALKYLTHIOPHENES

Poly-3-(hexylthiophene) has been observed [61] to change the conduction behaviour from a $T^{-1/4}$ dependence to a $T^{-1/2}$ dependence over a range of dopant concentrations. This is by no means unusual, and is also observed for polypyrrole [62], which apparently changes between three conduction mechanisms as the doping level is increased. These results indicated that at low temperatures, the charge carriers are pinned in deep potential energy states by the dopant ions themselves, thereby allowing only tunnelling to occur ($T^{-1/2}$ dependence). As the temperature increased, a two-step process for conduction occurs, involving the removal of the charge carriers from the potential energy well (T^{-1} dependence) and a hopping mechanism ($T^{-1/4}$ dependence) to the next available site.

Hourquebie *et al* [63] have measured the DC conductivity of undoped poly(3-butylthiophene) and poly(3-octylthiophene). The materials were separated into three fractions of decreasing molecular weight (M_w=1.13x10^5, 3.80x10^4 and 2.93x10^4 respectively).

The DC conductivity was plotted as a function of the polymer doping level. The results indicated that the greater the higher molecular weight material had an elevated conductivity, compared to the lower molecular weight fraction, which was corroborated by other researchers [64-65]. The increased conductivity may be assigned to an increased probability of intrachain motion as the intrachain conductivity is greater than the interchain conductivity [66], the conductivity at a given doping level will increase with molecular weight.

Thermally activated conductivity is generally characteristic of amorphous conducting polymers ie. as $\sigma \to 0$ as $T \to 0$, such as polypyrrole [67]. This type of conductivity is not always characteristic of polyaniline and polyacetylene [68], where the conductivity can show metallic behaviour when the temperature dependence is described by:

$$\sigma^{-1} = \rho_m \exp\left(\frac{-T_m}{T}\right) + \rho_t \exp\left[\frac{T_c}{(T_0 + T_s)}\right]$$

EQUATION 3.32

Where the pre-addition term describes the quasi-1D metallic term and the second term relates to the fluctuation-induced tunnelling between extended metallic regions. T_c and T_s are constants dependant on the barrier parameters; ρ_m, ρ_t, ρ_0, T_m and T_0 are constants with $T_m \sim 1000K$ and $T_0 \sim 1200K$.

Kaynak *et al* found that at frequencies of 10^{10}Hz, the $\sigma(\omega)_{mw}$ term was observed to be greater than the DC conductivity, σ_{DC} term for polypyrrole [69] for lightly doped films, using the equation:

$$\omega \, \varepsilon_0 \varepsilon^{''} = \sigma\left(\omega\right)_{mw} - \sigma_{DC}$$

EQUATION 3.33

For highly conducting films over the 90-290K temperature range, the AC component of both the AC and DC components, σ^* was not observed, but for semiconducting films, σ_{AC} was observed over all temperature ranges. There may be some inter-relation between σ_{AC} and σ_{DC} as σ_{DC} may not simply be subtracted from σ^*.

3.4.2 POLYANILINE

There are three main conduction mechanisms possible in polyanilines: 1D variable range hopping, 3D variable range hopping, coulombic interactions between conduction electrons and Sheng's charging energy limited tunnelling model, preventing a simple $T^{-1/2}$ dependence of the conductivity to be attributed to a hopping model; with the variety of possible processes accounting for the observed temperature dependencies. Several types of charges have been identified by various research groups [70-76].

The strength of the interchain hopping (quasi-1D behaviour) [77] is characterised by the interchain diffusion or transition rate, ω_d. If an electron is successfully able to transfer from one chain to another without being deflected by an impurity, defect etc, then at low temperatures, Motts' variable range hopping model will be the dominant conduction mechanism (when kT<< h/2$\tau i\pi$). For a strict 1D-disordered system, the variable range hopping model will produce a linear graph when $\log_e \sigma$ is plotted against T^{-1} [78]. For a quasi-1D disordered system, near the metal-insulator transition where the electron wave functions are extended over several polymer chains, there is a moderately high temperature below which the quasi 1D variable range hopping conductivity is given by:

$$\sigma = \sigma_0 \exp\left[-\left(\frac{T_0}{T}\right)^{1/2}\right]$$

EQUATION 3.34

where,

$$T_0 = \frac{8\alpha}{g(E_F)K} \qquad\qquad \sigma_0 = \frac{e^2 \upsilon_{ph}}{\alpha K T A}$$

EQUATION 3.35a   EQUATION 3.35b

e is known as the electronic charge, v_{ph} is the phonon frequency, k is the Boltzmann constant, A is the average cross-sectional area of the conducting chains, g(E_F) is the Fermi density of states with a single spin, α is the rate at which a single potential energy well decreases in size in relation to the wavefunction. L is the 1D localisation length and z is the number of nearest neighbour chains.

NOTE:

The phonon frequency may also be a function of temperature, depending on the electron-phonon interactions, and may additionally increase rapidly with increasing temperature and hopping energies.

For weak interchain interactions, the probability of an electron hopping between chains is low, however, intrachain variable range hopping still occurs perpendicular to the chain and is governed by the equation:

$$\sigma_{\perp} = \frac{2\,e^2\,g(E_F)\,b^2\,v_{ph}}{A}\left(\frac{t_*}{\hbar}\right)^2\exp\left[-\left(\frac{T_0}{T}\right)^{1/2}\right]$$

EQUATION 3.36

where,

$$T_0 = \frac{8\,\alpha}{g(E_F)\,2\,K}$$

EQUATION 3.37

where b is the interchain separation, and $t_* = t_{\perp} \times \tau_i$; where $t_{\perp}$ is the interchain transfer integral and τ_l is the mean free time.

These materials are thought to consist of essentially isolated metallic chains with the electrons being transported along the chains, and interchain hopping occurring as a secondary step and less dependent on bipolaron and polaron defects. As the materials are increasingly doped, the conductivity mechanism becomes more dependent on electrons [79] and the conductivities of the orientated highly conductive polymers are highly anisotropic.

$$\sigma(\xi)\alpha\exp\left(\frac{-e\,R\,\bar{E}}{kT}\right)$$

where R represents the hopping distance, ξ is the localisation length and $\bar{E}$ is the strength of the electric field. The temperature and electric field dependence observed by Wang *et al* [80] suggest that a quasi 1D variable range hopping model may be appropriate, with the relationship between the electric field and conductivity being described by the model:

$$\sigma\,(T\,)\alpha\;\exp\left[-\left(\frac{T_0}{T}\right)^{1/2}\right]$$

which favours a quasi 1D variable range hopping model of the type:

$$T_0 = \frac{16}{k\,N(E_F)L_{//}\,L_\perp^{\,2}}$$

where,

$$\sigma\,(\xi\,)\alpha\;\exp\left(\frac{-\xi_0}{\xi}\right)$$

hence,

$$\sigma\,(F\,)\alpha\;\exp\left(\frac{e\,R\,F}{k\,T}\right)$$

the hopping distance was calculated to be ~20Å. This value is much larger than the interchain distance (3.5-5Å). The dielectric constant data gained by Wang *et al* supports the existence of the 3D metallic regions with 'giant dielectric constants', which have also been observed by Khanna *et al* in TCNQ salts [81]. The major difference between TCNQ salts and polyaniline is that polyaniline has a much larger dielectric constant (~26) at low temperatures (TTF-TCNQ, ε~6). This is unlikely to be due to the lack of order along the polymer chains.

Polyaniline in the emeraldine state may therefore be described as a heterogeneous quasi 1D disordered system, composed of areas of highly crystalline and well-aligned material – 3D 'metallic' crystalline regions and individual polymer chains which can be said to be 1D localised amorphous regions.

The DC conductivity and microwave conductivity have both been observed for polyaniline doped with camphorsulphonic acid (CSA) [81]. The microwave dielectric constant ε_{mw} at 298K was observed to increase from ~800 to ~3x10^4, and is understood to be directly related to the

crystallinity of the sample, with an increasingly ordered system giving a lower dielectric constant. A negative ε_{mw} shows that the polymer has an intrinsic metallic nature [82] and the low temperature (T<=100K) data for polyaniline in the emeraldine state shows a $\varepsilon_{mw} \propto T^2$ dependency. This was attributed to the charge carriers being confined to the metallic islands. The thermal energy present was insufficient to overcome the potential energy barriers separating the islands within a hopping model, and an interrupted metallic strand model was therefore suggested [83]. The dielectric constant of polyaniline-CSA was observed to again be negative from 298-4.2K. The Drude model at low frequency $\{\omega\tau<<1\}$ describes the dielectric constant and conductivity as:

$$\sigma \cong \left(\frac{\omega_p^{\ 2}}{4\pi} \right) \tau$$

$$\varepsilon \cong -\omega_p^2 \tau^2$$

The plasma frequency, ω_p was estimated to be ~120cm^{-1} from the equation:

$$\omega_p \approx \frac{4\pi\sigma_{mw}}{\sqrt{-\varepsilon_{mw}}}$$

and τ to be ~1.2×10^{-11}s at 298K. The scattering time may be thought of as being particularly long and may originate from phonon back-scattering rather than forward scattering, and the low plasma frequency shows that only a small fraction of the available conduction electrons are used in conduction.

3.5   MEASUREMENT OF DIELECTRIC PERMITTIVITY

A Novocontrol BDS 4000/6000 system broadband dielectric spectrometer was used to obtain both dielectric and electrical data on the samples used. The system comprised a HP 4291A and a Solatron SI 1260 impedance analyser was used for the high frequency range (10^9-10^6 Hz) and low frequency range (10^7-10^{-6} Hz) respectively over a temperature range 113-673K.

In a dielectric measurement, a voltage U with a fixed frequency $\omega/2\pi$ is applied to the sample cell. U causes a current I at the same frequency in the sample cell, also causing a phase shift between the current I and voltage U described by the phase angle ϕ. The ratio of U, I and ϕ are determined by the electromagnetic properties of the sample and the sample geometry.

Samples were prepared in the form of discs, with a 5mm disc being used for low frequency measurement and 30mm discs used for the high frequency measurements. A known quantity of material was pelletised to a pressure of 3 tonnes. The sample thickness was then measured using a digital micrometer. Samples were coated with either silver paint, or vacuum-deposited gold to a thickness of 1000Å to provide good electrical contact between the electrodes plates of the sample holder.

Polytetrafluoroethylene (PTFE) was used for comparison against sample measurements and as a performance calibrant for the apparatus. Two types of PTFE sample were used. Dielectric measurements made above 1MHz were made on pellets pressed from PTFE powder and for frequencies below 1MHz; samples were cut from a PTFE sheet.
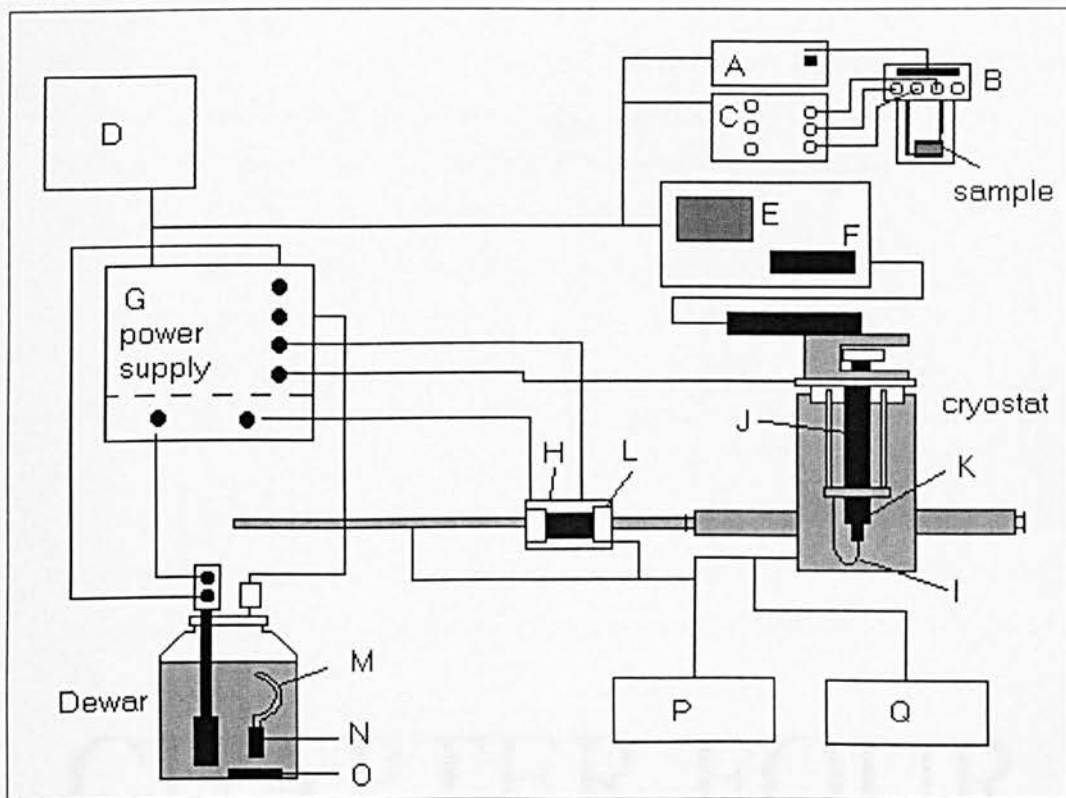
FIGURE 3.11

SCHEMATIC REPRESENATION OF THE NOVOCONTROL BDS 4000/6000 SYSTEM
BROADBAND DIELECTRIC SPECTROMETER

A=Novocontrol BDC remote interface

B= Novocontrol BDC analogue unit

C=Solartron SI 1260

D=Computer with controlling software

E=HP4291A impedance analyser

F=HP test station connector

G= Quattro temperature controller BDS 1330

H=gas heating module BDS 1310

I=PT 100 temperature sensor

J=RF extension line BDS 2200

K=RF sample cell BDS 2100

L=gas temperature sensor

M=vapourising module BDS 1320

N=Dewar temperature sensor

O=liquid nitrogen evaporator

P=vacuum pump BDS 1350

Q=vacuum gauge

CHAPTER FOUR

ELECTROMAGNETIC PROPERTIES OF CONDUCTING
POLYMERS

4.1 INTRODUCTION

Conducting polymers have a useful and variable ability to absorb the energy of electromagnetic fields passing through them. These materials have conductivities, dielectric permittivities, magnetic permeabilities and refractive indices that are complex. The imaginary component accounts for the loss in the material, where the incident radiation is dissipated in the form of heat. At frequencies of $\sim 10^9$ Hz, the losses may be accounted for by the molecular properties of the material providing loss mechanisms such as conductivity and heat dissipation.

When plane electromagnetic waves are incident on the boundary between different media, some of the energy crosses the boundary and some is reflected. The coefficients of reflection and transmission depend on the relative permittivities and permeabilities of the materials on either side of the boundary, and are expressions of the magnitude and phase of the reflected or transmitted signal.

Electromagnetic waves are sinusoidal waves that are uniform over any plane perpendicular to the direction of propagation. The directions of the electric field vector, $\bar{E}$ and the magnetic field vector, $\bar{B}$ are also perpendicular to each other and to the direction of propagation (Figure 4.1).
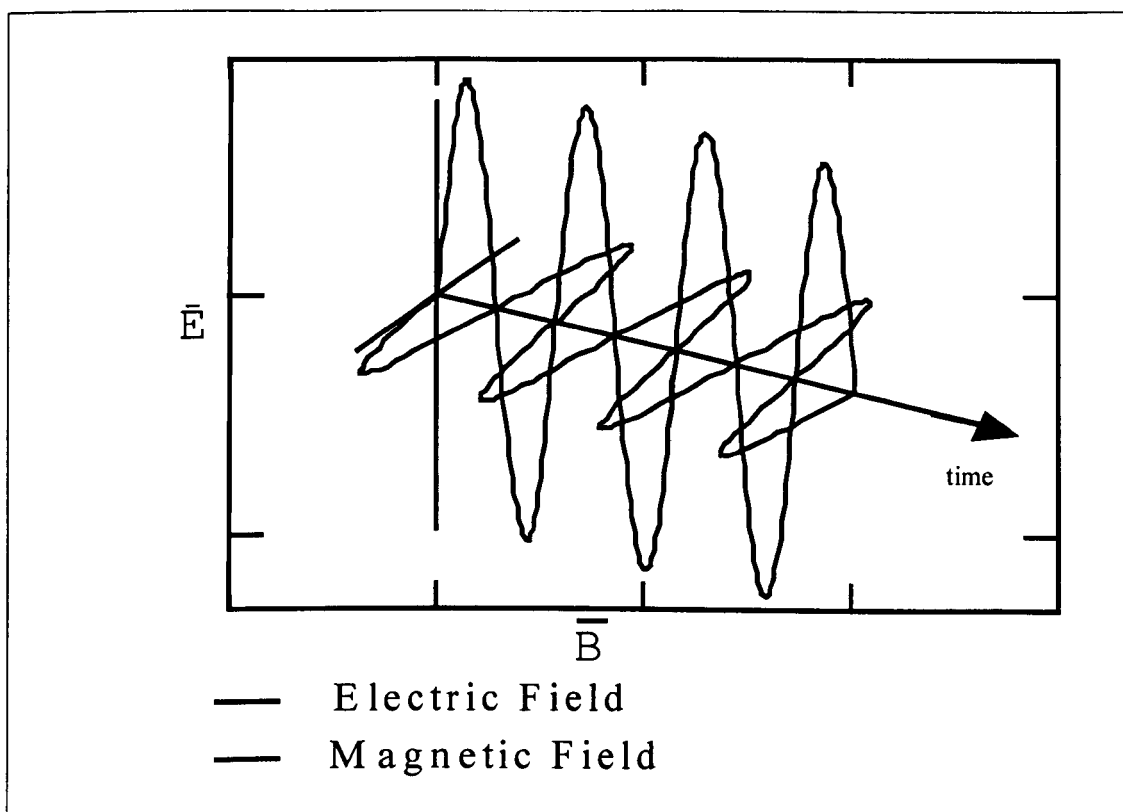
FIGURE 4.1

SCHEMATIC REPRESENTATION OF THE ELECTRIC FIELD AND MAGNETIC FIELD COMPONENTS OF THE ELECTROMAGNETIC WAVE

The dielectric and magnetic characteristics of the material will therefore determine the extent of dissipation of $\bar{E}$ and $\bar{B}$ components respectively.

4.2   REFLECTION AND TRANSMISSION OF ELECTROMAGNETIC WAVES

The solution to the properties of electromagnetic waves and the effect on the medium is governed by Maxwell's equations. These time-dependent equations allow regions of different permittivity and permeability observed at the boundary of different interfaces to be combined to give an overall picture of the $\bar{E}$ and $\bar{B}$ and fields.

Nicholson *et al* discovered that the solution for the scattering parameters are meaningless if the sample length, L is a multiple of $\lambda/2$ [84-85]. The resulting Weir algorithm used depends solely on the scattering parameters:

$$\Gamma = X \pm \sqrt{X^2 - 1}$$

EQUATION 4.1

where,

$$X = \frac{1 - V_1 V_2}{V_1 - V_2}$$

EQUATION 4.2

where,

$$V_1 = S_{21} + S_{11}$$

EQUATION 4.2

and,

$$V_2 = S_{21} - S_{11}$$

EQUATION 4.3

The coefficient of reflection may be defined as:

$$\Gamma = \frac{\dfrac{c_{vac}}{c_{exp}} \sqrt{\dfrac{\mu_r^\bullet}{\varepsilon_r^\bullet}} - 1}{\dfrac{c_{vac}}{c_{exp}} \sqrt{\dfrac{\mu_r^\bullet}{\varepsilon_r^\bullet}} + 1}$$

EQUATION 4.4

Since in most cases, the sample length is known, then the reference plane is not required for non-magnetic materials, and the scattering parameters are determined by:

$$|S_{11}| = \left| \frac{\Gamma(1-z^2)}{1-z^2 \, \Gamma^2} \right|$$

EQUATION 4.6A

$$|S_{21}| = \left| \frac{z(1-\Gamma^2)}{1-z^2 \, \Gamma^2} \right|$$

EQUATION 4.6B

Nicholson *et al* was able to relate the scattering parameters to the permittivity and permeability of the material to the scattering parameters. The transmission coefficient is determined by the condition that $|\Gamma_1| \le 1$:

$$z_1 = \frac{S_{11} + S_{21} - \Gamma_1}{1 - (S_{11} + S_{21})\Gamma_1}$$

EQUATION 4.7A

$$\frac{S_{11} S_{22}}{S_{12} S_{21}} = \frac{\left(1 - \dfrac{\varepsilon_r^*}{\mu_r^*}\right)^2}{\dfrac{4\varepsilon_r^*}{\mu_r^*}} \sinh^2 \gamma L$$

EQUATION 4.8

$$S_{21} S_{12} - S_{11} S_{22} = \exp\left[(-2\gamma_0)(L_{air} - L)\right]\frac{z^2\left[1-\Gamma^2\right]}{1-z^2 \, \Gamma^2}$$

EQUATION 4.9

and the magnetic permeability is given by:

$$\mu_r^* = \frac{1+\Gamma_1}{(1-\Gamma_1)\Lambda\sqrt{\frac{1}{\lambda_0^2}-\frac{1}{\lambda_c^2}}}$$

EQUATION 4.10

where λ_0 is the free space wavelength, and λ_c is the cut-off wavelength (which for X-band measurements is 4.5×10^{-2}m). Where Λ is a term relating to the group delay, and may be described by equation 4.11.

$$\frac{1}{\Lambda^2} = -\left[\frac{1}{2\pi L}\ln\left(\frac{1}{z_1}\right)\right]^2$$

EQUATION 4.11

The permittivity can then be described by:

$$\varepsilon_r^* = \frac{\lambda_0^2}{\mu_r^*}\left[\frac{1}{\lambda_c^2}-\left\{\frac{1}{2\pi L}\ln\left(\frac{1}{z_1}\right)\right\}^2\right]$$

EQUATION 4.12

These formulae were combined in an algorithm to calculate the magnetic permeability and dielectric permittivity from the scattering parameters.

Samples can range from two extremes: firstly a lossless medium that characterises insulators. (The electromagnetic radiation is not reflected or absorbed by the material and hence no loss occurs). The other extreme is a lossy medium where the reverse situation occurs, and the EM radiation is completely reflected. Conducting polymers may cover the area between these two regions, until a high doping level is reached and the surface is essentially metallic. At this point, nearly all of the incident radiation is expected to be reflected.

Both the $\bar{E}$ and $\bar{B}$ components are in phase and form a transverse electromagnetic (TEM) wave travelling forward long the z-axis, with a velocity ω/β. The ratio of $\bar{E}$ to $\bar{B}$ is known as the intrinsic impedance of the material under study, and is denoted by:

$$\eta = \frac{E_x^+}{H_y^+} = -\frac{E_x^-}{H_y^-} = \frac{\omega\mu}{\beta} = U\mu$$

EQUATION 4.13

where the phase constant, β is:

$$\beta = \omega\sqrt{\mu\varepsilon}\left\{\frac{1}{2}\left[\sqrt{1+\left(\frac{\sigma}{\omega\varepsilon}\right)^2}+1\right]\right\}^{1/2}$$

EQUATION 4.14

The velocity of the wave, U is $1/(\mu\varepsilon)^{1/2}$, which indicates that the velocity of the wave is completely dependent on the intrinsic properties of the material, and

$$\eta = U\mu = \frac{\mu}{\sqrt{\mu\varepsilon}} = \sqrt{\frac{\mu}{\varepsilon}}$$

EQUATION 4.15

The convention used here will be that incident waves travel in the z direction and the $\bar{E}$ and $\bar{B}$ fields noted as $\bar{E}_x^+$ and $\bar{B}_x^+$.

A reflected wave will therefore be denoted as $\bar{E}_x^-$ and $\bar{B}_x^-$ since it will be travelling in the negative direction.

4.2.1 LOSSLESS (PERFECT) DIELECTRICS $(\sigma/\omega\varepsilon')^2 \ll 1$

For a perfect dielectric, $\sigma=0$ and hence the attenuation constant, $\alpha=0$

and

$$\beta = \omega\sqrt{\mu\varepsilon}$$

also,

$$\eta = \sqrt{\frac{\mu}{\varepsilon}}$$

There is no attenuation of the electromagnetic waves and therefore of the $\bar{E}$ to $\bar{B}$ components.

The velocity,

$$U = \frac{\omega}{\beta} = \frac{1}{\sqrt{\mu\varepsilon}}$$

and

$$\lambda = \frac{2\pi}{\beta} = \frac{2\pi}{\omega\sqrt{\mu\varepsilon}}$$

4.2.2 LOSSY MATERIALS (DIELECTRICS) $(\sigma/\omega\varepsilon') \sim 1$

To calculate the intrinsic properties of the materials such as the conductivity, dielectric constant and magnetic permeability, the loss factors need to be considered, which require these parameters to be complex. The complex permittivity is:

$$\varepsilon = \varepsilon' - i\varepsilon'' = \left(\varepsilon_r'\varepsilon_0 - i\frac{\sigma}{\omega}\right)$$

EQUATION 4.16

Considering these complex quantities, the intrinsic impedance now becomes:

$$\eta = \sqrt{\frac{\mu}{\varepsilon}} = \sqrt{\frac{\mu}{\varepsilon'\left(1 - i\frac{\sigma}{\omega\varepsilon'}\right)}} = \frac{\sqrt{\mu/\varepsilon'}}{\sqrt{1 - i\frac{\sigma}{\omega\varepsilon'}}}$$

EQUATION 4.17

For a slightly lossy sample the phase constant β is approximately the same as that of a lossy material of the same permeability, therefore we can say that:

low loss $\sigma/\omega\varepsilon' < 0.1$

high loss $\sigma/\omega\varepsilon' > 10$

The $\bar{E}$ to $\bar{B}$ components are attenuated within the material slightly:

$$E = E_0\, e^{-\gamma z} a_x$$

EQUATION 4.18

$$H = \sqrt{\frac{\sigma + i\omega t}{i\omega\mu}}\, E_0\, e^{-\gamma z} a_y$$

EQUATION 4.19

Where γ is the propagation constant of the wave in the material and is defined in terms of real parts of the dielectric permittivity and magnetic permeability and the conductivity of the material:

$$\gamma = i\omega\sqrt{\mu\varepsilon'}\sqrt{1 - \frac{i\sigma}{\omega\varepsilon'}}$$

EQUATION 4.20

The propagation, attenuation and phase constant effects of a TEM wave travelling in a material may be summarised by the complex equation:

$$\gamma = \alpha + i\beta$$

EQUATION 4.21

4.2.3   HIGH LOSS MATERIALS (CONDUCTORS) $(\sigma/\omega\varepsilon')\gg 1$

A good conductor is a material in which a high degree of loss of the TEM wave energy occurs, the energy being dissipated by the conduction mechanism(s) of the material. This may be defined by $\sigma/\omega\varepsilon' > 100$. The intrinsic impedance of a conductor is therefore:

$$\eta_{cond} = \frac{\sqrt{\dfrac{\mu}{\varepsilon'}}}{\sqrt{-\dfrac{i\sigma}{\omega\varepsilon'}}}$$

EQUATION 4.22

and the propagation constant is:

$$\gamma \approx i\omega\sqrt{\mu\varepsilon'}\sqrt{-i\frac{\sigma}{\omega\varepsilon'}}$$
$$= \sqrt{\pi f \mu\sigma} + i\sqrt{\pi f \mu\sigma}$$
$$= \alpha + i\beta$$

EQUATION 4.23

As the TEM wave is more readily dispersed, a distance d is defined as the distance by which $\bar{E}$ to $\bar{B}$ are reduced by a factor of 1/e. This distance is known as the skin depth (Figure 4.2).
A summary of these equations is given in Table 4.1.
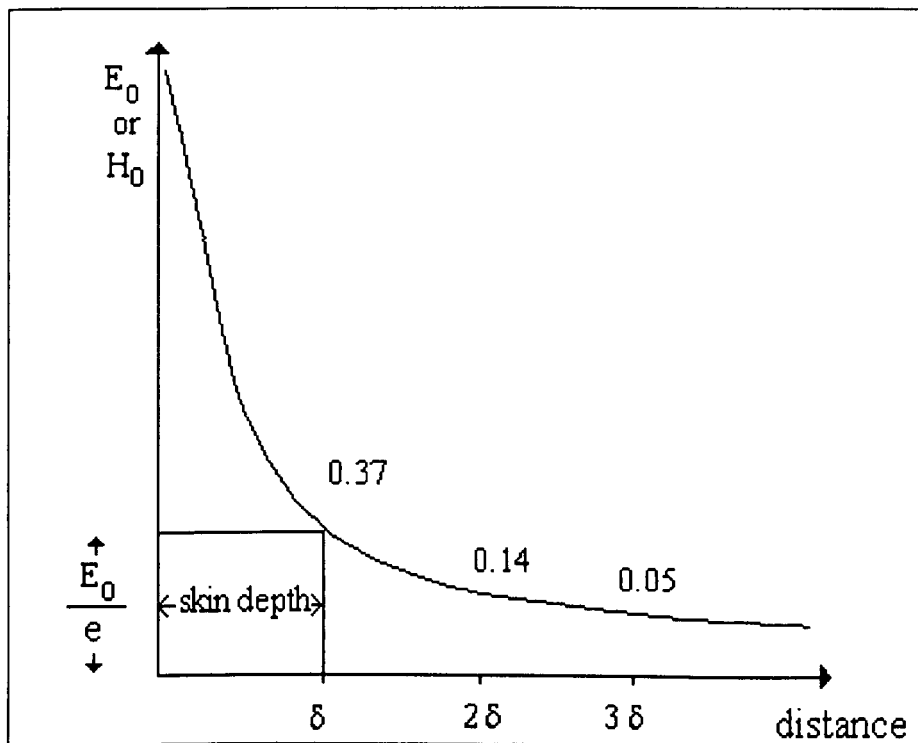
FIGURE 4.2

DIAGRAM SHOWING THE ATTENUATION OF THE ELECTRIC OR MAGNETIC FIELDS WHEN TRAVELLING INSIDE A GOOD CONDUCTOR

	Perfect Dielectric ($\sigma=0$)	Slightly Conducting Dielectric ($\sigma/\omega\varepsilon'$)<0.1	Good Conductor ($\sigma/\omega\varepsilon'$)>>1
Attenuation constant, α	$\omega\sqrt{\mu\varepsilon}\left\{\dfrac{1}{2}\left[\sqrt{1+\left(\dfrac{\sigma}{\omega\varepsilon}\right)^2}+1\right]\right\}$	$\approx\omega\sqrt{\mu\varepsilon}\left[\dfrac{1}{4}\left(\dfrac{\sigma}{\omega\varepsilon}\right)^2\right]^{1/2}=\dfrac{\sigma}{2}\sqrt{\dfrac{\mu}{\varepsilon}}$	$\approx\sqrt{\dfrac{\omega\mu\sigma}{2}}$
Phase Constant, β	$\omega\sqrt{\mu\varepsilon}\left\{\dfrac{1}{2}\left[\sqrt{1+\left(\dfrac{\sigma}{\omega\varepsilon}\right)^2}+1\right]\right\}$	$\approx\omega\sqrt{\mu\varepsilon}$	$\approx\sqrt{\dfrac{\omega\mu\sigma}{2}}$
Propagation Constant, γ	$\gamma=i\beta=i\omega\sqrt{\mu_0\,\varepsilon_0\,\mu_r\,\varepsilon_r}$	$i\omega\sqrt{\mu\varepsilon'}\left(\sqrt{1-i\dfrac{\sigma}{\omega\varepsilon'}}\right)$	$\approx\sqrt{\pi f\mu\sigma}\,(1+i)$
Intrinsic Impedance, η	$\sqrt{\dfrac{\mu}{\varepsilon}}=\sqrt{\dfrac{\mu_0\,\mu_r}{\varepsilon_0\,\varepsilon_r}}$	$\dfrac{\sqrt{\mu/\varepsilon'}}{\sqrt{1-i\sigma/\omega\varepsilon'}}$	$\sqrt{\dfrac{\omega\mu}{2\sigma}}$
Wavelength, λ	$\approx\dfrac{2\pi}{\omega\sqrt{\mu\varepsilon}}$		$2\pi\sqrt{\dfrac{2}{\omega\mu\sigma}}$
Velocity, U	$\approx\dfrac{1}{\sqrt{\mu\varepsilon}}$	$\dfrac{\omega}{\beta}=\sqrt{\dfrac{2\omega}{\mu\sigma}}$	$\dfrac{\omega}{\beta}=\sqrt{\dfrac{2\omega}{\mu\sigma}}$
Skin Depth, δ	$\approx\dfrac{2}{\sigma}\sqrt{\dfrac{\varepsilon}{\mu}}$	$\dfrac{1}{\omega\sqrt{\mu\varepsilon}\left\{\dfrac{1}{2}\left[\sqrt{1+\left(\sigma/\omega\varepsilon\right)^2}-1\right]\right\}^{1/2}}$	$\sqrt{\dfrac{2}{\omega\mu\sigma}}$

TABLE 4.1

4.3   BOUNDARY CONDITIONS

When a TEM wave reaches an interface between two different media, it is partially reflected and partially transmitted. The magnitude of the energy reflected and transmitted is dependent on the various magnetic and electric constants of the material (Figure 4.3).
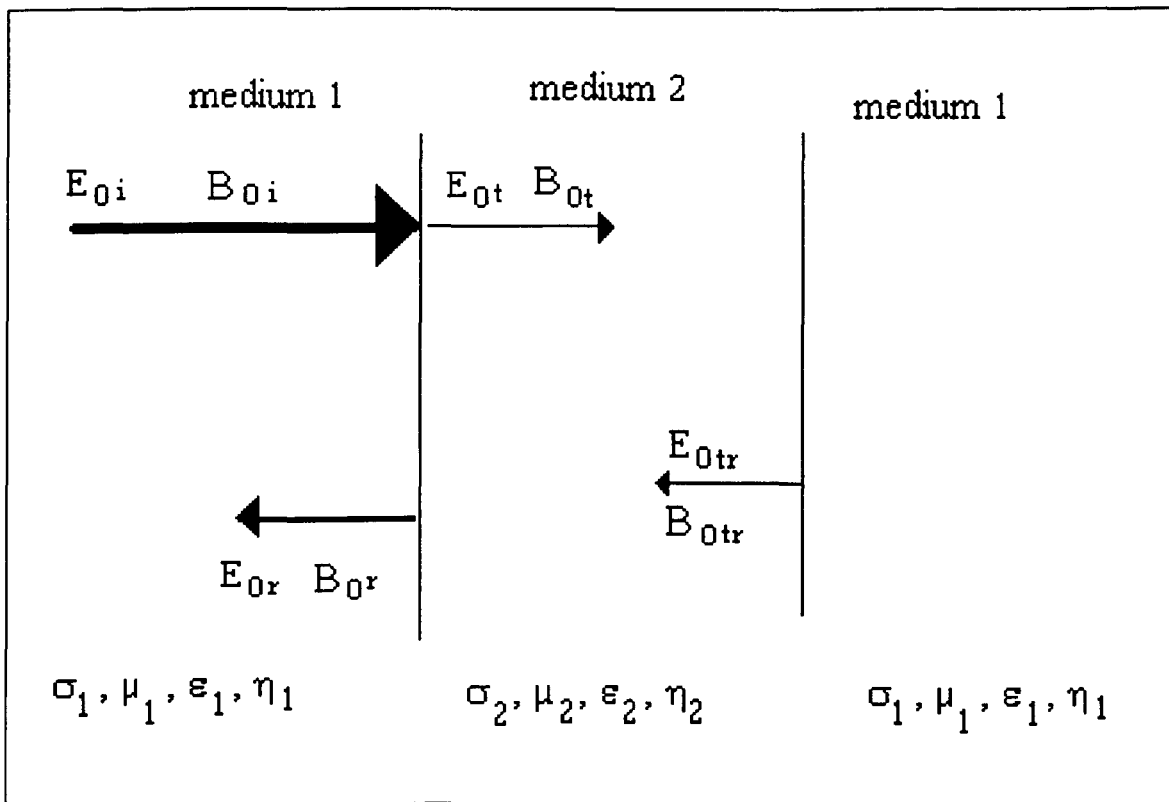
FIGURE 4.3

DIAGRAM SHOWING THE PARAMETERS THAT ARE OBSERVED WHEN A TEM WAVE TRAVELS BETWEEN DIFFERENT MEDIA

$E_{0,\,tr}$ and $B_{0,\,tr}$ will account for a very small proportion of the electric and magnetic components that are internally reflected within the material.

The transmission coefficient may then be defined in terms of the intrinsic impedance of the two media:

$$\Gamma = \frac{2\eta}{\eta_1 + \eta_2}$$

EQUATION 4.24

4.3.1   AIR-DIELECTRIC INTERFACE

Assuming that the conductivities of both dielectrics are equal to zero and that the material is non-magnetic, then we may assume that no loss will occur. If we assume that medium 1 is air and

medium 2 is a perfect dielectric in Figure 4.3, then ε_1 and ε_2 are both positive and real, as there is no loss component, and $\alpha_1=\alpha_2=0$ since the TEM wave is not attenuated.

The reflected E field component at the air-dielectric interface may change phase by π radians on reflection. The reflection coefficient may now be defined as the ratio between the incident and reflected $\bar{E}$ fields:

$$R = \frac{E_0{}^2{}_R}{E_0{}^2{}_I} = \left(\frac{1-n}{1+n}\right)^2$$

EQUATION 4.25

Similarly, the transmission coefficient is the ratio between the transmitted $\bar{E}$ field and the incident $\bar{E}$ field:

$$\Gamma = \frac{E_0{}^2{}_T \sqrt{\dfrac{\varepsilon_r\,\varepsilon_0}{\mu_r\,\mu_0}}}{E_0{}^2{}_I \sqrt{\dfrac{\varepsilon_0}{\mu_0}}}$$

EQUATION 4.26

If $\mu=0$, then

$$\Gamma = \frac{4n}{(1+n)^2}$$

The conservation of energy requires that:

$$\Gamma + R = 1$$

EQUATION 4.27

4.3.2 AIR-METAL INTERFACE

The TEM wave is almost completely reflected since no EM field can exist inside the conductor. The wave in the metal is attenuated, in which case the $\bar{E}$ is:

$$E = e_x\, E_{0T}\, \exp\{i(\omega t - \alpha z)\}\exp(-\alpha z)$$

EQUATION 4.28

and the $\bar{B}$ field is:

$$B = e_y \, B_{0T\exp} \left\{ i(\omega t - \alpha z) \right\} \exp(-\alpha z)$$

EQUATION 4.29

and

$$E_{0I} + E_{0R} = E_{0T}$$

EQUATION 4.30

also,

$$E_{0I} - E_{0R} = E_{0T} \sqrt{\frac{\sigma}{2\omega\mu\varepsilon_0}}(1-i)$$

EQUATION 4.31

$$\frac{E_{0R}}{E_{0I}} = -\frac{\sqrt{\dfrac{\sigma}{2\omega\varepsilon_0}}(1-i)-1}{\sqrt{\dfrac{\sigma}{2\omega\varepsilon_0}}(1-i)+1}$$

EQUATION 4.32

which is an expression of the amplitudes of the $\bar{E}$ field components at the boundary. If $\mu > 1$, then:

hence,

$$R = \left| \frac{E_{0R}}{E_{0I}} \right|^2$$

EQUATION 4.32

Expressed in terms of the intrinsic impedance, the transmission coefficient becomes:

$$\Gamma = \frac{2\eta_2}{\eta_1 + \eta_2} \approx \frac{2\eta_2}{\eta_1} \quad \text{if } \eta_2 << \eta_1$$

EQUATION 4.33

4.4 TRANSMISSION LINE THEORY

The relative permittivity and permeability may be defined from the scattering parameters by carrying out two sets of measurements. By using transmission line theory, a transmission line of length t, of characteristic impedance Z_2 and propagation constant k_2 is sandwiched between a pair of transmission line whose characteristic impedance and propagation constants are z_0 and k_0. This configuration is depicted in Figure 4.4.
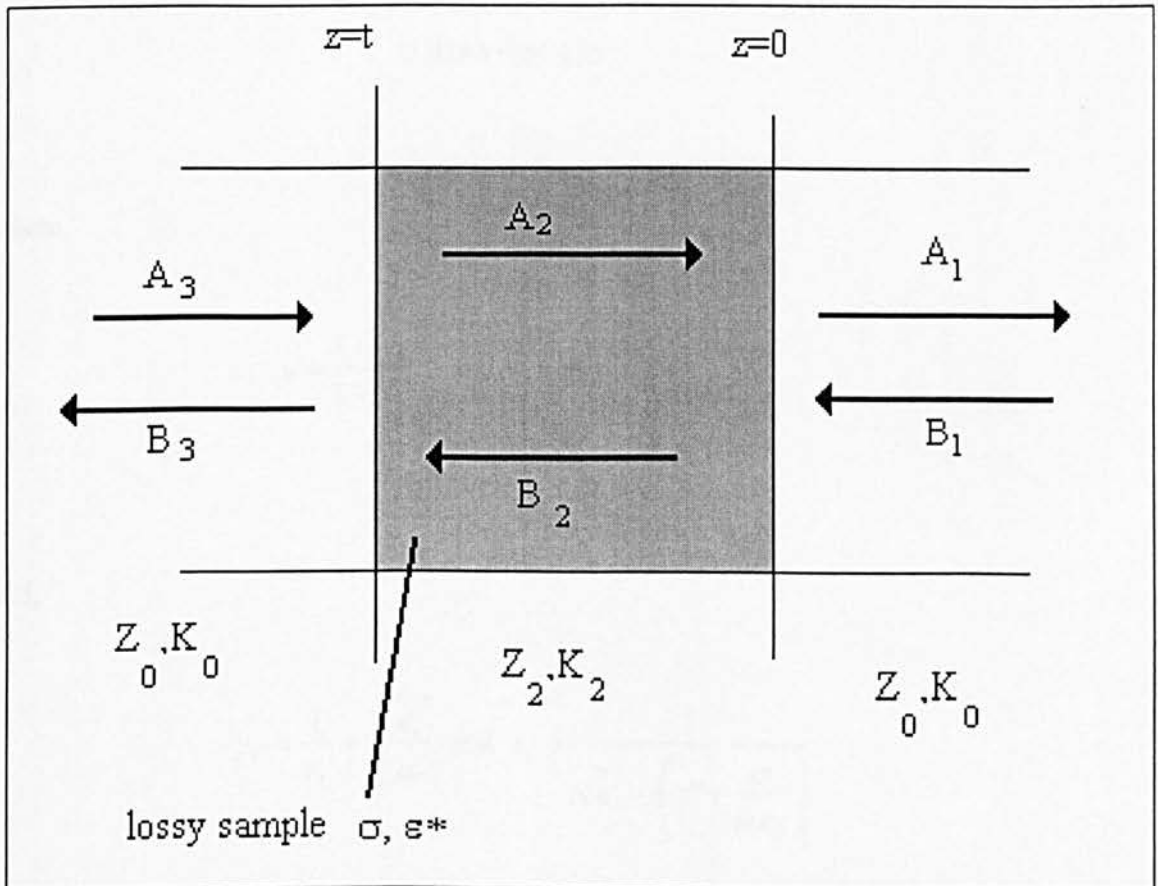
FIGURE 4.4

TEM WAVE PROPAGATION ALONG A SINGLE LINE TRANSMISSION LINE

The sample is placed in the central portion of the transmission line between z=0 and z=t, sandwiched between the input and output lines, whose characteristic impedance Z_0 and propagation constant, k_0 are also characteristic of the sample holder. Electromagnetic waves propagating toward the sample (forward) are given by A_1, A_2 and A_3; and those travelling back toward the source (reflected) B_1, B_2 and B_3 – all of which may be complex. A comparison of the measured data with and without a sample present allows an expression of the two scattering parameters:

$$S_{11} = \frac{u\left(1 - w^2\right)}{u^2 - w^2}$$

EQUATION 4.34

$$S_{21} = \frac{w\left(u^2 - 1\right)}{u^2 - w^2}$$

EQUATION 4.35

where,

$$u = \frac{1 - y_r}{1 + y_r} \quad \text{and w} = \exp\left(i k_2 t\right)$$

EQUATION 4.36

and,

$$y_r = \frac{1}{z_r} = \sqrt{\frac{\varepsilon_r}{\mu_r}} \quad \text{and } z_r = \frac{1}{\sqrt{\varepsilon'} - i\left(\varepsilon'' + \dfrac{\sigma}{\omega \varepsilon_0}\right)}$$

EQUATION 4.37

Since, S_{11} and S_{21} are known, then:

$$w^2 = \frac{u(1 - u S_{11})}{u - S_{11}}$$

$$u^2 + 2uQ + 1 = 0$$

EQUATION 4.38

where,

$$Q = \frac{[(S_{21})^2 - (S_{11})^2 - 1]}{2 S_{11}}$$

EQUATION 4.39

Now,

$$u = -Q \pm (Q^2 - 1)^{1/2}$$

EQUATION 4.40

and

$$U = \frac{u - 1}{u + 1}$$

$$\text{since} \quad U = \sqrt{\frac{\varepsilon_r}{\mu_r}}$$

$$\text{then} \quad W = \frac{u(1 - u S_{11})}{u - S_{11}}$$

$$\therefore \quad \sqrt{\mu_r \, \varepsilon_r} = \frac{\ln W}{i 2 k_0 t}$$

hence,

$$\varepsilon_r = \frac{U \ln W}{i 2 k_0 t}$$

$$\text{and,} \quad \mu_r = \frac{\ln W}{i 2 k_0 t W}$$

EQUATION 4.41

This also relates the fundamental properties of the TEM wave, α, β and γ:

Since,

$$\gamma = \alpha + i\beta = \beta_0 \left\{ -\varepsilon' + i\left(\varepsilon'' + \frac{\sigma}{\omega \varepsilon_0} \right) \right\}^{1/2}$$

EQUATION 4.42

$$\therefore \qquad \Gamma_0 = \frac{z-1}{z+1} = \frac{1 - \sqrt{\varepsilon' - i\left(\varepsilon'' + \dfrac{\sigma}{\omega \varepsilon_0} \right)}}{1 + \sqrt{\varepsilon' - i\left(\varepsilon'' + \dfrac{\sigma}{\omega \varepsilon_0} \right)}}$$

EQUATION 4.43

4.5 CONDUCTING POLYMERS

Conducting polymers are unusual electromagnetic materials. They are able to combine the characteristics of metals or insulators with the mechanical properties of plastics.

An analysis of the frequency dependent electrical properties of conducting polymers has led to two methods of study [86], where only the dielectric or conductivity presentation is used. These factors cannot be completely separated and analysed individually, since they are inextricably linked.

This research presents the reflection and transmission coefficients for polyalkythiophenes compared to the metal-complexed P3MT samples.

4.6 MEASUREMENT OF SCATTERING PARAMETERS

Measurements were made using a Hewlett Packard HP8510C Vector Network Analyser using an APC7 coaxial cell and WG16 waveguide transmission lines over the frequency range of 0.5 to 18GHz at intervals of 0.1GHz (Figure 4.5). A schematic representation of the network analyser is shown in Figure 4.6 Samples were sandwiched between two waveguide to coaxial transducers connected to the. Network Analyser calibrated in transmission mode to obtain reflection and transmission coefficients based on the scattering parameters. Several sample-holding techniques were used. Polymer films were either grown galvanostatically or solvent cast onto glass slides. It was found that the latter technique was preferable since this gave stronger films.

4.6.1   FREE STANDING FILMS

The properties of the polycarbonate blocks could be eliminated by the use of free-standing films placed between two waveguide to coaxial transducers. The polymer film was placed in a resonant window situated midway along rectangular cavity (Figure 4.7)
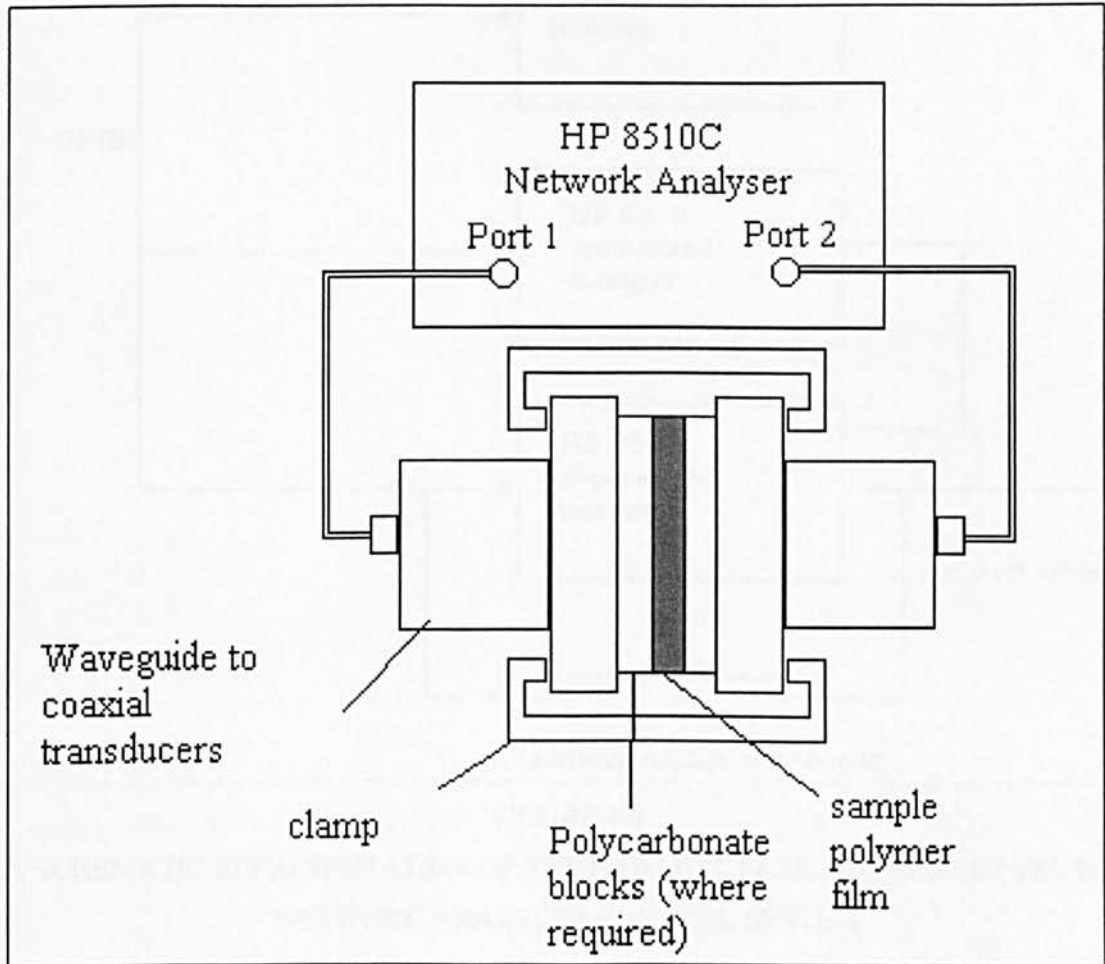
FIGURE 4.5

SCHEMATIC REPRESENTATION OF THE HEWLETT PACKARD HP8510C VECTOR NETWORK ANALYSER MEASUREMENT APPARATUS

In all cases, the sample was larger than the resonant window to avoid losses at the edges, and the instrument was calibrated in the transmission mode within the frequency range to be used.
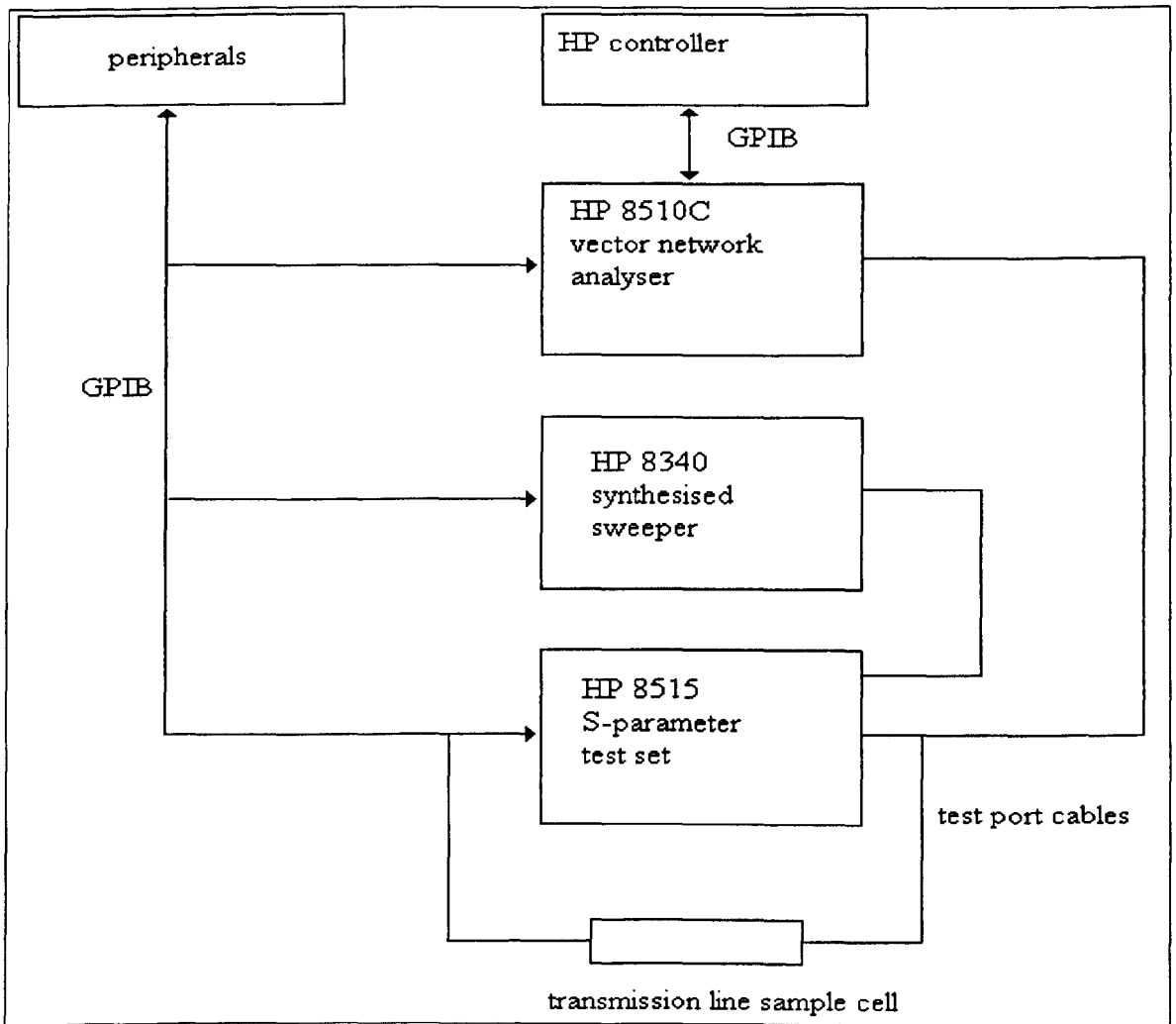
FIGURE 4.6

A SCHEMATIC REPRESENTATION OF THE HEWLETT PACKARD HP8510C VECTOR
NETWORK ANALYSER CONTROL SYSTEM
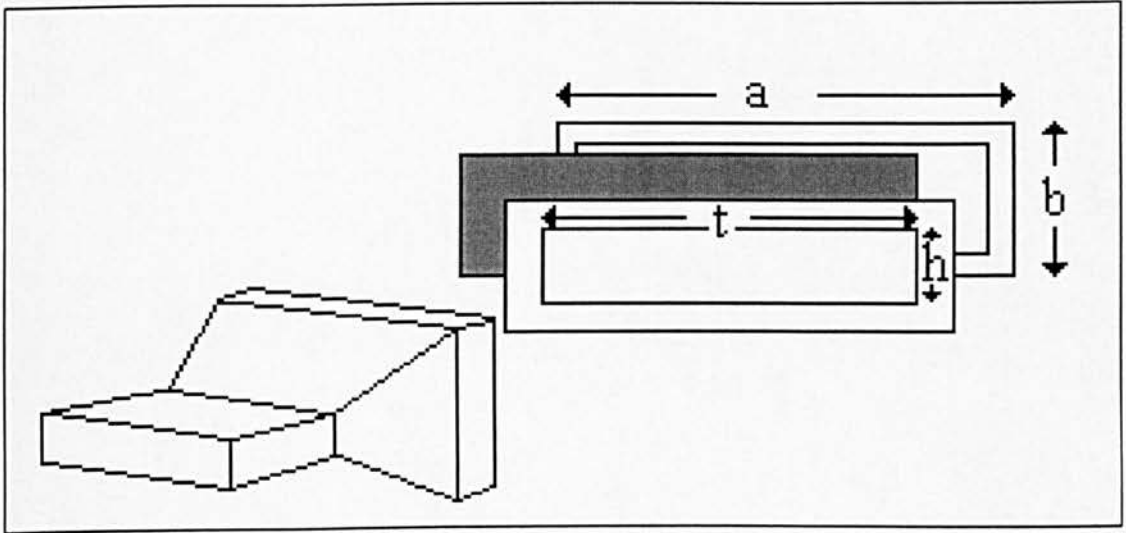
FIGURE 4.7

MEASUREMENT OF THE SCATTERING PARAMETERS USING THE RESONANT
WINDOW TECHNIQUE

CHAPTER FIVE

POLYMER PREPARATION AND ANALYSIS

5.1   INTRODUCTION

Polymer films were synthesised using both electrochemical methods and a more traditional oxidation of the monomer. The chemical synthesis involved the use of Grignard coupling of bromoalkanes and 3-bromothiophene to form the bromoalkylthiophene monomer. This was then chemically polymerised using an $FeCl_3$ solution.

5.1.1   ELECTROCHEMICAL POLYMERISATION

5.1.1.1   PREPARATION OF POLYPYRROLE AND POLY(3-METHYLTHIOPHENE)

A dry propylene carbonate solution of tetraethylammonium tetrafluoroborate (0.1 mol dm^{-3}) (TEATFB) was prepared and degassed using dry nitrogen gas. After degassing, the monomer ($1cm^3$ of either pyrrole (99%, Aldrich), or thiophene (99% Aldrich)) was added to the electrolyte solution (25 cm^3). Tetramethylammonium perchlorate (TMAP) and tetrabutylammonium tetraphenylborate (TBATPB) electrolyte solutions were made up to concentrations of 0.5 mol dm^{-3}, and 0.1mol dm^{-3} respectively, and degassed in a similar manner. The concentration and type of the electrolytes, and the electropolymerisation time were varied to determine their effect on the resulting film properties.

Electropolymerisation was carried out onto a low resistance indium-tin oxide (ITO) coated glass (Balzers), which was used as the working electrode. A saturated calomel electrode (SCE) was the reference electrode and stainless steel used as the counter electrode. A current density of approximately 30 mA cm^{-2} was used to initiate the growth of the polymer film was later reduced to ~5 mA cm^{-2}.

5.1.1.2   POLYANILINE

Hydrochloric acid was used as the electrolyte solution for the synthesis of polyaniline. Aniline (3ml, >99% BDH) was dissolved in HCl (97ml of 1.049mol dm^{-3}) to give a 3% polymerisation solution. The circuit shown in Figure 2.3 was used for the electrodeposition process and was adjusted to supply a current density of ~5mA cm^{-2} from a potentiostat operating in galvanostatic mode. The polymerisation reaction was consequently slow, producing patchy, uneven films. The electropolymerisation occurred more evenly over the ITO glass substrate when using a greater current density of up to 40mA cm^{-2}, producing smooth uniform films. The polymer films were grown to thicknesses between $1x10^2$ and $4x10^4$nm, with the thickness of the thicker films being measured directly using a micrometer, and the thinner films being determined by a Faraday's law calculation based on the charge passed, the molecular weight of the monomer used and the current density.

5.2   CHEMICAL SYNTHESIS OF MONOMERS AND POLYMERS
5.2.1   SYNTHESIS OF 3-DODECYLTHIOPHENE

To a suspension of magnesium (1.92g, 0.08moles) in anhydrous ether (50ml) was added dropwise 1-bromododecane (16.56g, 0.08moles) in ether. After complete disappearance of the magnesium, 3-bromothiophene (13.04g, 0.08moles) and nickel (II) 1,3-bis(diphenylphosphinopropane) chloride Ni(DPPP)Cl$_2$ (0.0048g, 1x10^{-3}moles) was added. The reaction was slightly exothermic and a brown coloration was observed. After refluxing for 18 hours, the reaction mixture was poured onto a mixture of crushed ice and HCl (2M), which was subsequently extracted with ether (3x50cm^3). The combined extracts were dried (anhydrous MgSO$_4$) and the solvent removed. The residue was then purified by vacuum distillation (2mmHg, 68°C) to give 3-dodecylthiophene (12g, 71% yield) by GCMS.

Spectroscopic identification of the monomer was carried out using ^{1}H NMR spectroscopy, ^{13}C spectroscopy and FTIR analysis. The ^{1}H and ^{13}C NMR spectra were obtained by dissolving ~1 drop if the monomer solution in ~0.5ml of deuterated chloroform. The analysis was carried out at 300MHz for ^{1}H NMR and 75.6MHz for the ^{13}C NMR. The spectra were measured in order to confirm the structural identity of the monomer and can be seen in Appendix I, Figures A1-A2.

The absorption spectra of the monomer was measured on a Perkin Elmer 1710 FTIR spectrometer between 400 and 4000 wavenumbers from a neat solution of the monomer. The FTIR spectrum can be seen in Appendix I, Figure A3.

5.2.2   SYNTHESIS OF 3-HEXYLTHIOPHENE

Magnesium turnings (1.92g) were added to a solution of 1-bromohexane (3.25g) in dry ether (200ml) to form the Grignard reagent. When the initial vigorous reaction had subsided, 1-bromohexane (3.91g) diluted with approximately the same volume of ether was added, to reinitiate it. When the diluted reagents were consumed, 3-bromothiophene (13.04g) and 1,3-bis(diphenylphosphinopropane) nickel (II) chloride (a few crystals) was added and the reagents refluxed for 24 hours.

The products were poured onto a mixture of dilute HCl (2M) and crushed ice (~200g) and then extracted by ether. The organic layer was dried with the minimum of anhydrous magnesium sulphate, and any residual ether was removed under rotary evaporation at room temperature. This method of extraction was repeated to yield 10.2g of product as determined by GCMS.

The 1H, 13C and FTIR spectra were measured in an identical manner to that detailed in section 5.2.1. The spectra can be seen in Appendix I, Figures A4-A6 respectively.

5.2.3 POLYMERISATION OF 3-DODECYLTHIOPHENE

Polymerisation of the alkylthiophene was carried out by adding the 3-dodecylthiophene (0.5g, 0.002moles) to anhydrous ferric chloride (9g, 0.056moles) in chloroform (50cm^3). The solution was initially purged with nitrogen, and stirred rapidly at 30°C for 4 hours to remove any residual solvents. As the reaction progressed, HCl gas was evolved. The mixture was filtered under vacuum and the filtrate was poured dropwise into a beaker of rapidly stirred methanol (200cm^3) to remove the excess ferric chloride, and to precipitate the polymer and dissolve the residual iron salts. The solid was then dried under vacuum at 40°C for 4 hours. The polymer was further purified by soxhlet extraction with refluxing methanol for 24 hours to remove any strongly attached ferric chloride. The solid residue was then dried under vacuum at 40°C for 4 hours and dissolved in hot chloroform using soxhlet extraction. When it was observed that no more oligomers were being extracted from the solid residue, the solution was allowed to cool to room temperature, the excess CHCl$_3$ being removed by rotary evaporation.

5.2.4 POLYMERISATION OF 3-HEXYLTHIOPHENE

The method used for the polymerisation of the 3-hexylthiophene monomer was identical in essence to that of the 3-dodecylthiophene monomer.

5.2.5 COMPLEXATION OF FERROMAGNETIC IONS INTO THE POLYMER CHAIN

Stoichiometric amounts of monomer, oxidant and transition metal compound were used to complex the metal ions into the polymer chain.

5.2.5.1 COMPLEXATION OF Fe INTO THE POLYMER CHAIN

0.1M of 3-methylthiophene monomer was added to a stirred solution of 0.25M FeCl$_3$ in CHCl$_3$ (50cm^3), and then the polymerisation was continued as described in section 5.2.3.

5.2.5.2 COMPLEXATION OF Ni INTO THE POLYMER CHAIN

Nickel (II) chloride (0.1moles) was added to a stirred solution of FeCl$_3$ (0.056moles) in CHCl$_3$ (50cm^3). The 3-methylthiophene monomer (0.5moles) was then added and the polymerisation continued as described in section 5.2.3.

5.2.5.3 COMPLEXATION OF Co INTO THE POLYMER CHAIN

Cobalt (II) chloride (0.1moles) was added to a stirred solution of FeCl$_3$ (0.056moles) in CHCl$_3$ (50cm^3). The 3-methylthiophene monomer (0.5moles) was then added and the polymerisation continued as described in section 5.2.3.

5.3   MEASUREMENT OF POLYMER ELECTROCHROMIC ACTIVITY

For the measurement of the rate of the electrochromic change, tetraethylammonium tetrafluoroborate (0.405g, 0.1M) was completely dissolved in monomer-free propylene carbonate and employed as the electrolyte solution. The counter electrode was placed along the edge of the glass cell away from the path of the beam (780nm, AlGaInP source) as was the reference electrode. The working electrode with polymer film was placed in the beam path (figure 2.4). The electrolyte solutions were made to the same concentration using the TMAP and TMATPB ionic salts.

5.4   ELECTROCHROMIC DEVICES

5.4.1   POLYPYRROLE-BASED ELECTROCHROMIC DEVICES

The polyethylene oxide (Aldrich, M_w=100,000) electrolyte matrix was used in a concentration of $3.8gdm^{-3}$, using an alkylammonium ion: network oxygen ratio of 1:8 as recommended for Li^+[87]. The electrolyte was prepared using $1.15x10^{-3}$ moles of TPC and 2.52g of PEO in approximately 10ml of acetonitrile, giving a ratio of 1:45 for Me_4N:O respectively. The ratio for Et_4N:O and Bu_4N:O were 1:34 and 1:38 respectively. Ion salts of this type were used to investigate the effect of the ionic volume of the cation on the electrochromic switching times. All solutions were degassed with dry nitrogen for 10 minutes.

5.5   UV-VISIBLE SPECTROPHOTOMETRY

The variation in the absorption of UV-visible radiation with the applied potential of the conducting polymer electrochromic devices was carried out on a KONTRON UVIKON 860 spectrophotometer. Spectra were measured in the 300-900nm range versus an optical reference sample consisting of an electrochromic device of the construction mentioned above but without the conducting polymer. The traces were recorded 'in-situ' in the double-beam spectrophotometer, with one beam being used for the sample beam and the dummy device used in the reference beam. The electrochromic device was controlled by a potentiostat (Thompson Ministat), and were held under constant potential until absorbances became steady. Spectra were run at intervals of 0.1V up to potentials of ±3 volts.

5.6 INDUCTIVELY COUPLED PLASMA ATOMIC EMISSION SPECTROSCOPY (ICP-AES)

Elemental analyses of the polymers were performed on a Jobin Yvon ICP Spectrometer, JY70 PLUS. The ICP conditions were a plasma power of 1KW, at a frequency of 40.68MHz. The plasma gas flow rate was $14l\ min^{-1}$ and a coating gas rate of $0.35l\ min^{-1}$. The sample uptake was $1ml\ min^{-1}$.

All glassware was thoroughly washed with concentrated HNO_3 (GLR grade). Samples were weighed into PTFE beakers and perchloric acid (neat, GLR grade, 5ml) was used to completely dissolve the sample. Identical procedures were carried out for the two standards, but without the addition of samples. The sample was pipetted into a 50ml volumetric flask and 'made-up-to-the-mark' with 2M HCl that was previously prepared using de-ionised water.

5.7 VACUUM DEPOSITION OF METALS AND SEMICONDUCTORS

Substrate materials were cleaned with IMS prior to evaporation, and then clamped within the vacuum chamber approximately 20cm away from the evaporation source. A few grains of metal or semiconductor (>99.999%, Balzers, 0.2-0.7mm pellets) were placed in a clean molybdenum boat supplied with a heating current by the stainless steel lead-through electrodes. The vacuum chamber was evacuated to a pressure of $\sim 10^{-5}$Pa. The quartz crystal-based thickness monitor was then started and a 60A current was applied to evaporate the metal or semiconductor. The evaporation was discontinued when the desired thickness of metal or semiconductor was obtained and the vacuum released. Samples were stored in sample vials under dry nitrogen until required.

5.8 DOPING OF POLYALKYLTHIOPHENE FILMS

Etched Fibre Reinforced Plastic (FRP) substrates of dimensions 0.8cm x 2.0cm x 2.2cm were used as supplied by DERA for testing. These substrates were weighed prior to coating using a five-figure balance and then coated several times with a concentrated (~2%) polymer solution. The substrates were then reweighed after thorough drying for 48 hours at 25°C in a fume cupboard. For each dopant concentration, the calculated mass of nitronium tetrafluoroborate was completely dissolved in methylated spirits (IMS) in a 15ml sample vial. The substrates were then placed in the solution and left for 36 hours. Upon removal from the solutions, the doped polymer films were quickly washed with IMS to remove any surface contaminants and then sealed in fresh sample vials under dry nitrogen.

The doping level was calculated by:

$$doping\ level = \frac{[dopant]}{[monomer]} \times 100$$

CHAPTER SIX

RESULTS AND DISCUSSION FOR ELECTROCHROMIC
PROPERTIES OF CONDUCTING POLYMERS

6.1   INTRODUCTION

This chapter discusses and examines the results from the investigation of the properties of the individual components involved in the construction of a portable electrochromic device. Polymer films were electrochemically prepared. The data was repeated when time permitted, and 5% error bars are depicted on the appropriate figures.

6.2   DC ELECTRICAL CONDUCTIVITY

Polymer films were grown to thicknesses of between 2000-4500nm using electropolymerisation. Table 6.1 shows a summary of the three types of conducting polymer made, the dopant ions used and their electrical conductivity. The polymers used were polypyrrole (PPY), poly(3-methylthiophene) (P3MT) and polyaniline (PANI) with ionic salts tetraethylammonium tetrafluoroborate (TEATFB), tetramethylammonium perchlorate (TMAP) and tetrabutylammonium tetraphenylborate (TBATPB). No data were produced for poly(3-methyl thiophene).tetraethylammonium tetraphenylborate (P3MT.TEATPB) due to the film being very brittle and incoherent.

Earlier studies [88-89] have quoted electrical conductivities of the order of $5\text{-}10\text{Scm}^{-1}$ for relatively smooth uniform films of polyaniline.

Polymer System	Film Thickness (nm)	Electrical Conductivity of doped state (as-synthesised) $\sigma(\text{S cm}^{-1})$
PPY.TEATFB	1970	$2.8\text{x}10^{3}$
PPY.TMAP	3320	17.5
PPY.TBATPB	3150	604.5
P3MT.TEATFB	4770	20.7
P3MT.TMAP	2240	236.6
PANI.HCl	3560	50.0

TABLE 6.1

ELECTRICAL CONDUCTIVITY OF CONDUCTING POLYMER FILMS

6.3   POLYMER ELECTROCHROMISM

Electrochromism was observed as the material was doped and undoped, and the rate of electrochromic switching analysed as a function of film thickness and dopant ion size. This

was repeated for each polymer and each dopant salt with the exception of polyaniline which was only doped with HCl.

6.3.1   POLYPYRROLE POLYMER FILMS

6.3.1.1   POLYPYRROLE AND TETRAFLUOROBORATE POLYMER FILM

Polypyrrole films doped with fluoroborate ions were electropolymerised to the thicknesses shown in table 6.2 below.

Film Thickness	Switching Time (s)	
(nm)	undoping	doping
130	2.50	0.75
150	3.25	1.43
190	3.45	1.64
280	3.63	1.85
290	3.88	1.61
360	4.00	2.43

TABLE 6.2

SWITCHING TIMES FOR POLYPYRROLE FILMS DOPED WITH FLUOROBORATE ANIONS

It should be noted that when the films were thickest, the switching time was slow in comparison to thinner films. The colour change is from a blue-black doped state to a yellow undoped state. Figure 6.1 compares the film thickness with the switching times.
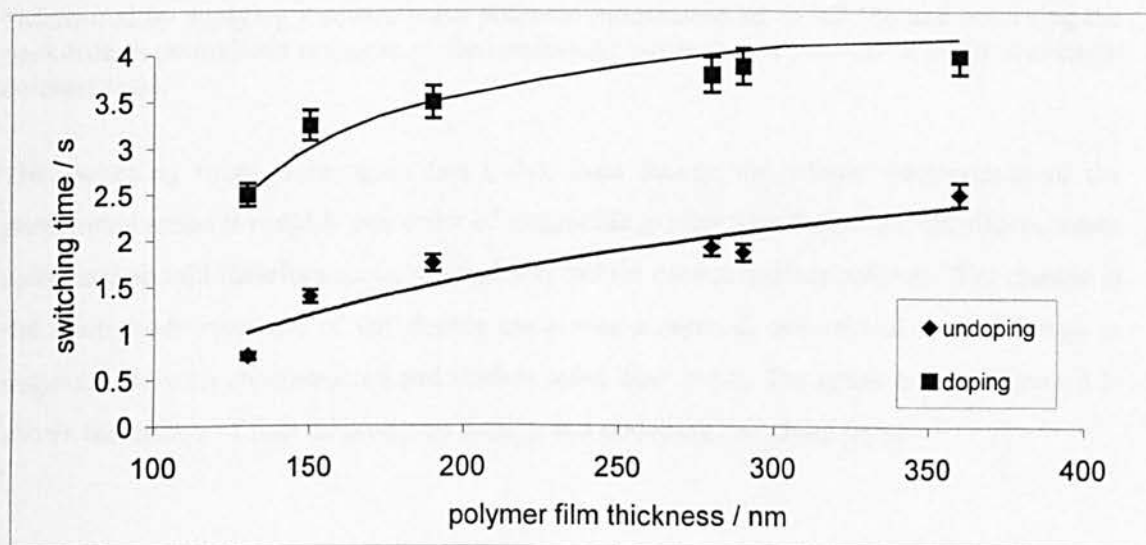
FIGURE 6.1

GRAPH DEPICTING THE RELATIONSHIP BETWEEN FILM THICKNESS AND SWITCHING TIMES FOR DOPING AND UNDOPING FILMS OF POLYPYRROLE WITH FLUOROBORATE ANIONS

The fluoroborate anion has the smallest ionic volume, is therefore expected to have the highest charge density, and will therefore move with greater velocity through a solution. Consequently, polymers doped with this cation can be expected to have the faster switching times.

6.3.1.2 POLYPYRROLE AND TETRAMETHYLAMMONIUM PERCHLORATE POLYMER FILMS

Polypyrrole films doped with perchlorate ions were grown to thicknesses within a range of approximately 100 to 1000nm and the observed doping and undoping switching times $\tau_{0.5}$ are shown in table 6.3 below.

Film Thickness (nm)	Switching of multiple cycles as a %age of total transmission*	Switching Time (s)	
		Undoping	Doping
98	-	1.00	2.00
225	9.29	1.25	2.75
476	10.00	2.38	4.00
732	10.81	2.50	4.63
965	35.75	3.75	4.75

TABLE 6.3

SWITCHING TIMES FOR POLYPYRROLE FILMS DOPED WITH PERCHLORATE ANIONS

*Measured by applying a square-wave potential programme set to 0.2 Hz, and observing the peak-trough photodiode response of the conducting polymer as a percentage of the maximum contrast ratio.

The switching times were again fast (<5s), even though the volume requirement of the perchlorate anion is roughly one order of magnitude greater than that of the tetrafluoroborate anion and should therefore move more slowly within the conducting polymer. The change in the photodiode response of the doping cycle was measured, and related to the change in response between an obstructed and unobstructed laser beam. The graph below (Figure 6.2) shows the effects of film thickness on doping and undoping switching times.
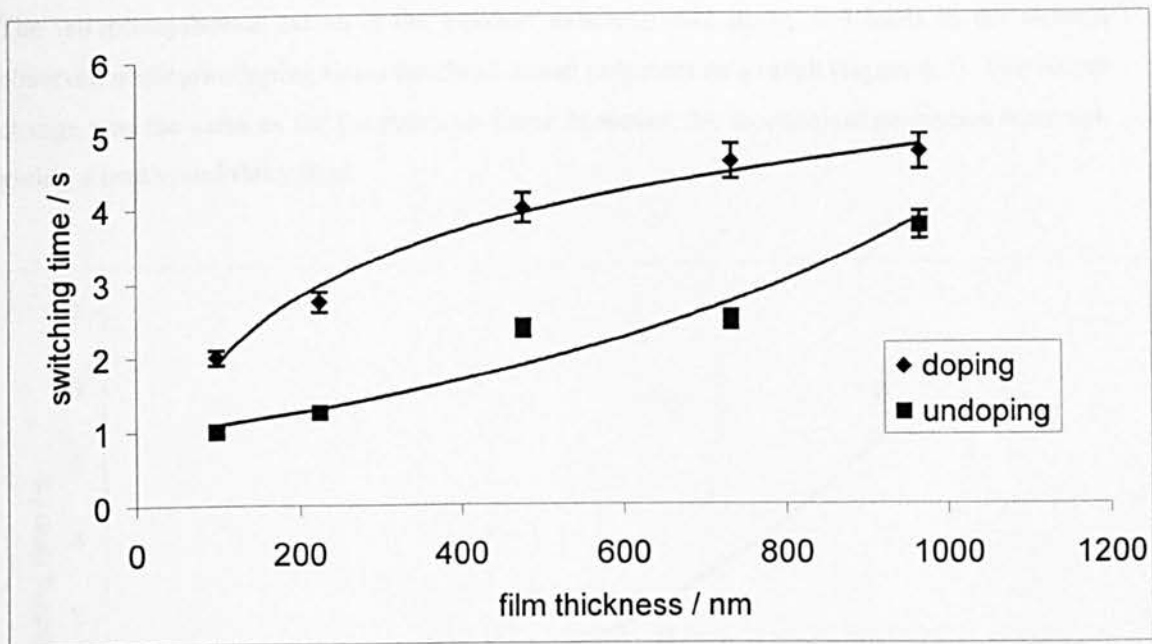
FIGURE 6.2

GRAPH DEPICTING THE RELATIONSHIP BETWEEN FILM THICKNESS AND
SWITCHING TIMES FOR DOPING AND UNDOPING FILMS OF POLYPYRROLE
WITH PERCHLORATE ANIONS

6.3.1.3 POLYPYRROLE TETRABUTYLAMMONIUMTETRAPHENYLBORATE FILMS

Polypyrrole films doped with the tetraphenylborate anion were grown to thicknesses of between 50 and 400nm. The corresponding switching times are shown in table 6.4 below.

Film Thickness	Switching of multiple cycles	Switching Time (s)	
(nm)	as a % of total transmission	undoping	doping
52	2.21	1.07	0.88
88	2.50	1.15	0.95
183	3.43	2.00	1.00
286	6.02	2.59	1.13
398	8.84	5.88	2.25

TABLE 6.4

SWITCHING TIMES FOR POLYPYRROLE FILMS DOPED WITH
TETRAPHENYLBORATE ANIONS

The tetraphenylborate cation is the bulkiest cation in this study, and leads to the slowest observed doping/undoping times for these doped polymers as a result (figure 6.3). The colour change was the same as for the previous films; however, the mechanical properties were not, giving a brittle and flaky film.
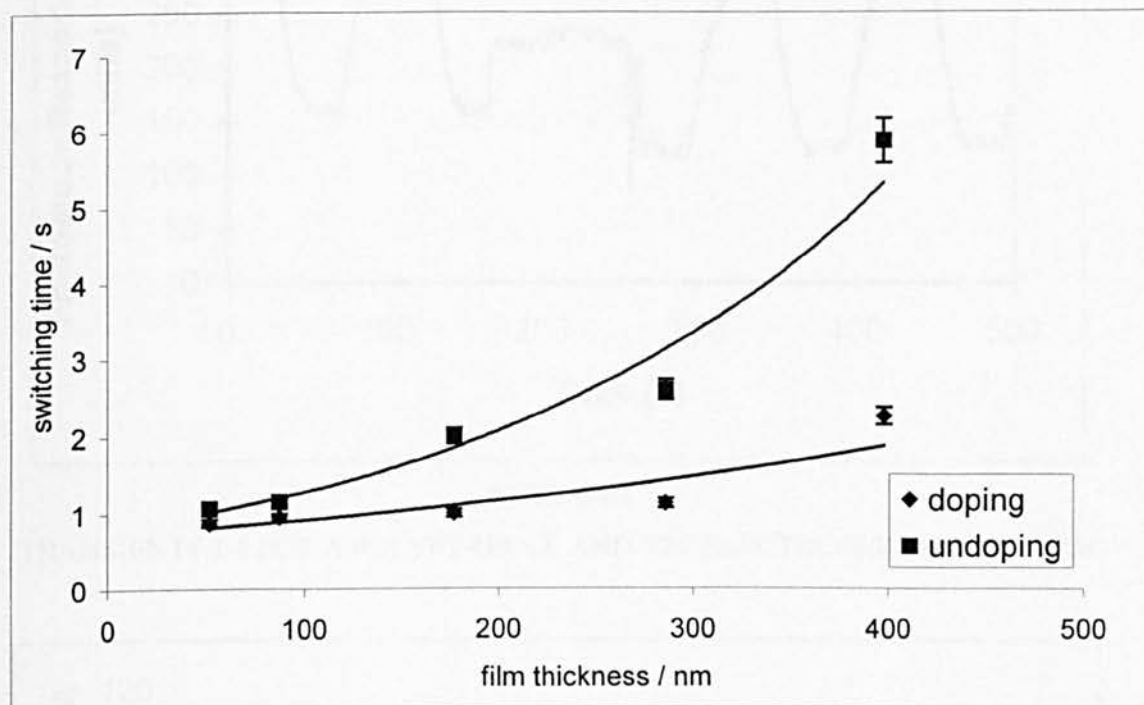
FIGURE 6.3

GRAPH DEPICTING THE RELATIONSHIP BETWEEN FILM THICKNESS AND
SWITCHING TIMES FOR DOPING AND UNDOPING FILMS OF POLYPYRROLE
WITH TETRAPHENYLBORATE ANIONS

6.3.1.4   POLYPYRROLE ELECTROCHROMIC DEVICE LONGEVITY STUDY

The films were switched between potentials of +1V and -1V. After approximately 5000 cycles, significant changes were observed in the transmitted light transient for these films indicating some polymer degradation. Figures 6.4 and 6.5 show the transmitted light transients for the respective films for transients 1-4 and transients 4996-5000 indicating the decrease in contrast between the doped and undoped states. The use of thinner films allows rapid switching but gives poorer contrast.
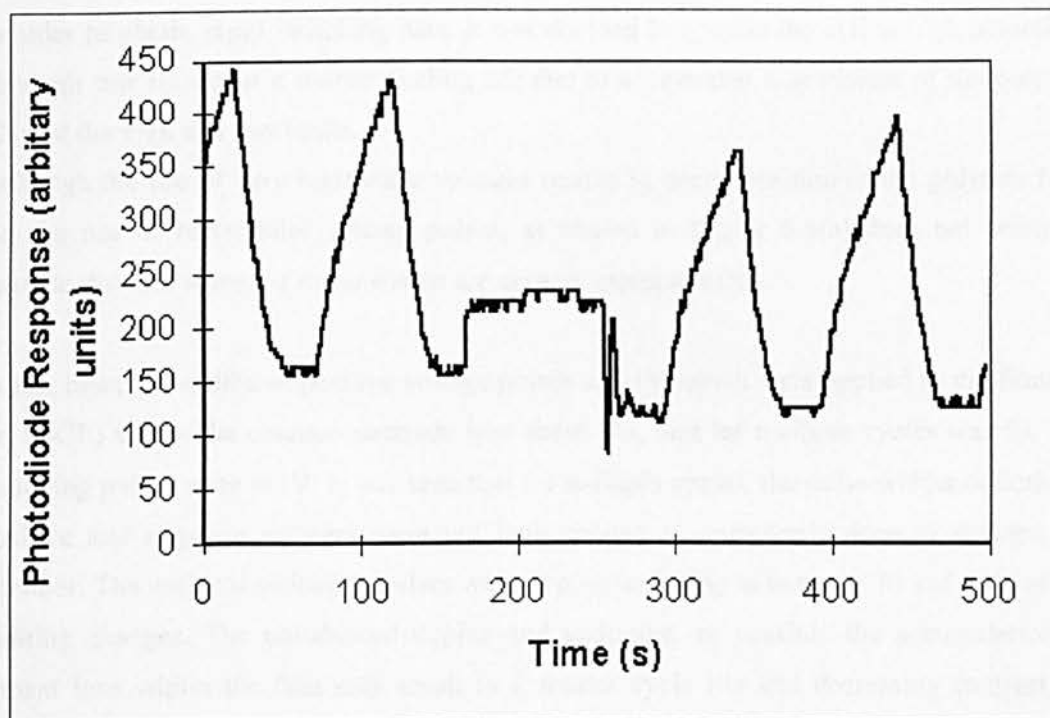
FIGURE 6.4

TRANSIENTS 1-4 FOR A POLYPYRROLE AND TPC ELECTROCHROMIC SYSTEM
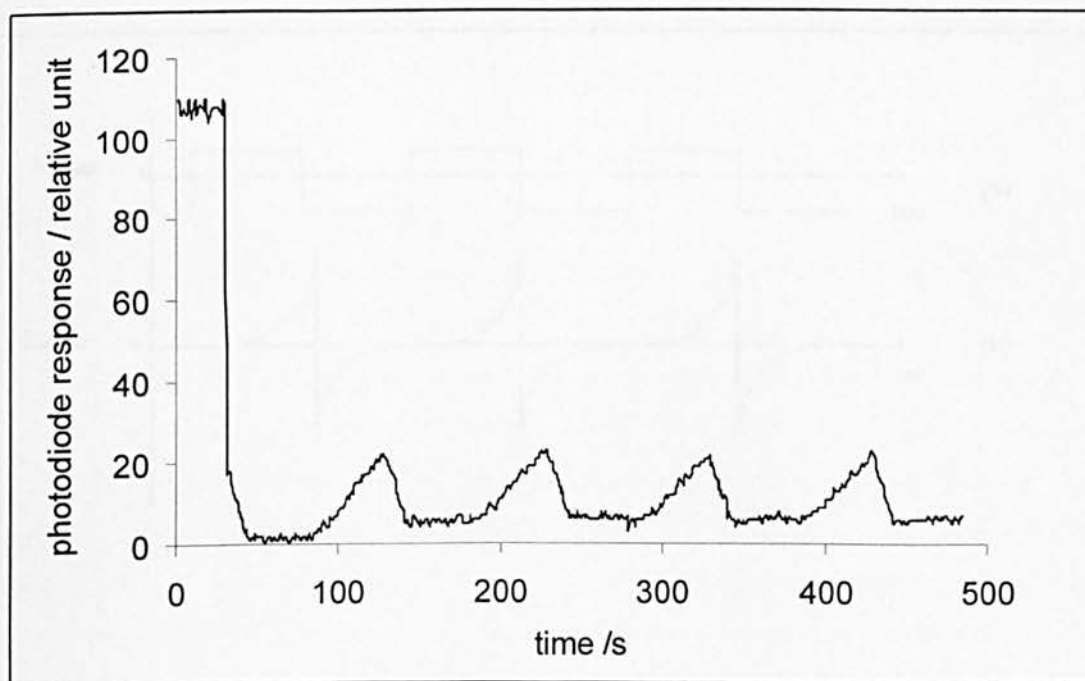
FIGURE 6.5

TRANSIENTS 4996-5000 FOR A POLYPYRROLE AND TPC ELECTROCHROMIC

SYSTEM

In order to obtain rapid switching data, it was decided to operate the cell at high potentials, although this results in a shorter cycling life due to accelerated degradation of the polymer films at the high and low limits.

Although the use of very high static voltages results in decomposition of the polymer film, but the use of rectangular voltage pulses, as shown in Figure 6.6(a) does not seriously degrade the film when the pulse widths are chosen appropriately.

In this case, the widths of positive voltage pulses of ~1V which were applied to the film(1V vs. SSCE) versus the counter electrode was about 50s, and for multiple cycles was 5s. The undoping pulses were ~-1V. It was seen that for multiple cycles, the pulse widths of both the positive and negative voltages were not long enough to completely dope or undope the polymer. The multiple switching pulses were doping/undoping to between 70 and 80% of the limiting changes. The unbalanced doping and undoping, or possibly the accumulation of dopant ions within the film may result in a shorter cycle life and decreasing contrast for longer operation periods.

Typical current transient response is shown in Figure 6.6(b) at the beginning of the operation, where the doping current was interrupted before coming to equilibrium.
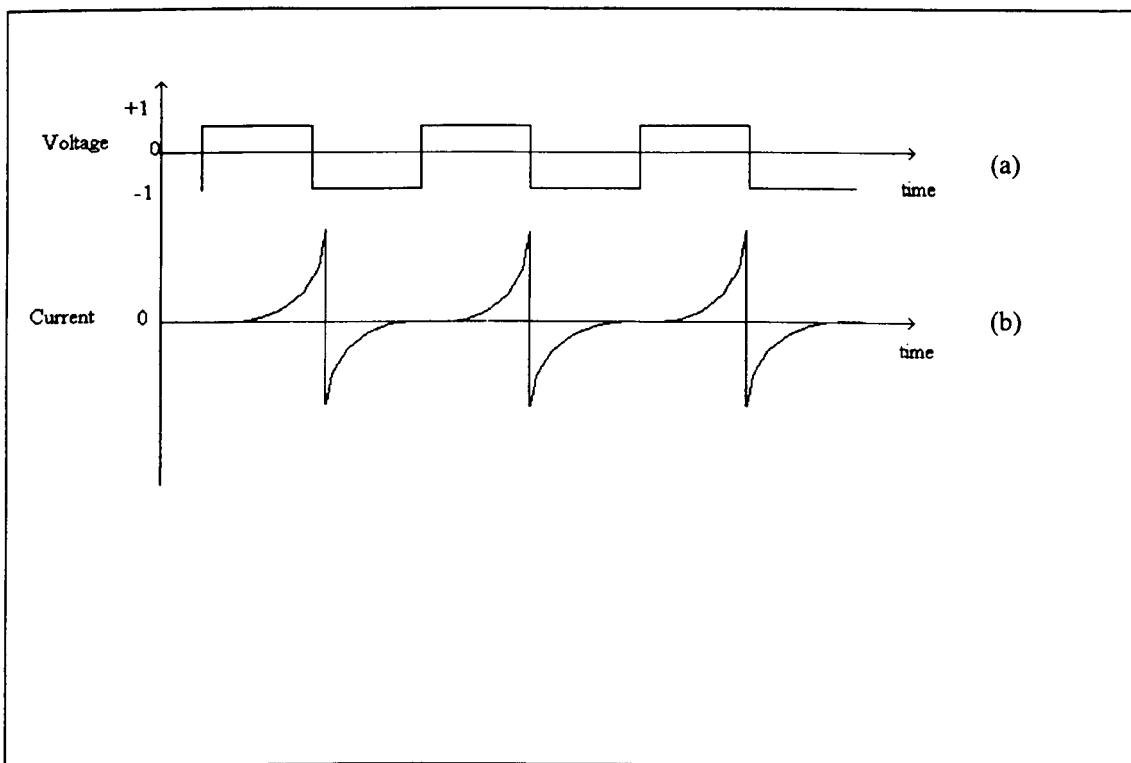
FIGURE 6.6

DIAGRAM SHOWING THE CURRENT CHANGES WHEN A SQUARE-WAVE
VOLTAGE IS APPLIED

Whilst charging during the doping cycle, the larger ions such as ClO_4^- and BPh_4^- permeate the film. However, the polymer structure does not easily allow the movement of bulky ions into or out of the polymer matrix. This film thickness is dependent on the polymer structure which can involve factors such as the rate of polymerisation, purity of monomers etc. This observation is indicated by the switching times for:

Polypyrrole.Perchlorate: $3.8s_{(965nm)}$ and $1.00s_{(98nm)}$
Polypyrrole.Tetraphenylborate: $5.9s_{(398nm)}$ and $0.3s_{(52nm)}$

and shown in figure 6.7:
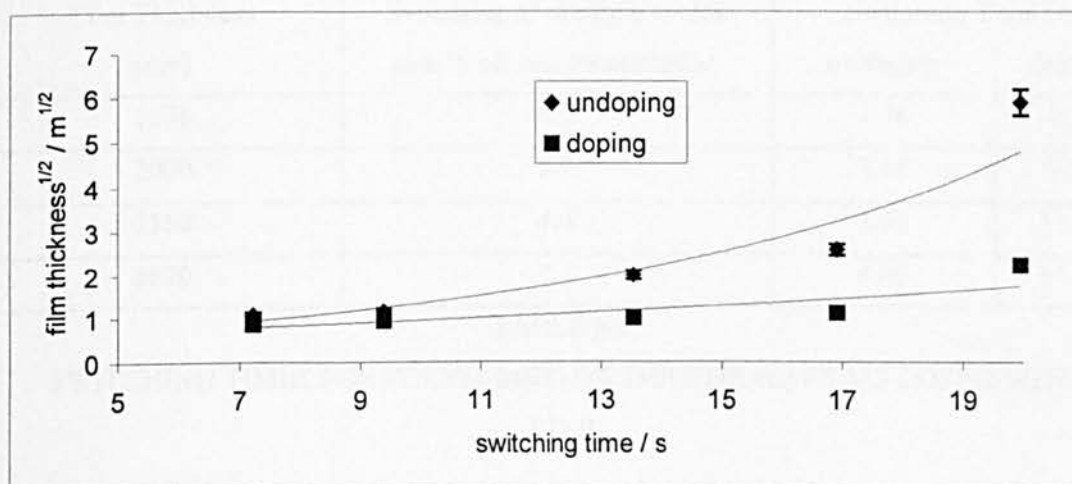
FIGURE 6.7

THE RELATIONSHIP BETWEEN THE FILM THICKNESS AND THE SWITCHING
TIME FOR A DOPING AND UNDOPING PROCESS FOR POLYPYRROLE

Switching times for thicker films are much greater than for thinner films, indicating either a diffusion or series resistance limiting control of the switching time. The dopant ions are able to travel into and out of the polymer film relatively unhindered for thinner films using small dopant ions of tetrafluoroborate. By plotting a graph of the switching time against the film thickness$^{1/2}$, a good indication of a diffusion-limited process may be observed by a deviation from a linear plot. Thinner films have a predictably higher rate of anion penetration as well as a faster response. The charging and discharging responses of different dopant ions indicated that the films in the solution of tetrafluoroborate ions had a faster response time than those of tetraphenylborate ions. We may summarise by saying that for equal film thicknesses of conducting polymers, smaller ion size may permeate more rapidly into and out of the polymer film.

6.3.2   POLY(3-METHYLTHIOPHENE) POLYMER FILMS

6.3.2.1   POLY(3-METHYLTHIOPHENE)   TETRAETHYLAMMONIUM TETRAFLUOROBORATE POLYMER FILMS

Doped polythiophenes are generally unstable to moisture in the doped state due to the release of dopants, and rapidly revert back to the undoped state, which is very stable in air. The instability of the doped state does not result from the decomposition of the films themselves. Poly(3-methylthiophene) polymer films were grown to thicknesses of between 1μm and 9μm and the electrochromic switching times in relation to their film thicknesses are shown in table 6.5.

Film Thickness (nm)	Switching of multiple cycles as a % of total transmission	Switching Time (s)	
		undoping	doping
1070	3.7	1.38	1.50
2000	3.9	2.38	9.50
5350	4.0	3.50	11.88
8820	7.1	4.00	17.50

TABLE 6.5

SWITCHING TIMES FOR POLY(3-METHYLTHIOPHENE) FILMS DOPED WITH TTFB

The colour change for the poly(3-alkylthiophene) conducting polymer is from the red undoped state to the blue doped state. Although the relative transmission through the polymer films was low, the undoping times were short in comparison to the polypyrrole films doped with the same counter-ion salt. The relationship between the doping and undoping times is shown in figure 6.8.

FIGURE 6.8

GRAPH DEPICTING THE RELATIONSHIP BETWEEN FILM THICKNESS AND
SWITCHING TIMES FOR DOPING AND UNDOPING FILMS OF POLY(3-
METHYLTHIOPHENE) WITH FLUOROBORATE ANIONS

6.3.2.2 POLY(3-METHYLTHIOPHENE) AND TETRAMETHYLAMMONIUM PERCHLORATE POLYMER FILMS

Poly(3-methylthiophene) films doped with perchlorate anions were grown to thicknesses of
between about 8μm and 40μm.

Film Thickness	Switching of multiple cycles	Switching Time (s)	
(nm)	as a % of total transmission	undoping	doping
8420	7.58	1.00	1.75
14000	8.91	1.88	2.00
21200	11.27	2.50	2.75
23200	12.28	2.58	4.75
34000	16.19	3.75	5.44
38600	25.64	3.75	7.50
48300	41.33	10.50	12.50

TABLE 6.6

SWITCHING TIMES FOR POLY(3-METHYLTHIOPHENE) FILMS DOPED WITH
PERCHLORATE ANIONS

Table 6.6 indicates that these polymer films showed the largest difference in the relative photodiode response of the rapid doping and undoping. The improved transmission values coupled with the slightly longer switching times as compared to polypyrrole doped with the same counter-ions indicate that the perchlorate ion causes more localised distortions within the polymer backbone.

FIGURE 6.9

GRAPH DEPICTING THE RELATIONSHIP BETWEEN FILM THICKNESS AND SWITCHING TIMES FOR DOPING AND UNDOPING FILMS OF POLY(3-METHYLTHIOPHENE) PERCHLORATE ANIONS
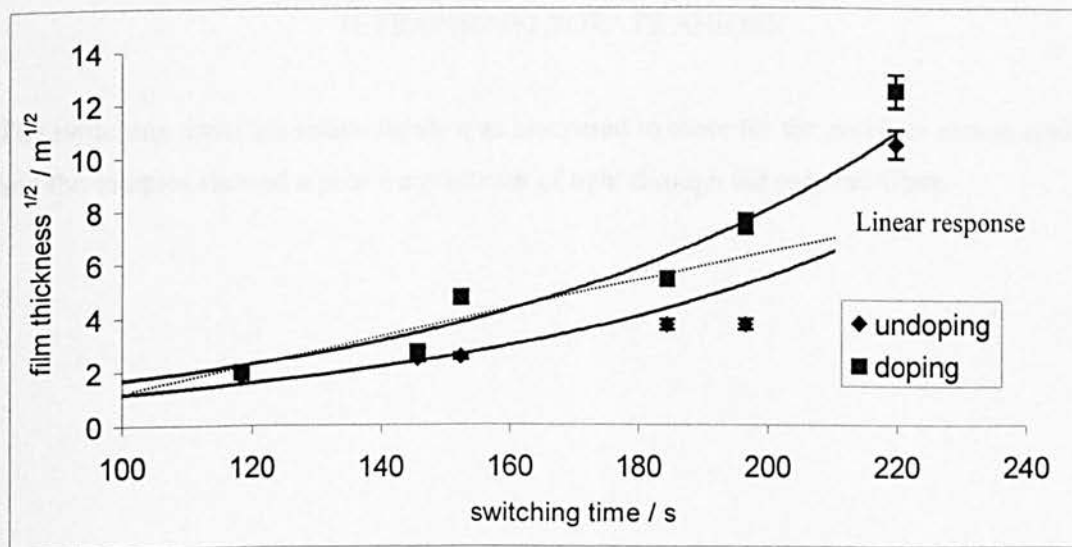
FIGURE 6.10

THE RELATIONSHIP BETWEEN THE FILM THICKNESS AND THE SWITCHING TIME FOR A DOPING AND UNDOPING PROCESS FOR POLYMETHYLTHIOPHENE

Figure 6.10 shows a switching time $\propto$ thickness$^{1/2}$ relationship between the film thickness and the switching times, therefore in comparison to previous measurements we can say that since a sharp deviation occurs at ~5.8, at film thicknesses of greater than approximately 34μm, the electrochromic process becomes diffusion limited.

6.3.2.3 POLY(3-METHYLTHIOPHENE) AND TETRABUTYLAMMONIUMTETRAPHENYLBORATE POLYMER FILMS

Poly(3-methylthiophene) films doped with tetraphenylborate anions were grown to thicknesses of between 2.5μm and 15.7μm as shown in table 6.7.

Film Thickness (nm)	Switching of multiple cycles as a % of total transmission	Switching Time (s) undoping	doping
3610	3.13	1.25	4.00
4750	4.51	1.50	4.25
7370	5.88	1.88	4.50
10140	6.94	2.00	5.75
12300	9.62	2.25	8.00
15700	11.27	8.00	8.25

TABLE 6.7

SWITCHING TIMES FOR POLY(3-METHYLTHIOPHENE) FILMS DOPED WITH TETRAPHENYLBORATE ANIONS

The switching times are relatively slow as compared to those for the previous anions studied, and the samples showed a poor transmission of light through the polymer films.
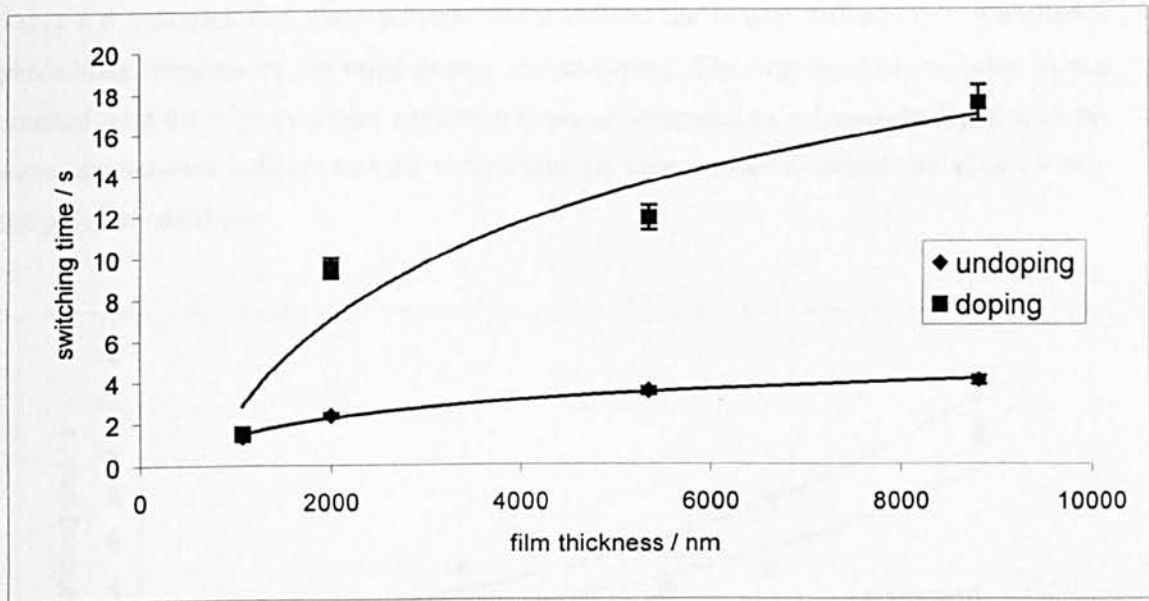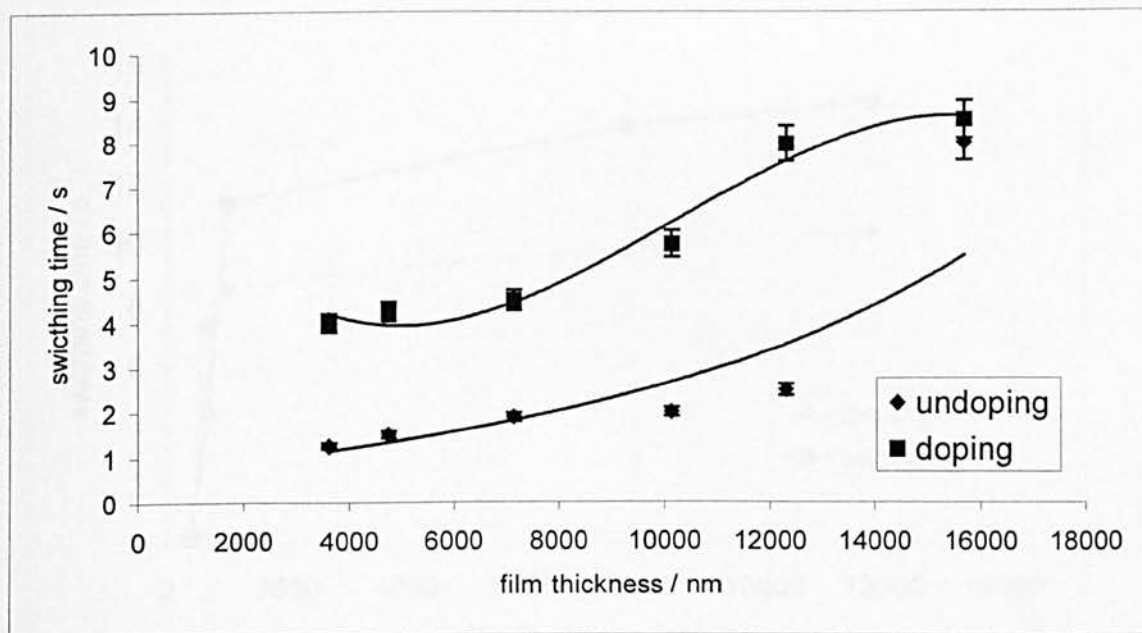
FIGURE 6.11

GRAPH DEPICTING THE RELATIONSHIP BETWEEN FILM THICKNESS AND SWITCHING TIMES FOR DOPING AND UNDOPING FILMS OF POLY(3-METHYLTHIOPHENE) WITH TETRAPHENYLBORATE ANIONS

Figure 6.11 shows the relationship between the doping and undoping times compared to the film thickness.

6.3.3.1 POLYANILINE CONDUCTING POLYMER FILMS

The polyaniline sample was switched between the conducting green (emeraldine) state and non-conducting yellow (leucoemeraldine) state by a potential change from +0.4V to -0.15V with respect to SSCE.

Film Thickness (nm)	Transmission Change (%)	Switching Time (s)	
		undoping	doping
390	1.43	<0.25	0.38
665	2.25	4.36	7.82
770	9.40	11.28	8374
7700	28.60	13.85	9.74
11800	33.20	14.62	10.26

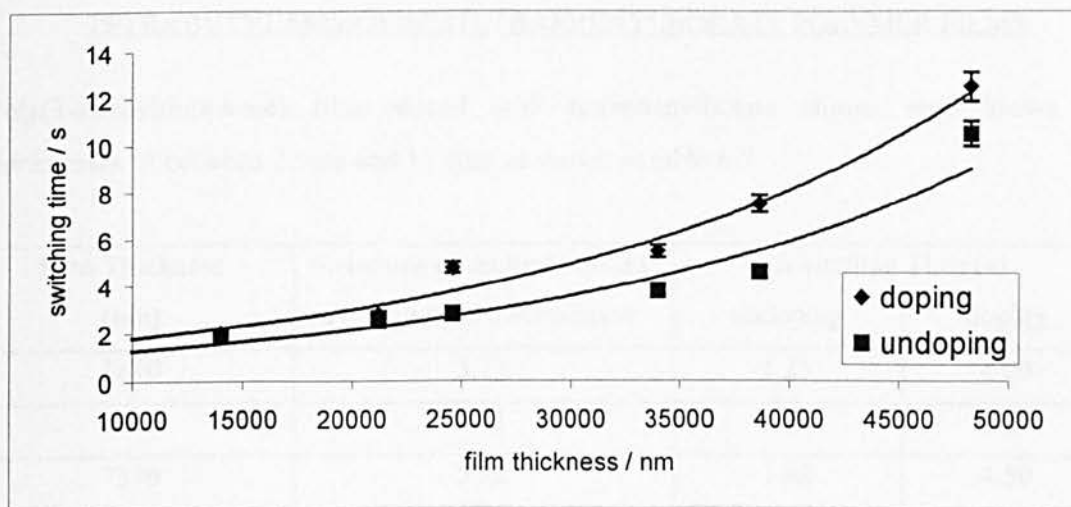TABLE 6.8

SWITCHING TIMES FOR POLYANILINE FILMS DOPED WITH CHLORIDE ANIONS
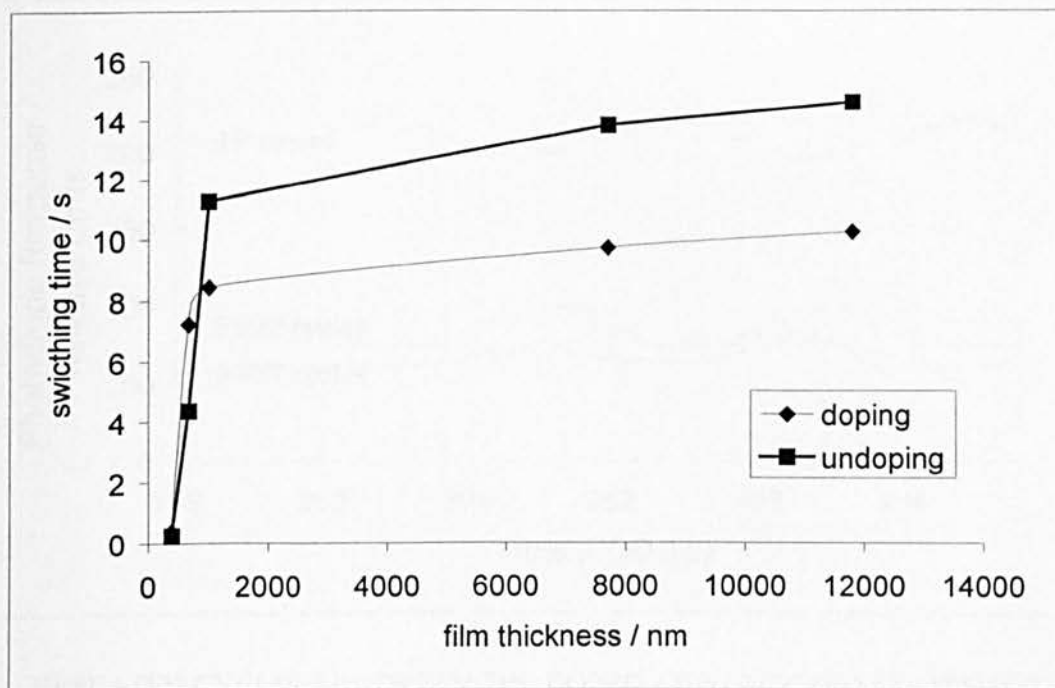
FIGURE 6.12

GRAPH DEPICTING THE RELATIONSHIP BETWEEN FILM THICKNESS AND SWITCHING TIMES FOR DOPING AND UNDOPING FILMS OF POLYANILINE WITH CHLORIDE ANIONS IN 2M HCL

Figure 6.12 shows that switching in polyaniline-based conducting polymers rapidly become diffusion-limited, plateauing at a stage where the movement of ions is not fast enough to alter the bulk polymer dopant concentration before the next voltage perturbation.

In this work the widths of the positive and negative voltage steps were 50s for single cycles and 5s for multiple cycles, and the potentials quoted were measured with respect to SSCE. It was noted that the use of rapid cycling did not dope/undope the polymer samples to the same extent as the slower doping/undoping cycles.

6.3.3.2 POLYANILINE ELECTROCHROMIC DEVICE LONGEVITY STUDY

Figure 6.13 gives the greatest contrast ratio compared to the polyalkylthiophene-based electrochromic device longevity study. This graph shows the raw data after 10, 1500 and 2000 cycles. There was a 38%, 60% and 65% decrease in the contrast ratio over the lifetime study respectively, indicative of polymer degradation or loss of interfacial contact.
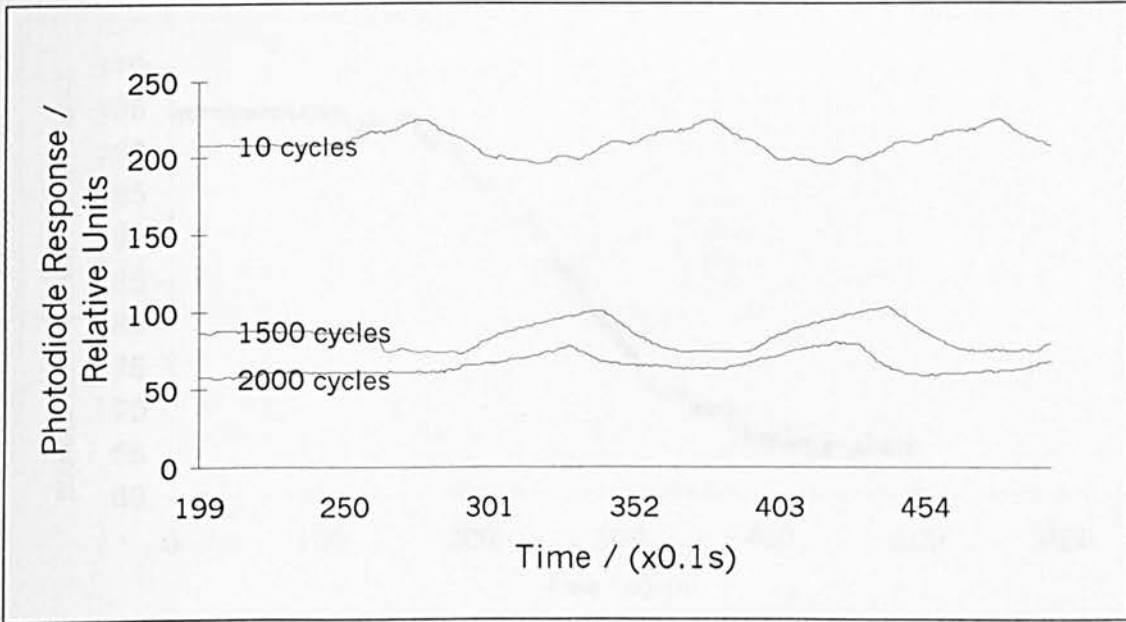
FIGURE 6.13

REPEATED CYCLING BETWEEN THE DOPED AND UNDOPED STATES FOR
POLYANILINE
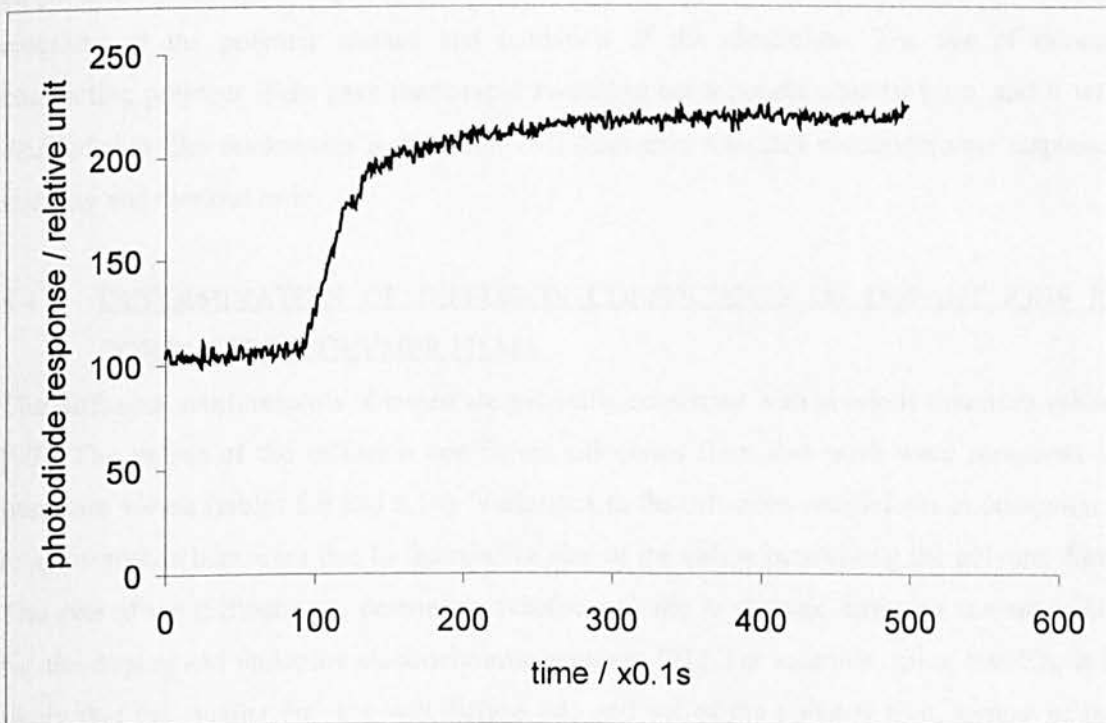
FIGURE 6.14

PHOTODIODE RESPONSE FOR THE DOPING CYCLE OF POLYANILINE
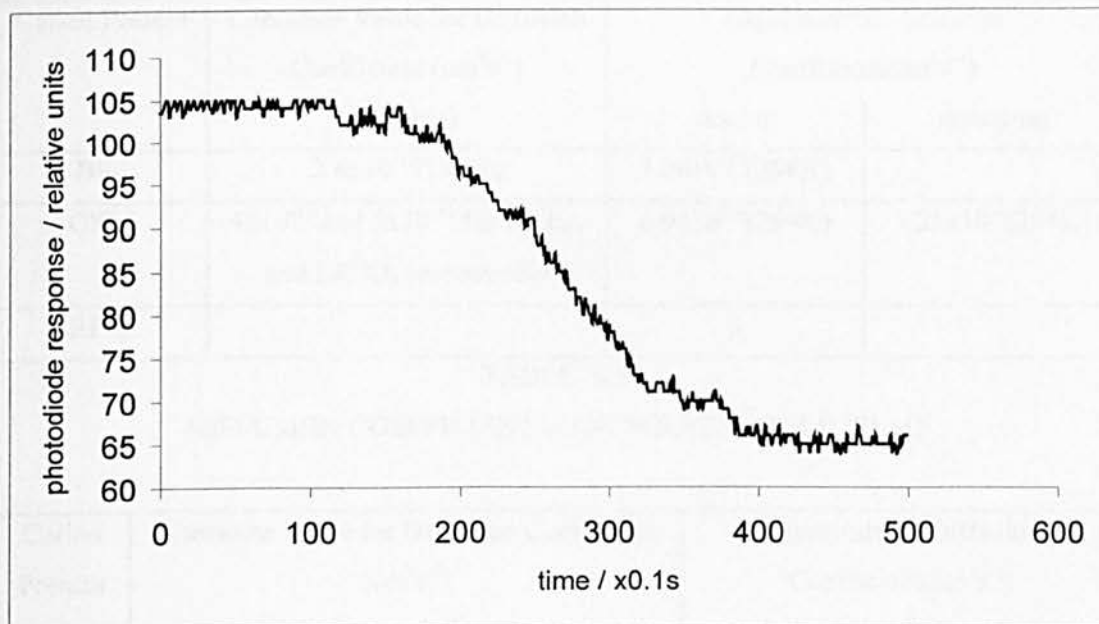
FIGURE 6.15

PHOTODIODE RESPONSE FOR THE UNDOPING CYCLE OF POLYANILINE

Application of a high voltage to the device resulted in a shorter cycle life due to irreversible reactions at the polymer surface and oxidation of the electrolyte. The use of thinner conducting polymer films gave more rapid switching but a poorer contrast ratio, and it was decided that film thicknesses in the range of 1-5μm gave adequate electrochromic response, stability and contrast ratio.

6.4   DETERMINATION OF DIFFUSION COEFFICIENTS OF DOPANT IONS IN CONDUCTING POLYMER FILMS

The diffusion measurements obtained are generally consistent with previous literature values [90]. The values of the diffusion coefficient calculated from this work were compared to literature values (tables 6.9 and 6.10). Variations in the diffusion coefficients in comparison to other researchers were due to the relative size of the cation penetrating the polymer film. The size of the diffusing ion determines whether anionic or cationic diffusion is responsible for the doping and undoping electrochromic response [91]. For example, using $NaClO_4$, it is likely that the smaller Na^+ ion will diffuse into and out of the polymer film, instead of the bulkier ClO_4^- ion. By selecting larger alkylammonium cations, we can remove this possible source of confusion, which may be the topic of further research.

Cation Present	Literature Value for Diffusion Coefficient (cm^2s^{-1}) (doping)	Experimental Diffusion Coefficient(cm^2s^{-1})	
		doping	undoping
BF_4^-	2.6×10^{-13}(298K)	3.2×10^{-13}(298K)	-
ClO_4^-	4×10^{-11} and 5×10^{-11} for $HClO_4$ and $LiClO_4$ respectively	6.9×10^{-14}(298K)	3.25×10^{-6}(298K)
BPh_4^-	-	-	-

TABLE 6.9

DIFFUSION COEFFICIENTS FOR POLYPYRROLE FILMS

Cation Present	Literature Value for Diffusion Coefficient (cm^2s^{-1})		Experimental Diffusion Coefficient(cm^2s^{-1})	
	doping	undoping	doping	undoping
BF_4^-	1.7×10^{-11}(273K)	1.9×10^{-11}(273K)	4.6×10^{-10}(298K)	4.9×10^{8} (298K)
ClO_4^-	2.1×10^{-12}(273K) $HClO_4$ 2.9×10^{-12}(273K) $LiClO_4$	-	6.6×10^{-12}(298K)	4.2×10^{7} (298K)
BPh_4^-	-	-	2.5×10^{-7}(298K)	-

TABLE 6.10

DIFFUSION COEFFICIENTS FOR POLY(3-METHYLTHIOPHENE) FILMS

In almost all the polypyrrole and poly(3-methylthiophene) polymer films, the undoping diffusion coefficient was observed to be higher than the doping diffusion coefficient at 298K. Diffusion of ions into the polymer film may not have fully penetrated into the bulk of the material, and only a surface doping effect will have occurred. As the polymer has been permeated by the diffusing ions, a path already exists for relatively unhindered movement back into solution, allowing the undoping diffusion coefficient to be much higher.

The ionic volume of the dopant ions used were BF_4^-, ClO_4^- and BPh_4^- are $7.46 \times 10^{-29}m^3$, $1.5 \times 10^{-28}m^3$ and $1.8 \times 10^{-27}m^3$ respectively. For polypyrrole, the diffusion coefficients decrease monotonically with increasing ion size (figure 6.16), however, for poly(3-methylthiophene) films, the trend is to increase and then decrease (figure 6.17).
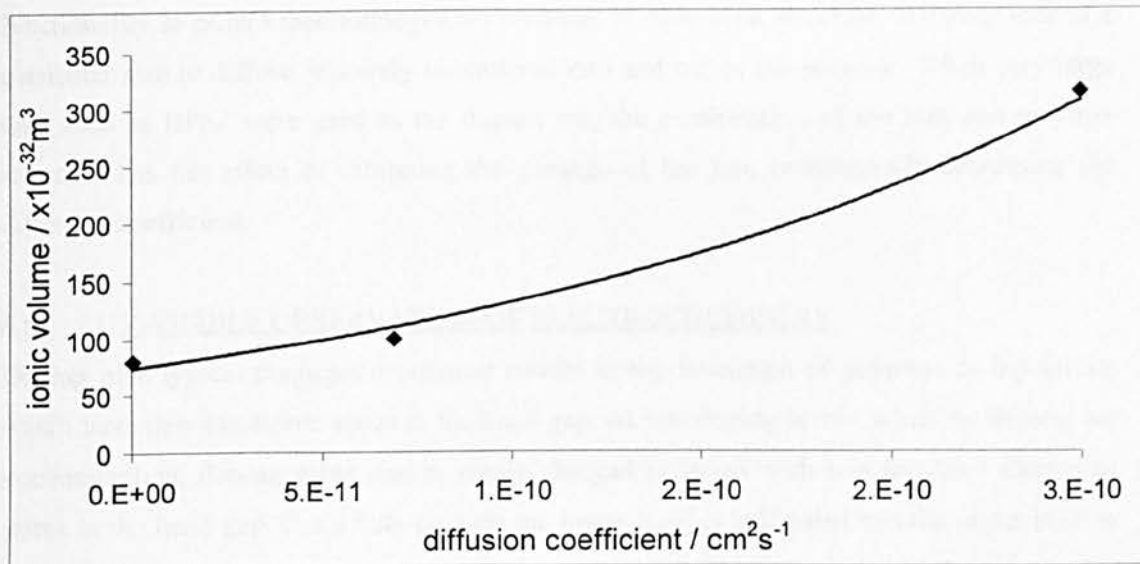
FIGURE 6.16

GRAPH SHOWING THE CHANGE IN DIFFUSION COEFFICIENT WITH
INCREASING DOPANT ION VOLUME FOR POLYPYRROLE

FIGURE 6.17

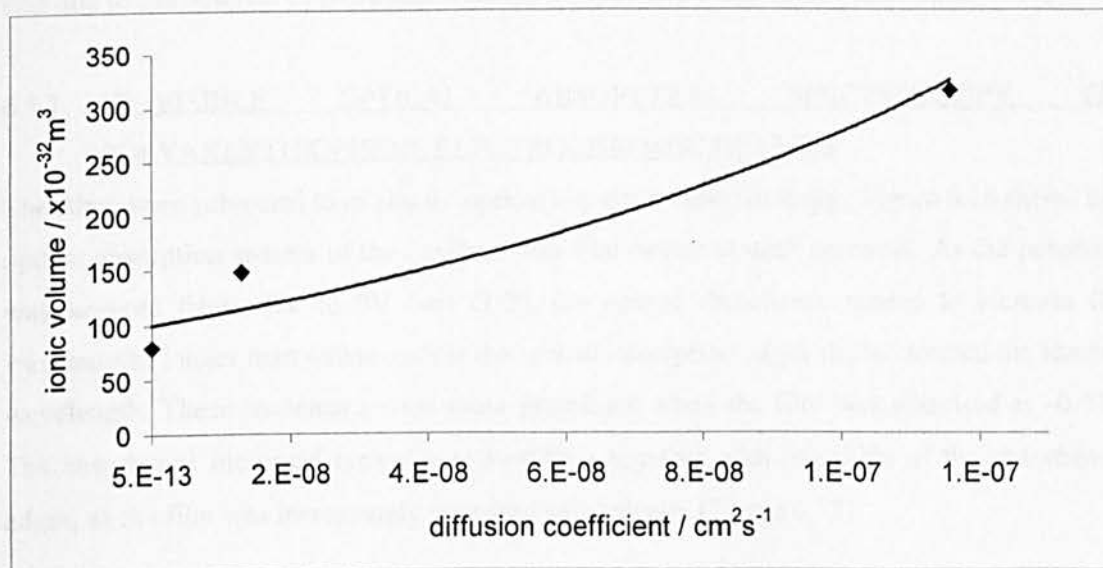GRAPH SHOWING THE CHANGE IN DIFFUSION COEFFICIENT WITH
INCREASING DOPANT VOLUME RADIUS FOR POLY(3-METHYLTHIOPHENE)

The diffusion coefficient does not seem to be related solely to the size of the dopant ion, but is
also an indication of the morphology of the polymer (as is the switching time). Although the
conducting polymers formed are known to be amorphous in nature, the presence of the methyl

functionality in poly(3-methylthiophene) produces a more open structure, allowing ions of a particular size to diffuse relatively unhindered into and out of the polymer. When very large ions such as BPh_4^- were used as the dopant ion, the combination of ion size and polymer structure has the effect of inhibiting the passage of the ion, consequently decreasing the diffusion coefficient.

6.5 UV-VISIBLE OBSERVATION OF ELECTROCHEMISTRY

Doping of a typical conjugated polymer results in the formation of polarons or bipolarons which have new electronic states in the band gap. At low doping levels, when the defects are not interacting, doping gives rise to singly charged polarons with two localised electronic states in the band gap. For a hole polaron the lower level is half-filled and the upper level is empty, allowing for sub-gap optical transitions, two of which are roughly degenerate. By increasing the dopant ion concentration, the probability of recombination of two polarons into one bipolaron increases; also, doubly charged bipolarons can be created by direct electron transfer from polarons to dopant molecules. For a hole bipolaron, the two intra-gap levels are empty and only two sub-gap transitions are possible. At higher doping levels, the bipolaron levels start to overlap; bipolaron bands are formed within the gap, and the latter increases in size due to the removal of p-orbitals from the valence and conduction band edges.

6.5.1 UV-VISIBLE OPTICAL ABSORPTION SPECTROSCOPY OF POLYAKLYTHIOPHENE ELECTROCHROMIC DEVICES

The films were subjected to in-situ uv-optical absorption spectroscopy. Figure 6.18 shows the optical absorption spectra of the oxidised thin film device at each potential. As the potential was lowered from +2V to 0V (wrt ITO), the optical absorbance tended to increase for wavelengths longer than 480nm, while the optical-absorption edges shifted toward the shorter wavelength. These tendencies were more prominent when the film was polarised at −0.5V. The absorbance increased typically at $\lambda > 400nm$ together with red shifts of the absorbance edges, as the film was increasingly polarised cathodically (Figure 6.18).

This technique established that the electronic and chemical changes caused by the electrochemical doping were entirely reversible (after equilibration) under cathodic polarisation, provided that the voltages applied were not too large. A safe range of polarising potentials was found to be -2V to +2V w.r.t. ITO; for an additional margin of safety over number of cycles, the limits should be set at about -1.5V to +1.5V for the polyalkylthiophene cells. Table 6.11 shows the observed maximum absorptions, λ_{max} and their corresponding electronic transitions associated with the UV-visible spectrum.
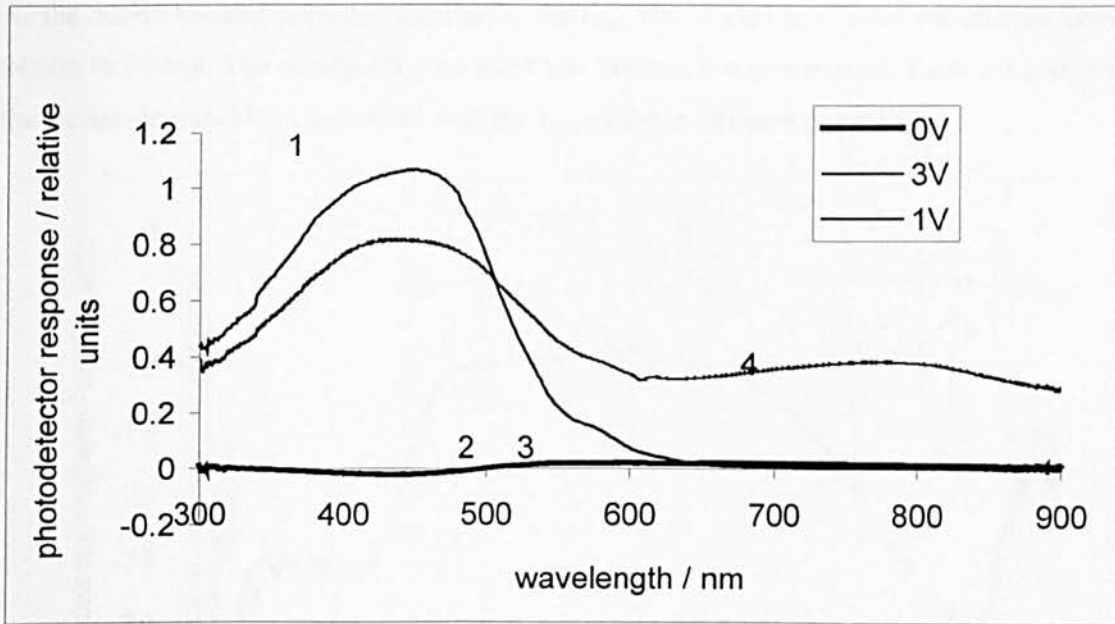
FIGURE 6.18

UV-VISIBLE ABSORPTION SPECTRUM FOR DOPED (POSITIVE VOLTAGE RANGE)
AND UNDOPED (NEGATIVE VOLTAGE RANGE) POLYALKYLTHIOPHENE WITHIN
AN ELECTROCHROMIC DEVICE

PEAK NUMBER	WAVELENGTH (nm)	TRANSITION ENERGY (eV)	TRANSITION
1	450	2.76	Fundamental $\pi-\pi^*$
2	570	2.18	$n-\pi^*$
3	600	2.07	Polaron band I
4	790	1.57	Polaron band II

TABLE 6.11

TABLE SHOWING THE ELECTRONIC TRANSITIONS FOR POLYAKLYTHIOPHENE

WITHIN AN ELECTROCHROMIC DEVICE

6.5.2   UV-VISIBLE OPTICAL ABSORPTION SPECTROSCOPY OF POLYANILINE ELECTROCHROMIC DEVICES

Figure 6.19 shows the optical absorption spectra of the thin film devices at each reduction potential. As the potential was lowered from -0.5V to –2.5V (wrt ITO) the optical absorbance peak tended to shift from 790nm to 830nm whilst the absorption edge at 420nm became more pronounced. Figure 6.20 shows the wavelength absorptions at +1V (wrt ITO).

As the device became polarized anodically, the λ_{max} was shifted to a lower wavelength from 840nm to 790nm. The absorption edge at 440nm became less pronounced. Table 6.12 shows the electronic transitions associated with the λ_{max} peaks at different potentials.
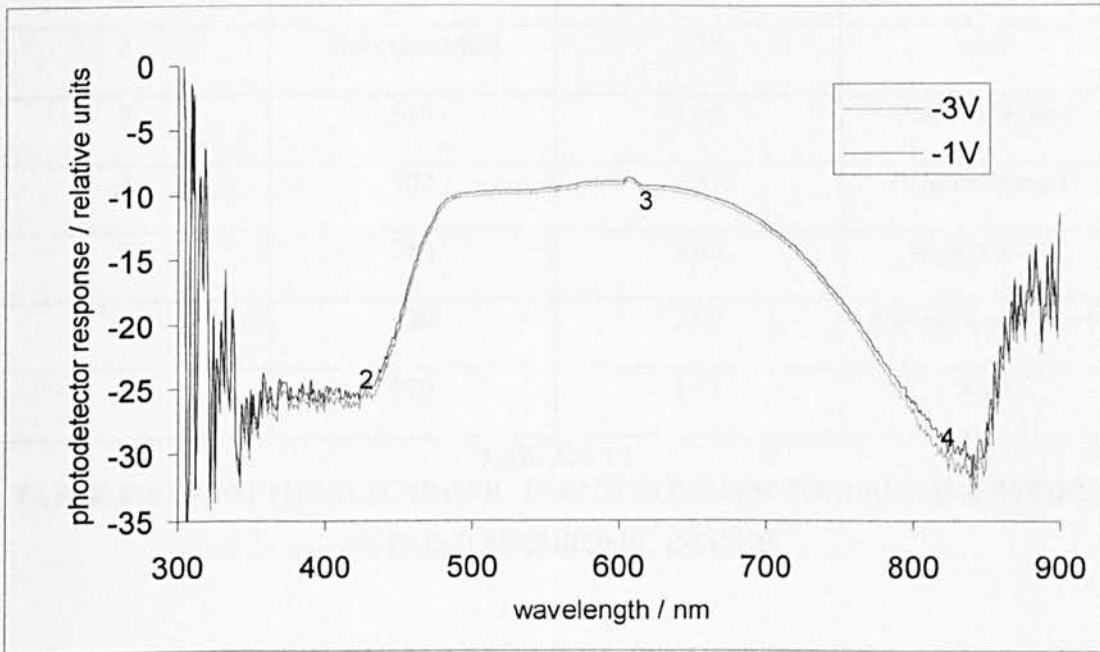
FIGURE 6.19

UV-VISIBLE ABSORPTION SPECTRUM FOR UNDOPED POLYANILINE WITHIN AN
ELECTROCHROMIC DEVICE
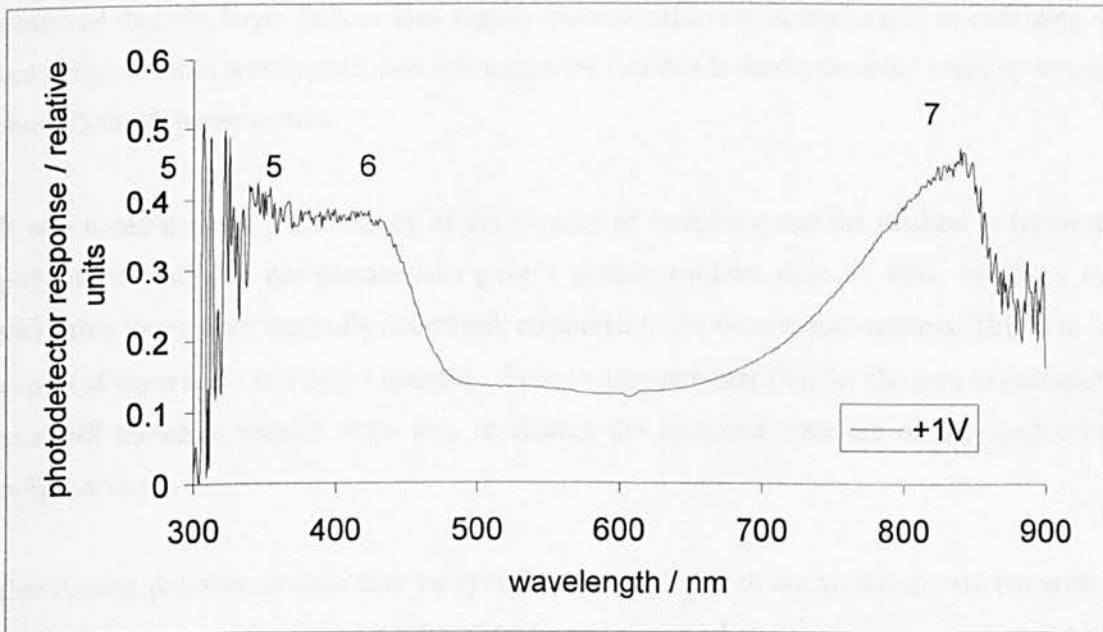
FIGURE 6.20
UV-VISIBLE ABSORPTION SPECTRUM FOR DOPED POLYANILINE WITHIN AN
ELECTROCHROMIC DEVICE

PEAK NUMBER	WAVELENGTH (nm)	TRANSITION ENERGY (eV)	TRANSITION
1	370	2.95	Fundamental π–π*
2	420 (shoulder)	3.35	n-π*
3	610	2.03	Polaron Band I
4	790	1.57	Polaron Band II
5	340	3.65	Higher π–π*
6	420	2.95	Fundamental π–π*
7	820	1.51	n-π*

TABLE 6.12

TABLE SHOWING THE ELECTRONIC TRANSITIONS FOR POLYANILINE WITHIN AN ELECTROCHROMIC DEVICE

6.6 SUMMARY OF ELECTROCHROMIC PROPERTIES OF CONDUCTING POLYMERS

Soluble conducting polymers in the polyalkylthiophene and polyaniline families were synthesized, and the effects of the doping ions on the switching times were studied. It was observed that the larger bulkier ions rapidly became diffusion limited when an oxidizing or reducing potential was applied, and it is suggested that this is due to the ions' inability to pass through the polymer matrix.

It was noted through a brief study of the kinetics of switching that the thickest polypyrrole polymer doped with perchlorate ions gave a greater contrast ratio of 36%, however, the switching times were markedly decreased, compared to the thinner counterparts. This is to be expected since there is a larger quantity of conducting polymer film for the ions to permeate, and will therefore require more ions to change the localized structure of the conducting polymer chain.

Conducting polymer devices may be cycled from the doped to the undoped state but with a marked decrease in the contrast ratio after several thousand switches. More rapid switching would involve the use of greater applied potentials, and from this study would shorten the lifetime of the electrochromic device by introducing an increased number of irreversible side

reactions at the polymer surface or at the molecular level. By the careful selection of voltage pulse widths, the side reactions can be reduced. The most stable polymer film was observed to be polyaniline due only a 5% decrease transmissive response of the photodetector after the polymer film had been cycled between 1500 and 2000 times. Response times of the polyaniline films to the applied voltage were often very different for the oxidising and reducing steps; and would not usually be expected if the process were diffusion-limited. This can be explained by different chemical reaction rates in the two directions, or by limitations of electrical conductivity or interfacial transport. A clear asymmetry was seen in the switching profiles, with a characteristic induction period when switching from the insulating state (figure 6.14) to the conductive state (Figure 6.15).

The diffusion coefficients were in agreement with literature values [90]. The size of the cation dictates the surrounding charge density, resulting in the bulkier and less densely charged tetraphenylborate ions having a diffusion coefficient that was 10^3 to 10^5 times slower than the fluoroborate and perchlorate ions respectively in the poly(3-methylthiophene) films.

CHAPTER SEVEN

RESULTS AND DISCUSSION FOR THE ELECTRONIC
PROPERTIES OF CONDUCTING POLYMERS

7.1 INTRODUCTION

This chapter describes and analyses the dielectric and electronic properties of poly(3-methylthiophene) and polyaniline and compares the data for these established conducting polymers to those for poly(3-methylthiophene) polymers complexed with Co, Ni and Fe.

7.2 THE ELECTRONIC PROPERTIES OF POLY(3-METHYLTHIOPHENE)

7.2.1 DETERMINATION OF THE COMPONENTS OF THE TOTAL CONDUCTIVITY

The log of the total conductivity (both the AC and the DC components) is shown as a function of the log of the frequency in the range 123K - 323K (Figure 7.1a). As the temperature increases, DC conduction processes can be seen to dominate at the lower frequencies. The DC component of the total AC conductivity measured by the broadband dielectric spectrometer can be determined by plotting a graph of the total conductivity against the applied frequency and extrapolating to 0Hz at a constant temperature, the results of which are shown in Table 7.1a.
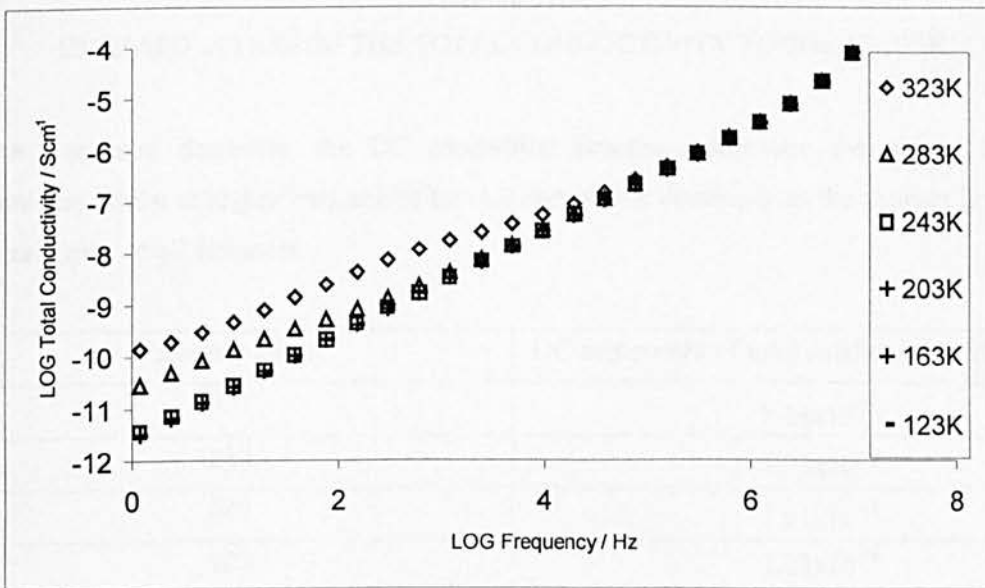
FIGURE 7.1a

DETERMINATION OF THE DC COMPONENT OF THE TOTAL CONDUCTIVITY FOR
POLY(3-METHYLTHIOPHENE)

Figure 7.1b shows the extrapolation to 0Hz for the total conductivity at 323K.
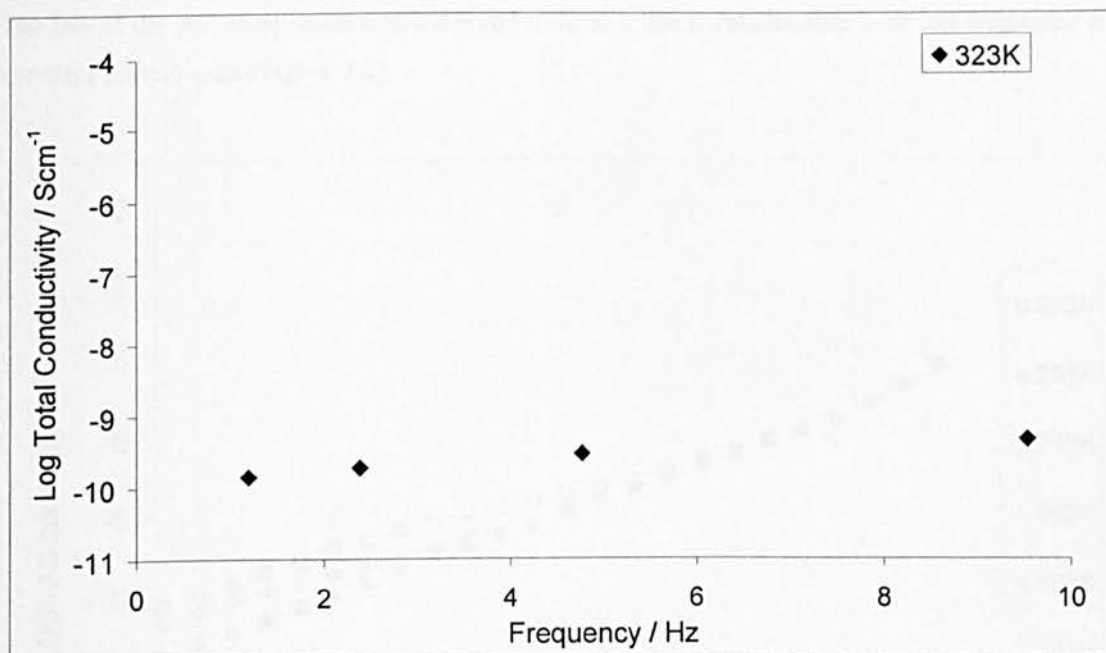
FIGURE 7.1b

EXTRAPOLATION OF THE TOTAL CONDUCTIVITY TO 0Hz AT 323K

As the frequency decreases, the DC conduction processes dominate the charge transfer mechanisms, whilst at higher frequencies the AC component dominates as the charges hop quite efficiently over small distances.

Temperature / K	DC component of total conductivity / Scm^{-1}
323	8.38×10^{-11}
283	7.73×10^{-12}
243	1.91×10^{-13}
203	1.23×10^{-14}
143	1.78×10^{-15}
123	2.05×10^{-15}

TABLE 7.1

TABLE SHOWING THE DC COMPONENT OF THE TOTAL CONDUCTIVITY FOR POLY(3-METHYLTHIOPHENE)

The log of the AC component was observed to have a linear relationship with log frequency at a constant temperature (Figure 7.2).
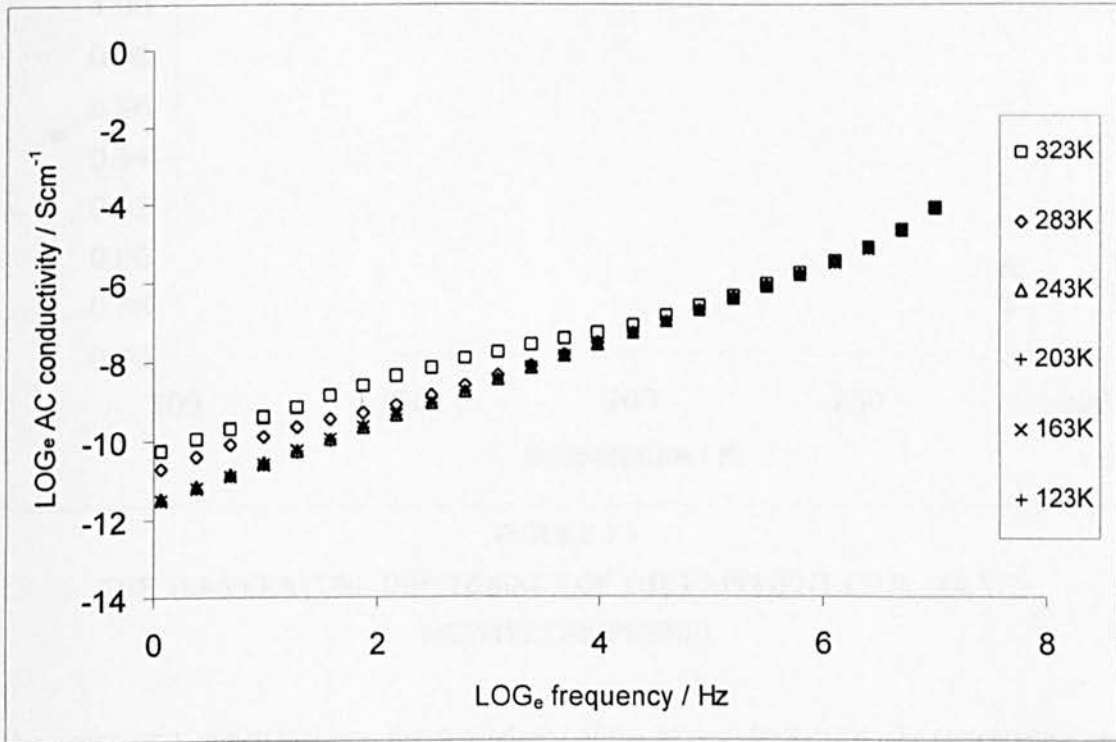
FIGURE 7.2

THE FREQUENCY DEPENDENCE OF THE PURE AC CONDUCTIVITY AT VARIOUS TEMPERATURES, AS OBTAINED FROM FIGURE 7.1 BY SUBTRACTING THE DC COMPONENT FROM THE TOTAL CONDUCTIVITY FOR POLY(3-METHYLTHIOPHENE)

The exponent, s was determined from the relationship shown in Equation 7.1.

$$\sigma_{AC} = \omega^s T^n$$

EQUATION 7.1

By plotting the slope of the $\log_e$ of the AC conductivity against the $\log_e$ of the frequency, the exponent s was determined, and its temperature dependence is shown in Figure 7.3.
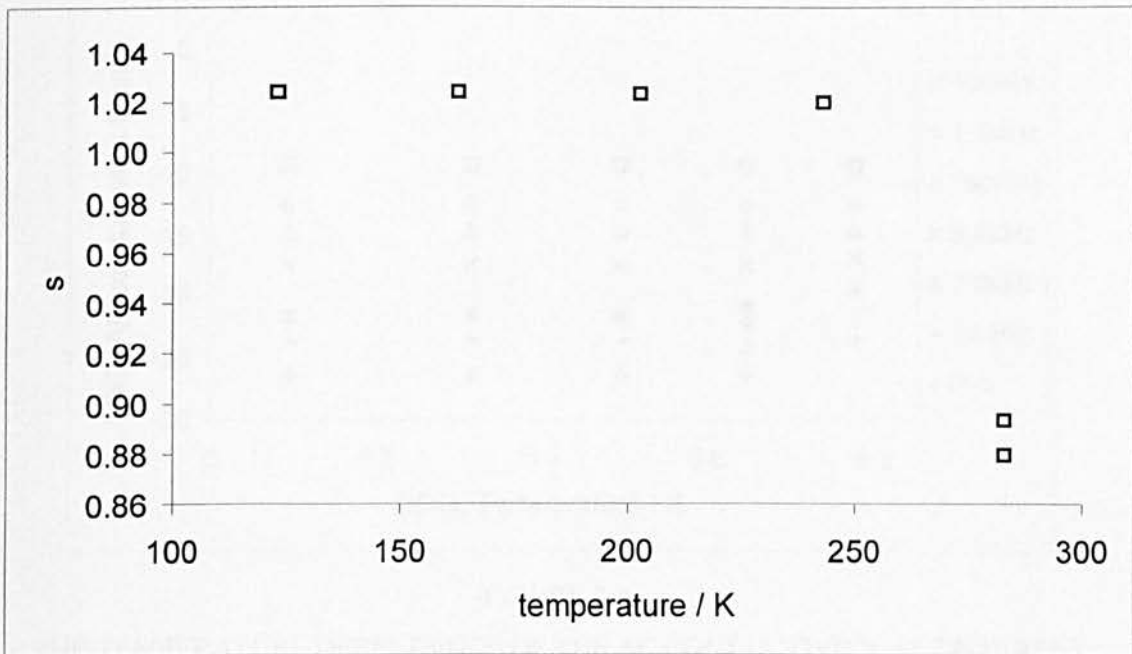
FIGURE 7.3

THE TEMPERATURE DEPENDENCE OF THE EXPONENT s FOR POLY(3-
METHYLTHIOPHENE)

The exponent n, which indicates the dependence of the AC conductivity on the temperature, was determined from slope of the plot of the $\log_e$ of the AC conductivity against the $\log_e$ temperature at a constant frequency (Figure 7.4a). A graph showing the $\log_e$ of the AC conductivity against the $\log_e$ temperature at 10MHz is shown in Figure 7.4b. The relationship between the temperature exponent, n and the frequency is shown in Figure 7.5.
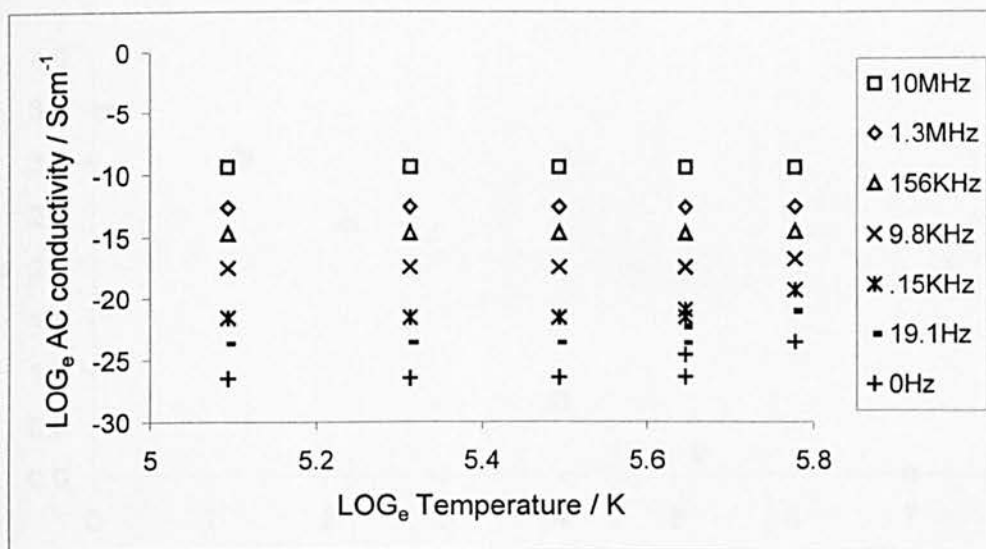
FIGURE 7.4a

THE TEMPERATURE DEPENDENCE OF THE AC CONDUCTIVITY AT DIFFERENT
FREQUENCIES FOR POLY(3-METHYLTHIOPHENE)
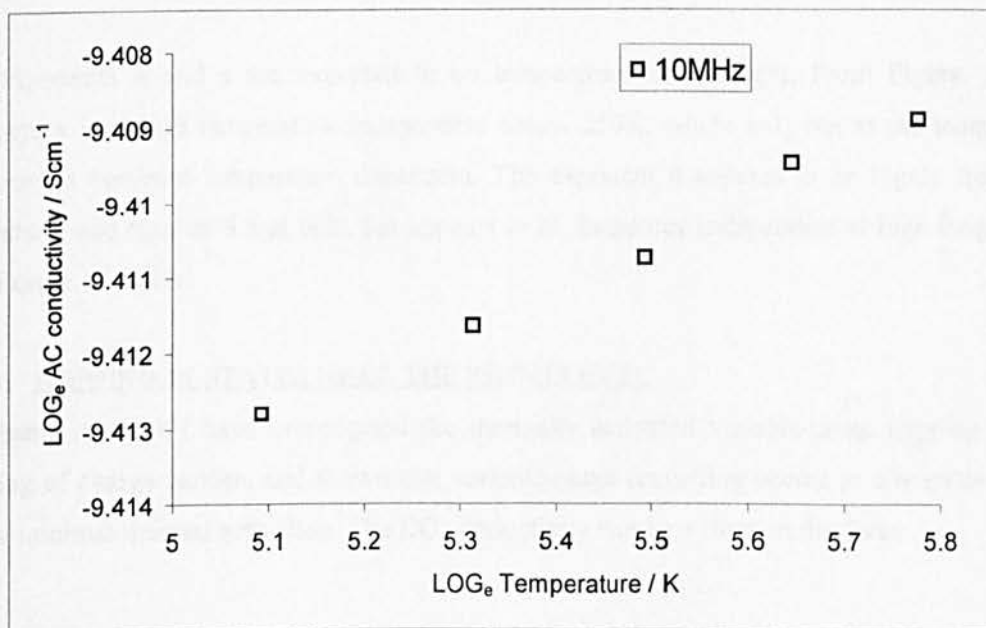
FIGURE 7.4b

THE TEMPERATURE DEPENDENCE OF THE AC CONDUCTIVITY AT 10MHz FOR
POLY(3-METHYLTHIOPHENE) TO SHOW THE NEGATIVE SLOPE
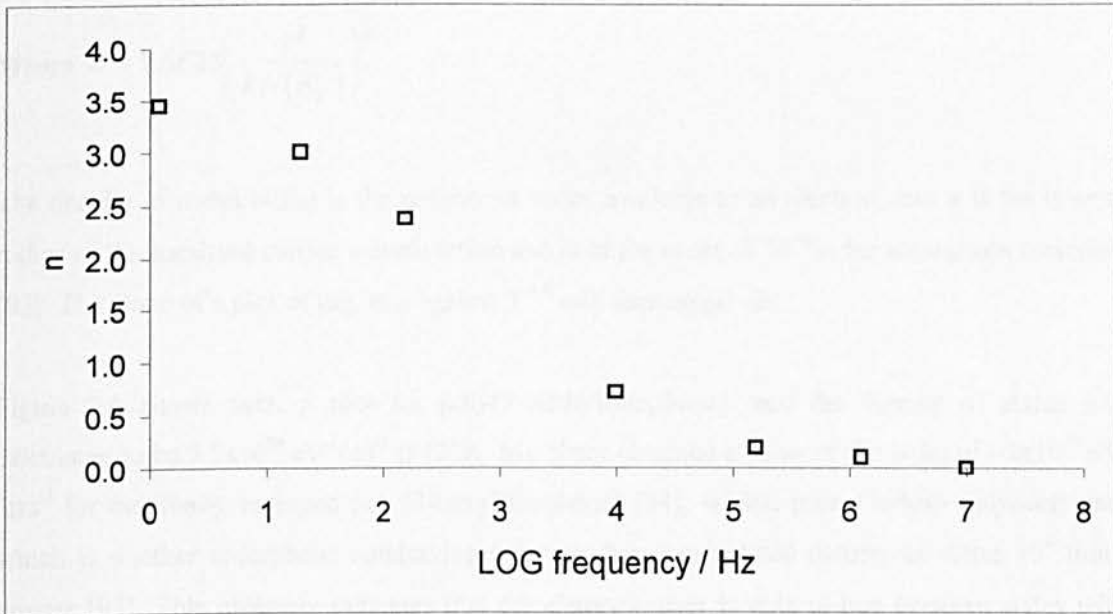
FIGURE 7.5

THE FREQUENCY DEPENDENCE OF THE EXPONENT n FOR POLY(3-
METHYLTHIOPHENE)

The exponents n and s are expected to be temperature independent. From Figure 7.3, the exponent s is indeed temperature independent below 250K, where s~1, but as the temperature increases, s becomes temperature dependent. The exponent n appears to be highly frequency dependent, and reaches 3.5 at 0Hz, but appears to be frequency independent at high frequencies of the order of 10^7Hz.

7.2.2 HOPPING IN STATES NEAR THE FERMI LEVEL

Abrahams et al [92] have investigated the thermally activated variable-range hopping or just hopping of charge carriers and shown that variable-range tunnelling occurs at low temperatures with a minimal thermal activation. The DC conductivity can be written in the form:

$$\sigma_{DC} = A\exp\left(\frac{-B}{T^{\frac{1}{4}}}\right)$$

EQUATION 7.2

Where $B = 1.6625 \left(\dfrac{\alpha^3}{k N(E_F)} \right)^{\frac{1}{4}}$

The density of states $N(E_F)$ is the number of states available to an electron, and α is the inverse radius of the localised carrier wavefunction and is of the order of 10^{-10}m for amorphous materials [93]. The slope of a plot of $\log_e \sigma_{DC}$ against $T^{-1/4}$ will then equal -B:

Figure 7.6 shows such a plot for poly(3-methylthiophene), and the density of states was calculated to be 5.2×10^{24} eV^{-1}cm^{-3} at 123K. Marchant obtained a value of the order of $\sim 3 \times 10^{25}$ eV^{-1}cm^{-3} for nominally undoped poly(3-hexylthiophene) [94], whilst, pure Durham polyacetylene, which is another amorphous conducting polymer, has a calculated density of states 10^6 times greater [95]. This probably indicates that the charge carrier is able to hop between states with very little input, thereby inferring that the trap depth is greater for poly(3-methylthiophene).
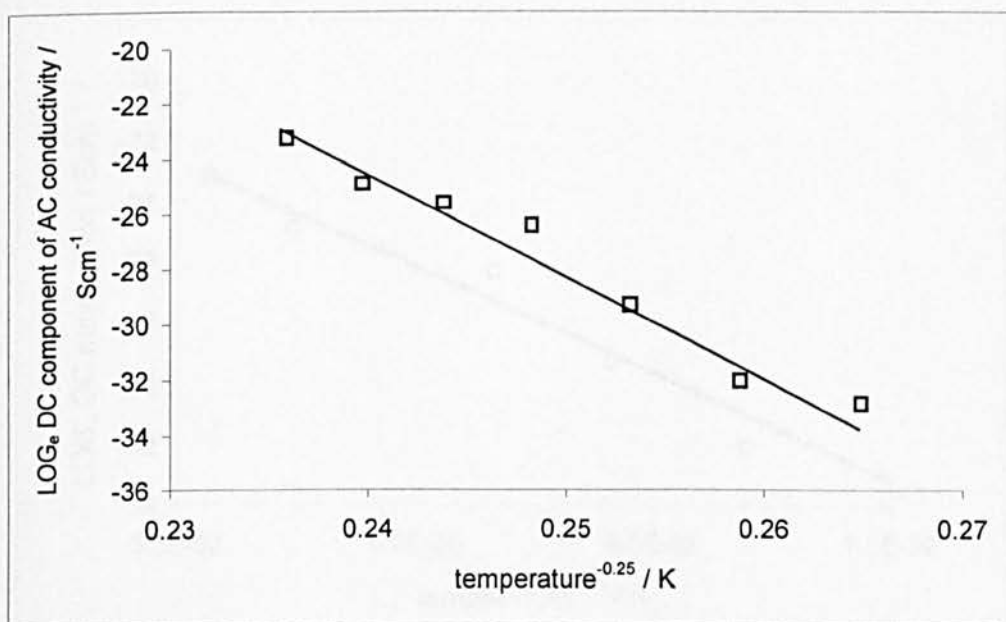
FIGURE 7.6

THE $T^{-1/4}$ TEMPERATURE DEPENDENCE OF THE PURE DC CONDUCTIVITY FOR POLY(3-METHYLTHIOPHENE)

7.2.3 BARRIER TUNNELLING

Sheng's thermal fluctuation-induced tunnelling model of conduction has been successfully applied to poly(p-phenylene) [96]. The theory proposes highly conducting (or metallic) islands surrounded by less conducting regions through which the charge carriers must tunnel. The insulating regions therefore act as barriers, and the charge carriers must overcome them. There is an effective activation energy of δE and barrier width W_b. The associated DC conductivity is:

$$\sigma_{DC}(T) = \sigma_0 \exp\left(\frac{-T_0}{T}\right)^{\frac{1}{2}}$$

EQUATION 7.3

where $T_0 = \dfrac{\delta E}{k}$ and $W_b = \dfrac{T_0\left(\dfrac{h}{2\pi}\right)}{2T\sqrt{2m_e\,\delta E}}$

m_e represents the electronic mass.
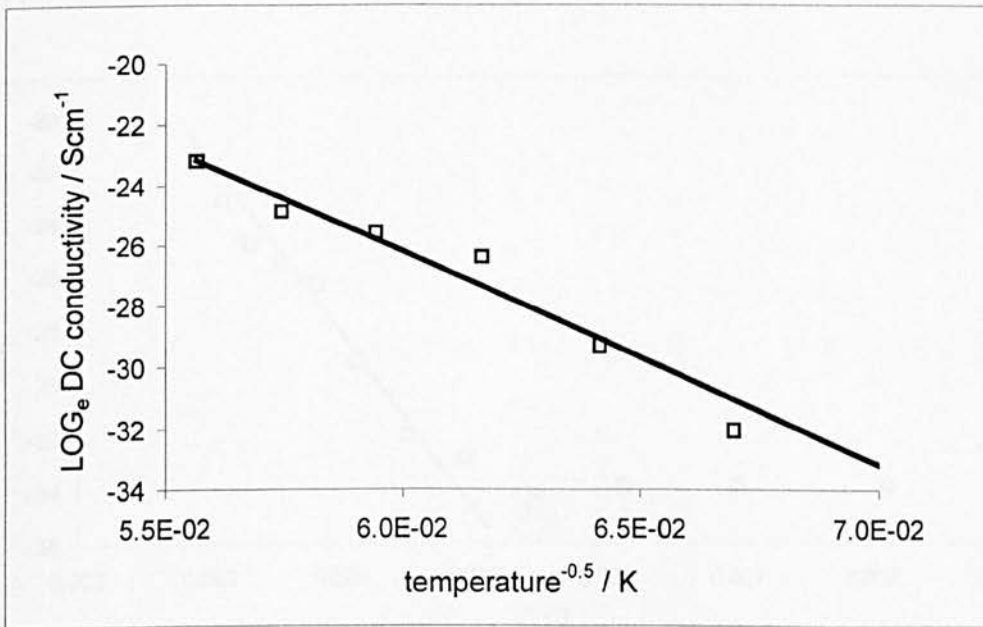
FIGURE 7.7

THE FITTING OF THE DC CONDUCTIVITY TO SHENG'S THERMAL FLUCTUATION – INDUCED TUNNELLING THEORY FOR POLY(3-METHYLTHIOPHENE)

A slope of –697.24 was obtained for the low temperature sample plot (Figure 7.7) measured between 183-123K, yielded an impossibly high energy barrier height of 41.9eV. The unusually high barrier height was not corroborated by Vakiparta *et al* [97] whose calculation for poly(3-hexylthiophene) gave a barrier height of 0.3eV at 359K and 0.53eV at 193K. This appears to indicate a lack of fitting to Sheng's model for poly(3-methylthiophene).

7.2.4   POLARON HOPPING

Polaron hopping has an activation energy, W_2 and is represented by the following relationship to the DC conductivity:

$$\sigma_{DC}(T) = A \; \exp\left(\frac{-W_2}{kT}\right)$$

EQUATION 7.5

By plotting the $\log_e$ of the DC component of the AC conductivity against 1/T, the activation, W_2 for the process can be determined (Figure 7.8).

FIGURE 7.8

THE T^{-1} TEMPERATURE DEPENDENCE OF THE PURE DC CONDUCTIVITY FOR POLY(3-METHYLTHIOPHENE)

At temperatures between 323K-183K, a good fit to the polaron hopping model is obtained from the linear region in figure 7.8, yielding an activation energy, W_2 of 0.48eV for polaron hopping conduction. As the temperature decreases below 183K, the plot becomes non-linear and the conductivity is not temperature dependent. This is in agreement with data published by Marchant, who notes a bipolaron bandwidth of 0.055eV, a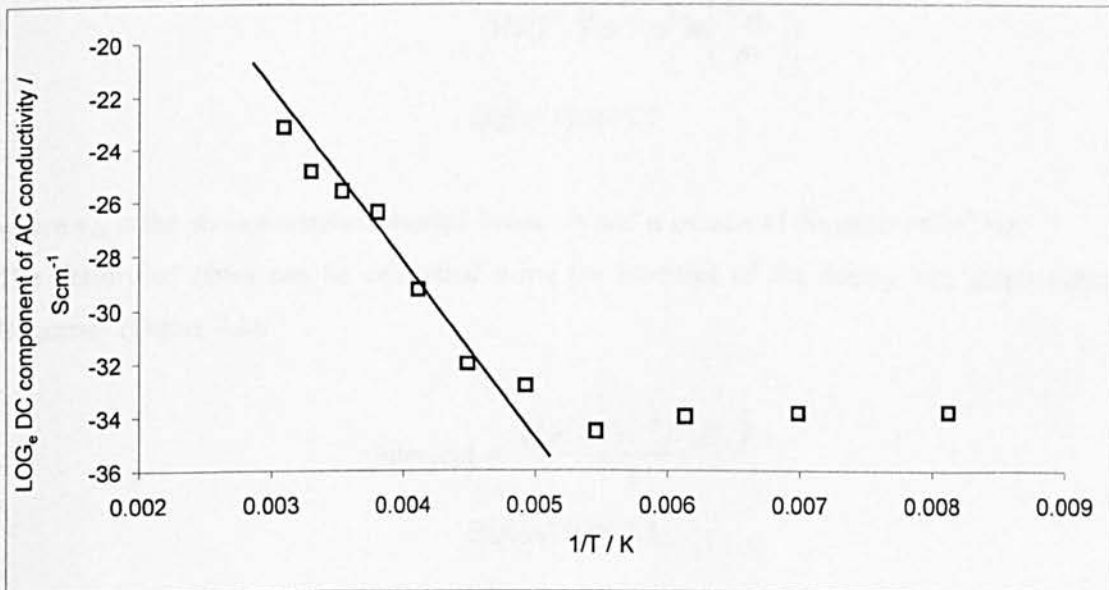nd points out that this value is in agreement with the absorption band width of the two polaronic states of doped poly(3-hexylthiophene) films, indicating that the polaron bandwidth is very narrow.

7.3   AC CONDUCTIVITY

7.3.1   VARIABLE RANGE HOPPING

The AC conductivity for variable range hopping is described by equation 7.1. The calculation of the density of states and dependence of the exponents s on the frequency and n on the temperature allow a comparison of established models of hopping [98] have determined that hopping near the Fermi Level is described by equation 7.7.

$$\sigma_{AC}(\omega, T) = \frac{\pi e^2 kT}{3N(E_F)^2 \alpha^{-5} \omega \left[\ln\left(\frac{\upsilon_{ph}}{\omega} \right) \right]}$$

EQUATION 7.7

where υ_{ph} is the phonon-assisted attempt frequency and is usually of the order of 10^{12}Hz.

The density of states can be calculated using the intercept of the doubly $\log_e$ graph against frequency (Figure 7.2):

$$\text{intercept} = \frac{\pi^2 e^2 kT \alpha^{-5} N(E_F)}{3}$$

EQUATION 7.8

At 123K, the density of states was calculated to be 1.9×10^{58} $J^{-2}cm^{-3}$ or $1.1 \times 10^{29} eV^{-1}cm^{-3}$. This value for $N(E_F)$ is approximately 10^4 times greater than that calculated from the DC conductivity, but is in good agreement with calculations using Durham polyacetylene [99].

A possible reason for this discrepancy is that the DC conductivity measurements are not as sensitive to the hopping mechanisms as AC conductivity, since the charge carriers do not have enough time to relax in their localised states as they pass through the material.

7.3.2   BARRIER HOPPING

This model predicts that the frequency exponent, s will decrease linearly as the temperature increases according to equation 7.9:
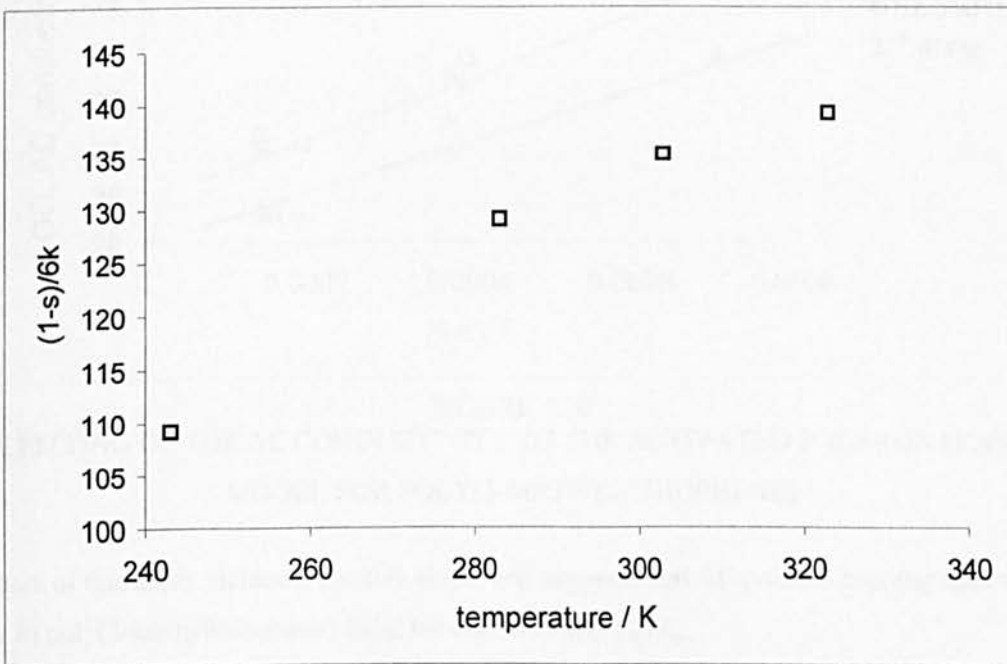
$$1 - s = \frac{6kT}{W_h}$$

EQUATION 7.9

FIGURE 7.9

THE FITTING OF THE AC CONDUCTIVITY TO THE BARRIER HOPPING MODEL FOR POLY(3-METHYLTHIOPHENE)

Calculation of the barrier height based on figure 7.9 gives a barrier height of 2.6eV, and suggests that this model does not describe the charge transport within this temperature range.

7.3.3 ACTIVATED POLARON HOPPING MODEL

The AC conductivity on the polaron hopping model can be described by the expression:

$$\sigma_{AC}(\omega, T) \propto \omega^s \exp\left(\frac{-W_2(1-s)}{kT}\right)$$

By plotting $\log_e \sigma_{AC}$-($s \log_e \omega$) against 1-s/T, a negative linear slope indicates the activation energy, W_2 (Figure 7.10).
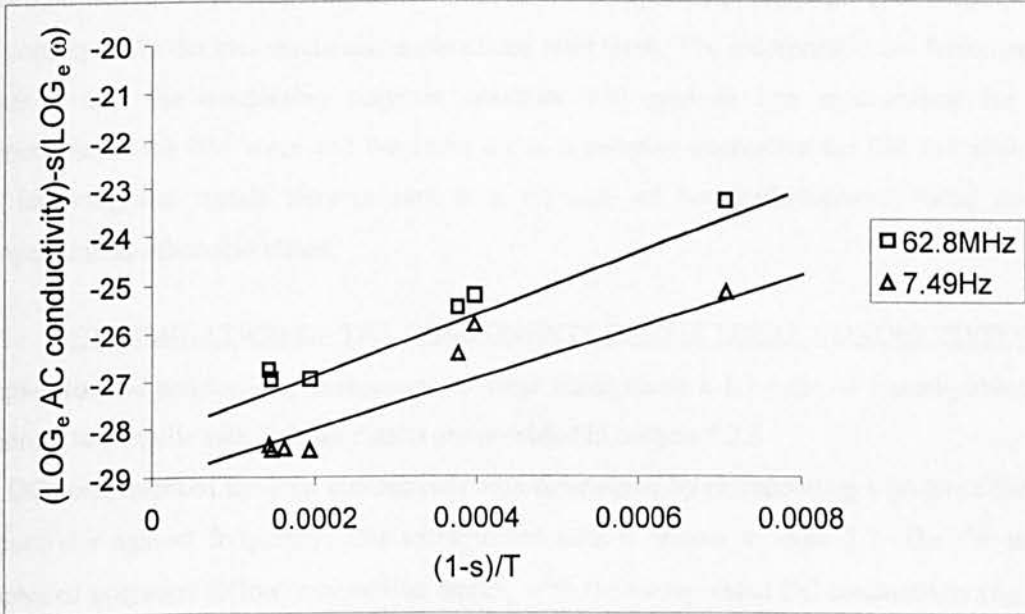
FIGURE 7.10

THE FITTING OF THE AC CONDUCTIVITY TO THE ACTIVATED POLARON HOPPING MODEL FOR POLY(3-METHYLTHIOPHENE)

The data of this study yielded a positive slope, and suggests that AC polaron hopping does not occur in poly(3-methylthiophene) films between 323 and 123K.

7.3.4 SUMMARY OF ELECTRONIC CONDUCTION MODELLING FOR PURE POLY(3-METHYLTHIOPHENE)

The data of this study appears to fit a variable range hopping theory at low temperatures (<250K). As the temperature increases to 183K, the conduction mechanism deviates to an activated process where the charge carriers overcome a barrier of 0.48eV. This energy barrier is consistent with the bi(polaronic) states observed in the UV-visible spectrophotometry, and may be due to the excitation of a valance band electron to the bi(polaron) state.

7.4   COMPLEXED POLY(3-METHYLTHIOPHENE) POLYMERS

The dissipation of the electromagnetic wave when incident upon a surface is dependent on the presence of loss mechanisms for $\bar{E}$ and $\bar{B}$; the more loss mechanisms that are available, the more rapidly the EM wave is attenuated. These loss mechanisms are mainly conductivity dependent, and hence a study of the electronic properties of these materials will aid in the design and selection of the loss mechanisms most appropriate for their use. Most modern materials concerned with this EM scattering concentrate on the dissipation of either the $\bar{E}$ or B component, and consequently the loss mechanisms associated with them. The incorporation of ferromagnetic metals within the conducting polymer structure will provide loss mechanisms for both components of the EM wave and therefore act as a superior alternative for EM radiation loss. The ferromagnetic metals were present in a 1:1 ratio of 3-methylthiophene: metal ion and undoped unless otherwise stated.

7.4.1   DETERMINATION OF THE COMPONENTS OF THE TOTAL CONDUCTIVITY

Samples for the conductivity measurements were made using a 1:1 ratio of 3-methylthiophene monomer to metallic salt. Further details are provided in section 5.2.5

The DC component of the total conductivity was determined by extrapolating a graph of the total conductivity against frequency. The extrapolated data is shown in table 7.2. The Co and Ni complexed polymers follow very similar trends, with the extrapolated DC conductivity (σ_{DCC}) of the Ni complexed polymer at constant temperature being 2.08×10^{-4} Scm^{-1} and the Co complexed polymer 2.14×10^{-5} Scm^{-1}.

	Ni	Fe	Co
σ_{DCC}(this work)/Scm^{-1}	2.08×10^{-4}	2.52×10^{-5}	2.14×10^{-5}
σ_{DC} [100]	7.32×10^{-6}	-	-
σ_{DC} [101]	1.30×10^{-4}	-	3.40×10^{-5}

TABLE 7.2

TABLE COMPARING THE DC COMPONENT OF THE TOTAL CONDUCTIVITY FROM THIS WORK WITH THE DC CONDUCTIVITY OF OTHER RESEARCHERS

The extrapolated data, σ_{DCC} is compared to the Van der Pauw DC four probe conductivity measurements carried out by Budd (σ_{DC}) [101].

The conductivities of both Ni and Co complexed polymers are independent of frequency to 1×10^6 Hz, and then show a linear increase as the frequency increases to 1.8×10^9 Hz.

The Fe complexed polymer shows a different conductivity-frequency relationship, and this shown in Figure 7.11.
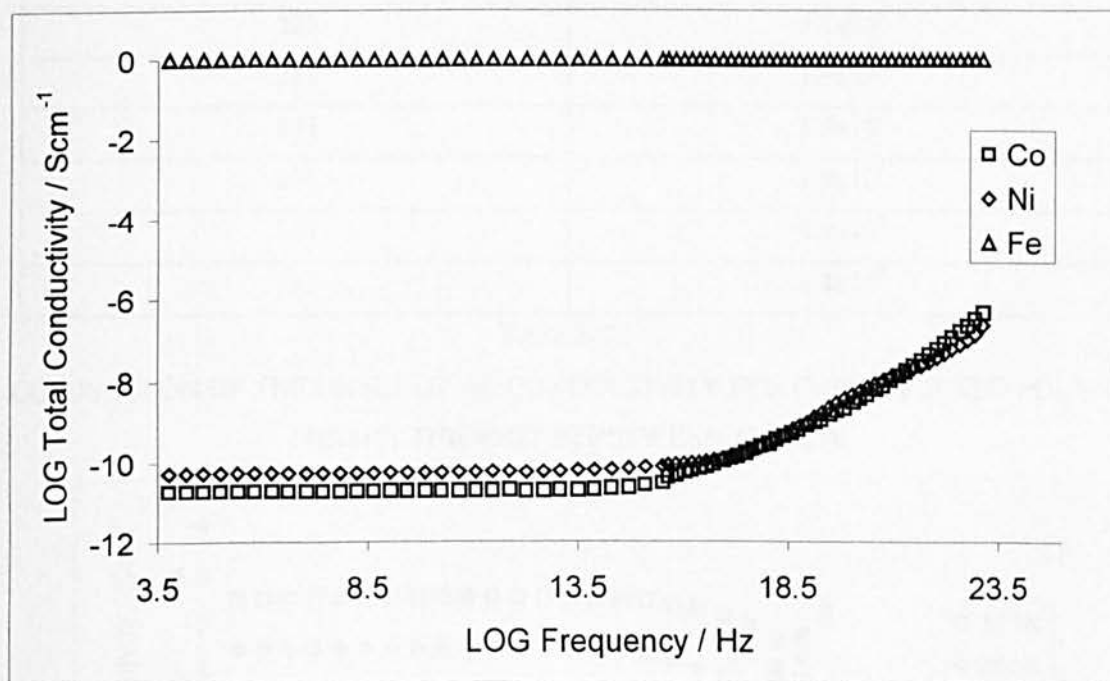

FIGURE 7.11

THE FREQUENCY DEPENDENCE OF THE TOTAL CONDUCTIVITY FOR Co, Ni AND Fe COMPLEXED POLY(3-METHYLTHIOPHENE)

7.4.2   Co COMPLEXED POLY(3-METHYLTHIOPHENE) POLYMERS

The cobalt complexed material clearly shows a hopping mechanism for the conductivity as the conductivity increases based on the schematic plot described in section 3.3.2.6. The onset of the ω^s behaviour occurs at a progressively lower frequency as the temperature decreases, as shown in Table 7.3, and Figure 7.12a and therefore becomes less of a contribution to the total conductivity of the material as the temperature decreases. Figure 7.12b shows the relationship of the total conductivity and the linear frequency at 323K.

The complexation of a Co ion within the polymer chain instigates a sharp dependence on the frequency (and thus a ω^s-type behaviour for the conductivity) between 323K-123K, in

comparison to the non-complexed poly(3-methylthiophene), which shows a gradual increase in the total conductivity as the frequency increases and a contribution from both the AC and DC mechanisms to the overall conductivity.

Temperature / K	Onset of ω^s behaviour / Hz
323	3.1×10^5
283	1.6×10^5
243	3.9×10^4
203	1.9×10^4
163	4.9×10^3
123	2.4×10^3

TABLE 7.3

COMPARISON OF THE ONSET OF AC CONDUCTIVITY FOR Co COMPLEXED POLY(3-METHYLTHIOPHENE) BETWEEN 123-323K
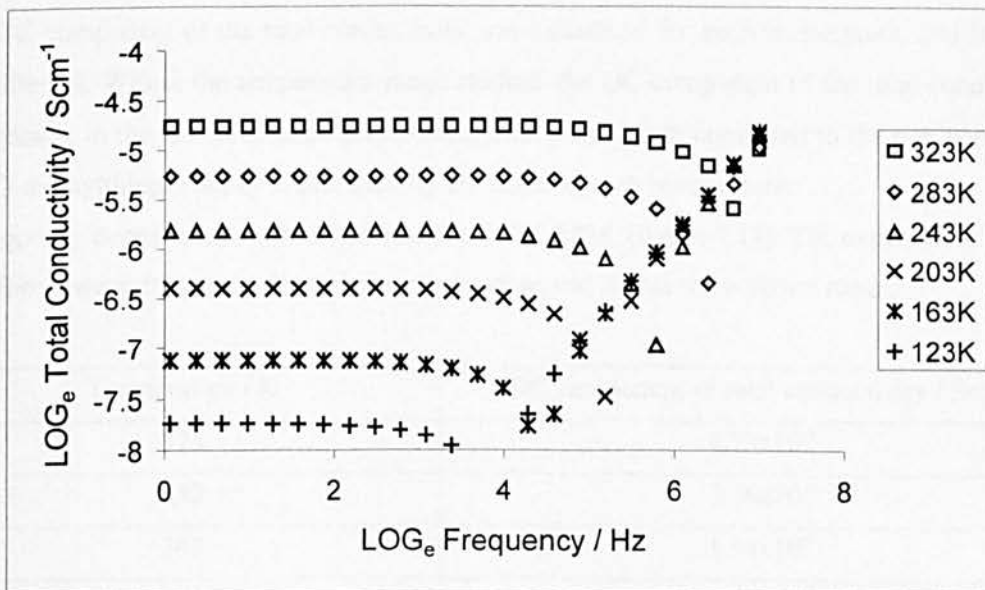

FIGURE 7.12a

THE FREQUENCY DEPENDENCE OF THE TOTAL CONDUCTIVITY AT VARIOUS TEMPERATURES OBTAINED BY SUBTRACTING THE DC COMPONENT FROM THE TOTAL CONDUCTIVITY FOR Co COMPLEXED POLY(3-METHYLTHIOPHENE)
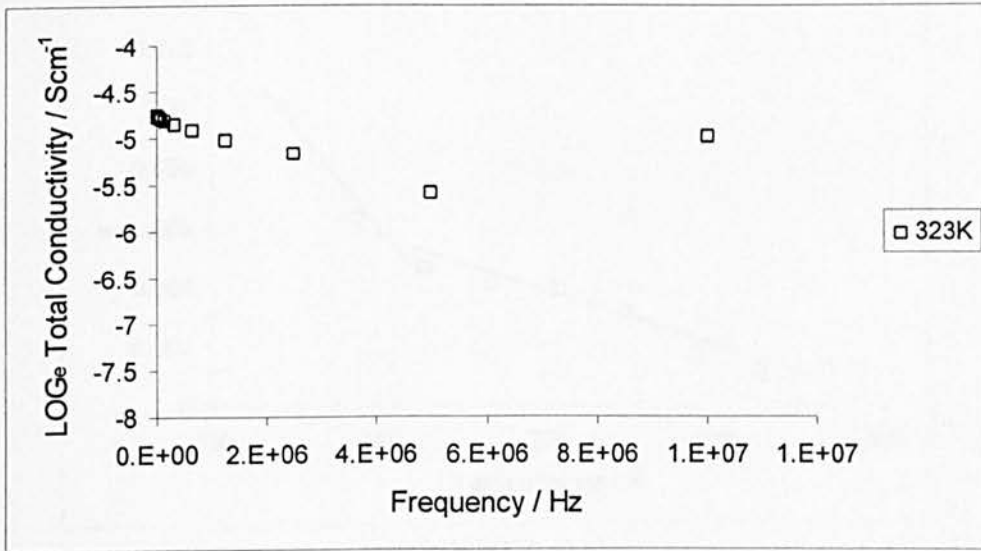
FIGURE 7.12b

THE FREQUENCY DEPENDENCE OF THE TOTAL CONDUCTIVITY AT 323K FOR Co

COMPLEXED POLY(3-METHYLTHIOPHENE)

The DC component of the total conductivity was calculated for each temperature, and is shown in Table 7.4. Within the temperature range studied, the DC component of the total conductivity was greater in the Co complexed poly(3-methylthiophene) film compared to the non-complexed poly(3-methylthiophene) by approximately 10^6 times at each temperature.

A frequency dependence is observed between 143K-283K (figure 7.13). The exponent s<<1, and therefore a weak frequency dependence can be observed in this temperature range.

Temperature / K	DC component of total conductivity / Scm^{-1}
323	1.73×10^{-5}
283	5.56×10^{-6}
243	1.54×10^{-6}
203	3.96×10^{-7}
143	7.6×10^{-8}
123	1.85×10^{-8}

TABLE 7.4

TABLE SHOWING THE DC COMPONENT OF THE TOTAL CONDUCTIVITY FOR Co
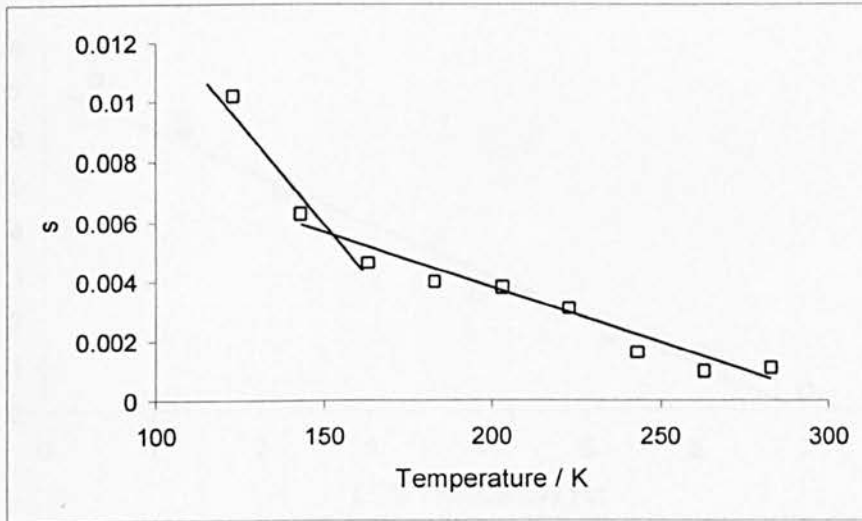
COMPLEXED POLY(3-METHYLTHIOPHENE)

FIGURE 7.13

THE TEMPERATURE DEPENDENCE OF THE EXPONENT s FOR Co COMPLEXED

POLY(3-METHYLTHIOPHENE)

The temperature dependent exponent n was calculated from the slope of $\log_e$ of the AC component of the total conductivity against $\log_e$ T at constant frequency (Figure 7.14). Some temperature dependence is observed over the entire frequency range studied (Figure 7.15).
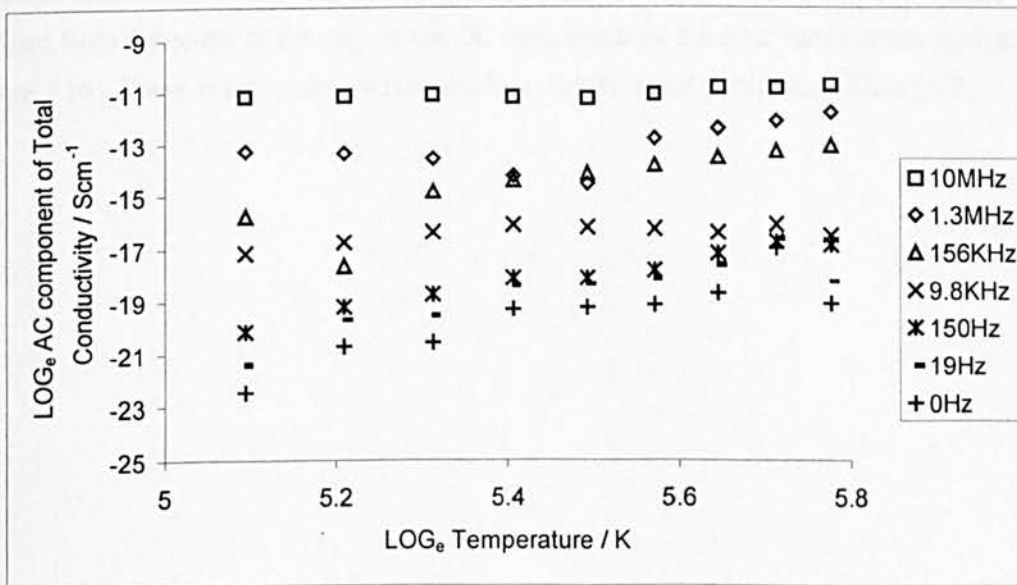

FIGURE 7.14

THE TEMPERATURE DEPENDENCE OF THE AC CONDUCTIVITY AT DIFFERENT

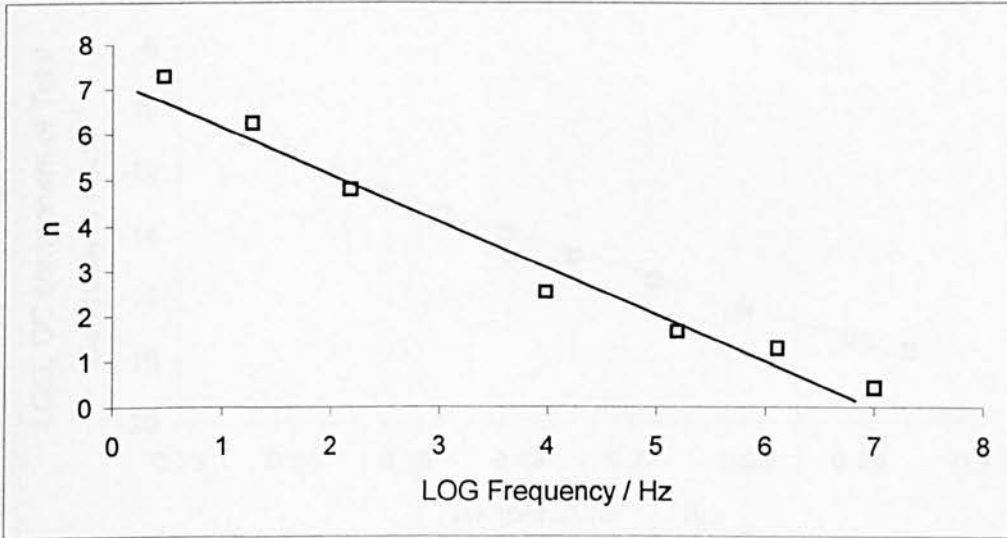FREQUENCIES FOR Co COMPLEXED POLY(3-METHYLTHIOPHENE)

FIGURE 7.15

THE FREQUENCY DEPENDENCE OF THE EXPONENT n FOR Co COMPLEXED POLY(3-
METHYLTHIOPHENE)

7.4.2.1 HOPPING IN STATES NEAR E_F

At ambient temperatures, the density of states at E_F for undoped poly(3-hexylthiophene) was estimated by Marchant to be of the order of 3.2×10^{25} eV^{-1}cm^{-3}. A value of 1.8×10^{22} eV^{-1}cm^{-3} was obtained from the slope of the $\log_e$ of the DC component of the total conductivity against $T^{-0.25}$ (Figure 7.16). These values compare favourably to lightly doped polypyrrole films [102].
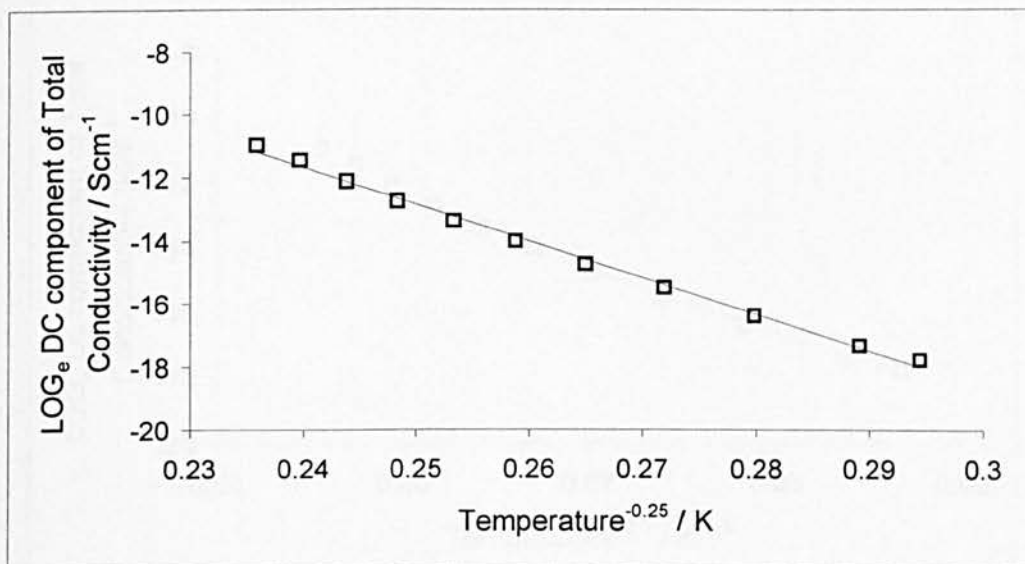
FIGURE 7.16

THE $T^{-1/4}$ TEMPERATURE DEPENDENCE OF THE PURE DC CONDUCTIVITY FOR Co
COMPLEXED POLY(3-METHYLTHIOPHENE)

7.4.2.2 BARRIER TUNNELLING

A straight line graph of $\log_e$ DC component of the total conductivity against $T^{-0.5}$ was obtained (Figure 7.17), with a slope of −274.1 over the temperature range 123K to 223K and a correlation coefficient of 0.997. The slope of the graph represents $T_0^{1/2}$, and the energy of the barrier δE was calculated to be 0.02eV. The barrier width was estimated to be 2.5nm at 300K and 2.3nm at 123K indicating that the barrier width is not temperature dependent. The complexation of Co produces a closer fit to the barrier tunneling model at 300K compared to the non complexed polymer.
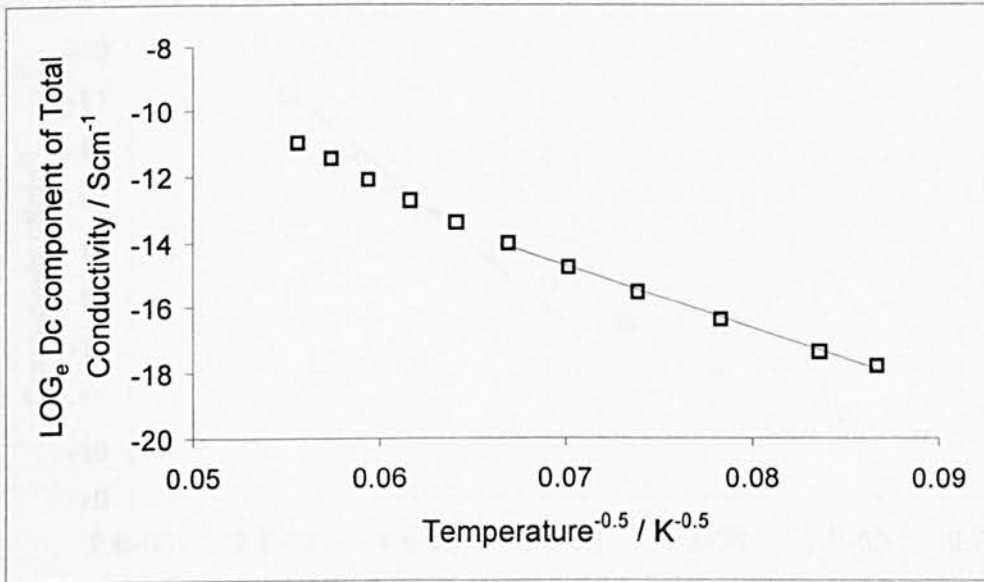
FIGURE 7.17

THE FITTING OF THE DC CONDUCTIVITY TO SHENG'S THERMAL FLUCTUATION–
INDUCED TUNNELLING THEORY FOR Co COMPLEXED POLY(3-
METHYLTHIOPHENE)

7.4.2.3 POLARON HOPPING

A linear plot was approximated for $\log_e$ of the DC component of the total conductivity against T^{-1} between 323K and 123K (Figure 7.18), yielding a slope of –2389.2 between 323-243K. A value of 0.21eV was calculated for the activation energy for polaron hopping. It was observed that as the temperature decreased, there was an increasing deviation from the linear curve fitting, indicating that the polaron hopping became less of a contributory factor in the overall conductivity of the material, and that the polaron defect bandwidth is indicative of a narrow band.

FIGURE 7.18

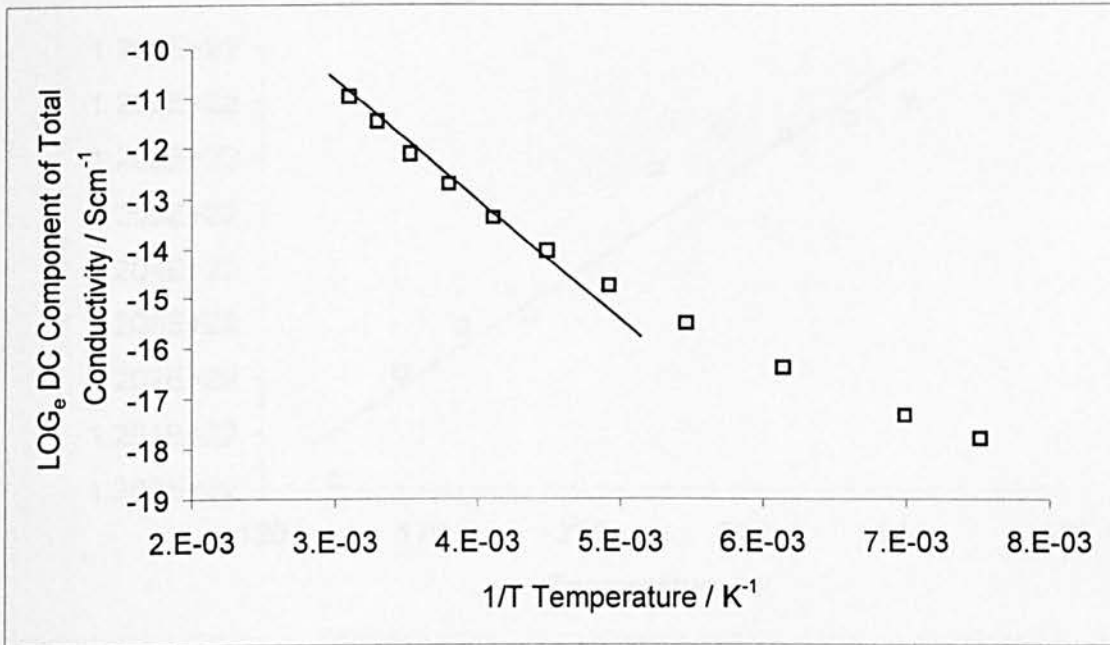THE T^{-1} TEMPERATURE DEPENDENCE OF THE PURE DC CONDUCTIVITY FOR Co
COMPLEXED POLY(3-METHYLTHIOPHENE)

7.4.2.4 ACTIVATED BARRIER HOPPING

The Co complexed poly(3-methylthiophene) does not show a linear relationship derived from
equation 7.9 over the temperature range 123K to 323K (Figure 7.19), since the exponent s<<1,
and shows a temperature dependence over the entire frequency range studied.
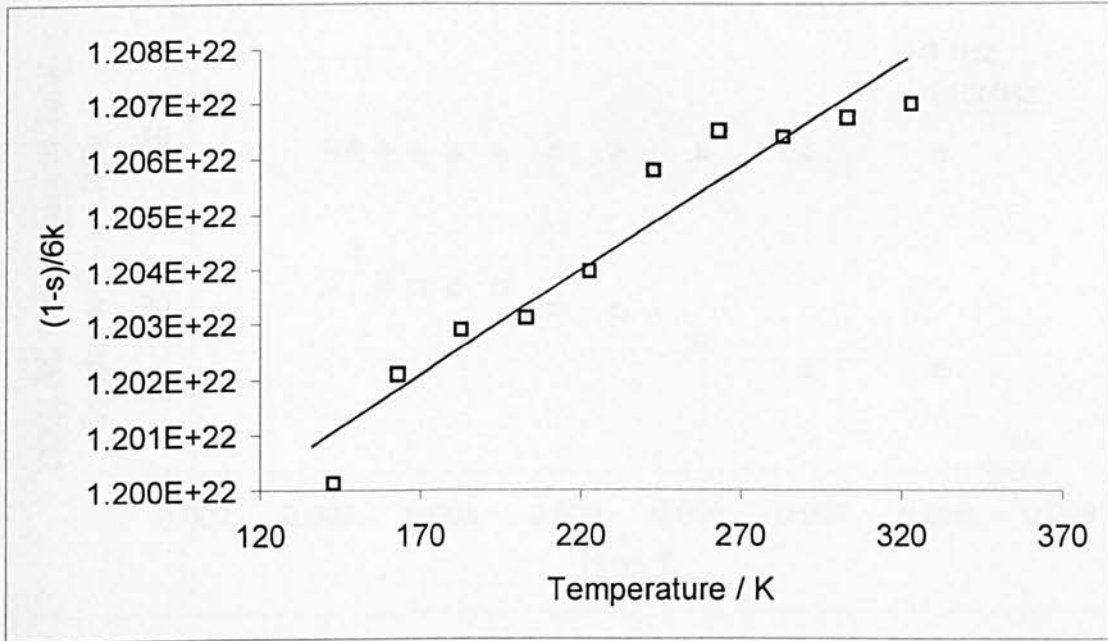
FIGURE 7.19

THE FITTING OF THE AC CONDUCTIVITY TO THE BARRIER HOPPING MODEL FOR

Co COMPLEXED POLY(3-METHYLTHIOPHENE)

7.4.2.5 ACTIVATED POLARON HOPPING MODEL

By plotting $\log_e \sigma_{AC} - s \log_e(\omega)$ against $(1-s)/T$, a straight line plot will indicate the activation energy W_2. The graph obtained is shown in Figure 7.20, and a negative slope is obtained at both frequencies indicating a lack of fitting to this model.
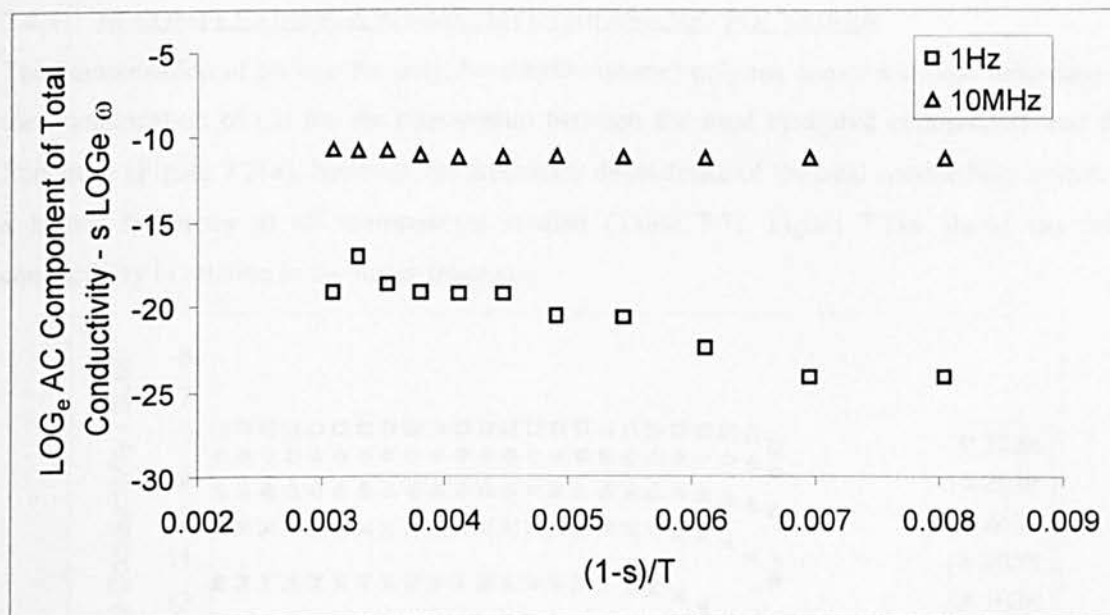
FIGURE 7.20

THE FITTING OF THE AC CONDUCTIVITY TO THE ACTIVATED POLARON HOPPING
MODEL FOR Co COMPLEXED POLY(3-METHYLTHIOPHENE)

7.4.2.6 SUMMARY OF ELECTRONIC CONDUCTION MODELLING IN Co COMPLXED POLY(3-METHYLTHIOPHENE)

The data suggests that charge transfer occurs by variable-range hopping over the entire temperature range studied (323-123K), but deviates from a $T^{-1/2}$ dependence at low temperatures (<223K) where the insulating barrier height was calculated to be 0.02eV and the barrier width 2.3nm 123K. As the temperature increases above 223K, polaron hopping becomes the main charge transfer process with an activation energy of 0.21eV as the polarons are no longer localized.

7.4.3 Ni COMPLEXED POLY(3-METHYLTHIOPHENE) POLYMERS

The complexation of Ni into the poly(3-methylthiophene) polymer shows a similar behaviour to the complexation of Co for the relationship between the total measured conductivity and the frequency (Figure 7.21a), however, the frequency dependence of the total conductivity occurs at a higher frequency at all temperatures studied (Table 7.5). Figure 7.21b shows the total conductivity in relation to the linear frequency.
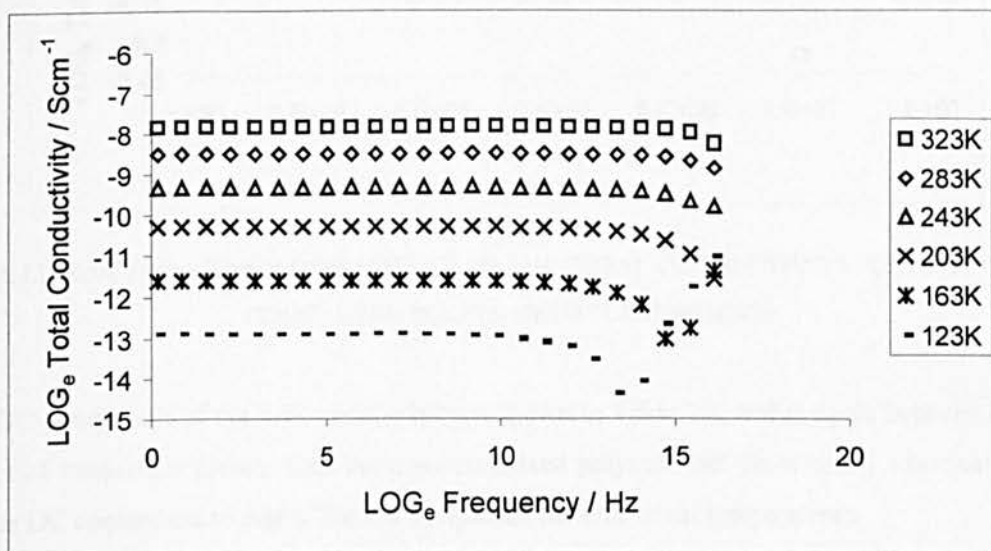
FIGURE 7.21a

THE FREQUENCY DEPENDENCE OF THE TOTAL CONDUCTIVITY AT VARIOUS TEMPERATURES OBTAINED BY SUBTRACTING THE DC COMPONENT FROM THE TOTAL CONDUCTIVITY FOR Ni COMPLEXED POLY(3-METHYLTHIOPHENE)

Temperature / K	Onset of ω^s behaviour / Hz
323	1.0×10^7
283	5.0×10^6
243	2.5×10^6
203	2.5×10^6
163	6.3×10^5
123	1.56×10^5

TABLE 7.5

COMPARISON OF THE ONSET OF AC CONDUCTIVITY FOR Ni COMPLEXED POLY(3-METHYLTHIOPHENE) BETWEEN 123-323K
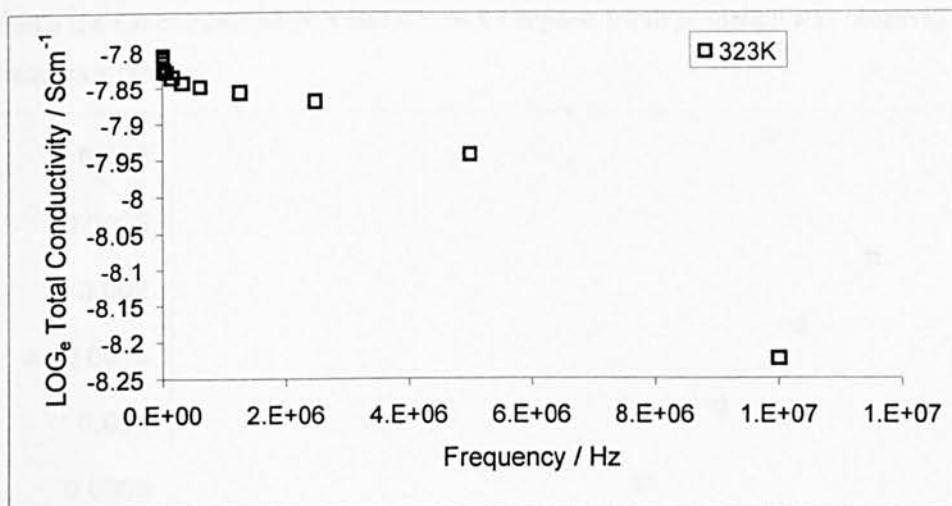
7.21b

THE LINEAR FREQUENCY DEPENDENCE OF THE TOTAL CONDUCTIVITY AT 323K FOR Ni

COMPLEXED POLY(3-METHYLTHIOPHENE)

The DC component of the total conductivity is shown in Table 7.6, and is again between 6 and 7 orders of magnitude greater than the non-complexed polymer, but gives nearly identical values for the DC component to that of the Co complexed material at all temperatures.

Temperature / K	DC Component of Total Conductivity / Scm^{-1}
323	1.7×10^{-5}
283	5.5×10^{-6}
243	1.5×10^{-6}
203	3.9×10^{-7}
163	7.6×10^{-8}
123	1.8×10^{-8}

TABLE 7.6

TABLE SHOWING THE DC COMPONENT OF THE TOTAL CONDUCTIVITY FOR Ni

COMPLEXED POLY(3-METHYLTHIOPHENE)

A weak frequency dependence is observed from 203 – 323K (Figure 7.21) since the values of s are <<1, and a temperature dependence is observed at frequencies greater than 1.3×10^6Hz (Figure

7.22) unlike the Co complexed polymer where a temperature dependence was observed over the entire frequency range.
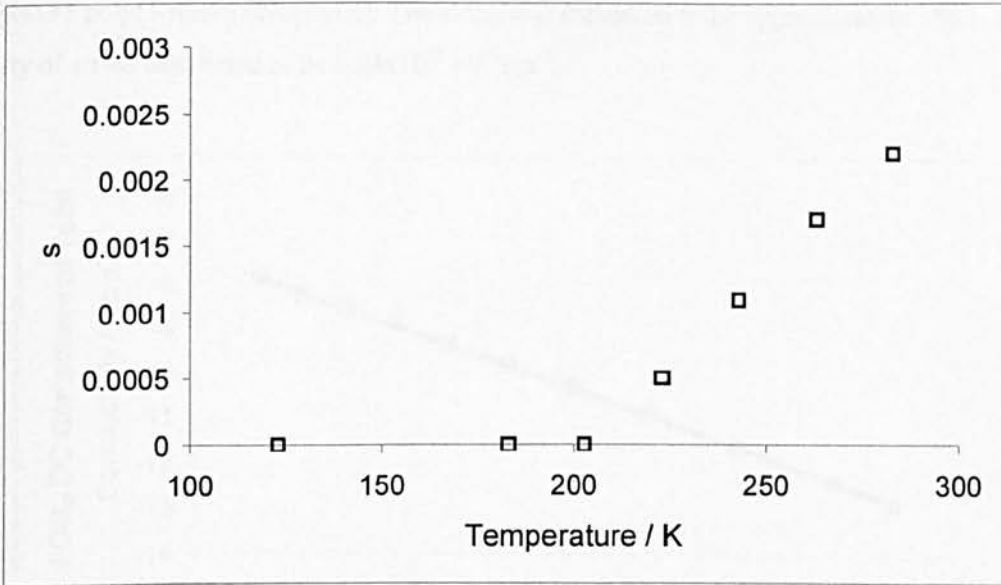

FIGURE 7.22
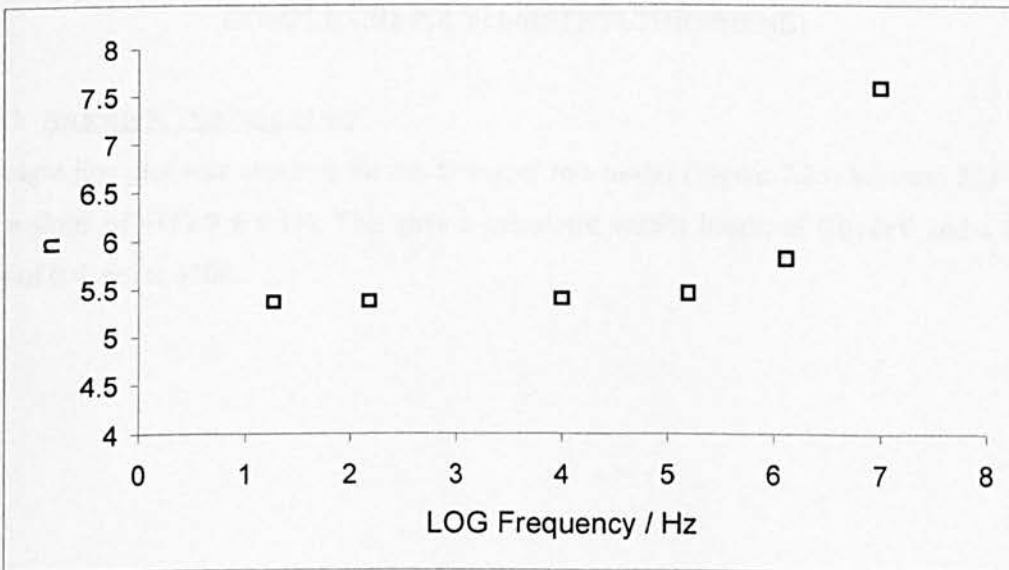THE TEMPERATURE DEPENDENCE OF THE EXPONENT s FOR Ni COMPLEXED
POLY(3-METHYLTHIOPHENE)

FIGURE 7.23
THE FREQUENCY DEPENDENCE OF THE EXPONENT n FOR Ni COMPLEXED POLY(3-
METHYLTHIOPHENE)

7.4.3.1 HOPPING IN STATES NEAR E_F

Figure 7.24 shows the temperature dependence of σ_{DC} component of the total conductivity for Ni complexed poly(3-methylthiophene). The slope was estimated to be approximately -86.1, and the density of states calculated to be 6.28×10^{22} $eV^{-1}cm^{-3}$.
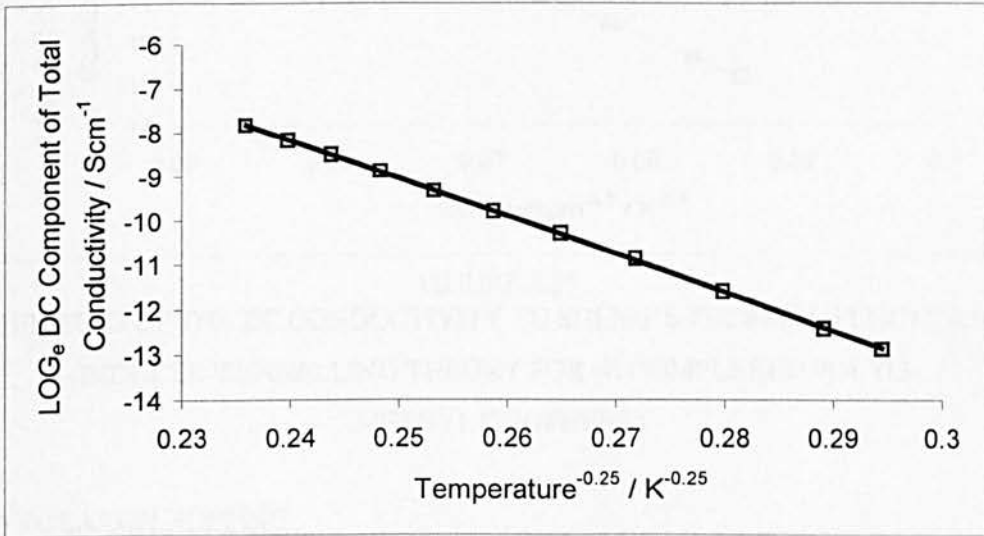

FIGURE 7.24

THE $T^{-1/4}$ TEMPERATURE DEPENDENCE OF THE PURE DC CONDUCTIVITY FOR Ni COMPLEXED POLY(3-METHYLTHIOPHENE)

7.4.3.2 BARRIER TUNNELLING

A straight-line plot was obtained for the fitting of this model (Figure 7.25) between 223-123K, with a slope of $-162.9 \pm 0.1\%$. This gave a calculated barrier height of 0.014eV and a barrier width of 0.41nm at 300K.
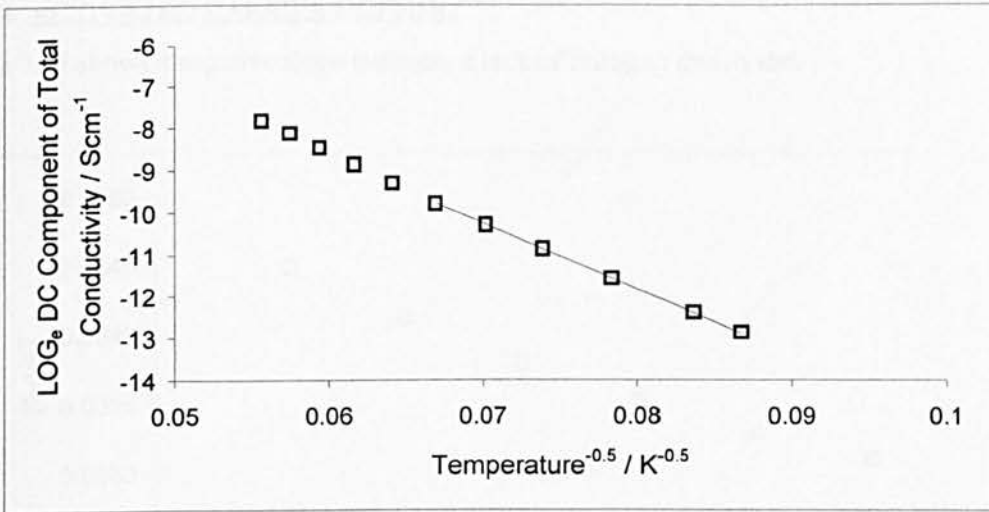
FIGURE 7.25

THE FITTING OF THE DC CONDUCTIVITY TO SHENG'S THERMAL FLUCTUATION–
INDUCED TUNNELLING THEORY FOR Ni COMPLEXED POLY(3-
METHYLTHIOPHENE)

7.4.3.3 POLARON HOPPING

A linear plot was obtained from 323K to 223K (Figure 7.26), with a slope of –1139.63 ± 0.1%.
This gave a calculated value of 0.098eV for the activation energy of the polaron hopping.
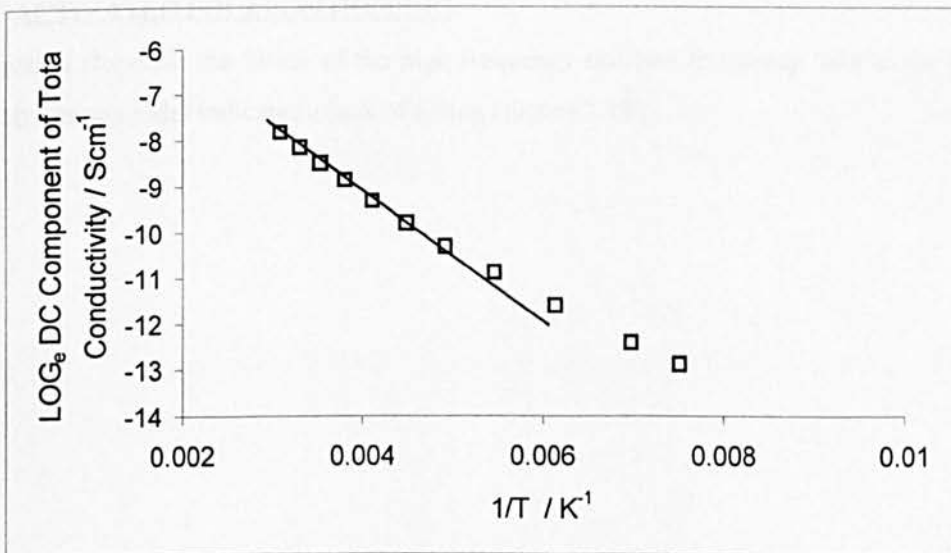
FIGURE 7.26

THE T^{-1} TEMPERATURE DEPENDENCE OF THE PURE DC CONDUCTIVITY FOR Ni
COMPLEXED POLY(3-METHYLTHIOPHENE)

7.4.3.4 ACTIVATED BARRIER HOPPING

Figure 7.27 shows a negative slope indicates a lack of fitting to this model.
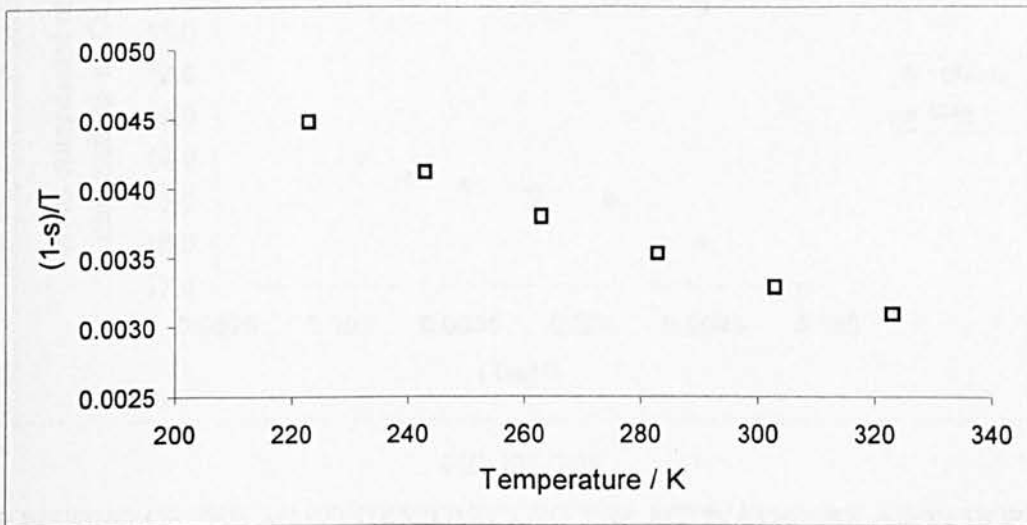

FIGURE 7.27

THE FITTING OF THE AC CONDUCTIVITY TO THE BARRIER HOPPING MODEL FOR
Ni COMPLEXED POLY(3-METHYLTHIOPHENE)

7.4.3.5 ACTIVATED POLARON HOPPING

The negative slope for the fitting of the high frequency and low frequency data to the activated
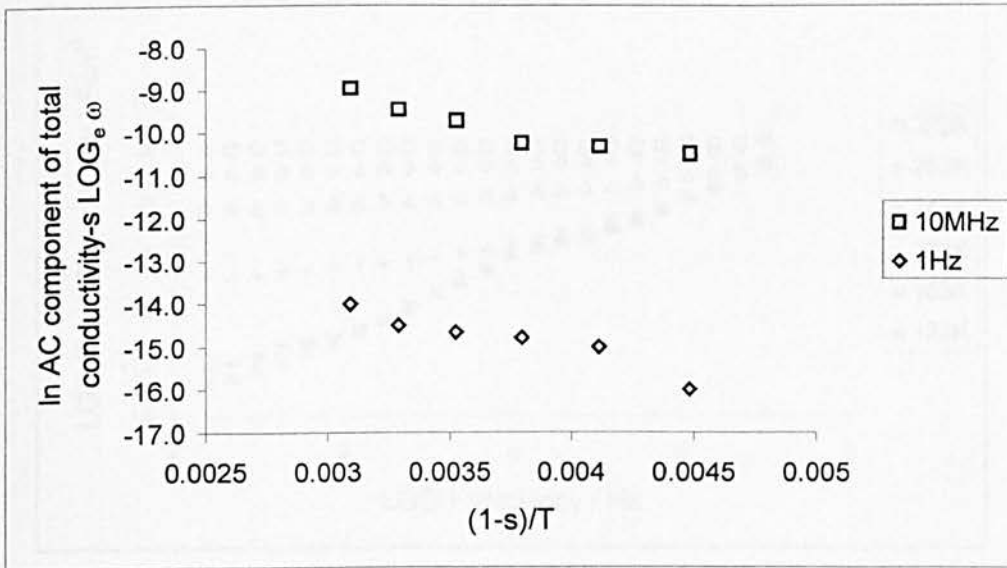polaron hopping model indicates a lack of fitting (Figure 7.28).

FIGURE 7.28

THE FITTING OF THE AC CONDUCTIVITY TO THE ACTIVATED POLARON HOPPING

MODEL FOR Ni COMPLEXED POLY(3-METHYLTHIOPHENE)

7.4.3.6 SUMMARY OF ELECTRONIC CONDUCTION MODELLING IN Ni COMPLXED POLY(3-METHYLTHIOPHENE)

The density of states was calculated to be $6.3 \times 10^{22} eV^{-1} cm^{-3}$ for hopping near E_F, with variable-range hopping occurring over the entire temperature range studied (323-123K). The barrier tunnelling model gave a barrier height of 0.01eV and barrier width of 0.41nm at 300K, and appears to contribute to charge transfer between 123-223K. Polaron hopping also contributed to the conductivity with a small activation energy of ~0.1eV at higher temperatures (323-223K).

7.4.4 Fe COMPLEXED POLY(3-METHYLTHIOPHENE) POLYMERS

The combined AC and DC conductivities of Fe complexed P3MT appears to remain essentially frequency independent above 243K, below which a considerable frequency dependence is observed and increasingly so as the temperature is decreased to 123K (Figure 7.29).
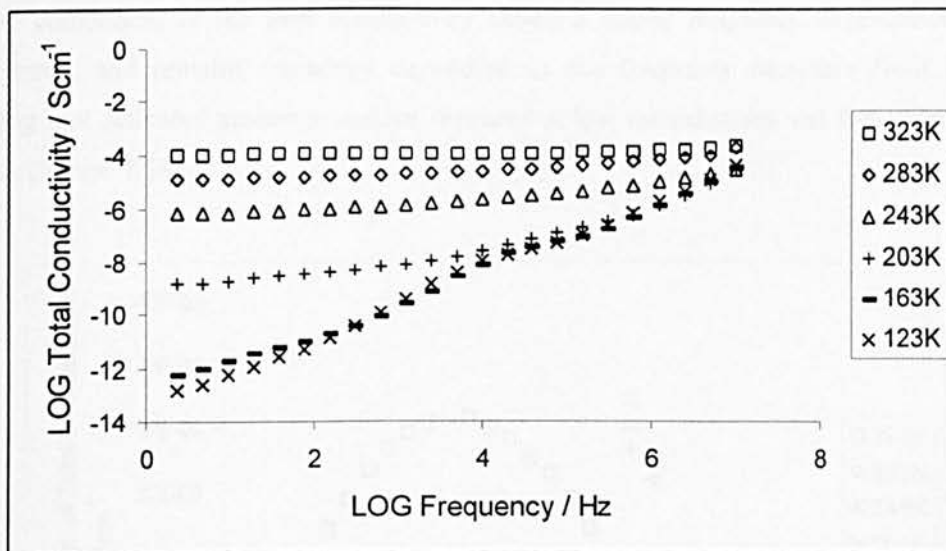
FIGURE 7.29
THE FREQUENCY DEPENDENCE OF THE TOTAL CONDUCTIVITY AT VARIOUS
TEMPERATURES OBTAINED BY SUBTRACTING THE DC COMPONENT FROM THE
TOTAL CONDUCTIVITY FOR Fe COMPLEXED POLY(3-METHYLTHIOPHENE)

The extrapolated DC conductivities are shown in table 7.7, which show a much lower DC component of the total conductivity compared to the Co and Ni complexed polymers below 243K.

Temperature / K	DC Component of Total Conductivity / Scm^{-1}
323	8.6×10^{-5}
283	1.0×10^{-5}
243	5.2×10^{-7}
203	9.0×10^{-10}
163	5.8×10^{-11}
123	5.7×10^{-11}

TABLE 7.7
TABLE SHOWING THE DC COMPONENT OF THE TOTAL CONDUCTIVITY FOR Fe
COMPLEXED POLY(3-METHYLTHIOPHENE)

The AC component of the total conductivity shows a strong frequency dependence at high temperatures, and remains frequency dependent as the frequency increases from 2×10^4Hz, indicating that activated processes are not favoured at low temperatures and frequencies below 2×10^4Hz (Figure 7.30).
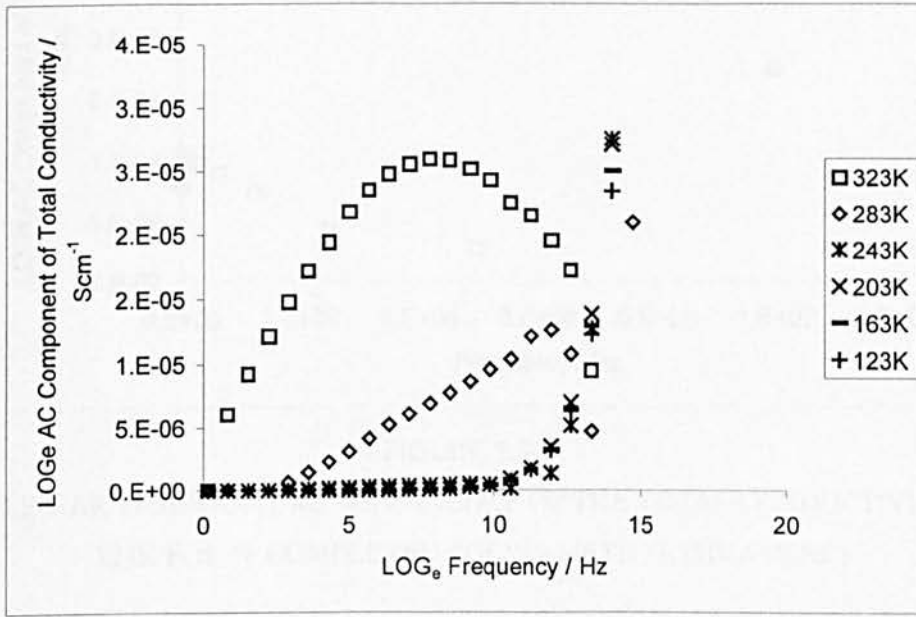
FIGURE 7.30a

THE FREQUENCY DEPENDENCE OF THE PURE AC CONDUCTIVITY AT VARIOUS TEMPERATURES, AS OBTAINED FROM FIGURE 7.31 BY SUBTRACTING THE DC COMPONENT FROM THE TOTAL CONDUCTIVITY FOR POLY(3-METHYLTHIOPHENE)

The exponent, s shows a very similar behaviour to that of the Ni complexed poly(3-methylthiophene) (Figure 7.31), indicating that there is a weak temperature dependence of the AC conductivity, predicting that variable range hopping will not contribute to the conductivity of Fe complexed poly(3-methylthiophene).
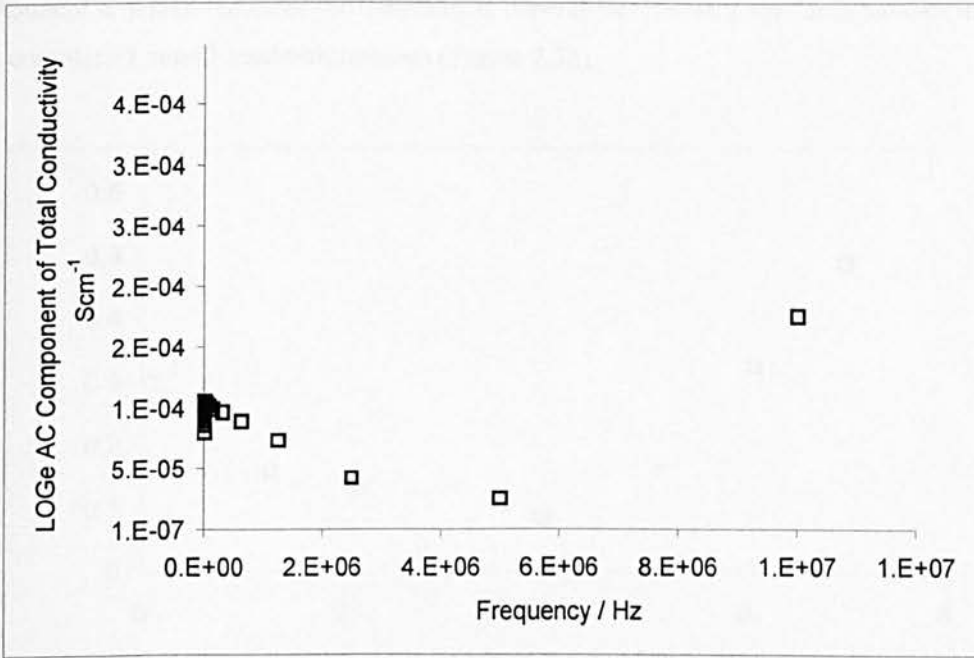
FIGURE 7.30b

THE LINEAR TEMPERATURE DEPENDENCE OF THE TOTAL CONDUCTIVITY AT
323K FOR Fe COMPLEXED POLY(3-METHYLTHIOPHENE)

FIGURE 7.31
THE TEMPERATURE DEPENDENCE OF THE EXPONENT s FOR Fe COMPLEXED
POLY(3-METHYLTHIOPHENE)

The exponent n, which indicates the temperature dependence shows a similar behaviour to that of the Ni complexed poly(3-methylthiophene) (Figure 7.32).

FIGURE 7.32

THE FREQUENCY DEPENDENCE OF THE EXPONENT n FOR Fe COMPLEXED POLY(3-METHYLTHIOPHENE)

7.4.4.1 HOPPING IN STATES NEAR E_F

Figure 7.33 shows a representation of the model used to describe hopping conduction near E_F. A calculation based on the slope of the temperature dependent region between 323K and 183K yielded a density of states of 2.5×10^{20} eV^{-1} cm^{-3}.

FIGURE 7.33

THE T$^{-1/4}$ TEMPERATURE DEPENDENCE OF THE PURE DC CONDUCTIVITY FOR Fe

COMPLEXED POLY(3-METHYLTHIOPHENE)

7.4.4.2 BARRIER TUNNELLING

Calculated barrier heights based on the slopes of Figure 7.34 yields an insulating barrier height of 0.02eV and barrier width of 1.2nm at 123K for the low temperature results (223-123K); with the high temperature (323-223K) barrier height increasing slightly to 0.023eV and barrier width decreasing to 0.54nm at 323K. The barrier width results are in agreement with Marchants data for undoped poly(3-hexylthiophene) [94], where a barrier width of 4.6nm was based on a DC conductivity of ~10^{-5} Scm^{-1} at 168K. However, the value for δE is indicative of a doped polymer [97].

7.4.4.3 POLARON HOPPING

The high temperature region based on the data obtained between 323K and 203K (Figure 7.35) yielded a barrier height of 0.52eV.
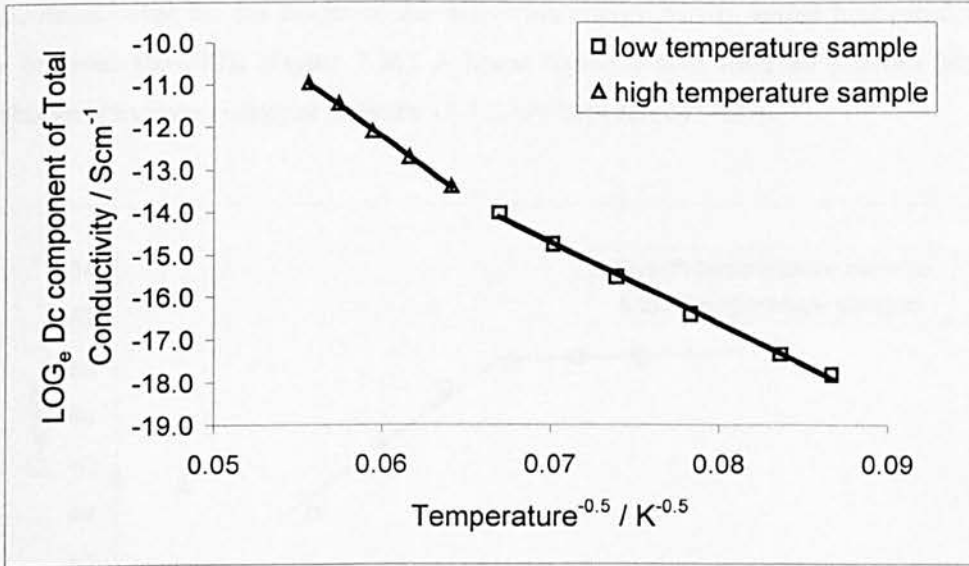
FIGURE 7.34

THE FITTING OF THE DC CONDUCTIVITY TO SHENG'S THERMAL FLUCTUATION–
INDUCED TUNNELLING THEORY FOR Fe COMPLEXED POLY(3-
METHYLTHIOPHENE)
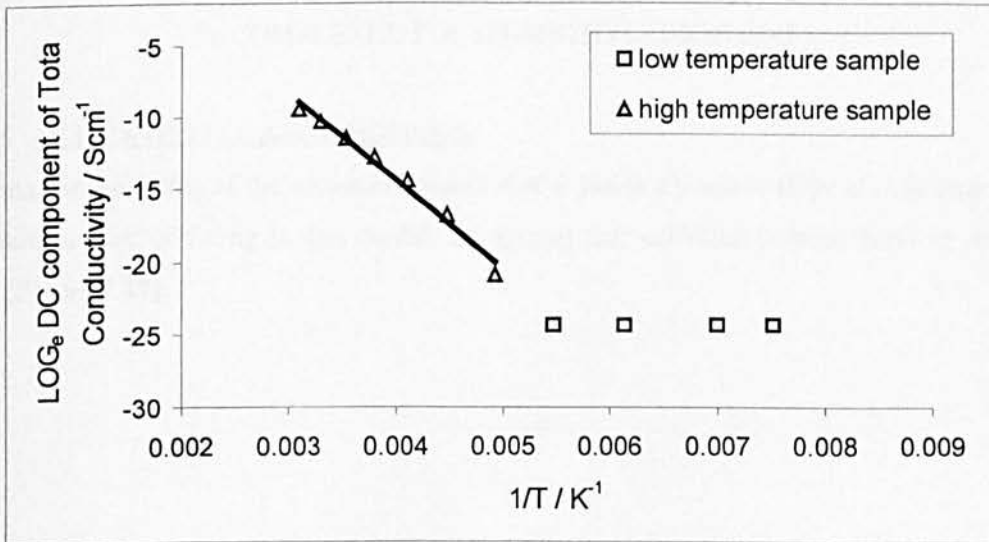
FIGURE 7.35

THE T^{-1} TEMPERATURE DEPENDENCE OF THE PURE DC CONDUCTIVITY FOR Fe
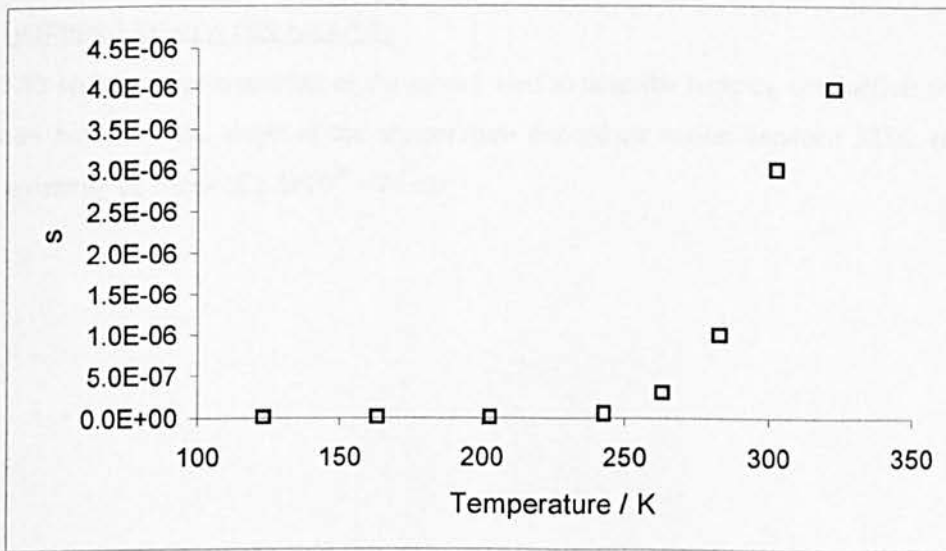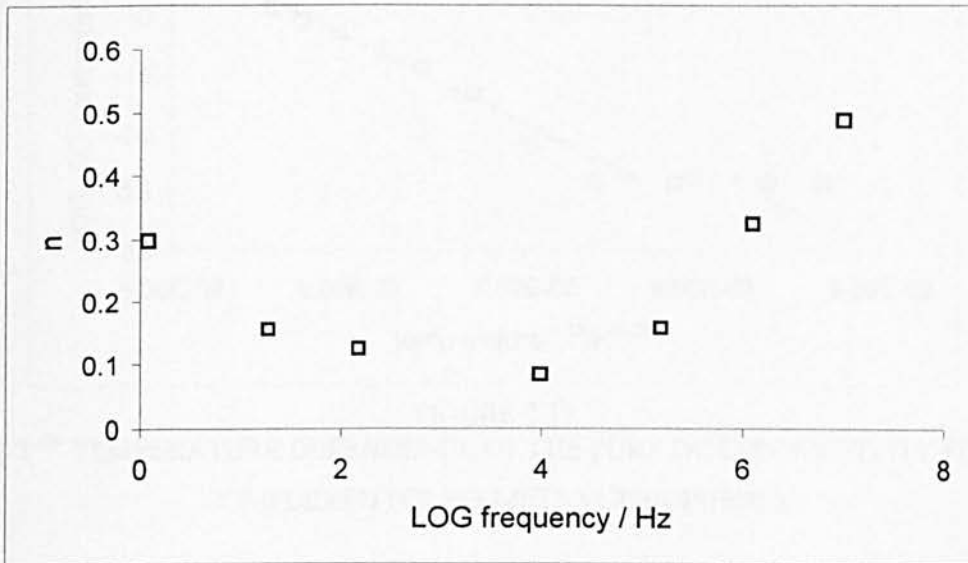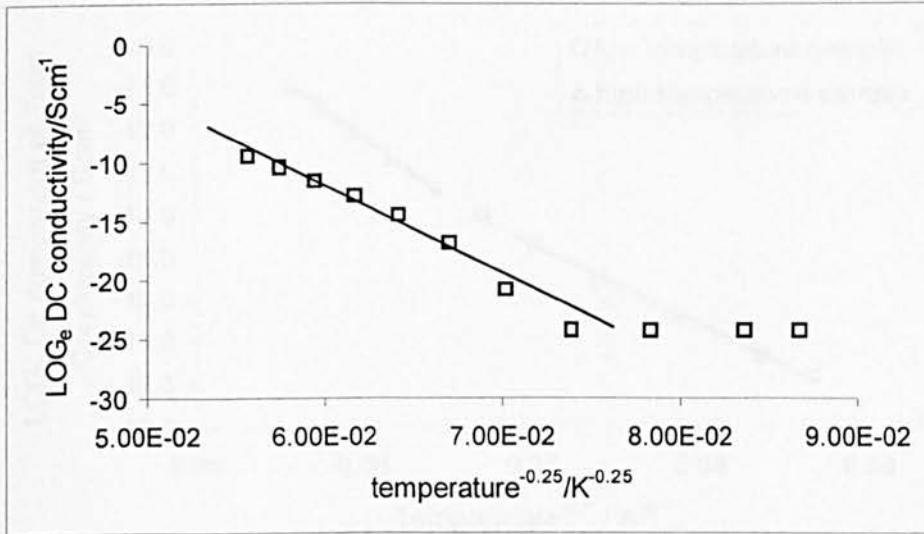COMPLEXED POLY(3-METHYLTHIOPHENE)

7.4.4.4 ACTIVATED BARRIER HOPPING

The calculated value for the height of the activation energy barrier varied between 0.45eV to 0.59eV between 183-243K (Figure 7.36). A linear region is also observed between 243-323K, and yields an activation energy of between 14.8-20eV between 243-323K.

FIGURE 7.36

THE FITTING OF THE AC CONDUCTIVITY TO THE BARRIER HOPPING MODEL FOR Fe COMPLEXED POLY(3-METHYLTHIOPHENE)

7.4.4.5 ACTIVATED POLARON HOPPING

The data for the fitting of the activated polaron model yields a positive slope at both frequencies indicating a lack of fitting to this model, suggesting that activated polaron hopping does not occur (Figure 7.37).

FIGURE 7.37

THE FITTING OF THE AC CONDUCTIVITY TO THE ACTIVATED POLARON HOPPING
MODEL FOR Fe COMPLEXED POLY(3-METHYLTHIOPHENE)

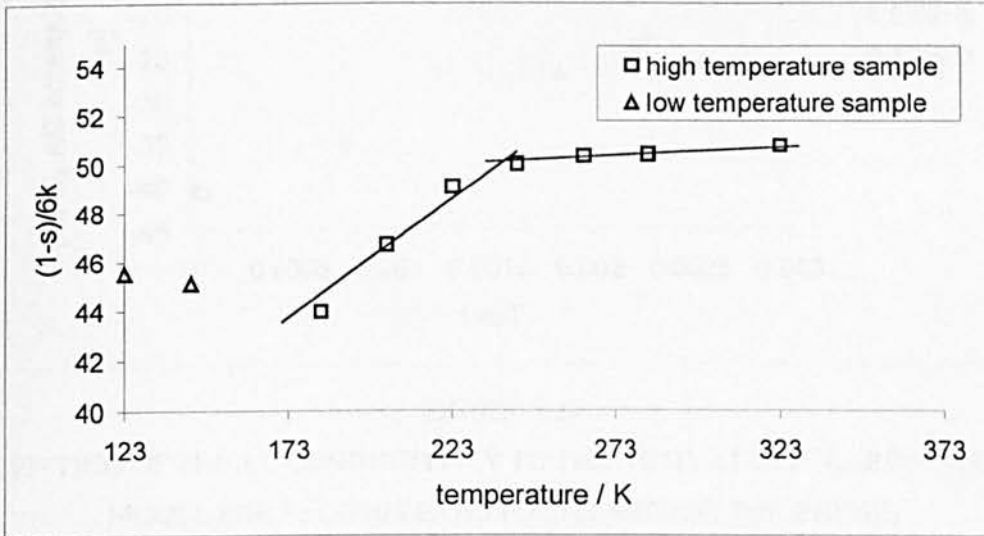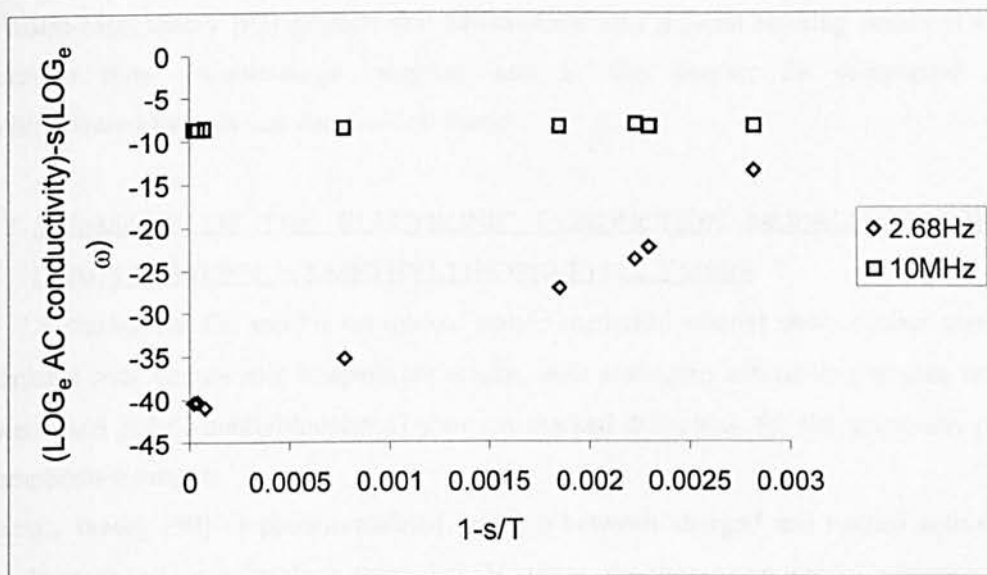### 7.4.4.6 SUMMARY OF ELECTRONIC CONDUCTION MODELLING IN Fe COMPLEXED POLY(3-METHYLTHIOPHENE)

The results of the analysis of the modelling of conductivity data shows that Fe complexed poly(3-methylthiophene) changes from a $T^{-1/2}$ dependence at lower temperatures (123-223K, $\delta E \sim 0.02 eV$) to a $T^{-1/4}$ (183-323K) dependence at higher temperatures. The density of states was calculated to be $2.5 \times 10^{20} eV^{-1} cm^{-3}$ for a hopping near E_F - a relatively high value for an undoped polymer, however, the DC conductivity is $\sim 2.5 \times 10^{-5} Scm^{-1}$. This low DC conductivity can be attributed to the 'pinning' of polarons within the localised states by the presence of the Fe^{2+} and Fe^{3+} ions.

The Fe^{2+} and Fe^{3+} ions essentially act as an insulating barrier to the movement of the charge carriers, but the high activation energy observed for the activated barrier hopping between 183-243K of 0.45eV-0.59eV shows that a lower temperature hopping is favoured over higher temperature hopping, where implausibly high activation energies are in the region of $\sim 20eV$. As the temperature is increased, the polymer chains become increasingly more mobile, thereby increasing the average distance between the metal ions - providing an explanation of the increase in the activation energy between the potential barriers as the temperature increases.

The Austin-Mott theory [98] predicts that Miller-Abrahams polaron hopping occurs at a higher temperature than variable-range hopping, and in this respect Fe complexed poly(3-methylthiophene) follows that Austin-Mott theory.

7.4.4.7 SUMMARY OF THE ELECTRONIC CONDUCTION MODELLING FOR THE COMPLEXED POLY(3-METHYLTHIOPENE) POLYMERS

Table 7.8 shows that Co and Ni complexed poly(3-methylthiophene) show similar conduction mechanisms over comparable temperature ranges, with analogous activation energies, however, Fe complexed poly(3-methylthiophene) shows a marked difference for the activation energies and temperature ranges.

Kivelson's theory [99] of phonon-assisted hopping between charged and neutral solitons may originally seem to be applicable to these data. However, the theory requires the presence of both charged and neutral solitons, which are only present when the polymer doping level <0.005mol%.

	Variable-Range Hopping	Barrier tunnelling	Polaron Hopping
P3MT	123-250K $N(E_F)=5.2\times10^{24}$ eV^{-1}cm^{-3}	Not applicable to P3MT	323-183K $W_2=0.48$eV
Fe	323-183K $N(E_F)=2.5\times10^{20}$eV^{-1}cm^{-3}	223-123K $\delta E=0.023$eV $W_b=1.2$nm at 123K	323-203K $W_2=0.52$eV
Co	323-123K $N(E_F)=1.8\times10^{22}$eV^{-1}cm^{-3}	123-223K $\delta E=0.02$eV $W_b=2.5$nm at 300K	323-243K $W_2=0.21$eV
Ni	323-123K $N(E_F)=6.3\times10^{22}$eV^{-1}cm^{-3}	123-223K $\delta E=0.01$eV $W_b=0.01$nm at 300K	323-223K $W_2=0.1$eV

TABLE 7.8

SUMMARY OF THE CONDUCTION MECHANISMS FOR COMPLEXED POLY(3-METHYLTHIOPHENE) POLYMERS

Budd has described the presence of metal-sulphur bonds [101], and inter-metallic ion hopping is favoured at a lower temperature, when the Fe-S bonds are in relatively close proximity to each other. An idealised situation is shown in Figure 7.38.
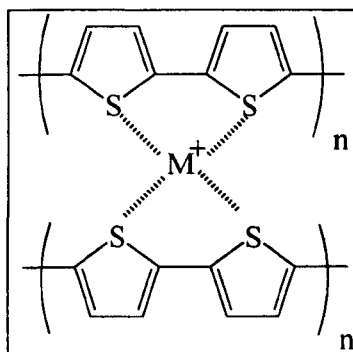

FIGURE 7.38

REPRESENTATION OF HOW METAL IONS ARE ARRANGED BETWEEN THE POLYMER CHAINS

The presence of the Fe^{2+} and Fe^{3+} ions (also confirmed by ICP analysis) act as a barrier to the movement of charge carriers within the polymer chain, thereby deepening the potential wells. This results in quantum tunnelling as the favoured method of charge conduction.

7.5 DIELECTRIC PROPERTIES OF CONDUCTING POLYMERS

This area of work investigates the effects of frequency and temperature on the pure P3MT polymer and complexed polymers, by observation and analysis of the dielectric properties using dielectric spectroscopy. By the observation and analysis of the conduction and polarisation processes, these materials may be characterised with regard to their properties for electromagnetic absorption.

7.5.1 POLY(3-METHYLTHIOPHENE)

The measured real (ε_r') and imaginary (ε_r'') parts of the dielectric constant (ε^*) are shown in Figures 7.39-7.40 respectively, in relation to the log of the applied frequency.

FIGURE 7.39

RELATIONSHIP BETWEEN THE REAL PART OF THE DIELECTRIC CONSTANT AND
THE FREQUENCY FOR POLY(3-METHYLTHIOPHENE)

In Figure 7.39 it appears that ε_r' remain constant (~5.8) for T<203K until the applied frequency is ~10^6 Hz. At frequencies less than 10^6 Hz, a strong frequency dependence is observed for poly(3-methylthiophene) samples measured at 323-243K. As the applied frequency is increased, ε_r' can be seen to increase to ~1.1 .
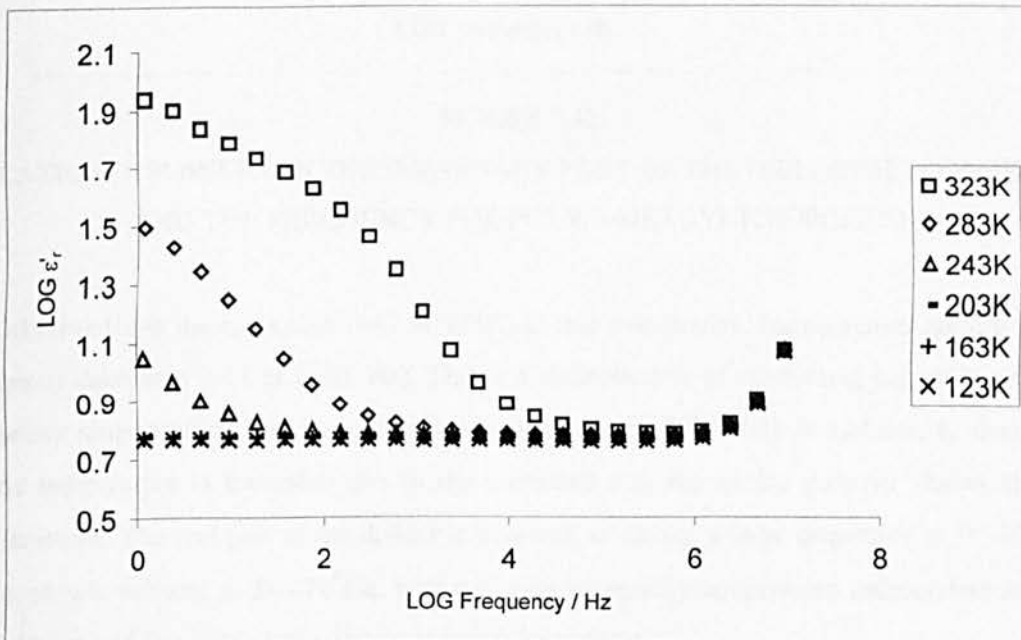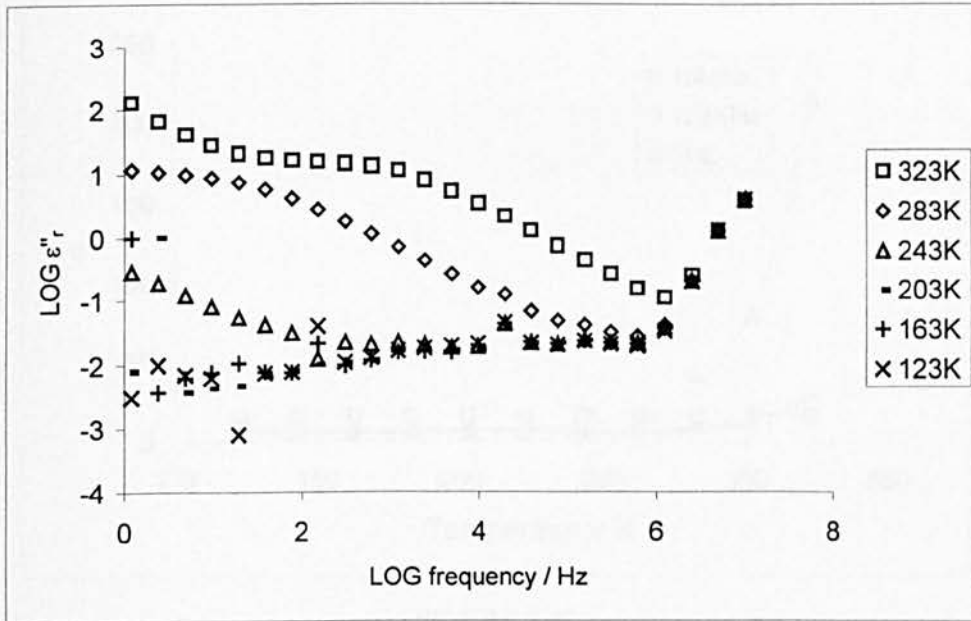
FIGURE 7.40

RELATIONSHIP BETWEEN THE IMAGINARY PART OF THE DIELECTRIC CONSTANT
AND THE FREQUENCY FOR POLY(3-METHYLTHIOPHENE)

It is observed that the ε_r' is high (~87 at 323K) at low frequencies, but decreases rapidly as the frequency decreases (~11 at 1×10^7 Hz). This is a characteristic of conducting polymers over the frequency range studied, and is consistent with other reports [103-108]. In addition, ε_r' decreases as the temperature is increased due to the increased mobility of the polymer chains at high temperatures. The real part of the dielectric constant, ε_r' shows a large dispersion at $f<\sim10^5$ Hz, which slowly reduces at $f> \sim10^5$Hz; with ε_r' being essentially temperature independent at high frequencies and frequency independent at low temperatures.

The dielectric loss, ε_r'' shown in Figure 7.40 also shows a rapid decrease as the frequency increases, and shows a similar behaviour to that shown in Figure 7.39, but at $f> 2.5\times10^6$ Hz. Figures 7.41 and 7.42 show the dependence of ε' and ε_r'' on temperature.
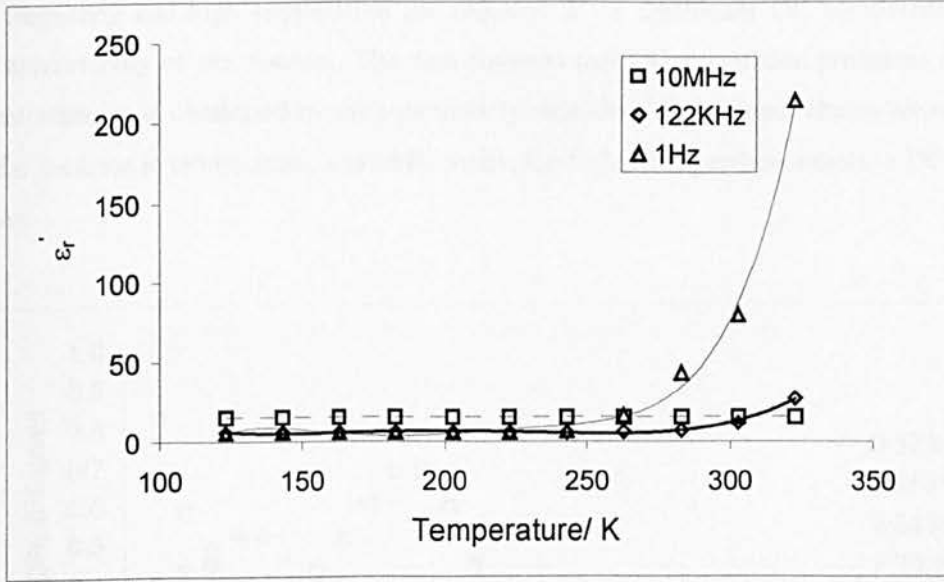
FIGURE 7.41

RELATIONSHIP BETWEEN THE REAL PART OF THE DIELECTRIC CONSTANT AND
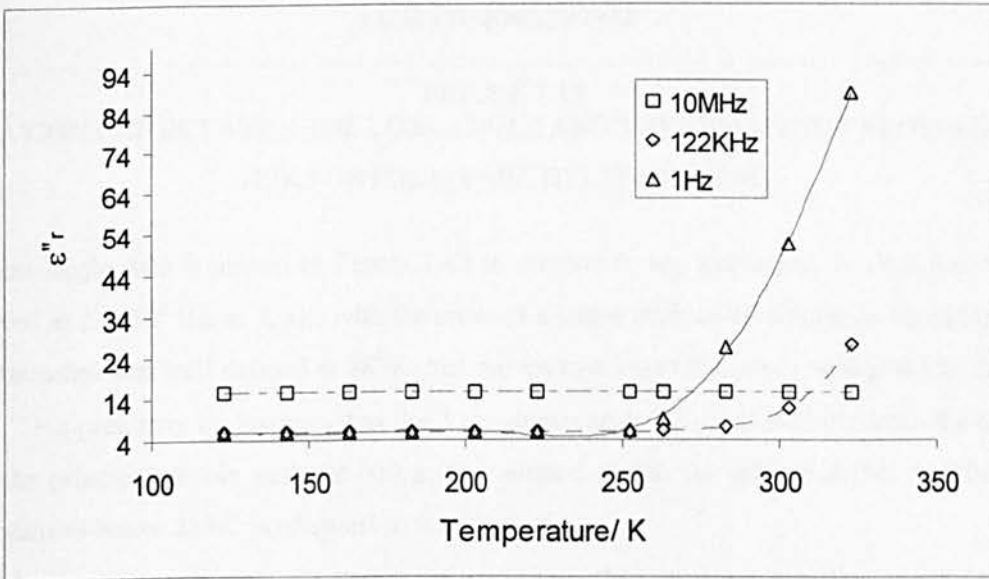THE TEMPERATURE FROM 1Hz TO 10MHz FOR POLY(3-METHYLTHIOPHENE)

FIGURE 7.42

RELATIONSHIP BETWEEN THE IMAGINARY PART OF THE DIELECTRIC CONSTANT
AND THE TEMPERATURE FROM 1Hz TO 10MHz FOR POLY(3-METHYLTHIOPHENE)

A low frequency and high temperature are required for a significant DC contribution to the overall conductivity of the material. The data suggests that DC conduction processes dominate these materials, as is confirmed by the conductivity data since the polymer chains are mobilised due to the increase in temperature, and additionally, the higher temperature assists in DC hopping processes.
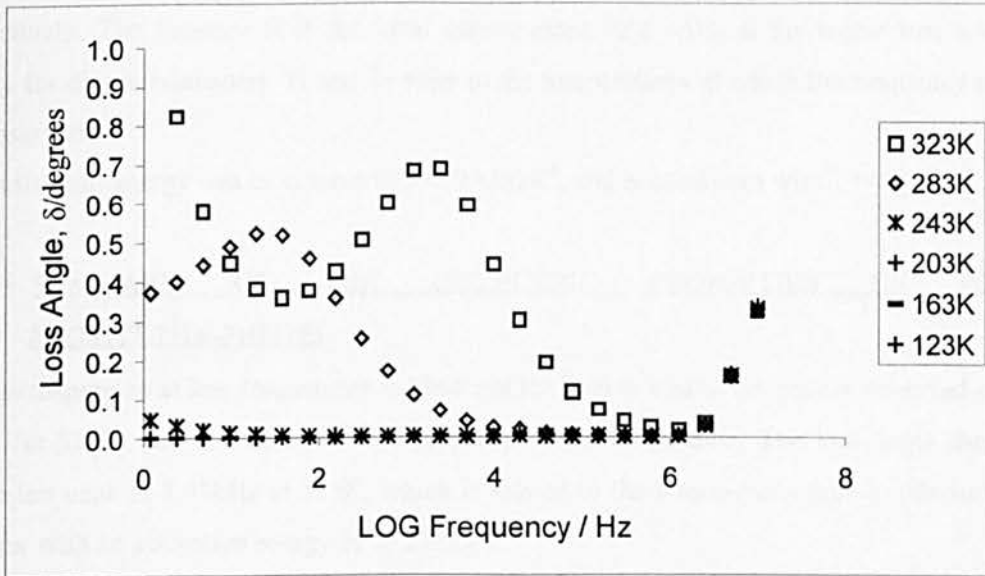
FIGURE 7.43

RELATIONSHIP BETWEEN THE LOSS ANGLE AND THE FREQUENCY FROM 323K TO 123K FOR POLY(3-METHYLTHIOPHENE)

The loss angle data is shown in Figure 7.43 in relation to log frequency. A clear loss peak is observed at 2.4×10^3 Hz, at 323K, with the onset of a larger peak as the frequency decreases. This peak becomes less well defined at 283K, and moves to a lower frequency, and peaks at 38 Hz at 283K. This peak may be designated as the β dispersion peak, which is characteristic of a material with the principal dipole moment being incorporated within the main polymer backbone. At temperatures below 283K, no dispersion is observed.

The β loss peak occurs when the temperature is greater than the glass transition temperature, T_g; and is associated with an activation energy ΔH_β, of the form:

$$\ln \frac{f_{\max(T_1)}}{f_{\max(T_2)}} = -\frac{\Delta H_\beta}{R}\left(\frac{1}{T_1} - \frac{1}{T_2}\right)$$

EQUATION 7.10

Where $f_{\max(T1)}$ refers to the maximum of the first peak, and $f_{\max(T2)}$ refers to the maximum of the second peak of the tan δ plot vs frequency (Figure 7.43). The maxima are 2441Hz and 38Hz respectively. The constant R is the ideal gas constant, and $-\Delta H_\beta$ is the molar free activation energy for dipole relaxation. T_1 and T_2 refer to the temperatures at which the frequency maxima are observed.

The activation energy was calculated to be 79 kJmol^{-1}, and is consistent with T<<T$_g$.

7.5.1.1 SUMMARY OF THE DIELECTRIC PROPERTIES OF POLY(3-METHYLTHIOPHENE)

A large dispersion at low frequencies is observed for both $\varepsilon_r{}'$ and $\varepsilon_r{}''$. A peak is observed at 5kHz for $\varepsilon_r{}''$ at 323K, and is indicative of a dipolar polarisation process. The loss angle shows a γ dispersion peak at 2.43kHz at 323K, which is related to the a side-chain type oscillation of the polymer with an activation energy of 79 kJmol^{-1}.

As T~T$_g$, the relaxation time of the dipoles, τ is of the order of several seconds since increasing the temperature affects both the proximity of the polymer chains to each other and increases the mobility of the polymer chains. The relaxation time of P3MT was calculated to be ~3.2x10^{-10}s, indicating that the polymer chains are closely packed. In order to increase the loss of the polymer in the 10^9 Hz range, an increase in temperature is recommended.

7.5.2 THE DIELECTRIC PROPERTIES OF Co COMPLEXED POLY(3-METHYLTHIOPHENE)

The $\varepsilon_r{}'$ and $\varepsilon_r{}''$ both decrease rapidly as the frequency increases, with the evolution of a peak observed at 1.56 x 10^{5}Hz for $\varepsilon_r{}'$ (log frequency) (Figure 7.44) at 323K. This peak is probably due to a minor dipolar relaxation process, with the peak becoming broader as the temperature decreases to 123K, indicating a broad and asymmetrical distribution of the relaxation times of the dipoles. This relaxation peak also moves toward a lower frequency as the temperature decreases.
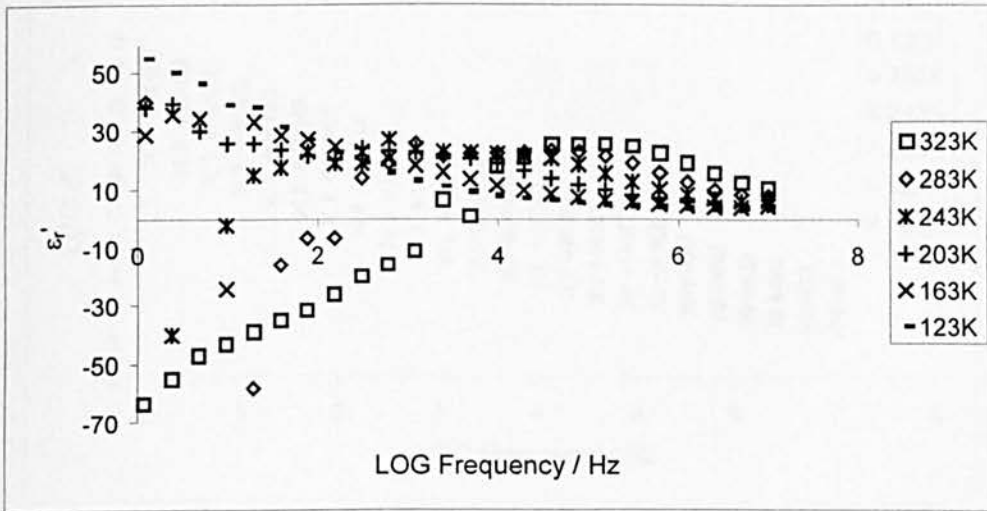
FIGURE 7.44

RELATIONSHIP BETWEEN THE REAL PART OF THE DIELECTRIC CONSTANT AND
THE FREQUENCY FOR Co COMPLEXED POLY(3-METHYLTHIOPHENE)

The log $\varepsilon_r^{''}$ versus the log frequency graph shown in Figure 7.45 is almost linear with a slope of -1 (particularly at high temperatures), indicating that $\varepsilon_r^{''}$ is proportional to 1/f. This phenomenon has also been observed for the salt form of polyaniline – another conducting polymer [109-111], and provides further evidence of Austin-Mott hopping conduction [112-114].
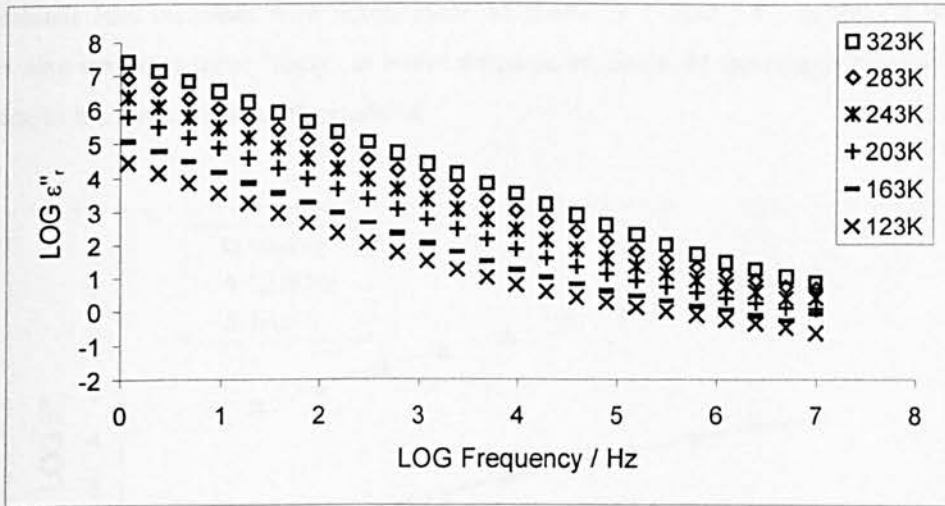
FIGURE 7.45

RELATIONSHIP BETWEEN THE IMAGINARY PART OF THE DIELECTRIC CONSTANT
AND THE FREQUENCY FOR Co COMPLEXED POLY(3-METHYLTHIOPHENE)

When ε_r' is plotted against temperature, as shown in Figure 7.46, the real part of the dielectric constant exhibits a peak at 122Hz with a value of ε_r' ~26 at 263K. Two peaks are observed at 1Hz with a value of ~40 at 263K, and a value of ~35 at 203K.
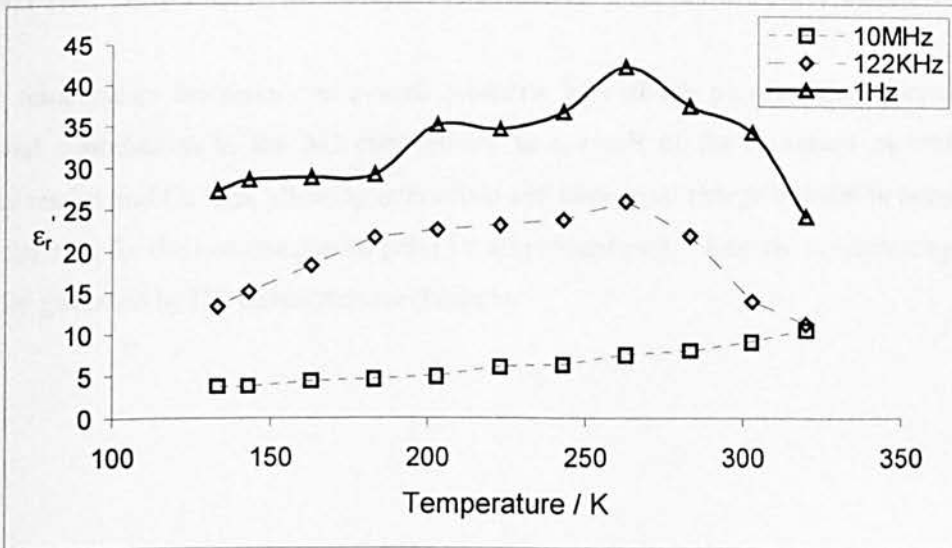

FIGURE 7.46

RELATIONSHIP BETWEEN THE REAL PART OF THE DIELECTRIC CONSTANT AND
THE FREQUENCY FOR Co COMPLEXED POLY(3-METHYLTHIOPHENE)

The dielectric loss increases with temperature, as shown in Figure 7.47, as the Co complexed polymer also becomes more 'lossy' at lower frequencies, since all the relaxation processes can contribute to the overall loss of the material.
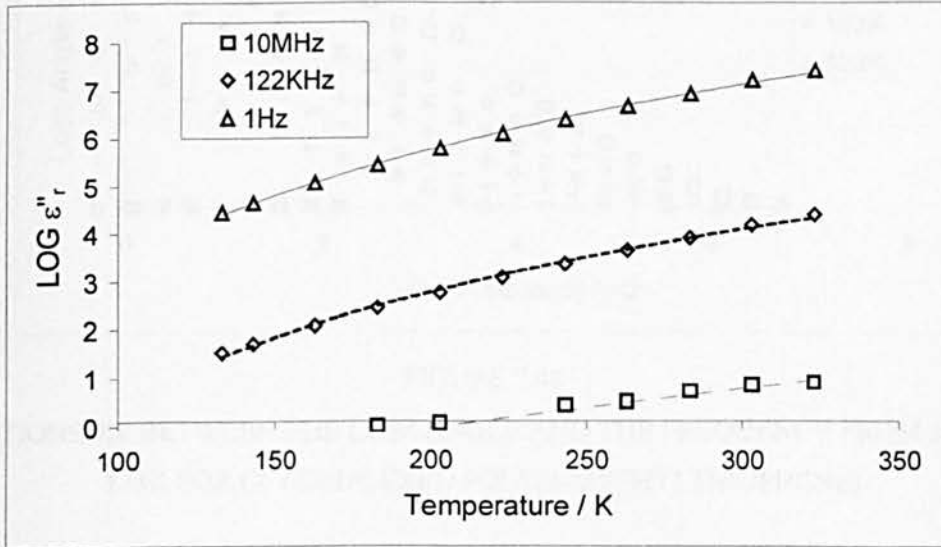

FIGURE 7.47

RELATIONSHIP BETWEEN THE IMAGINARY PART OF THE DIELECTRIC CONSTANT
AND THE TEMPERATURE FOR Co COMPLEXED POLY(3-METHYLTHIOPHENE)

As the temperature increases, the overall dielectric loss of the polymer increases due to an additional contribution to the AC conductivity as a result of the increased mobility of the polymer chains and Co ions, allowing inter-chain and inter-ionic charge transfer to occur. This is unlike the case for the non-complexed poly(3-methylthiophene), where the conduction process is generally governed by DC conduction mechanisms.
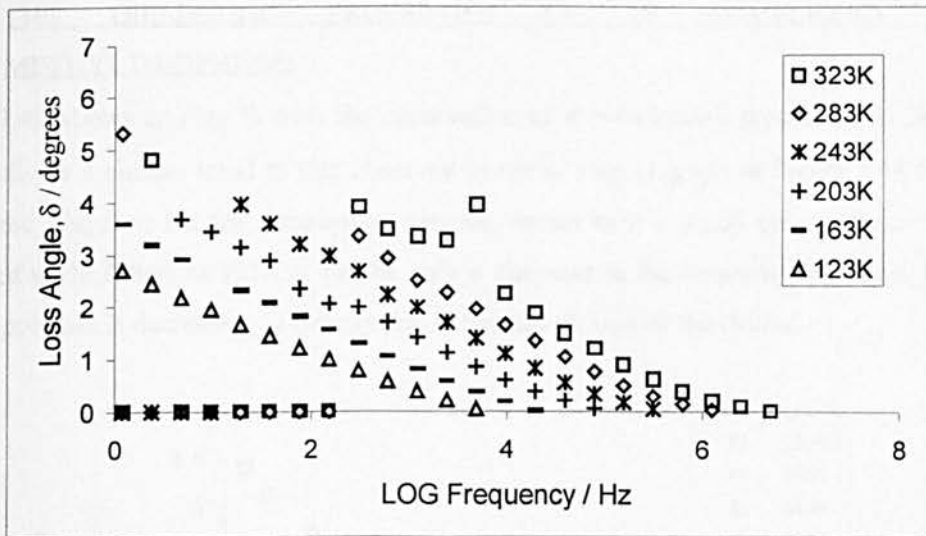
FIGURE 7.48

RELATIONSHIP BETWEEN THE LOSS ANGLE AND THE FREQUENCY FROM 323K TO
123K FOR Co COMPLEXED POLY(3-METHYLTHIOPHENE)

The loss angle, δ shown in Figure 7.48 as a function of frequency shows that no clear dispersion
peak is observed between 323-123K indicating that there is a very broad distribution of dipolar
relaxation times.

7.5.2.1 <u>SUMMARY OF THE DIELECTRIC PROPERTIES OF Co COMPLEXED POLY(3-METHYLTHIOPHENE)</u>

The dielectric properties of Co complexed P3MT favour confirm that variable range hopping is
the favoured charge transfer process. Due to the lack of structure of the loss data, it can be
assumed that there is a very broad distribution of relaxation times of the dipoles and hence, the
polymer chains are closely packed.

7.5.3 THE DIELECTRIC PROPERTIES OF Ni COMPLEXED POLY(3-METHYLTHIOPHENE)

Figure 7.49 shows $\varepsilon_r^{'}$ (log f) with the observation of a polarisation process at 31.3KHz. The graph follows a similar trend to that observed in the $\varepsilon_r^{'}$ (log f) graph in Figure 7.44 for the Co complexed polymer, but the polarisation process occurs over a much greater frequency range compared to the latter. At 123K $\varepsilon_r^{'}$ can be seen to decrease as the frequency increases, indicating that the polymer is decreasing in density due to thermal motion of the chains.
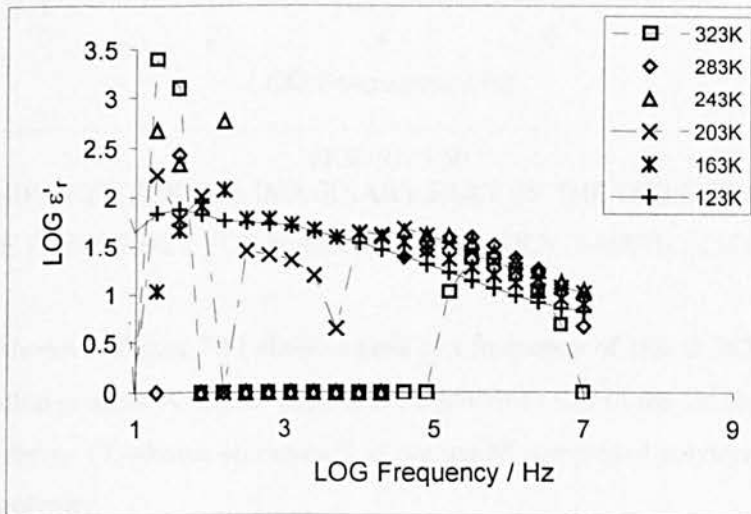

FIGURE 7.49

RELATIONSHIP BETWEEN THE REAL PART OF THE DIELECTRIC CONSTANT AND THE FREQUENCY FOR Ni COMPLEXED POLY(3-METHYLTHIOPHENE)

Figure 7.50 shows an identical behaviour to the Co complexed polymer for $\varepsilon_r^{''}$ (log f), indicating that $\varepsilon_r^{''}$ is proportional to 1/f within the frequency and temperature range studied.
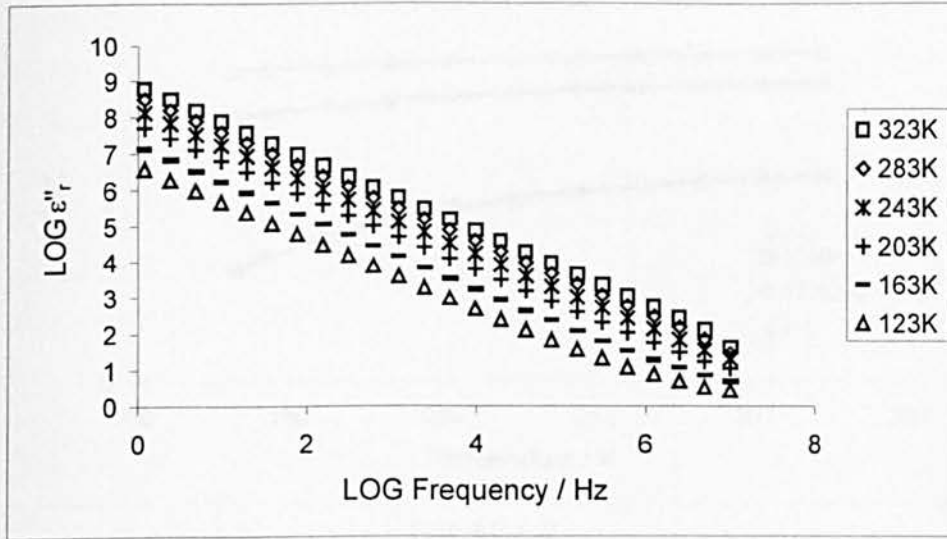
FIGURE 7.50
RELATIONSHIP BETWEEN THE IMAGINARY PART OF THE DIELECTRIC CONSTANT
AND THE FREQUENCY FOR Ni COMPLEXED POLY(3-METHYLTHIOPHENE)

The log ε_r' (T) shown in Figure 7.51 shows a peak at a frequency of 1Hz at 303K – indicative of a dipolar relaxation process. A similar pattern of behaviour to that of the Co complexed polymer is observed for the ε_r'' (T) shown on Figure 7.52 for the Ni complexed polymer compared to the Co complexed polymer.
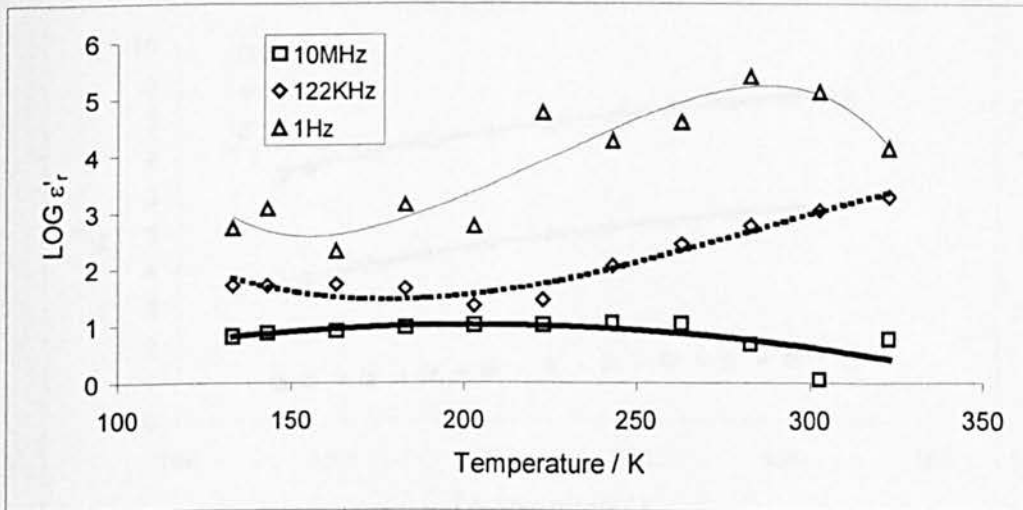

FIGURE 7.51
RELATIONSHIP BETWEEN THE REAL PART OF THE DIELECTRIC CONSTANT AND
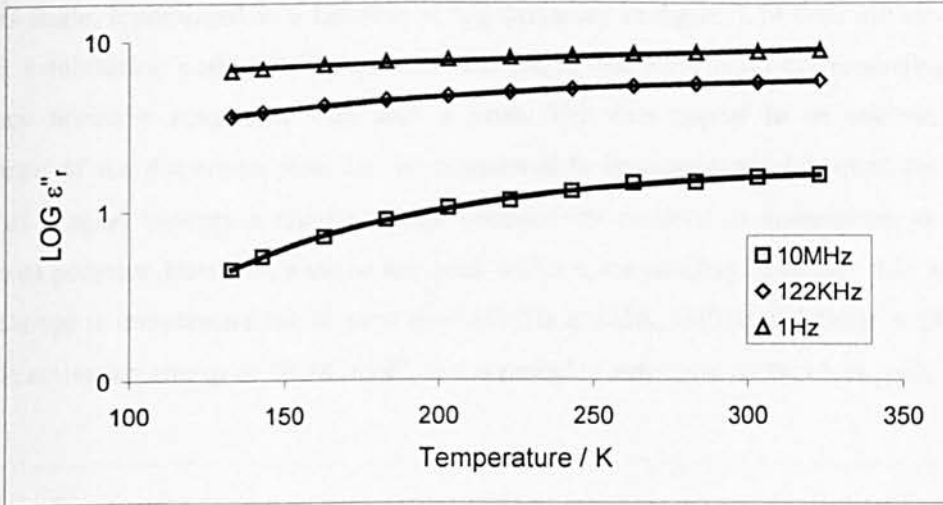THE TEMPERATURE FOR Ni COMPLEXED POLY(3-METHYLTHIOPHENE)

FIGURE 7.52

RELATIONSHIP BETWEEN THE IMAGINARY PART OF THE DIELECTRIC CONSTANT AND
THE TEMPERATURE FOR Ni COMPLEXED POLY(3-METHYLTHIOPHENE)

Since σ_{DC} is related to the temperature, the σ_{DC} conductivity can be expected to increase due to
contributions from hopping conduction. Therefore, $\varepsilon_r^{\bullet}$ is low at low frequencies since this
quantity is directly affected by the AC conduction mechanisms, and hence the complex dielectric
constant does again appear to be dominated by the DC conduction mechanisms as shown in
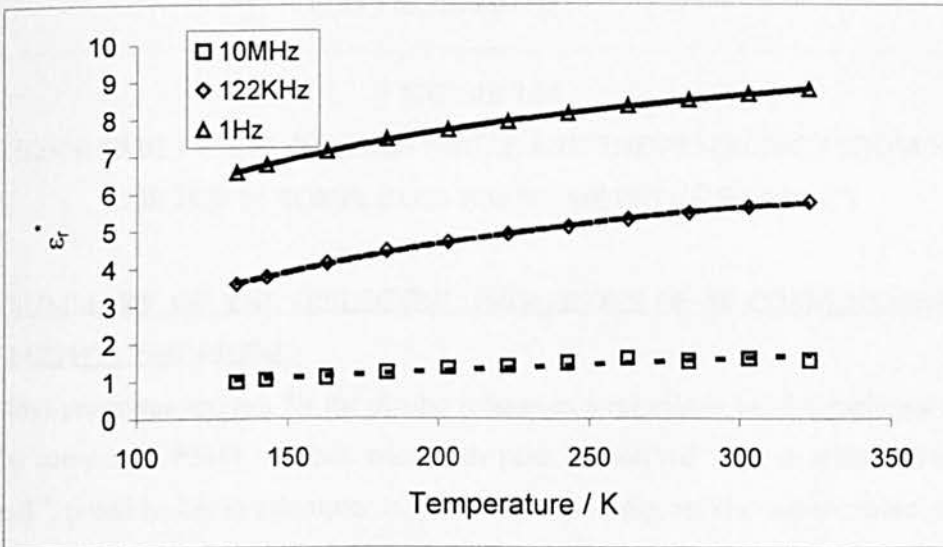Figure 7.53.

FIGURE 7.53

RELATIONSHIP BETWEEN THE COMPLEX DIELECTRIC CONSTANT AND THE TEMPERATURE
FOR Ni COMPLEXED POLY(3-METHYLTHIOPHENE)

The loss angle, δ presented as a function of log frequency in figure 7.54 does initially seem to produce a relaxation peak at 19Hz between 323-163K, but there is no corresponding shift in frequency normally associated with such a peak. The data appear to be unclear, and the appearance of the dispersion peak can be considered to be anomalous, however, the absolute values of δ again indicate a relatively high conductivity material in comparison to the non-complexed polymer. However, a minor loss peak with a corresponding frequency shift associated with a change in temperature can be seen at ~0.16MHz at 323K, shifting to 39KHz at 283K. This yields an activation energy of 26.3KJmol^{-1}, and is probably indicative of the γ loss peak.
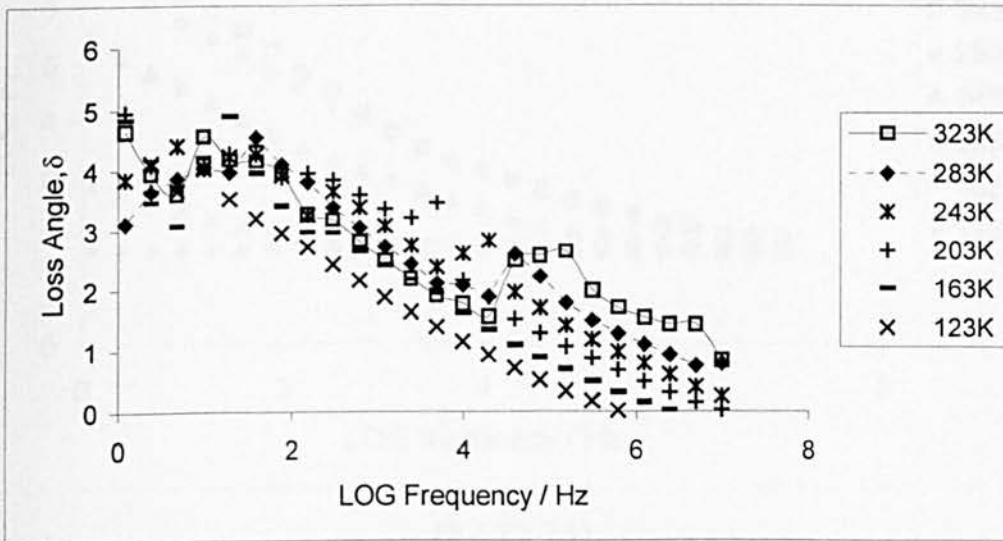

FIGURE 7.54

RELATIONSHIP BETWEEN THE LOSS ANGLE AND THE FREQUENCY FROM 323K TO 123K FOR Ni COMPLEXED POLY(3-METHYLTHIOPHENE)

7.5.3.1 SUMMARY OF THE DIELECTRIC PROPERTIES OF Ni COMPLEXED POLY(3-METHYLTHIOPHENE)

Similar loss processes account for the dipolar relaxation mechanisms in Ni complexed P3MT as in the Co complexed P3MT. A small minor loss peak is observed, with an activation energy of ~26KJmol^{-1}, possibly due to a damped oscillation of a local dipole. The complexation of Ni ions into the poly(3-methylthiophene) backbone has again contributed to the bulk conductivity of the material, but to a lesser extent than in the Co complexed polymer.

7.5.4 THE DIELECTRIC PROPERTIES OF Fe COMPLEXED POLY(3-METHYLTHIOPHENE)

A large dispersion of ε_r' is observed at low frequencies for ε_r' (log frequency) as shown in Figure 7.55, ranging from ~73 at 323K to ~44 at 123K at a frequency of 1Hz. At the higher temperatures (323-243K), ε_r' decreases rapidly, but at lower temperatures (163-123K), ε_r' remains independent of frequency.
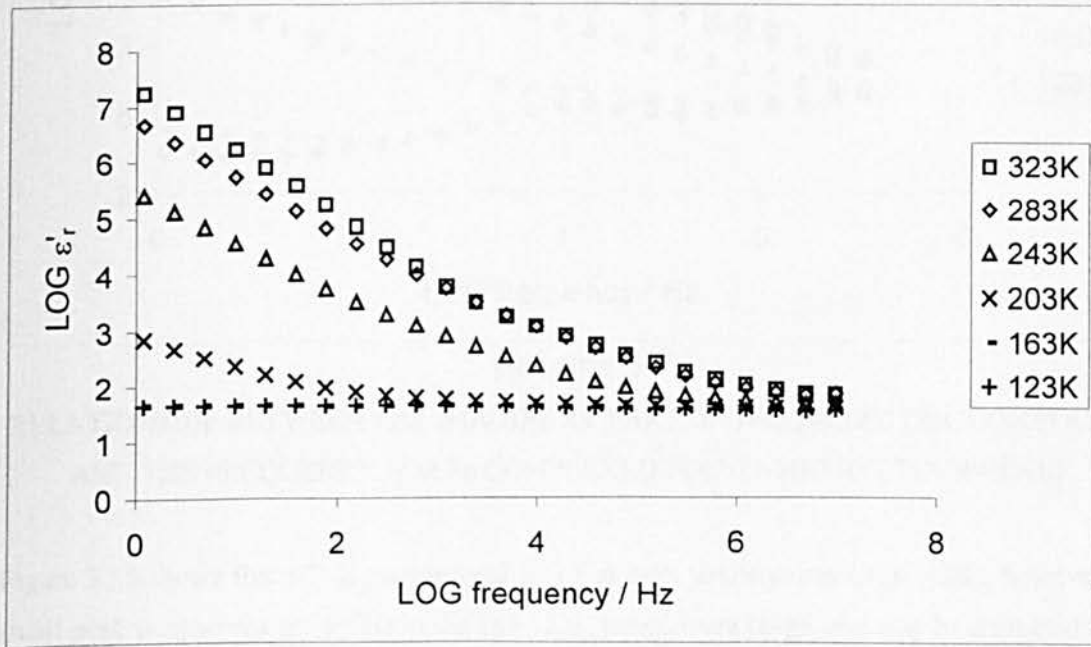

FIGURE 7.55

RELATIONSHIP BETWEEN THE REAL PART OF THE DIELECTRIC CONSTANT AND THE FREQUENCY FOR Fe COMPLEXED POLY(3-METHYLTHIOPHENE)
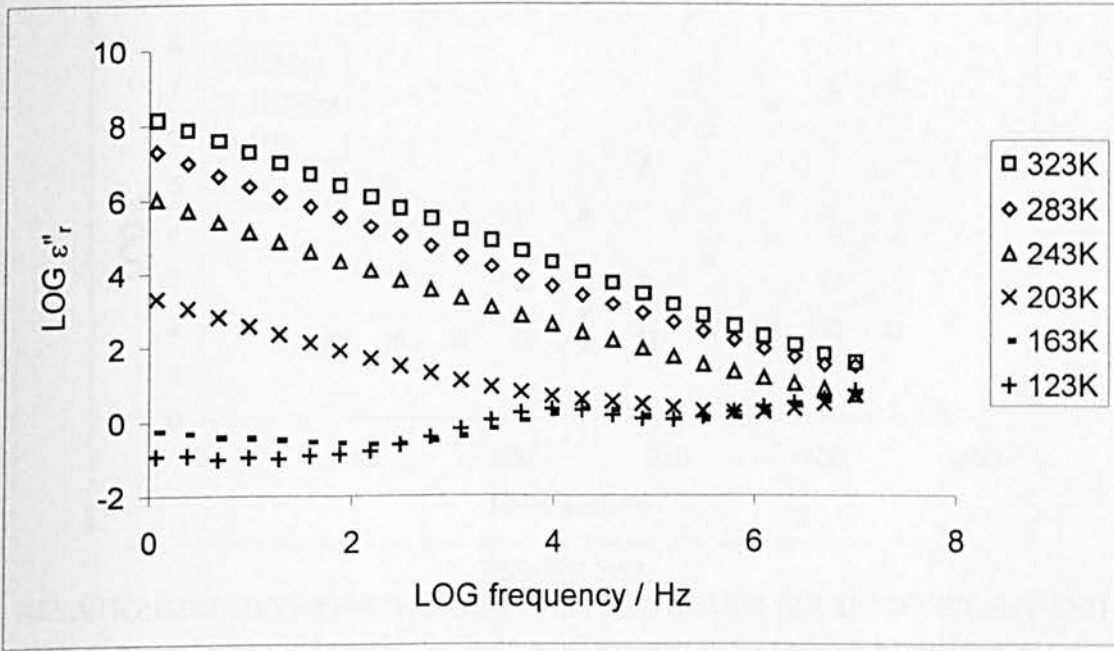
FIGURE 7.56

RELATIONSHIP BETWEEN THE IMAGINARY PART OF THE DIELECTRIC CONSTANT
AND THE FREQUENCY FOR Fe COMPLEXED POLY(3-METHYLTHIOPHENE)

Figure 7.56 shows that ε_r'' is proportional to $1/f$ at high temperatures (323-243K), however, a small peak is observed at $\sim 10^4$Hz in the 163-123K temperature range, and may be attributed to a secondary loss mechanism such as a 'crankshaft' type movement of the polymer chains.

When the real part of the dielectric constant is plotted against the temperature as in Figure 7.57, it is seen that ε_r' remains constant at all frequencies until ~ 200K. ε_r' then increases significantly with the temperature, and peaks at $\sim 1.7 \times 10^7$ at 323K at 1Hz. At 122KHz, $\varepsilon_r'(T)$ peaks at 9.15×10^3 and at 10MHz, peaks at ~ 82 at 323K.

This behaviour has been observed in cross-linked polyaniline emeraldine salt [115], and indicates a $\varepsilon_r' \propto T^2$ behaviour. The model suggests that the charge carriers have insufficient energy to overcome the potential energy barriers, and that multiple hopping between metallic islands can be considered to account for this behaviour.

FIGURE 7.57

RELATIONSHIP BETWEEN THE REAL PART OF THE DIELECTRIC CONSTANT AND

THE TEMPERATURE FOR Fe COMPLEXED POLY(3-METHYLTHIOPHENE)

The ε_r'' (T) (Figure 7.58) and the complex dielectric constant, ε_r^* (figure 7.59) show a similar
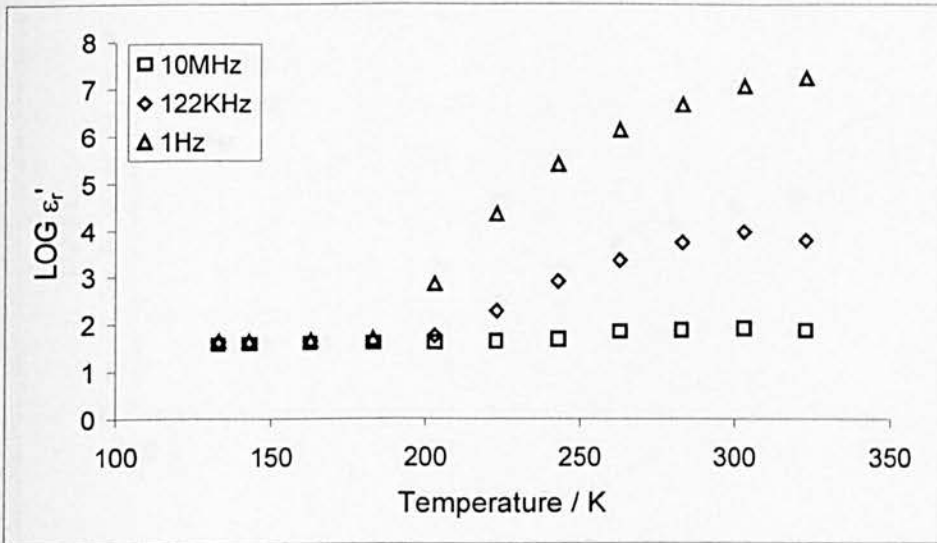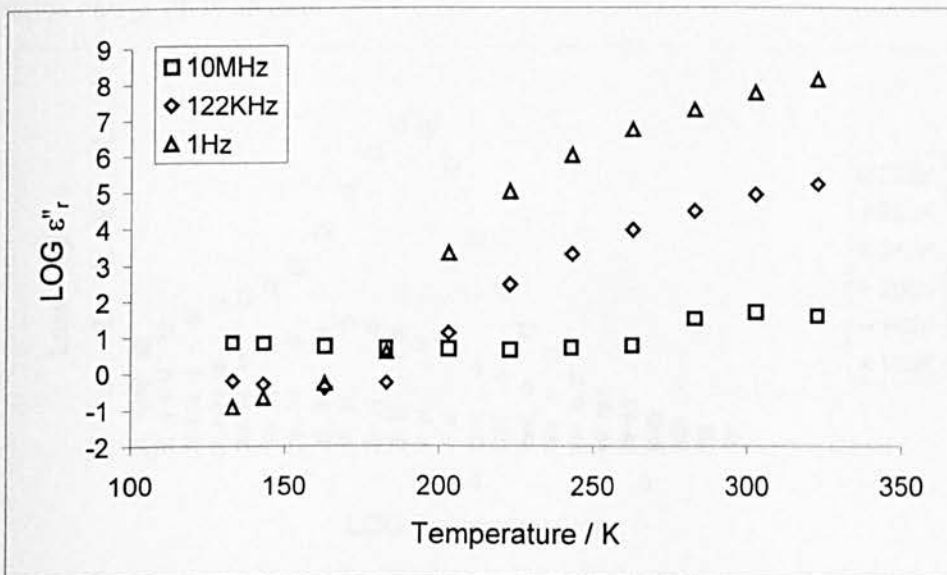
trends to that of ε_r'

FIGURE 7.58

RELATIONSHIP BETWEEN THE IMAGINARY PART OF THE DIELECTRIC CONSTANT

AND THE TEMPERATURE FOR Fe COMPLEXED POLY(3-METHYLTHIOPHENE)
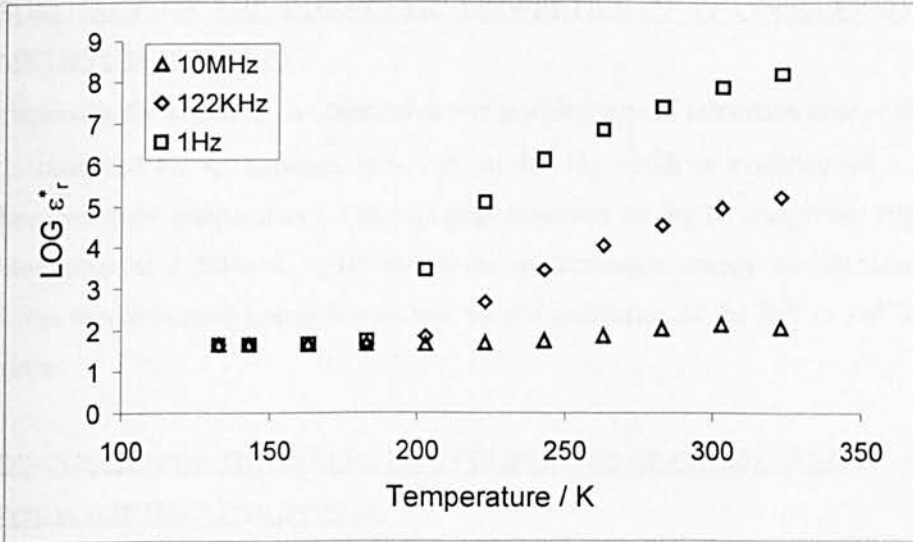
FIGURE 7.59

RELATIONSHIP BETWEEN THE COMPLEX DIELECTRIC CONSTANT AND THE
TEMPERATURE FOR Fe COMPLEXED POLY(3-METHYLTHIOPHENE)

A very prominent loss peak is observed at 1.2KHz, with $\delta=26.9$ at 323K. This decreases in amplitude, and shifts to a lower frequency as the temperature decreases (Figure 7.60). This yields an activation energy of 39.5KJmol^{-1}.

FIGURE 7.60

RELATIONSHIP BETWEEN THE LOSS ANGLE AND THE FREQUENCY FROM 323K TO
123K FOR Fe COMPLEXED POLY(3-METHYLTHIOPHENE)

7.5.4.1 SUMMARY OF THE DIELECTRIC PROPERTIES OF Fe COMPLEXED POLY(3-METHYLTHIOPHENE)

A large dispersion for ε_r' and ε_r'' is observed due to a wide range of relaxation time of the dipoles. A peak is obser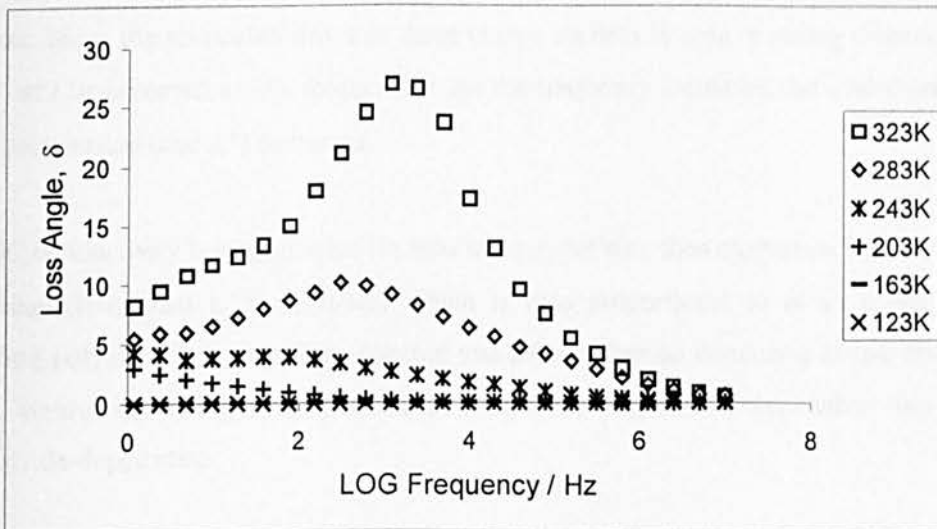ved for ε_r'' between 163-123K at 10^4 Hz which is evidence for a relaxation process between these temperatures. The loss peak observed for the Fe complexed P3MT shows a dispersion peak at 1.2kHz at 323K and gives an activation energy for 39.5kJmol^{-1}. It is proposed that this activation energy is required for the oscillation of the Fe^{2+} or Fe^{3+} ion at high temperatures.

7.5.5 DISCUSSION OF THE DIELECTRIC PROPERTIES OF COMPLEXED POLY(3METHYLTHIOPHENE)

Conducting polymers usually contain a large number of hopping charge carriers, which may then lead to a great difference in the dielectric properties of these materials in comparison to insulators. The hopping charge carriers can make a significant contribution to the real and imaginary parts of the dielectric constant, which are related to the polarisation. Epstein *et al* [116] has mentioned that the static value of ε_r' depends on the density of states, the inter-site distance and the temperature. The application of an AC electric field will cause ε_r' to exhibit a relaxation process that is analogous to a dipolar system, where the localised state is described as a polaron. Since the relaxation times of these charge carriers is long, a strong dispersion of ε_r' and ε_r'' will be observed at low frequencies. As the frequency increases, the contribution to the overall polarisation (and ε_r^*) decreases.

If the DC conductivity is insignificant (in insulating materials), then $\sigma_{AC}=\omega\varepsilon_0\varepsilon_r''$, however if σ_{DC} is non-negligible, then $\varepsilon_r''\approx \sigma_{DC}/(\omega\varepsilon_0)$ which is also proportional to ω^{-1} as is the case for conducting polymers. It is therefore expected that DC conduction dominates at low frequencies, and AC conduction at higher frequencies in conducting polymers, except when they are in a rigorously de-doped state.

Figures 7.36 and 7.38 for poly(3-methylthiophene) together with Figures 7.53 and 7.54 for Fe complexed poly(3-methylthiophene) indicate that the density of the charge carriers is much higher in the non-complexed poly(3-methylthiophene) and the Fe complexed poly(3-

methylthiophene) since the dispersion of ε_r' and ε_r'' is far greater than the dispersion observed in figures 7.42 and 7.44 for the Co complexed poly(3-methylthiophene) and figures 7.49 and 7.50 for the Ni complexed poly(3-methylthiophene) at low frequencies. At high frequencies (>10^5 Hz for the non complexed poly(3-methylthiophene) and ~10^7Hz for the Fe complexed poly(3-methylthiophene)), there is a negligible DC contribution to the conductivity of the materials. The activation energy of the Fe complexed P3MT is 39.5 kJmol^{-1}, in comparison to the uncomplexed P3MT, which has an activation energy of 79kJmol^{-1}. This is due to the oscillation of the Fe-S bond in the Fe complexed P3MT. The activation energy of the uncomplexed P3MT is due to the oscillation of the 3-methylthiophene units along the polymer chain.

This reduction in the activation energy for the Fe complexed P3MT favours DC hopping processes, and, in summary, a low σ_{DC} may generally be associated with a high microwave absorption.

CHAPTER EIGHT

RESULTS AND DISCUSSION FOR THE
ELECTROMAGNETIC PROPERTIES OF CONDUCTING
POLYMERS

8.1 INTRODUCTION

This chapter describes and analyses the 'optical' electromagnetic properties of the poly(3-hexylthiophene) polymer films using a variety of sample holding techniques. Samples were analysed using a resonant window when a strong cohesive free-standing polymer film could be synthesised.

8.2 POLY(HEXYLTHIOPHENE) FREE-STANDING FILMS

Measurements have been taken of the scattering parameters (section 5.10), and calculations of the reflection, transmission and absorption coefficients have been made and presented in this work.

8.2.1 POLYMER DOPING LEVEL

The transmission, reflection and absorption coefficients at 1, 3, 5 and 7 mole% doping as a function of frequency are shown in Figures 8.1 – 8.3 respectively. The doping level is calculated as described in section 5.8.

The initial results indicate that the high frequency reflection, transmission and absorption coefficients are strongly dependent on the doping level of the conducting polymer.

The DC conductivities and film thicknesses of the samples were measured using the Van der Pauw four probe technique and calculated using solution concentration, area of solvent casting and volume of solution cast data respectively. These values are shown in Table 8.1:

DOPING LEVEL / MOLE %	FILM THICKNESS / μm	DC CONDUCTIVITY / Scm^{-1}
2	1.1	3×10^{-4}
3	2.1	0.12
4	2.3	0.27
6	4.4	0.49
8	1.6	0.75
11	1.8	5.22

TABLE 8.1

TABLE SHOWING THE MEASURED DC CONDUCTIVITIES FOR POLY(3-HEXYLTHIOPHENE) IN RELATION TO THE POLYMER FILM THICKNESS

At very low doping levels (<3 mole%), the polymer acts as a good insulator ($\sigma/\omega\varepsilon_0 << 1$), resulting in a high transmission of the incident EM radiation (Figure 8.1), together with a low reflection (Figure 8.2) of the microwave radiation. At these doping levels, only a maximum of 0.24% of the microwaves is absorbed (-0.021dB) (Figure 8.3).
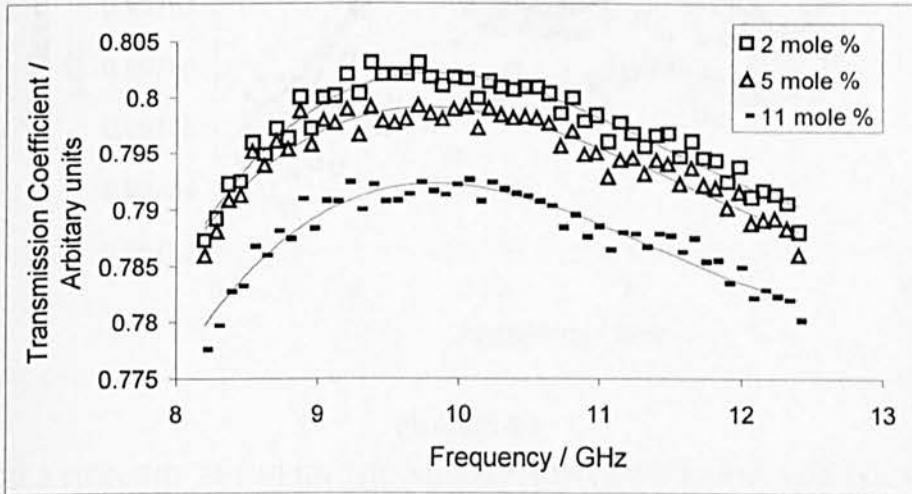

FIGURE 8.1

RELATIONSHIP BETWEEN THE TRANSMISSION COEFFICIENT FOR POLY(3-HEXYLTHIOPHENE) POLYMER FILMS AND FREQUENCY DOPED BETWEEN 2mol% AND 11 mol%
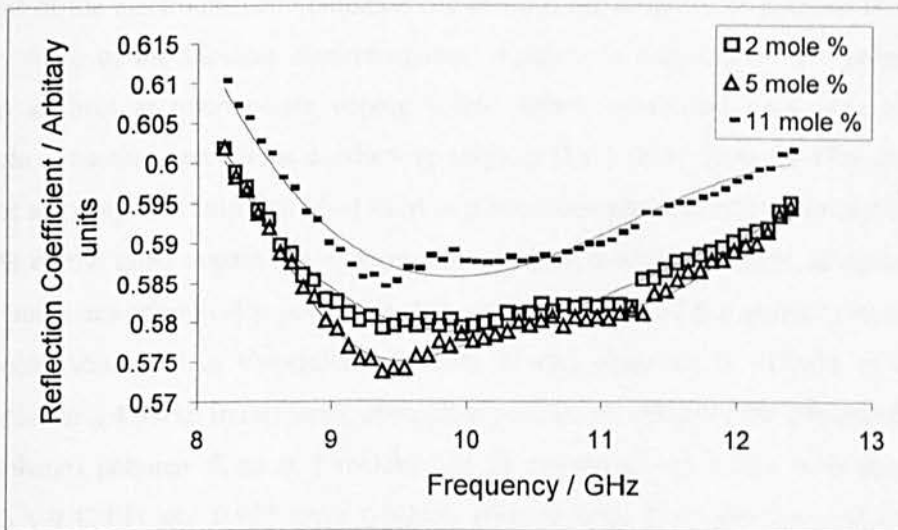

FIGURE 8.2

RELATIONSHIP BETWEEN THE REFLECTION COEFFICIENT FOR POLY(3-HEXYLTHIOPHENE) POLYMER FILMS AND FREQUENCY DOPED BETWEEN 2 mol% AND 11 mol%
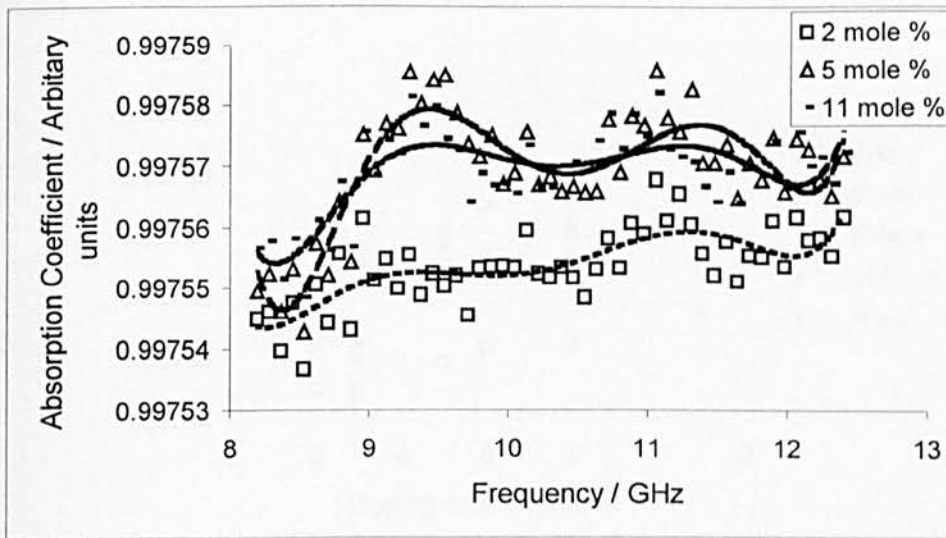
FIGURE 8.3

RELATIONSHIP BETWEEN THE ABSORPTION COEFFICIENT FOR POLY(3-
HEXYLTHIOPHENE) POLYMER FILMS AND FREQUENCY DOPED BETWEEN 2mol%
AND 11mol%

At very high doping levels, the polymer film acts as a metal, with the collapse of the electric field component of the electromagnetic radiation occurring at the air/polymer-polymer film interface. However, some of the incident electromagnetic radiation is absorbed by the polymer and is dissipated as heat at intermediate doping levels. Other researchers have observed this for polypyrrole – another amorphous conducting polymer [117]. They report a 47% absorption at 10GHz for a doping concentration of ~19mM of p-toluenesulphonate, and an absorption of ~15% at ~35mM of the same dopant ion concentration. A bulk solution of 0.2M of aqueous pyrrole solution was electrochemically polymerised in an equivalence of the quoted concentration of dopant anion solution. An absorption of ~55% is also observed at ~19mM of dopant ion concentration at 2.45GHz. In this work, absorption peaks were observed for free-standing poly(3-hexylthiophene) polymer films at 5 mole% and 11 mole% at ~11.1GHz, with absorptions of 0.998units (-0.42dB) and 0.997 units (-0.2dB) (Figure 8.4). The reflection and transmission coefficients as functions of the doping level are shown in Figures 8.5 and 8.6 respectively. These data indicate that the increase in the metallic conduction mechanisms of the polymer provides a more reflective and less transmissive polymer resulting from the increased doping level.
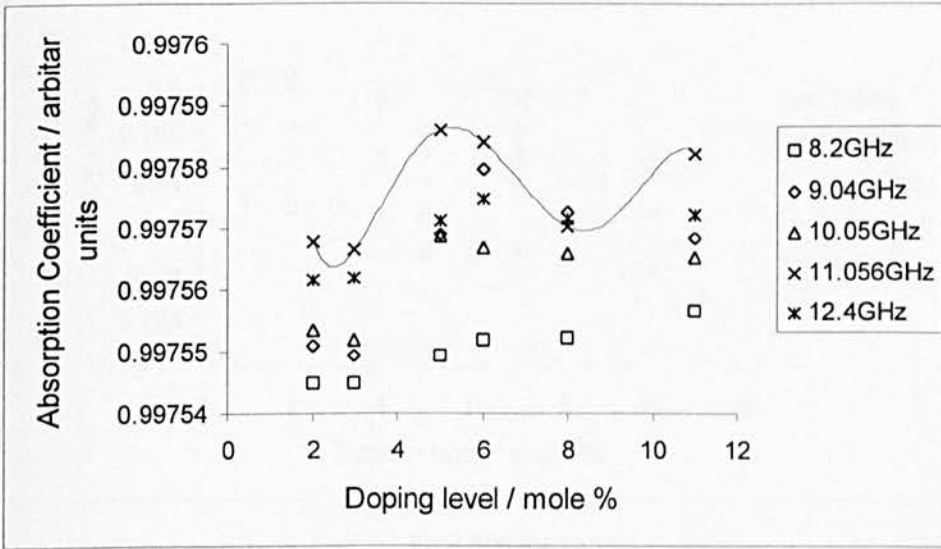
FIGURE 8.4

RELATIONSHIP BETWEEN THE ABSORPTION COEFFICIENT AND THE DOPING
LEVEL FOR POLY(3-HEXYLTHIOPHENE) BETWEEN 8.2GHz AND 12.4GHz
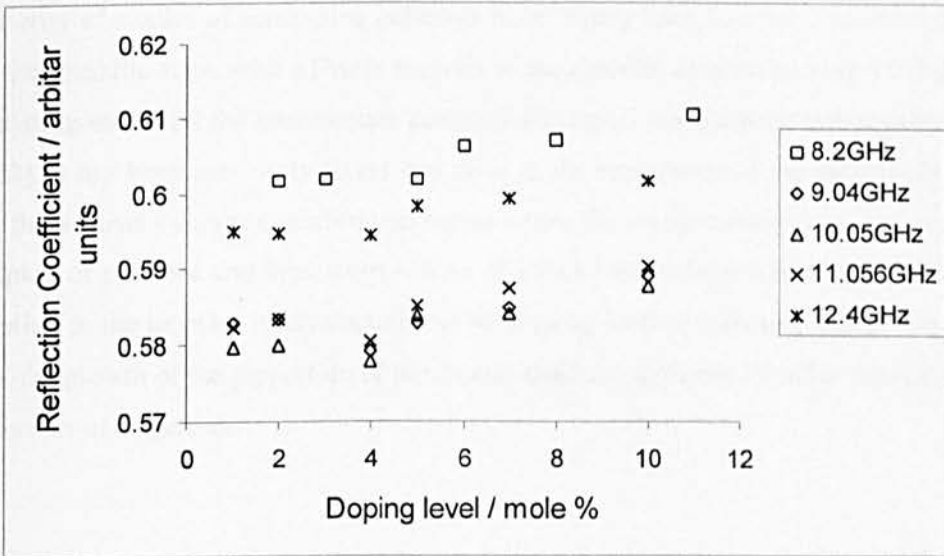

FIGURE 8.5

RELATIONSHIP BETWEEN THE REFLECTION COEFFICIENT AND THE DOPING
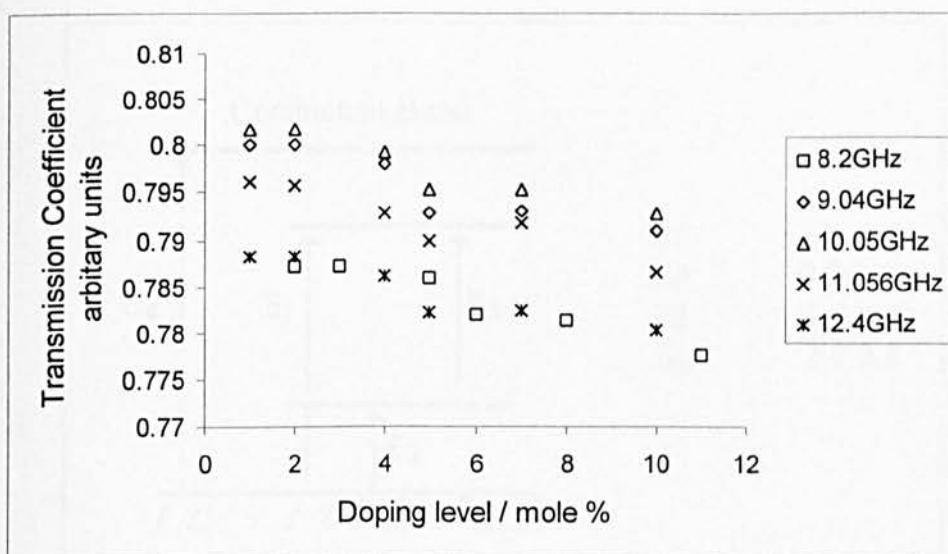LEVEL FOR POLY(3-HEXYLTHIOPHENE) BETWEEN 8.2GHz AND 12.4GHz

FIGURE 8.6

RELATIONSHIP BETWEEN THE TRANSMISSION COEFFICIENT AND THE DOPING

LEVEL FOR POLY(3-HEXYLTHIOPHENE) BETWEEN 8.2GHz AND 12.4GHz

The majority of studies of conducting polymers have largely been focussed on either the highly conducting metallic state, with a Drude analysis of the metallic conduction [118-119] or else on the insulating state, and the intermediate conductivity region has not been investigated in detail [120-122]. It has been previously found that prior to the appearance of the metallic Drude-type regime, there exists a charge concentration region where the charge transport can be described by the hopping of polarons and bipolarons – both of which have different mobilities. Therefore, a contribution to the increase in conductivity as the doping level is increased can be explained in terms of the growth of the proportion of bipolarons that have a greater mobility than the polarons by two orders of magnitude.
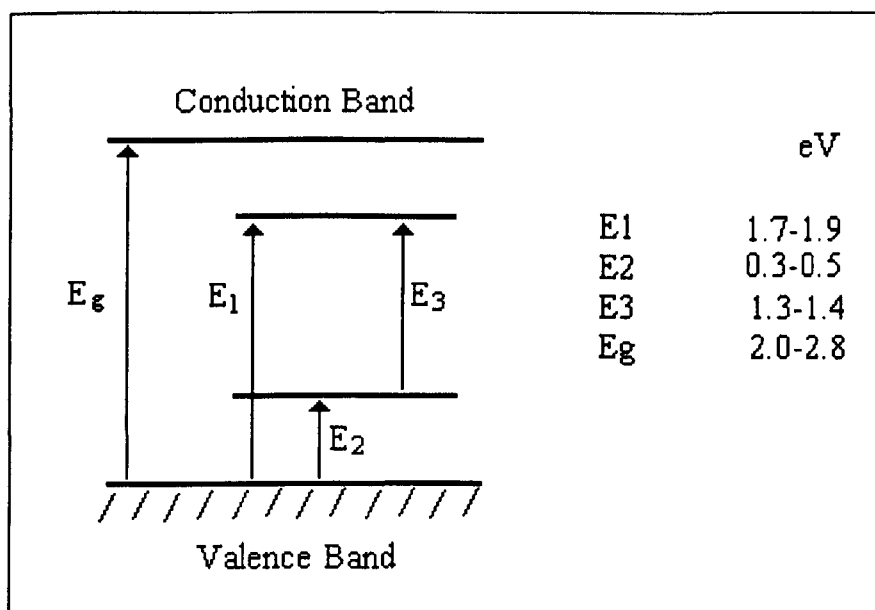
FIGURE 8.7

BAND STRUCTURE OF LIGHTLY DOPED (1-10mol%) POLY(3-HEXYLTHIOPHENE)

At this intermediate doping level, in the range of 1-10%, the electronic band gap is interrupted by comparatively localised polaronic energy levels (Figure 8.7).

The presence of an AC signal would therefore modulate the occupation of all states. This can be observed by comparing Figures 8.8 and 8.9, which represent the DC conductivity and the microwave conductivity as a function of the dopant level.

At low doping levels (<3 mole%), the spin density increases as the number of polarons increases. Further doping (3-10 mole%) further increases the number density of polarons and bipolarons, with a resultant increase in the DC conductivity, thereby implying that both polarons and bipolarons contribute to the charge transfer process in this conducting polymer. Based on the ESR observations of a linear dependence of the spin density on dopant concentration for polythiophenes [123] using ESR and for poly(3-methylthiophene) [124-125] in the doping of range 1-10 mole%, and the levelling off of the density of spins at higher doping levels, it has been concluded that polarons are the dominant charge carriers, and that metallic conduction begins at 10 mole% doping level.
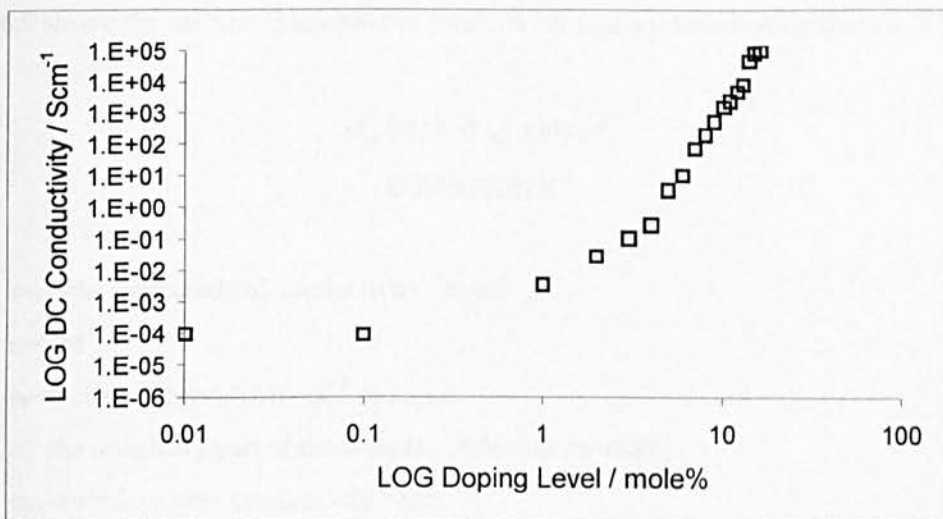
FIGURE 8.8

THE MEASURED DC CONDUCTIVITY IN RELATION TO THE DOPING LEVEL FOR
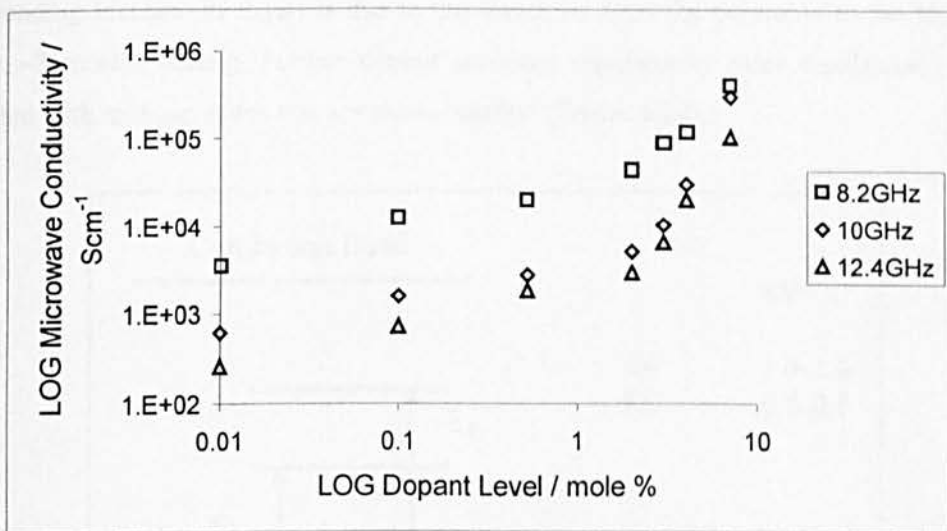POLY(3-HEXYLTHIOPHENE)

FIGURE 8.9

THE CALCULATED HIGH FREQUENCY CONDUCTIVITY IN RELATION TO THE
DOPING LEVEL FOR POLY(3-HEXYLTHIOPHENE)

Figure 8.9 shows the calculated microwave conductivity ($\sigma_m(\omega)$) based on equation 8.1:

$$\sigma_m(\omega) = \sigma_{DC} + \omega\varepsilon_0\varepsilon''$$

EQUATION 8.1

Where σ_{DC}=the measured DC conductivity / Scm^{-1}

ω=2πf

ε_0=dielectric permittivity of free space

ε'' the imaginary part of the complex dielectric constant

$\sigma_m(\omega)$=microwave conductivity / Scm^{-1}

By relating $\sigma_m(\omega)$ to the doping level, an enhancement in the conductivity can be observed in comparison to the DC conductivities at analogous doping levels. Since the DC conductivity primarily involves activated (bi)polaron hopping at ambient temperatures, it is proposed that the corresponding increase in $\sigma_m(\omega)$ is due to the transition from the polaronic to the bipolaronic state at ~5 mole% doping. Further doping produces significantly more bipolarons, which is associated with mid-gap states that are closer together (Figure 8.10).
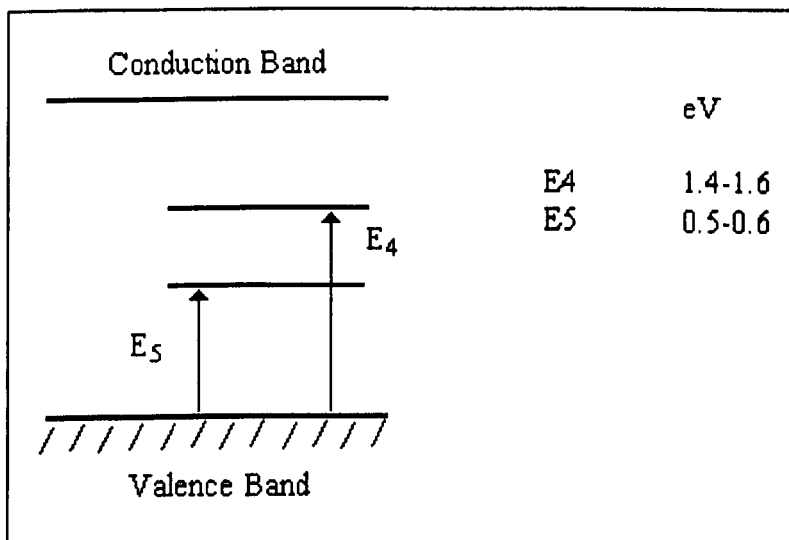

FIGURE 8.10

BAND STRUCTURE OF HEAVILY DOPED (>10mol%)POLY(3-HEXYLTHIOPHENE)

peak observed at ~11 mole% at 11GHz may be suggestive of free carrier absorption from within the bipolaron states due to the formation of a partially filled metallic band from the polaron states.

8.3   METAL-COMPLEXED POLY(3-METHYLTHIOPHENE)

It has been established earlier that the presence of metal ions decreases the density of states near the Fermi level, and contributes to activated hopping conduction.

8.3.1   Co COMPLEXED POLY(3-METHYLTHIOPHENE)

The reflection and transmission coefficients follow conventional behaviour with regard to the applied frequency (Figure 8.11), however, the absorption coefficient shows two absorption peaks at 7.95GHz and 10.56GHz, both with absorbances of –0.015dB, with a possible larger absorbance of –0.16dB at 13.63GHz (Figure 8.12).
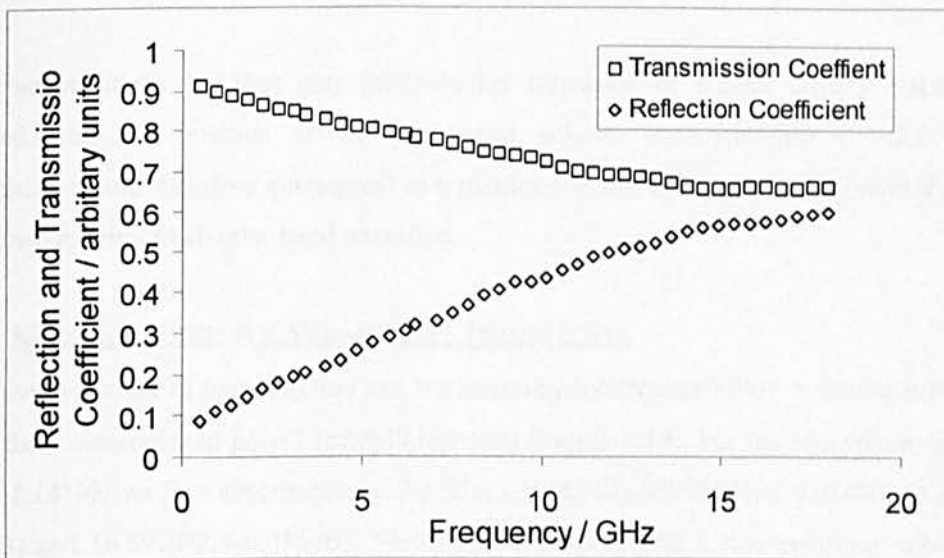

FIGURE 8.11

RELATIONSHIP BETWEEN THE RELECTION AND TRANSMISSION COEFFICIENT FOR UNDOPED Co COMPLEXED POLY(3-METHYLTHIOPHENE) POLYMER FILMS AND FREQUENCY
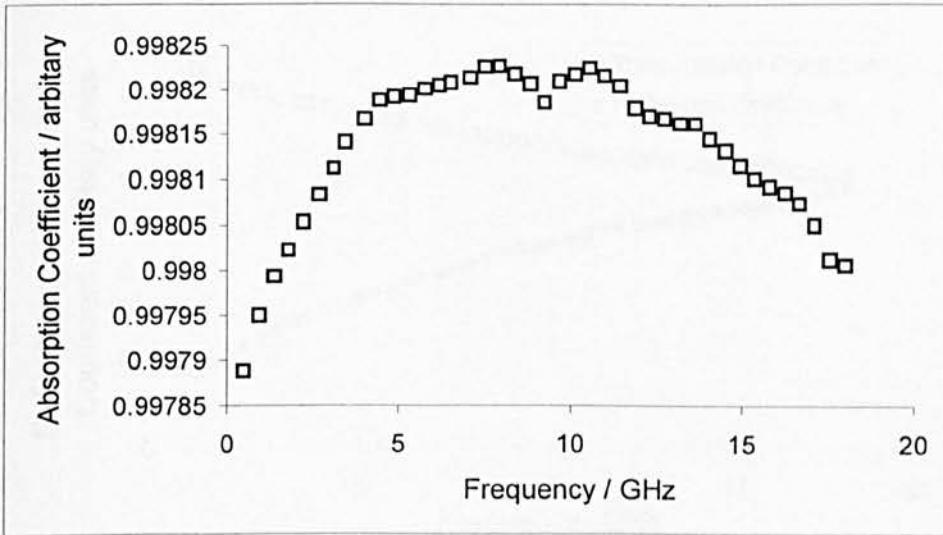
FIGURE 8.12

RELATIONSHIP BETWEEN THE ABSORPTION COEFFICIENT FOR UNDOPED Co
COMPLEXED POLY(3-METHYLTHIOPHENE) POLYMER FILMS AND
FREQUENCY

The presence of the Co ions may facilitate the formation of a new 'bound' polaron band displaced from the position of the established polaron band between 1.57-2.07eV. The absorbances would therefore correspond to transitions within these new states, with the smaller absorbance relating to an inter-band transition.

8.3.2   Ni COMPLEXED POLY(3-METHYLTHIOPHENE)

Again, the behaviour of the reflection and transmission coefficients follow a similar behaviour to that of the Co-complexed poly(3-methylthiophene) (Figure 8.13), but the absorption coefficient (Figure 8.14) shows four absorbances at 7.9 GHz (-0.015dB), 10.56GHz (-0.01dB), 13.63GHz (-0.014dB) and 16.69GHZ (-0.015dB). We therefore propose that a fine polaronic sub-structure has been created by the complexation of the Ni ions, and that the incident electromagnetic radiation is absorbed by the polarons that are then promoted to these closely neighbouring levels.
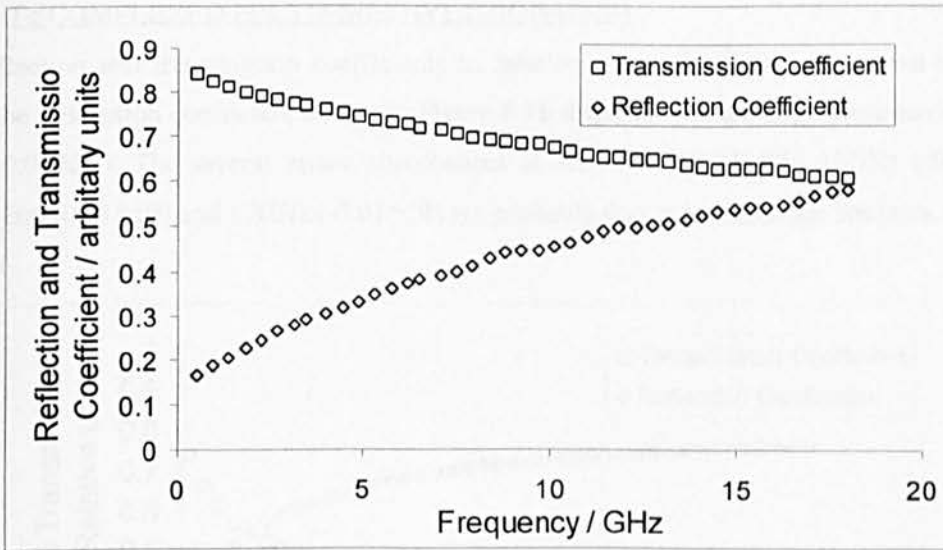
FIGURE 8.13

RELATIONSHIP BETWEEN THE RELECTION AND TRANSMISSION COEFFICIENT FOR
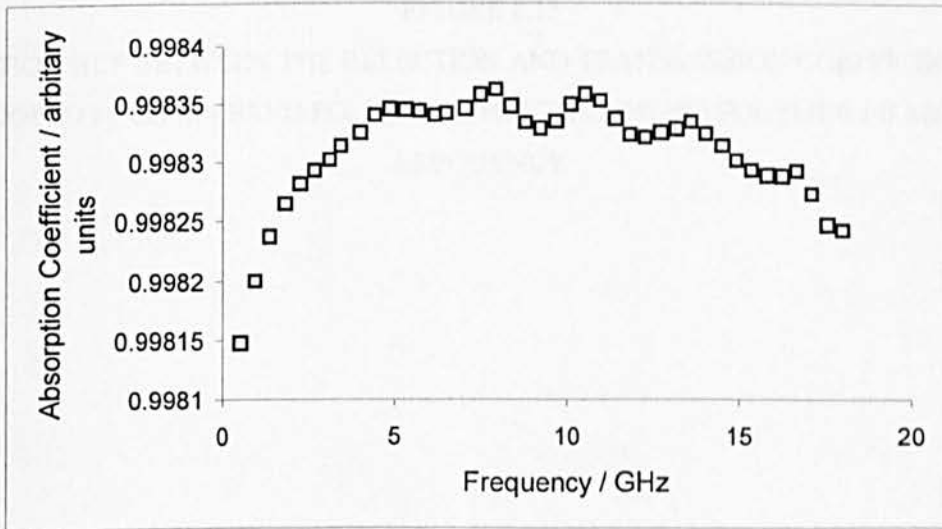UNDOPED Ni COMPLEXED POLY(3-METHYLTHIOPHENE) POLYMER FILMS AND
FREQUENCY

FIGURE 8.14

RELATIONSHIP BETWEEN THE ABSORPTION COEFFICIENT FOR UNDOPED Ni
COMPLEXED POLY(3-METHYLTHIOPHENE) POLYMER FILMS AND FREQUENCY

8.3.3   Fe COMPLEXED POLY(3-METHYLTHIOPHENE)

The reflection and transmission coefficients in relation to the frequency are shown in Figure 8.15. The absorption coefficient shown in Figure 8.16 displays a single large absorbance at 2.25 GHz (-0.013dB). The several minor absorbances at 7.94GHz (-0.013dB), 11GHz (-0.017dB), 14.06GHz (-0.014dB) and 17GHz (-0.015dB) are probably due to instrumental artefacts.
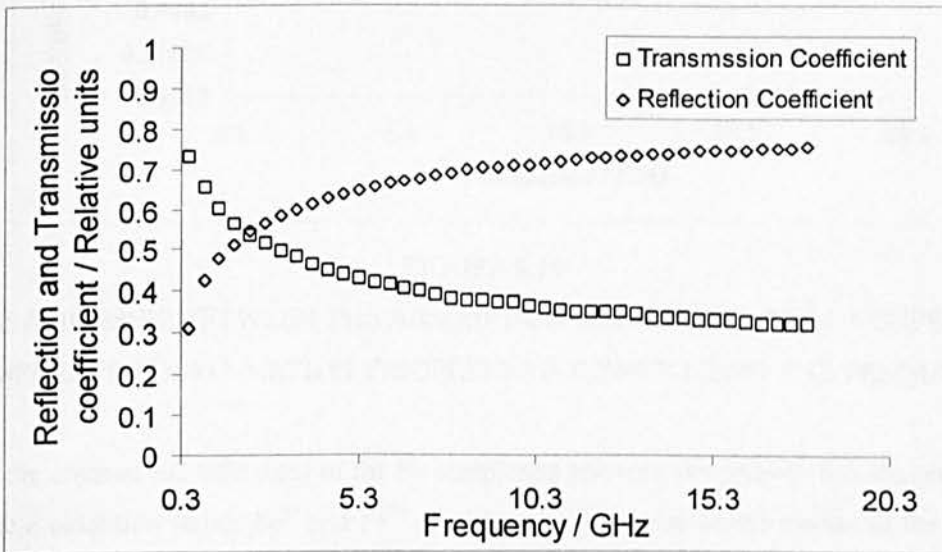

FIGURE 8.15

RELATIONSHIP BETWEEN THE RELECTION AND TRANSMISSION COEFFICIENT FOR UNDOPED Fe COMPLEXED POLY(3-METHYLTHIOPHENE) POLYMER FILMS AND FREQUENCY
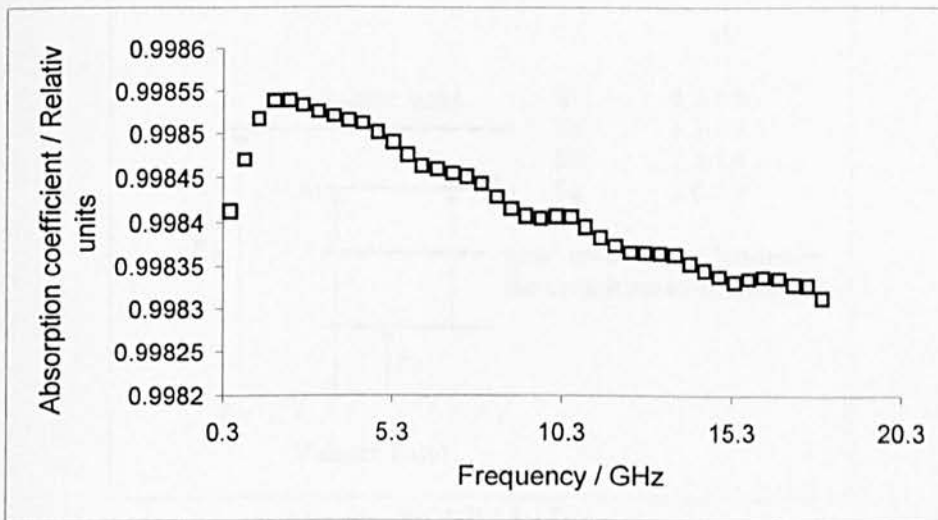
FIGURE 8.16

RELATIONSHIP BETWEEN THE ABSORPTION COEFFICIENT FOR UNDOPED Fe
COMPLEXED POLY(3-METHYLTHIOPHENE) POLYMER FILMS AND FREQUENCY

Due to the unusual AC behaviour of the Fe complexed polymer, we propose that the presence of two stable oxidation states: Fe^{2+} and Fe^{3+} provides a large barrier to the motion of the polarons and, upon further doping, bipolarons, and thereby lowering the DC conduction. This might also provide a substantial barrier to the microwave conductivity, resulting in less absorption of the microwave radiation.

8.4   SUMMARY OF THE ELECTROMAGNETIC PROPERTIES OF POLY(3-ALKYLTHIOPHENE)

The complexation of ferromagnetic ions has made a significant contribution to the absorbance of the incident high frequency electromagnetic radiation by the formation of a new polaron band at approximately 1.3-1.7eV (Figure 8.17). The application of EM radiation excites the polarons to the bipolaronic state.
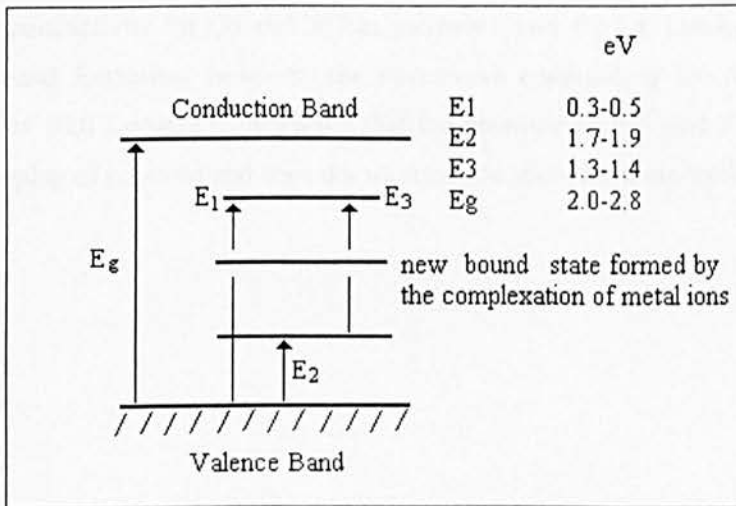
	eV
E1	0.3-0.5
E2	1.7-1.9
E3	1.3-1.4
Eg	2.0-2.8

FIGURE 8.17

THE PROPOSED CREATION OF A NEW INTER-POLARON ENERGY LEVEL UPON COMPLEXATION OF THE Ni AND Co METAL IONS WITH POLY(3-METHYLTHIOPHENE)

The microwave conductivity has therefore been increased by the contribution of the new polaron band, and the microwave conductivity for the complexation of Co, Ni and Fe is shown in Figure 8.18.
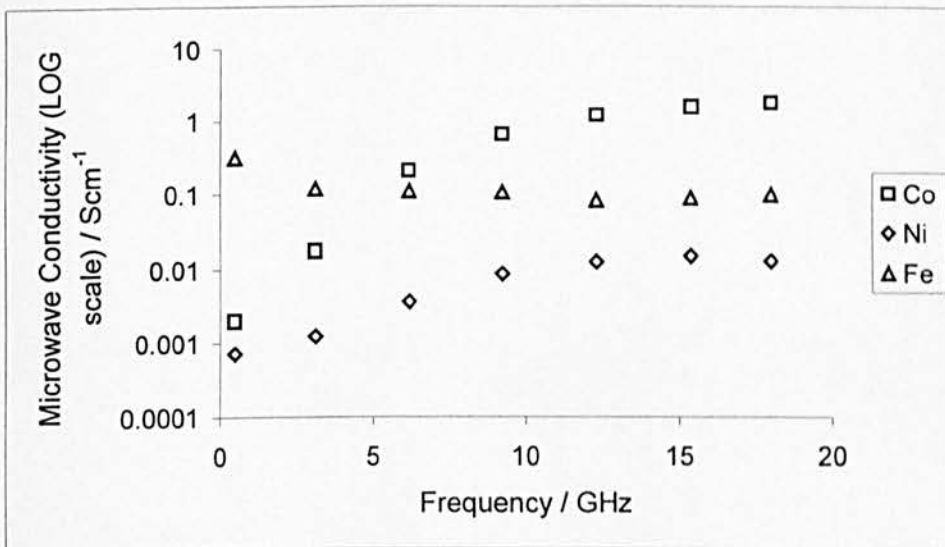

FIGURE 8.18

THE CALCULATED HIGH FREQUENCY CONDUCTIVITY FOR Co, Ni AND Fe FOR UNDOPED COMPLEXED POLY(3-METHYLTHIOPHENE)

The microwave conductivity for Co and Ni has increased over the DC conductivity, indicating new polaronic band formation, however, the microwave conductivity for the Fe complexed polymer decreases with frequency, indicating that the presence of Fe^{2+} and F^{3+} ions provides a barrier to the hopping of polarons and does not increase the microwave absorption.

CHAPTER NINE

CONCLUSIONS AND FURTHER WORK

9.1 CONCLUSIONS

The work in this thesis has involved a study of the factors involved in electrochromic switching with a view to using this data to provide controllable electromagnetic absorption. This should be considered in conjunction with a preliminary investigation into the effect of complexing ferromagnetic ions into poly(3-methylthiophene) to provide superior electromagnetic absorption.

Polyalklylthiophenes and polyanilines have been synthesised using two different techniques. Electrochemical polymerisation was found to give insoluble very high molecular weight films, and the nature of the product was very dependent upon the polymerisation conditions, particularly the presence of residual water. The films that were produced by this method were very brittle and porous, but could be used for use over small areas. However, this method was later replaced by chemical synthesis of polymer films that could be solvent cast from solution. The superior mechanical characteristics of the solvent cast films better suited the study.

The electrochromic properties of polyaniline, polypyrrole and poly(3-methylthiophene) were investigated using a variety of dopant ion sizes. The bulkiest dopant ion: tetraphenylborate, was observed to become rapidly diffusion-limited due to an inability to pass through the polymer when an oxidising or reducing potential was applied. Thinner polymer films switched more rapidly, but gave a reduced contrast ratio. This is to be expected since there is a larger quantity of conducting polymer film for the ions to permeate, and will therefore require more ions to change the localized structure of the conducting polymer chain. Polymer films were also cycled continuously to study the possible effects on the polymer degradation for extended usage. It was found that polymers could be cycled repeatedly between the doped and undoped states with only a small decrease in the contrast ratio after several thousand switches. The longevity of the polymer film could be increased if a suitable voltage pulse amplitude was used.

The DC and AC study of the conduction processes of poly(3-methylthiophene) revealed that at temperatures below 250K, the conduction is due to variable range hopping. As the temperature was increased to 183K, the conduction mechanism deviates to an activated process, with polaron hopping occurring with an activation energy of 0.48eV. This value of the energy barrier is consistent with a transition from the lower polaron band to the upper (bi)polaron band to form a new polaron.

The complexation of Co appears to favour variable range electron hopping over the entire temperature range. Low temperature conduction (<223K) is due to quantum tunnelling between the potential barriers, with an activation energy of 0.02eV across a barrier width of 2.3nm at 123K. As the temperature is increased above 223K, an activated polaron hopping is favoured with an energy barrier of 0.21eV in comparison to 0.48eV to the non complexed poly(3-methylthiophene). Therefore the DC conductivity of the material is lower, since the density of states is reduced by ~300$eV^{-1}cm^{-3}$ in the Co complexed polymer, but AC conduction mechanisms are favoured, with the possibility of the upper polaron band moving closer to the conduction band by 0.35eV.

The complexation of Ni follows a similar trend to that of the Co complexed P3MT, with variable range hopping occurring over the entire temperature range studied (123-323K), but favours barrier

tunnelling at temperatures below 223K through a barrier of 0.01eV in height and 0.41nm in width. Activated polaron hopping occurs by moving the upper polaron band even closer to the conduction band to 0.098eV at temperatures >223K.

The low density of states for the Fe complexed polymer ($2.5 \times 10^{20} eV^{-1} cm^{-3}$) gives a low DC conductivity, with barrier tunnelling occurring between 123-223K with $\delta E \sim 0.02eV$. A further increase in temperature to 183K fits the $T^{-\frac{1}{4}}$ model, with the variable range electron hopping model, occurring from 183-323K. The presence of the Fe^{2+} and Fe^{3+} ions appears to form an insulating barrier to the movement of polarons. However, the presence of metal-sulphur bonds as a result of the complexation of the Fe^{2+} and Fe^{3+} ions may additionally contribute an additional charge transfer mechanism at low temperature due to hopping between the metallic islands, with an activation energy of 0.45eV at 123K. The activation energy for hopping between the metallic sites increases as the temperature increases, since the metal sites further apart at higher temperatures.

The presence of a large number of hopping charges present in conducting polymers leads to a large

difference for ε_r' and ε_r'' in comparison to insulators. Uncomplexed poly(3-methylthiophene) and Fe complexed poly(3-methylthiophene) show a large dispersion of ε_r' and ε_r'' at low frequencies whereas Co and Ni complexed polymers show less of a dispersion, indicating that

the relaxation times are slower for the uncomplexed and Fe complexed polymers, possibly due to an inherent disorder of the polymer.

ε_r'' shows a 1/f dependency for both Co and Ni complexed polymers which is indicative of a DC dominated conduction process, which is not the case for the uncomplexed and Fe complexed polymers. No loss angle peak is observed for the Ni and Co complexed polymers, which indicates that there the dipoles associated with the polymer chain have a very wide distribution of relaxation times.

Budd *et al* have confirmed the complexation of the Fe^{2+} and Fe^{3+} ions. This data, confirms that the high concentration of metal ions results in a reduction of the activation energy since the main dipole of the molecule has been transferred to the Fe-S bond. Oscillations of this moiety explain the loss at 1.2KHz and 323K. A schematic diagram of this species is shown in Figure 9.1. The Fe^{x+} ion is unlikely to be situated mid-way between polymer chains, and is more likely to be closely bonded to one polymer chain than to another.
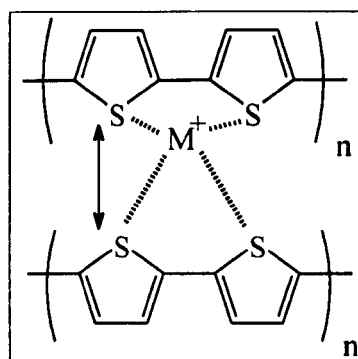

FIGURE 9.1

PREDICTION OF THE POSITION OF THE METAL ION IN A POLYMER CHAIN

This model would explain the large dispersion that is observed with a decrease in frequency and an increase in temperature. Only small oscillations of the Fe-S moiety are possible at high frequencies and low temperatures, resulting in a small dielectric loss. Larger oscillations are possible at low frequencies and as the temperature increases, resulting in a larger contribution of the dielectric loss. Complexation by Co, Ni and Fe was found to make a contribution to the

microwave absorption characteristics of poly(3-methylthiophene). Doping of the uncomplexed polymer produces absorbances at 5 and 11 mole% corresponding to the transition from the polaronic to the bipolaronic state at 5 mole% doping. Further doping produces significantly more bipolarons, which move the mid-gap states closer together resulting in a further absorption at 11 mole%. In contrast to this, complexation of Co and Ni produces a new polaronic state at 1.3-1 7eV, with a corresponding increase in the microwave conductivity due to the contribution from polarons promoted to this level. The complexation of Fe, with the presence of Fe^{2+} and Fe^{3+} decreases the microwave conductivity by either widening the polaronic energy states or by providing deeper localisations along the polymer chain.

Since a domination of the DC conduction processes is required to provide enhanced electromagnetic absorbers, it is the recommendation of the author that Co complexed polymers be used at doping levels of 5 mole% [121].

9.2   FURTHER WORK

Much of the work carried during this research could be investigated further. The author makes the following suggestions:

i)   Preparation of highly annealed P3MT to observe the new bound polaron band using UV-visible spectrometry.

ii)   A study of the effect of the doping level on the absorption of the incident electromagnetic radiation with magnetic complexed polymer would provide additional data on the optimisation of electromagnetic radiation absorption.

iii) This research concentrated on investigating the possibility of enhanced electromagnetic absorption by the complexation of a conducting polymer with magnetic ions. Since it is appears that the electromagnetic radiation is absorbed more readily as a result of the complexation of a conducting polymer with magnetic ions, further work is required in the optimisation of the precise concentration of the magnetic ions to provide superior electromagnetic radiation absorption whilst maintaining the integrity of the conducting polymer films.

iv)   Observation of the magnetic components, μ_r' and μ_r'' in addition to the ε_r' and ε_r'' would provide additional evidence that the complexation of Fe, Co and Ni into the polymer has contributed to the magnetic loss of the electromagnetic wave.

REFERENCES

[1]   H. Shirakawa, S. Ikeda; Polym. J. **2** (1971) 231.

[2]   S. M. Sze; Semiconductor Devices-Physics and Technology; J. Wiley and Sons pp14

[3]   A.I. Gubanov; Quantum electron theory of amorphous semiconductors Consultants Bureau New Nork (1963)

[4]   L. Banyai; Physique de Semiconducteurs (ed. M. Hulin) Dunod Paris (1964)

[5]   N.H. Mott; Phil. Mag (1968) 1259

[6]   P.W. Anderson; Phys. Rev. **109** (1970) 1492

[7]   N.F. Mott; Adv Phys. **16** (1967) 40

[8]   M.H. Cohen, H. Fritzsche and S.R. Ovshinskv; Phys. Rev. lett. **22** (1969) 1065

[9]   A.I. Gubanov; Quantum electron theory of amorphous conductors (1963) Consultants Bureau, New York 1965

[10]   L. Banyai; *Physiquee des Semiconducteurs* (ed. M. Hulin) (1964) Dunod Paris

[11]   P.W. Anderson; Phys. Rev. **109** (1958) 1042

[12]   NF. Mott; Electronic Processes in Non-Crystalline Materials, Clarendon Press Oxford (1979)

[13]   N.W. Ashcroft. N D. Mermin; Solid State Physics Rinehart and Wilson (1976)

[14]   P.W Anderson Phys. Rev. **109** (1958) 1492.

[15]   H. Nalwa; Handbook of Organic Conductive Molecules and Polymers J. Wiley and Sons New York 1997 (1st Edn)

[16]   W.P. Su and JR Schrieffer; Proc. Natl. Acad. Sci. U.S.A. **77** (1980) 5626

[17]   D.K. Campbell and K. Fesser; Mol. Cryst. Liq. Cryst. **77** (1981) 253

[18]   S.A. Brazovskii and N. Kirova; J.E.P.T. Lett. **33** (1981) 4.

[19]   A.R. Bishop, D.K. Campbell and K. Fesser; Mol. Cryst. Liq. Cryst. **77** (1981) 218

[20]   J.L. Brèdas, R.R Chance and R. Silbey Mol. Cryst. **77** (1981) 319

[21]   J.L. Brèdas, S.C. Scott, K. Yakushi and GB. Street; Phys. Rev. B Cond. Matt. **30** (1984) 1023

[22]   P.W. Anderson; Phys. Rev. Lett **34** (1975) 953

[23]   W.P. Su, J. R. Schrieffer and A.J. Heeger; Phys. Rev. Lett **42** (1979)1698

[24]   C.S. Yannoui and T.C. Clarke; Phys. Rev. Lett. **51** (1983) 1191

[25]   C. Rebbi; Sci. Am. **40** (1979) 92

[26]   W.P. Wu, J.R. Schrieffer and A.J. Heeger; Phys. Rev. Lett;. B (1979) 1698

[27]   D.S. Boudreaux, R.R. Chance, J.L. Brèdas and R. Silbey; Phys. Rev. B Cond. Matt.

28 (1983) 6927

[28]   H. Thomann, L.R. Dalton, Y Tomkiewicz, N. S. Shiren and T.C. Clarke; Phys. Rev. Lett. **50** (1983) 533

[29]   D. Moses, A. Denenstein, J. Chen, A.J. Heeger, P. McAndrew, T. Woemer, A.G. Macdiarmid and Y.W. Park; Phys. Rev. B Cond. Matt. **25** (1982) 7652

[30]   E.J. Mele and M. J. Rice; Phys. Rev. B Cond. Matt. **23** (1981) 5397

[31]   J. M André, I.A. Burke, J. Dehalle, G. Nicholas and P.H. Durand; Int. J. Quantum. Chem. Quantum Chem. Symp. **13** 283 (1979).

[32]   A.J. Epstein, H. Rommelmann, R.W. Bigelow, H.W. Ibison. D.M. Hoffman and D. B. Tanner; Phys. Rev. Lett. **51** (1983) 2020

[33]   J.C. Scott, M. Krounbi, P. Pfluger and G.B. Street: Phys. Rev. B Cond. Matt. **28** (1983) 2140

[34]   J.C. Scott, J.L. Brèdas, J.H. Kaufman, P. Pfluger, G.B. Street and K. Yakushi: Mol. Cryst. Liq. Cryst. **118** (1985) 163

[35]   J L. Brèdas , J.C. Scott. K. Yakushi and G.B. Street: Phys Rev B Cond. Matt. **30** (1984) 1023

[36]   J.L. Brèdas, B. Thérnans, J.G. Fripat, J. M André and R.R. Chance; Phys. Rev. B Cond. Matt. **29** (1984) 6761

[37]   J.L. Brèdas, B. Thérnans, J.G. Fripat, J. M André and R.R. Chance; Phys. Rev. B Cond. Matt. **29** (1984) 6791

[38]   T.C. Chung, J.H. Kaufman, A.J. Heeger and F. Wudl; Phys. Rev. B Cond. Matt. **30** (1984) 702

[39]   D. Moses. A. Denenstein, J. Chen, A.J. Heeger, P. McAndrew. T. Woemer, A. G. Macdiarmid and Y.W. Park: Phys. Rev. B Cond. Matt. **25** (1982) 7652

[40]   J.J. Ritsko, J. Finke and G. Creceline; Solid State. Commun. **46** (1983) 477

[41]   C. K. Chiang, C.R. Fincher, Y.W. Park, A.J. Heeger, H. Shirakawa, E.J. Louis, A.G. Macdiarmid; Phys. Rev. Lett **39** (1977) 1098.

[42]   C. K. Chiang, Y.W. Park, A.J. Heeger, H. Shirakawa, E.J. Louis and A.G. Macdiarmid Chem. Phys. **69** (1978) 5098.

[43]   T.C. Chung, J.H. Kaufman, A.J. Heeger and F. Wudl; Mol. Cryst. Liq. Cryst; **118** (1985) 205

[44]   K. Kaneto, H. Agawa, H. Yoshino; J. Appl. Phys. **61** 1197-1205 (1992)

[45]   S.M. Sze, Physics of Semiconductor Devices; 2nd Ed. Wiley International and Sons

[46]   N.Schockley, W.T. Read; Phys Rev. **87** (1952)835-342

[47]   N.F. Mott, E.A. Davis; Electronic Processes in Non-Crystalline Materials, Oxford University Press. London (1971)

[48]   S. Marchant, PhD Thesis; University of Greenwich (1992)

[49]   A.J. Grant and E.A. Davis; Solid State Commun. **15** 563 (1974)

[50]   P.N. Butcher; J.Phys. C: Solid State Phys. **7** 2645 (1974)]

[51]   A. Miller and S. Abrahams; Phys. Rev. **120** 745 (1960)

[52]   G.E. Pike and C.H. Seager; Phys. Rev. B **10** 1421 (1974)

[53]   A.R. Blythe; Electrical Properties of Polymers, Cambridge University Press, Cambridge (1979)

[54]   M.S. Ahmed, A.M. Zihilif, E. Martuscelli G. Ragosta and E. Scafora; Polymer Composites **13 (1)** (1992) 53

[55]   A.J. Epstein, H. Rommelmann, M. Abkowitz and H.W Gibson; Polym. Prep. **12 (1)** (1982) 88

[56]   A. Feldblum; Y W. Park, A.J. Heeger, A.G. Macdiarmid , G Wnek, F. Karasz and J.C.W. Chien; J Polym. Sci. Polym. Phys. Edn. **19** (1981) 173

[57]   A.K. Jonscher; Dielectric Relaxation in Solids. Chelsea Dielectric. London (1983)

[58]   P.W. Debye; Polar Molecules. Dover Publications, New York (1945)

[59]   J.R. Macdonald; Impedance Spectroscopy J. Wiley and Sons (1987)

[60]   N.F. Mott; Phil. Mag. **22** 903

[61]   S Marchant and P.J.S. Foot: data to be published (1995)

[62]   M. Reghu, S.V. Subramanyam and S. Chatterjee: Phys Rev. B **43(5)** (1991) 4236

[63]   P. Hourquebie; L. Olmedo; Synth. Met. **65** (1994) 19-26

[64]   A.G. Macdiarmid, A.J. Epstein; Proc. 1st Int. Conf. Frontiers of Polymer Research. New Delhi. India Jan. 20-25 (1991)

[65]   H. Ishikawa. X. Xu. A. Kobayashi; J. Phys. D Appl. Phys. **25** (1992) 897-900

[66]   K. Mizoguchi, M Nechtschein, J.P. Travers; Phys. Rev. Lett. (1989) 63-66

[67]   A.B. Kaiser, C.J. Liu, P.W. Gilberd, B. Chapman, N.T. Kemp, B. Wenling, A.C. Partridge, W.T. Smith, J.S. Shapiro; Synth. Met. (ICSM 1996).

[68]   A. Kaynak, J. Unwvorth, G.E. Beard, R. Clout; Mat. Res. Bull **28** (1993) 1109-1125.

[69]   A. Kaynak, J. Unsworth, B.A. Lunn; J. Mat. Sci. **28** (1993) 3307-3312.

[70]   F. Genoud. M. Nechtschein, C. Santier; Synth. Met. **55** (1993) 642

[71]   F. Zuo, M. Angelopoulos, A.G. Macdiarmid , A.J. Epstein; phys. Rev. B **36** (1997) 3475

[72]   Z. H. Wang, C. Li, E.M. Scherr, A.G. Macdiarmid, A.J. Epstein; Phys. Rev. B **45** (1992) 4190

[73]   H.K. Roth, H. Gruber, Z. Wissenschaft; Liepzig **15** (1991) 369

[74]   S.A. Jansen, T. Duong, A. Major, Y. Wei and I.T. Sein Jr; Synth. Met. **105** (1999) 107

[75]   E.M. Genies and M.J. Lapowski, J. Electroanal. Chem **236** (1987) 199

[76]   RH. Bauguam, J.F. Wolf, H. Echhardt, L.W. Shacklette; Synth. Met. **25** (1988) 121

[77]   Z H. Wang, A. Ray, A.G. Macdiarmid, A.J. Epstein; Phys. Rev. B **343(5)** (1991) 4373

[78]   J Kijarui; Phys. Rev B **83** (1983) 922

[79]   A.J. Heeger, S A. Kievelson, J.R. Schrieffer and W.P. Su; Rev. Mod. Phys. **60** (1988) 781

[80]   Z. H. Wang, A. Ray, A.G. Macdiarmid and A.J. Epstein; Phys. Rev. B **43(5)** (1992) 4373

[81]   S.K. Khanna, F Ehrenfreud, A.F. Garito, A.J. Heeger; Phys Rev B **10** (1974) 2205.

[82]   Z.H. Wang, E.M. Scherr, AG. Macdiarmid and A.J. Epstein. Phys Rev Lett. **66** (1991) 1745.

[83]   J.Joo, Z. Oblabouski, G. Du, J.P. Pouget, A.J. Epstein, E J. Oh, J.M. Wiesinger, Y.Min and AG. Macdiarmid; Phys. Rev. B (Rap. Commun.) **49(4)** (1994) 2977.

[84]   A M. Nicholson and G. Ross; IEEE Trans. Instrum.. Meas. **IM-19** (1970) 377-382

[85]   W B Weir; Proc IEEE **62** (1974) 33

[86]   A.K. Jonscher; Nature **267** (1977) 673

[87]   J.E. Weston, B.C H. Steele; Solid Stare Ionics **2** (1981) 327-364

[88]   T A. Skotheim (ed) Handbook of Conducting Polymers; (1986) Vol.1 &2.

[89]   A.J. Bard and L.R. Faulkner, Electrochemical Methods - Fundamentals and Applications; J. Wiley and Sons LTD (1980)

[90]   F.Mohammed, Ph D. thesis, University of Sussex (1987)

[91]   J.M. Bureau, M. Gazard. M. Champagne, J.C. Dubois, G. Tourillon and F. Garnier; Mol. Cryst. Liq. Cryst; **118** (1985) 235-239

[92]   A.Miller and S.Abrahams; Phys. Rev. **120** (1960) 745

[93]   S.M. Sze; Physics of Semiconductor Devices; John Wiley and Son (1981)

[94]   S.Marchant and P.J.S. Foot; Chemtronics **5** (1991) 131

[95]   P.J.S. Foot; unpublished data

[96]   R.Callaerts, H.Krikor, R.Mertiens and P.Nagels; Synth. Met. **37** (1990) 107

[97]   K. Vakiparta, J. Moulton, A.J. Heeger, P.Smith, H.Isotalo, H.Stubb and M. Loponen; Synth. Met. **41** (1991) 903

[98]   N.H. Mott and E.A. Davis; Electronic Processes in Non-crystalline Materials Clarendon Press (1979)

[99]   S. Kivelson; Phys. Rev. Lett. **47** (1981) 1549

[100]   D. Budd, R. Davis and P.J.S. Foot; 4th International Autumn School on Conducting Polymers - Transport Phenomena eds. J. Przyluski (1992)

[101]   D. Budd, R. Davis and P.J.S. Foot; Proc. European Materials Research Society Symposium on Polyconjugated Materials Strasbourg (1991)

[102]   R. Singh, R.P. Tandon, V.S. Panwar and S. Chandra; J. Appl. Phys **69(4)** (1991) 2504

[103]   K.L. Ngai and R.W.Rendell; in T.A. Skotheim (ed) Handbook of Conducting Polymers. (1986) 967

[104]   S Chen and C.Liao; Macromol. **26** (1993) 2810

[105]   F. Zuo, M. Angelopoulos, A.G. Macdiarmid and A.J. Epstein; Phys Rev. B (1989) 3570

[106]   Hsun-Tsing Lee, Chien-Shiun Liao and Show-An Chen; Makromol. Chem. **194** (1993) 2443

[107]   C.R. Lawrence, Miah, T. Stickland, T.S. Treen and I. Youngs; IEE Proc.-Sci. Meas. Technol. **145 4** (1998) 166

[108]   K. L. Ngai and R.W. Rendell in TA. Skotheim (ed.) Handbook of Conducting Polymers (1986) 967.

[109]   T.J. Lewis; Dielectric and related Molecular processes 3 (1977) Chem. Soc. London

[110]   F. Zuo, M. Angelopoulos A.G. Macdiarmid and A.J. Epstein; Phys. Rev. B (1989) 3570

[111]   A.K. Jonscher; Dielectric Relaxation in Solids Chelsea Dielectric Press London (1983)

[112]   J. Unsworth, A. Kaynak, B.A. Lunn and G.E. Beard; J. Mat. Sci 28 (1993) 3307-3312

[113]   A.J.Epstein, J.Joo, R.S.Kohlman, G. Du, A.G. Macdiarmid, E.J.Oh, Y.Min, J.Tsukamoto,
        H.Kaneto and J.P. Pouget; Synth. Met. **65** (1994) 149

[114]   J.Joo, E.J.Oh, G. Min, AG. Macdiarmid and A.J.Epstein; Synth. Met. **69** (1995) 251

[115] R.S. Kohlman, J.Joo, Y.Z. Wang, J.P. Pouget, H. Kaneto, T. Ishiguro and A.J. Epstein; Phys. Rev. Lett 74(5) (1994) 773

[116] J. Joo, Z. Oblahowski, G. Du, J.P. Pouget, E.J. Oh, J.M. Wiesinger, Y. Min, A.G. Macdiarmid and A.J. Epstein; Phys. Rev. B 49(4) (1993) 2977

[117] Z.H.Wang, E.M. Scherr, AG. Macdiarmid and A.J. Epstein; Phys. Rev. B 45 (8) (1991) 4190

[118] T. Yamabe, K. Tanaka, S.Yamanaka, T. Koike and F. Fukui: J. Chem. Phys. 82 (1985) 5737

[119] K Mizoguchi, M.Nechtschein, J.P. Travers and C. Menardo; Phys. Rev. Lett. 63 (1989) 66

[120] T.H. Gilani and T. Ishiguro; J. Phys. Soc. Jpn. 66 (1997) 727

[121] J. Chen, A.J. Heeger and F. Wudl; Solid State Commun. 58 (1986) 251

[122] Colaneri, M Nowak, D. Spiegel, S. Hotta and A.J. Heeger; Phys Rev. B 36 (1987) 7964

[123] Z.W. Sun and A.J. Frank; J. Chem. Phys. 94 (1991) 4600

[124] J. Usworth, A. Kaynak, BA. Lunn and G.E. Beard; J. Mat. Sci 28 (1993) 3307-3312

[125] M. Reghu, S.V Subramanyam and S. Chatterjee; Phys Rev B 43(5) (1991) 4236

APPENDIX I

SPECTROSCOPIC DATA
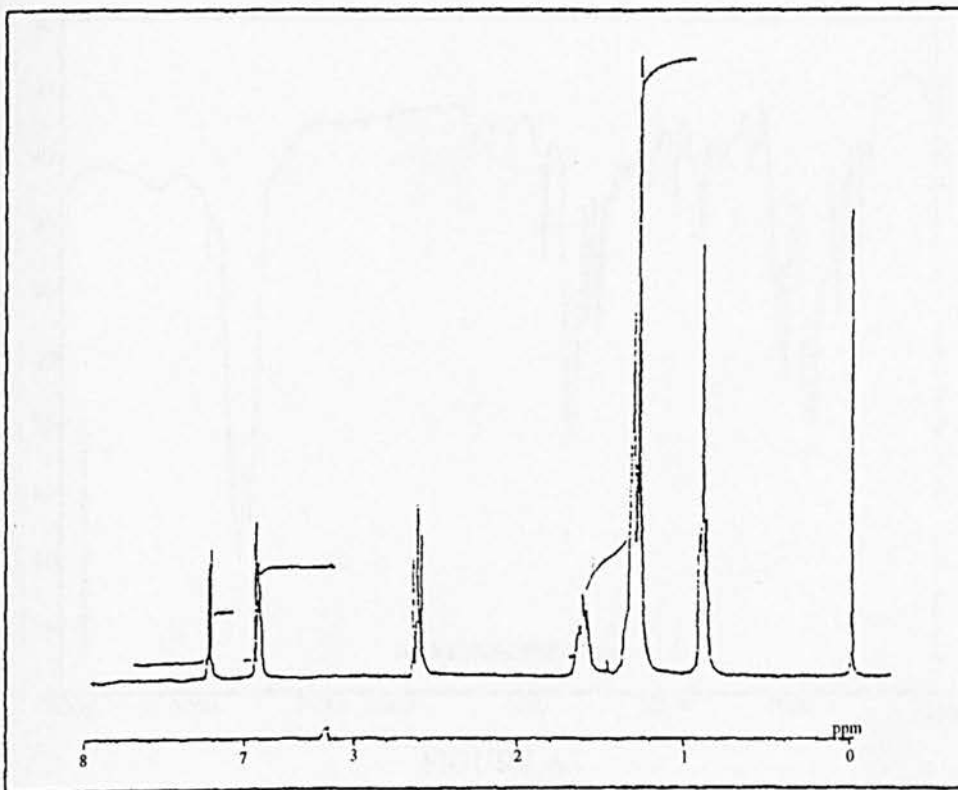
FIGURE A1
^{1}H NMR SPECTRUM OF 3-HEXYLTHIOPHENE MONOMER
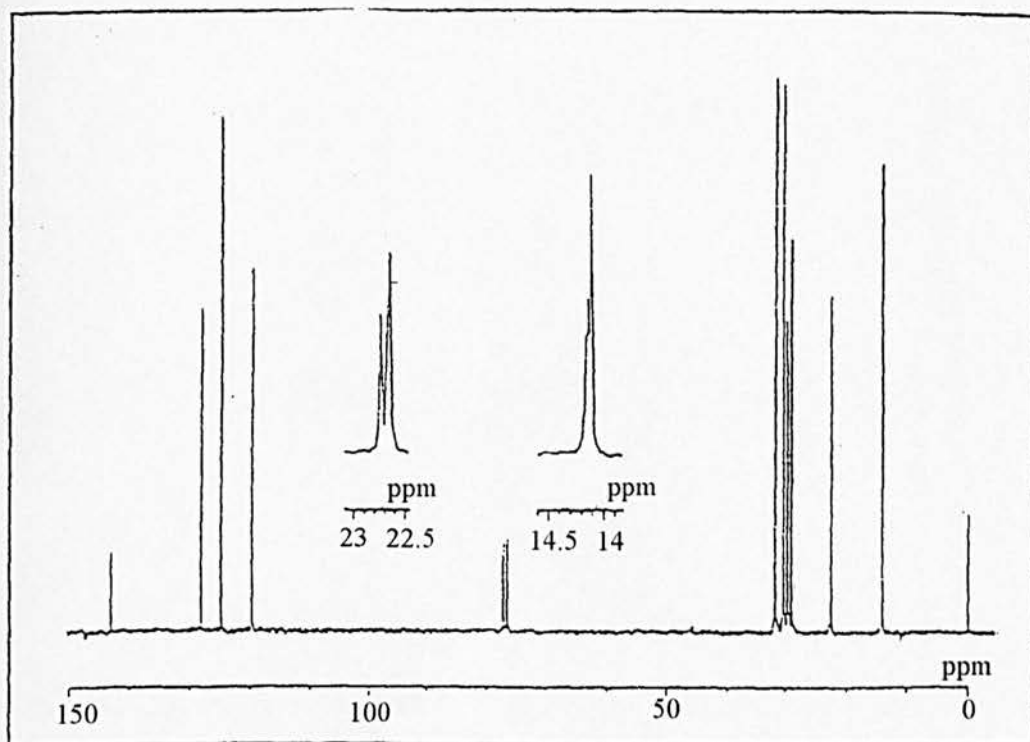
FIGURE A2
^{13}C NMR SPECTRUM OF 3-HEXYLTHIOPHENE
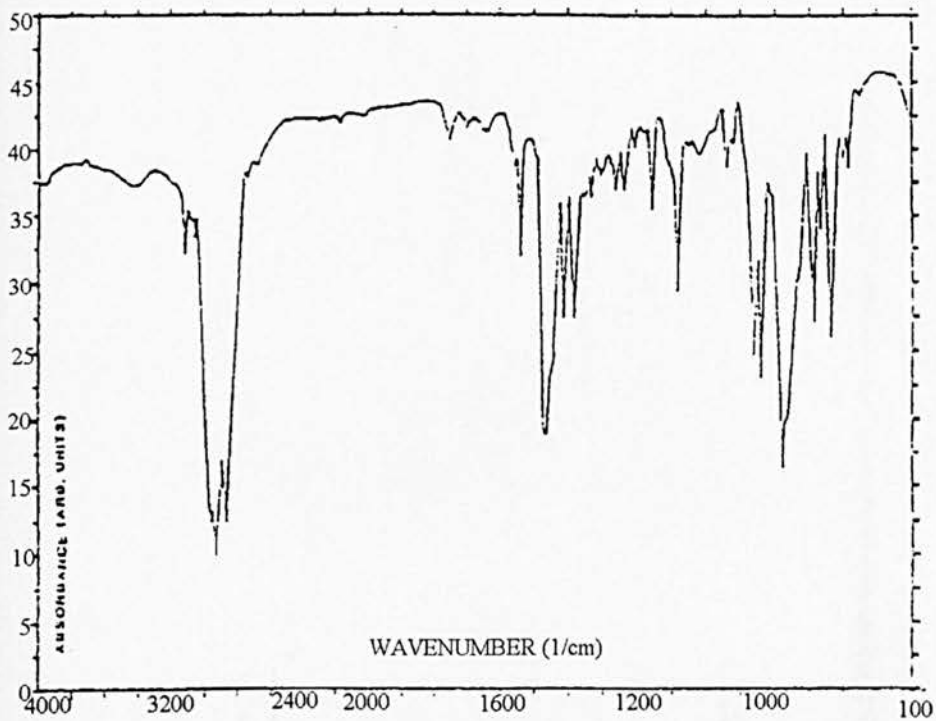
FIGURE A3
FTIR SPECTRUM OF 3-HEXYLTHIOPHENE
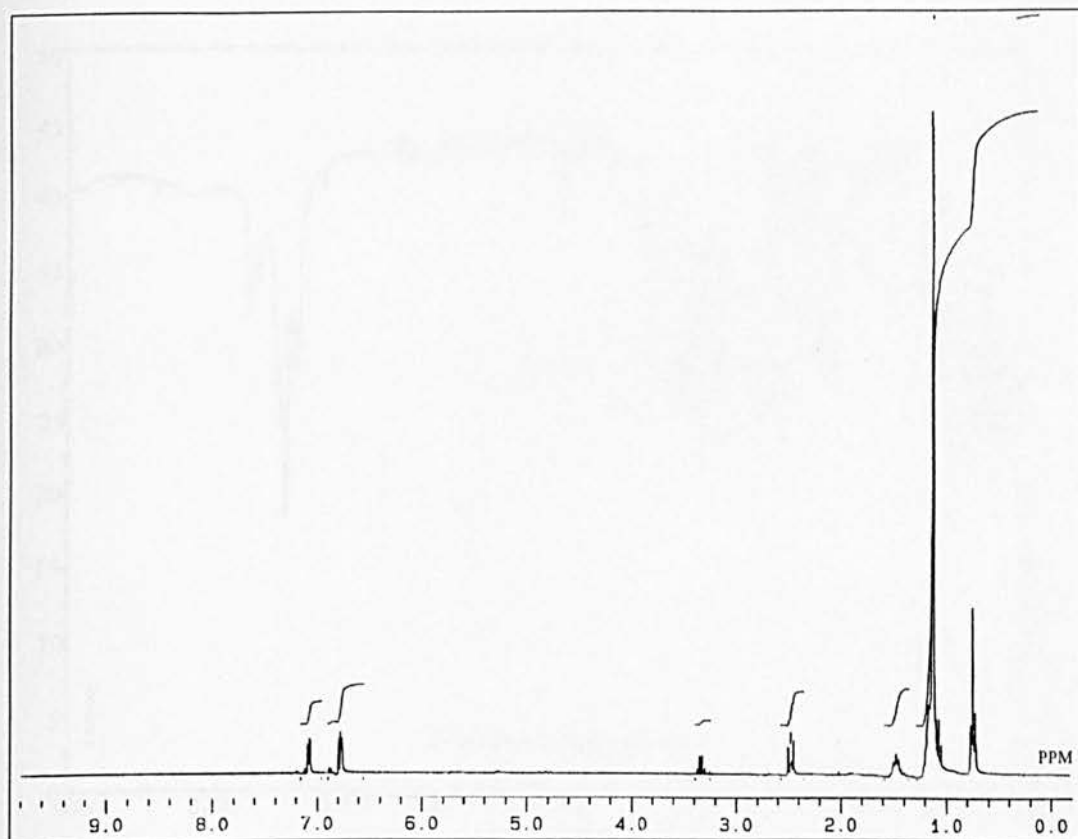
FIGURE A4
^{1}H NMR SPECTRUM OF 3-DODECYLTHIOPHENE
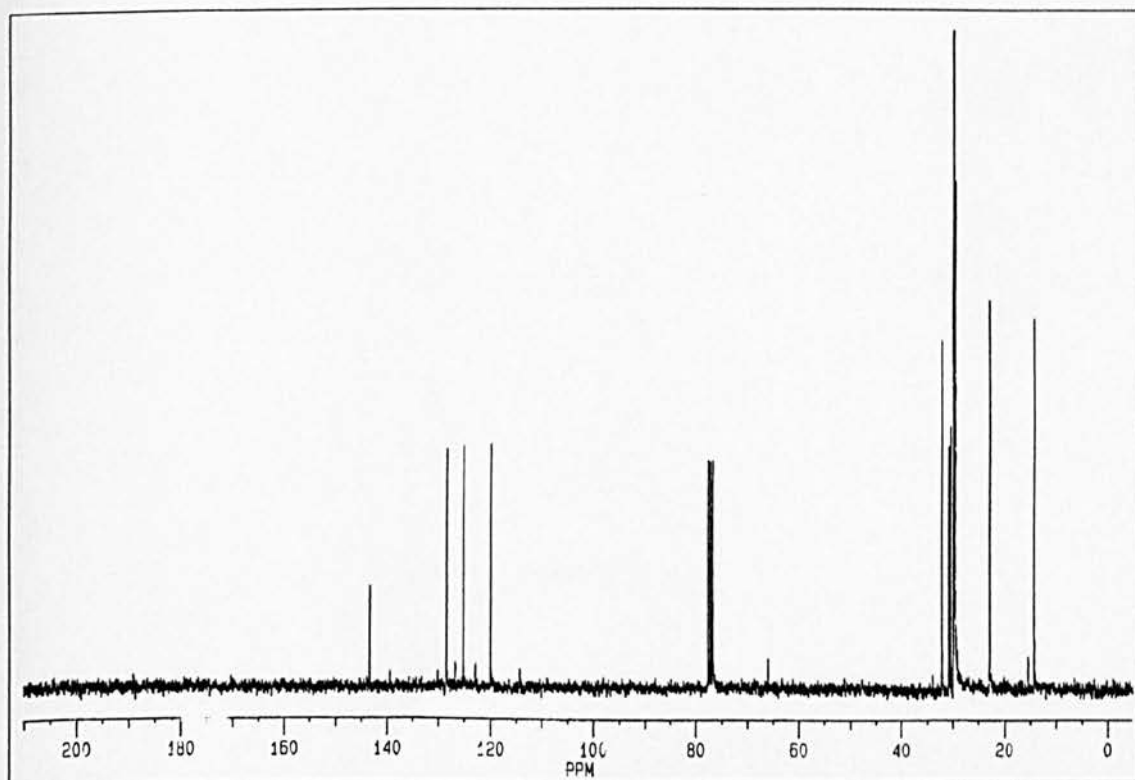
FIGURE A5
^{13}C NMR SPECTRUM OF 3-HEXYLTHIOPHENE
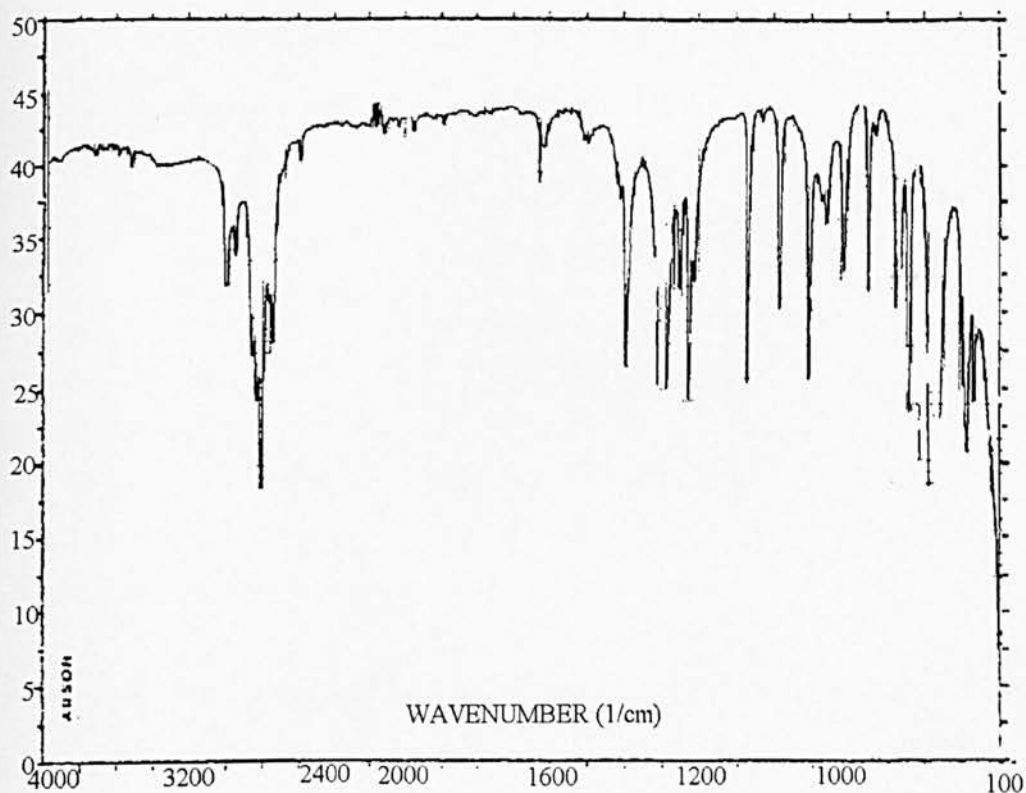
FIGURE A6
FTIR SPECTRUM OF 3-HEXYLTHIOPHENE

APPENDIX II

PUBLICATIONS RESULTING FROM THIS WORK

The following presentations resulted from this research:

- Poly(3-alkylthiophene)-based Solid-State Electrochromic Device Using an Elastomeric Polymer Electrolyte', Electrochem '95, Bangor, Wales (1995) (poster presentation).

- 'A poly(o-alkoxyaniline) and poly(3 -alkylthiophene)-based Solid-State Electrochromic Device using an Elastomeric Electrolyte', 2nd International Conference on Materials Chemistry, University of Kent, UK (1996) (poster presentation)

- 'Dielectric Measurement and Analysis of Poly(3-alkylthiophene) at High Frequencies', International MRS Meeting, San Francisco, California, USA (1997) (aural and paper presentation)

- 'Broadband Dielectric properties of polyanilines' A. Lawrence, M. Miah, T. Stickland, A. Treen, I. Youngs; WE Proc. Sci Meas. Technol. 145 No.4 (1998)

The authors are currently preparing several more papers based on more recent research which include similar investigations into NiO and Au thin films using vector network analysis, the dielectric and electromagnetic characteristics of conducting polymer films dispersed in a polytetrafluoroethylene matrix and further electromagnetic and dielectric studies into metal complexed poly(3-methylthiophene) polymer films.

Poly(3-alkylthiophene)-based Solid-State Electrochromic Device Using an Elastomeric Polymer Electrolyte

Electrochem '95, Bangor, Wales (1995) (poster presentation).

P.Foot[a], M.Miah[a], I. Youngs[b]

a   Department of Chemistry, Kingston University, Penrhyn Road, Kingston Upon Thames, KT1 2EE, UK

b   Structural Materials Centre, DERA, Farnborough, Hampshire, GU14 0LX, UK

INTRODUCTION

One may form electrochromic devices (ECD) from thin-film cells having conducting polymers deposited on transparent electrodes. By investigating the mechanism of such a devices, it may be possible to produce a viable alternative to current liquid-crystal devices (LCD).

AIMS

- Produce electrochromic device
- Improve on current liquid electrolyte systems by using a polymer electrolyte
- Investigate factors limiting switching speed of device
- Characterise the observed electrochromic effects using spectroelectrochemistry, cyclic voltammetry (CV) and chronoelectrochromic transmission data.

BASIC PRINCIPLE OF CONDUCTING POLYMERS

• Conjugated polymer systems are similar to inorganic semiconductors:

• Normally the valence and conduction bands in polymers are separated by an electronic band-gap of approximately 1eV.

Conduction Band

$E_g\uparrow$ $\quad\downarrow E_g$ $\updownarrow E_g$

Valence Band

Metal	Semiconductor	Insulator
$E_g<0$ eV	$E_g\sim0.1\text{-}0.5eV$	$E_g>3eV$
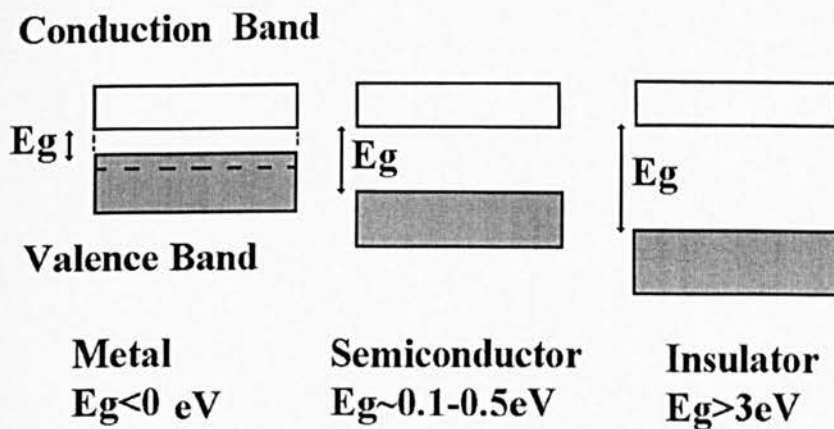
• Addition or removal of electrons from polymers based on conjugated systems, by insertion or subtraction of appropriate ions (dopants) causes p or n-type doping depending on the ions' charge.

Doping produces new midgap electronic states and effectively lowers the optical band gap.

a)   b)   c)   d)

Polaron Defect   **Bipolaron Levels**   **Bipolaron Bands**
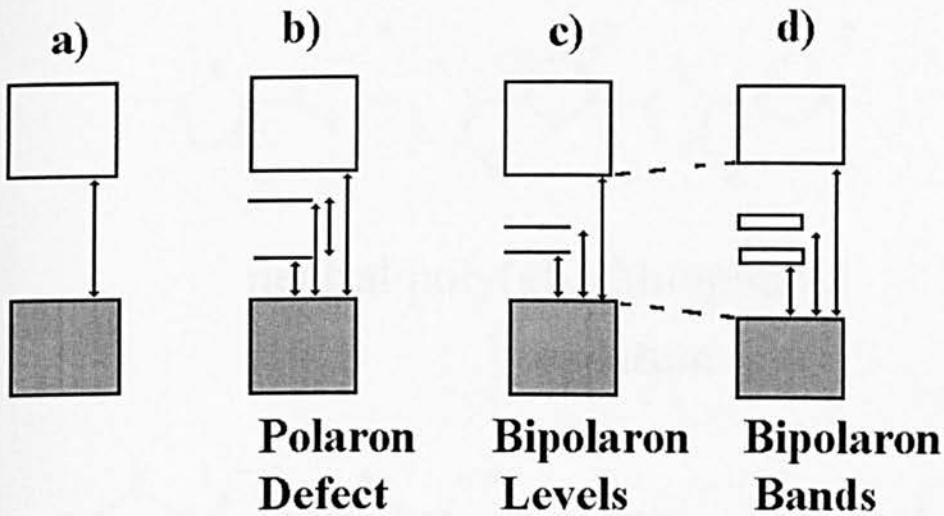
The structural changes manifest themselves as radical ions along the polymer chain.
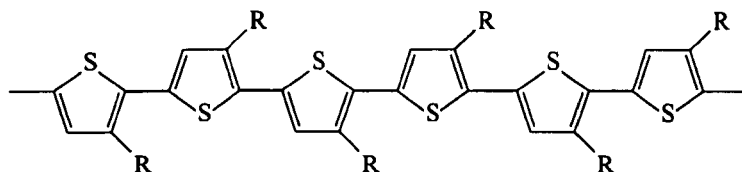
neutral poly(alkylthiophene)

oxidation
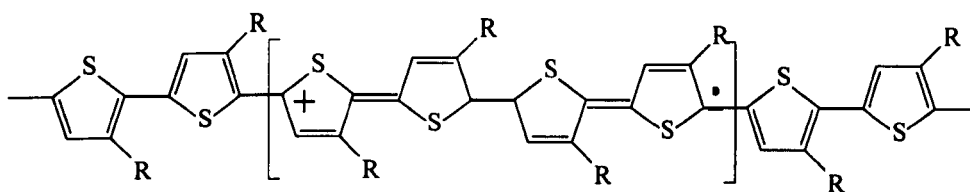
light doping(1-10mole%)
single radical cation formation

further oxidation
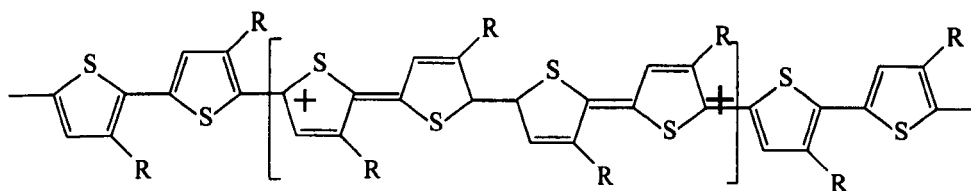
heavy doping(>20mole%)
progressive radical ion formation

heavy doping (>20mole%)

progressive di-cation formation

- Production of Conducting Polymer
  - Electrosynthesis (Galvanostatic)
  - Chemical synthesis (soluble polymers) and   film casting

- Direct electrosynthesis onto transparent   (ITO) substrate

A doped polymer film is deposited at a constant rate on the working electrode.

A Transparent electrode
B Conducting polymer
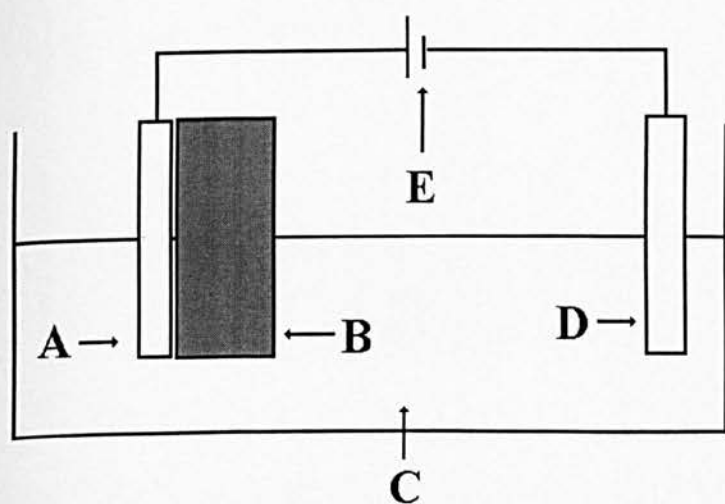
C Electrolyte
D Counter electrode
E Constant current Source

Electrolyte contains monomer and $Et_4N^+X^-$ in propylene carbonate. ($X=BF_4^-$, ClO_4^-, BPh_4^-)

Chemical Synthesis

- Synthesis of functionalised thiophene or aniline monomers. Polymerisation using FeCl3 initiator. Casting or spin-coating of transparent thin films onto ITO glass.

Comparison of LCD's vs ECD's

ECD	LCD
Low power consumption	Low power consumption
Wide viewing angle	Narrow viewing angle
Current induced change	Voltage (field) induced change
Electrolyte required	None required
Long cycling life	Very long cycling life
Memory maintained without power	Power normally required for memor
Response may be as short as μs	Normally ms response time

ECD Construction

ITO working electrode

polymer film

electrolyte

ITO counter and pseudo reference electrode

viewing angle
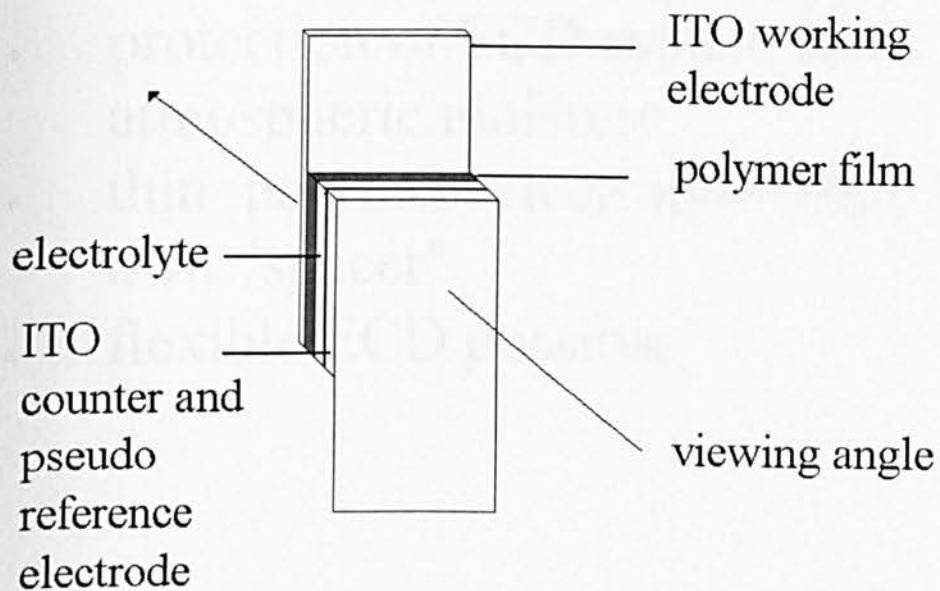
Electrolyte

Choice of polymeric solid electrolyte is due to:

- low viscosity electrolyte may leak
- protection of ECD system from atmospheric moisture
- thin polymer electrolyte film acts as its own "spacer"
- flexible ECD possible

Study of Electrochromism

Conducting polymers may be switched from the doped to the undoped state by forming cationic species along the conjugated backbone of the polymer. This may be induced by an electric field.

Electrochromism in conducting polymers is characterised by:

a) Colour change
b) amperometric decay
c) Switching between stable oxidation states

Doping transient of poly(3-dodecylthiophene) as observed by laser (670nm) and photodiode.

Undoping transient of poly(3-dodecylthiophene) as observed by laser (670nm) and photodiode.
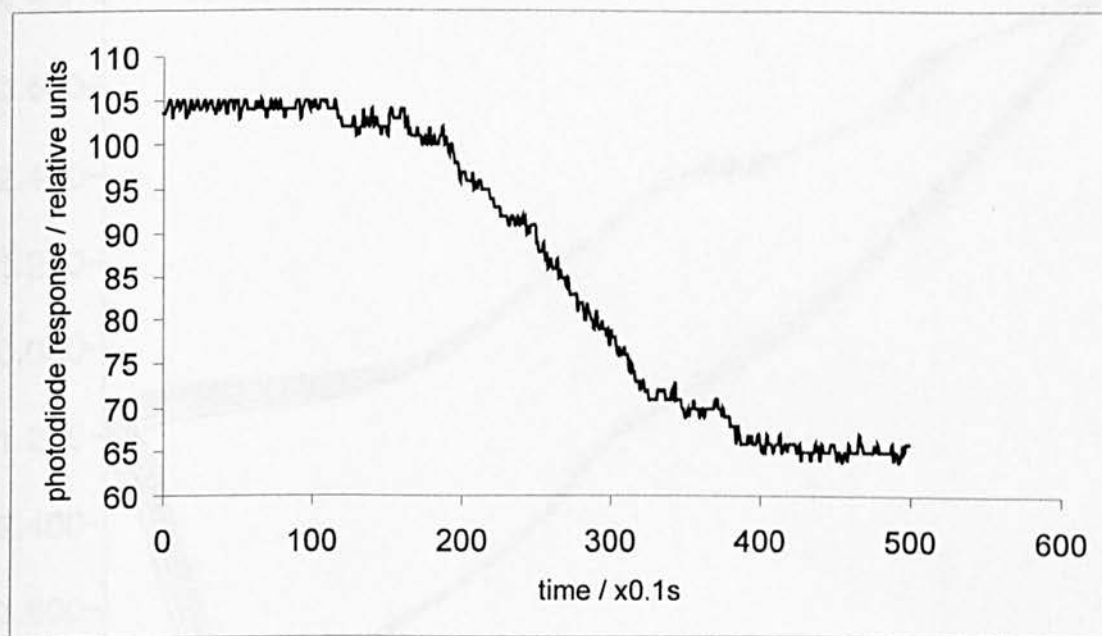
Observation of the oxidation-reduction cycle by CV shows a stable undoping peak at +0.9V(red) and a doping peak at +1.8V(blue) wrt ITO pseudo reference electrode.
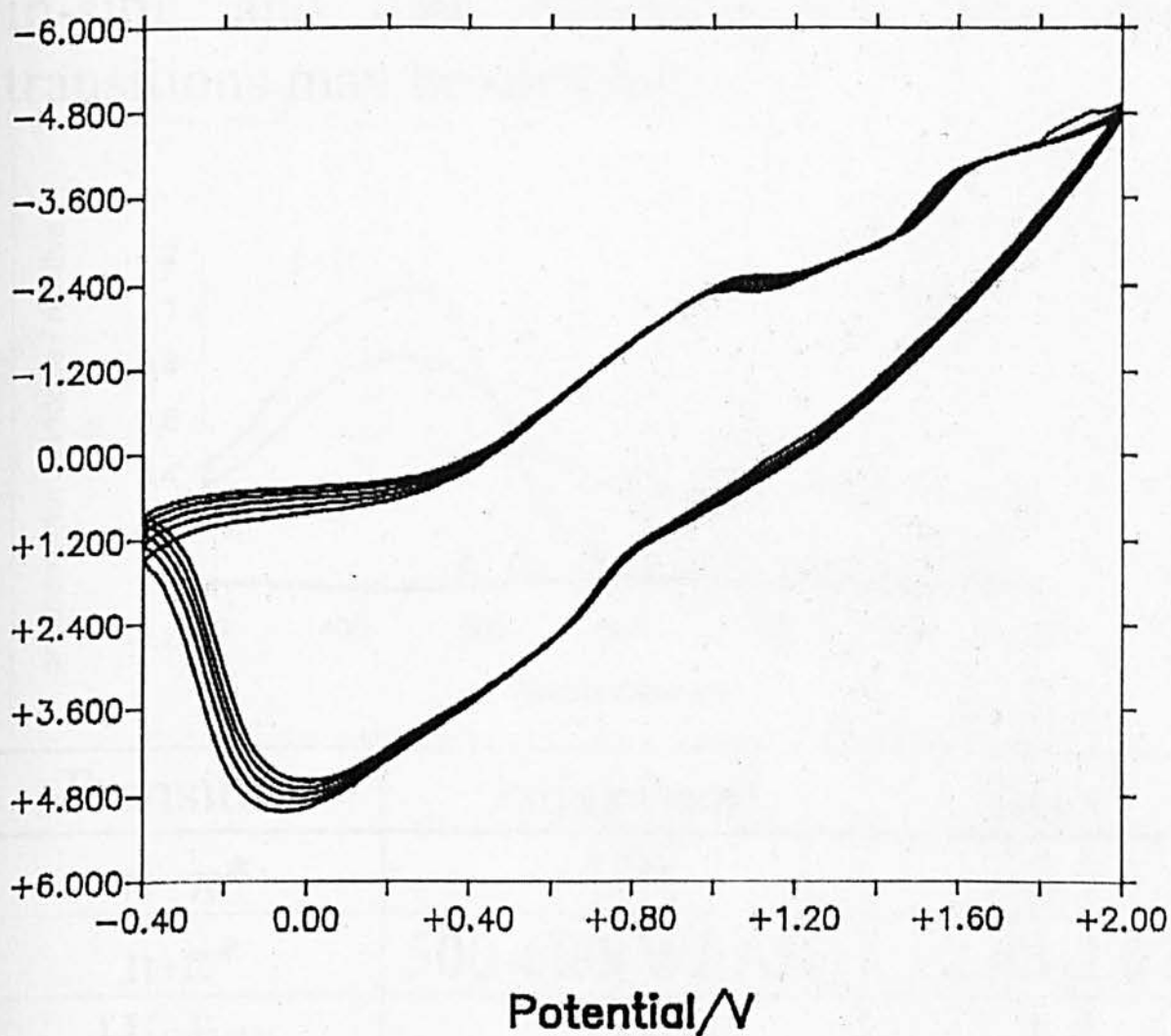
Spectroelectrochemistry

While maintaining a series of working electrode potentials within a UV-vis spectrophotometer, spectra may be recorded in-situ, and data regarding the electronic transitions may be obtained.
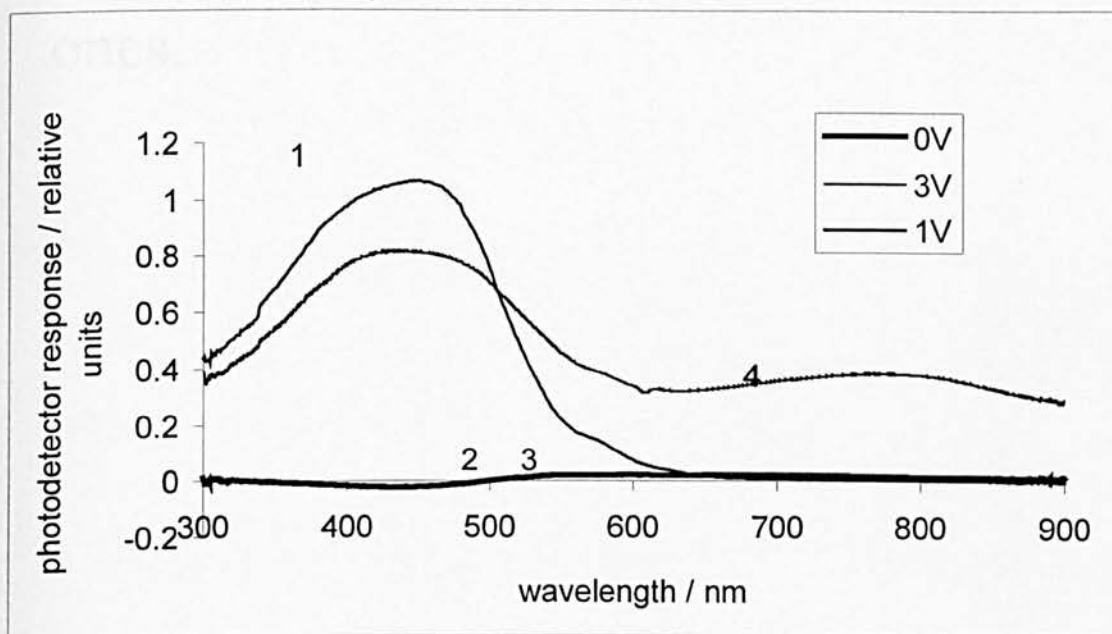
Transition	λmax*nm)	E(ev)
$\pi-\pi^*$	420	2.9
$n-\pi^*$	500-600(WEAK)	2.48-2.07
Higher polaron band	780 850	1.6 1.5

lower polaron band $\pi-\pi^*\sim$0.2-0.3eV. The colour change is caused by:

- production of charged polaron/bipolaron states or polymer backbone (balanced by injection of "dopant" counter-ions)

- this results in new near-IR absorption peaks at the expense of fundamental UV-visible ones.

Conclusion

Factors found to influence rate of colour change:

- choice of dopant ions - smaller ions don't neccessarily move faster!

$(BF_4^- < ClO_4^- < BPh_4^-)$

- Electrochromic polymer film thickness - thick films switch colour slowly, due to ionic diffusion becoming limiting.

- electrolyte conductivity - higher resistance produces greater voltage loss in ECD

- voltage range used - but excessive applied voltages cause polymer degradation!

Dielectric Measurement and Analysis of Poly(3-alkylthiophene) at High Frequencies

P.Foot[a], M.Miah[a], I. Youngs[b]

a   Department of Chemistry, Kingston University, Penrhyn Road, Kingston Upon Thames, KT1 2EE, UK

b   Structural Materials Centre, DERA, Farnborough, Hampshire, GU14 0LX, UK

ABSTRACT

The dielectric properties of polypyrrole doped to a range of conductivities has previously been well characterised at microwave frequencies [1,2]. In this present work, the variation in the complex permittivity at room temperature are presented over a wide range of dopant concentration to study the impact on the high frequency conductivity. In contrast to previous studies on polypyrrole which measure either the electrochemically prepared films or powder compacts, the use of poly(3-alkylthiophene)

enables the investigation of thin films prepared by solution casting. The high frequency measurements were undertaken using waveguide transmission line techniques and confirm that the transmission properties are highly dependent on film conductivity.

[1]   G. Phillips, R. Suresh, J. Waldmann, J. Kumar, J-I Chen, S. Tripathy and J.C. Juang; J. Appl. Phys. 69 **2** (1991) 899

[2]   A. Kaynak, J. Unsworth, G.E. Beard and R. Clout; Mat. Res. Bull. 283 (1993) 1109.
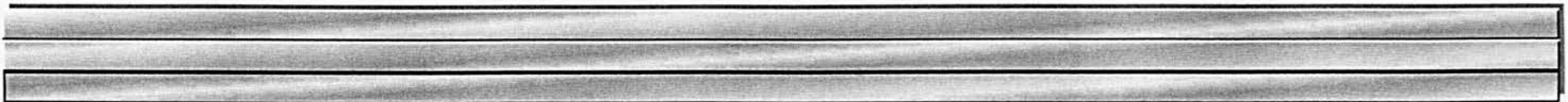
Formation of Alkylthiophene Monomer

Formation of Polymer

$$\text{FeCl}_3/\text{CHCl}_3$$

DOPING OF POLYMERS

CONDUCTION BAND

CONDUCTION BAND

2.6eV

1.7eV

$E_g \sim 2.3eV$

0.6eV

VALENCE BAND

VALENCE BAND

MEASUREMENT TECHNIQUE

HP 8510A
NETWORK
ANALYSER

PORT 1   PORT 2

S21
transmission
coefficient
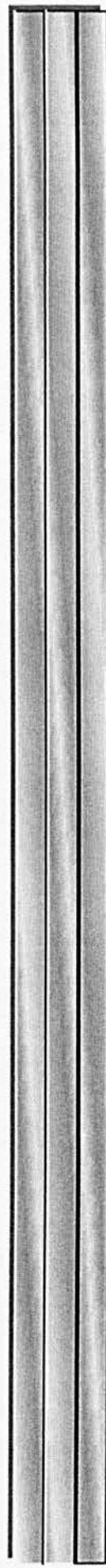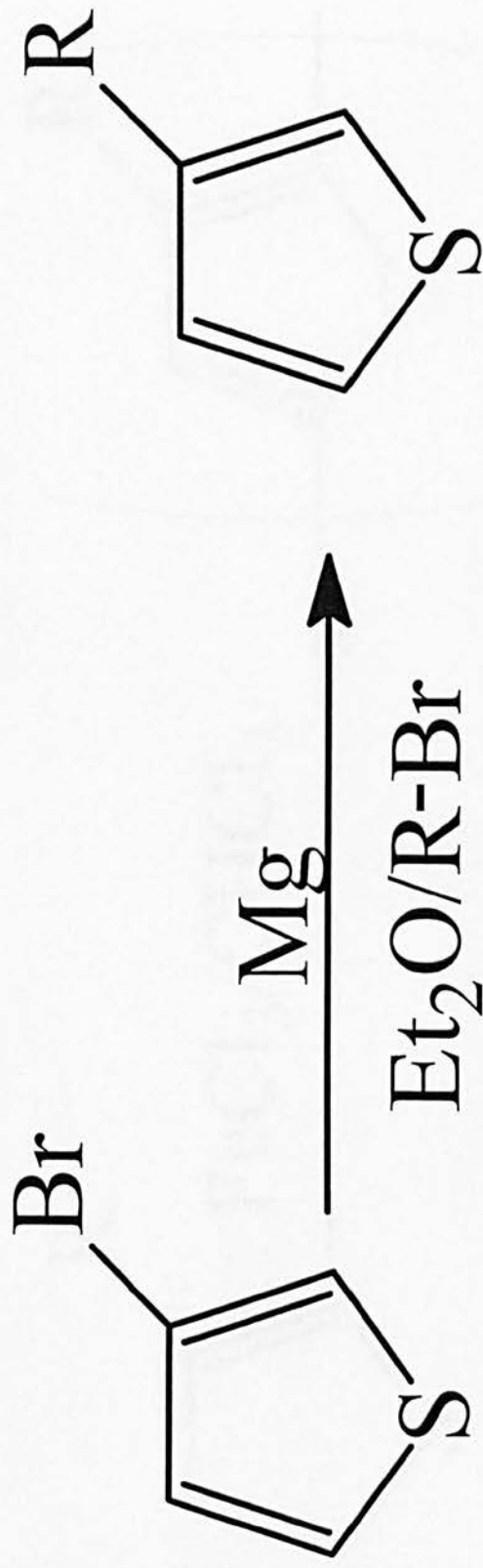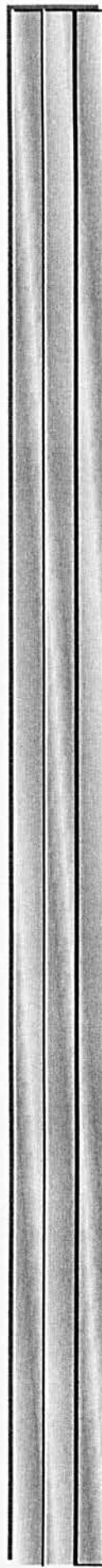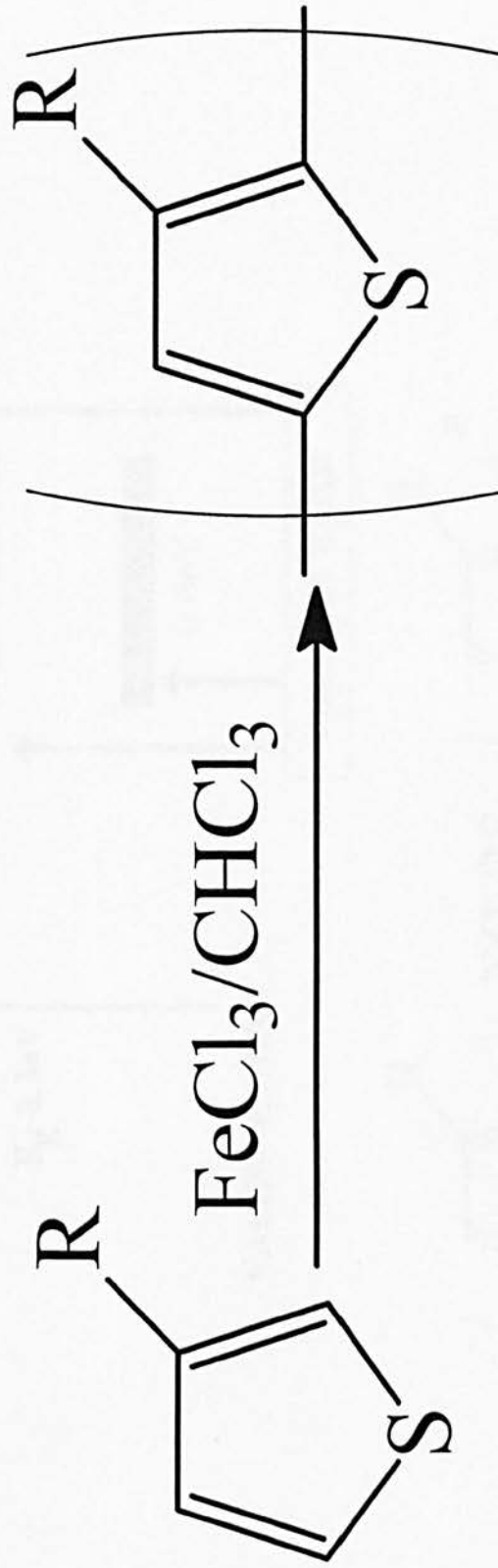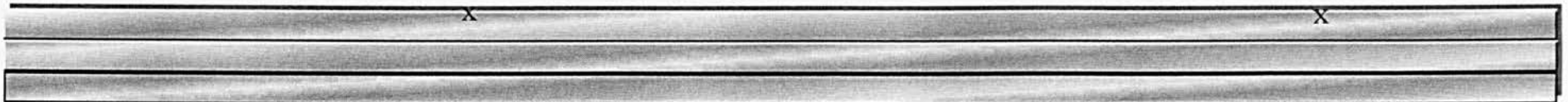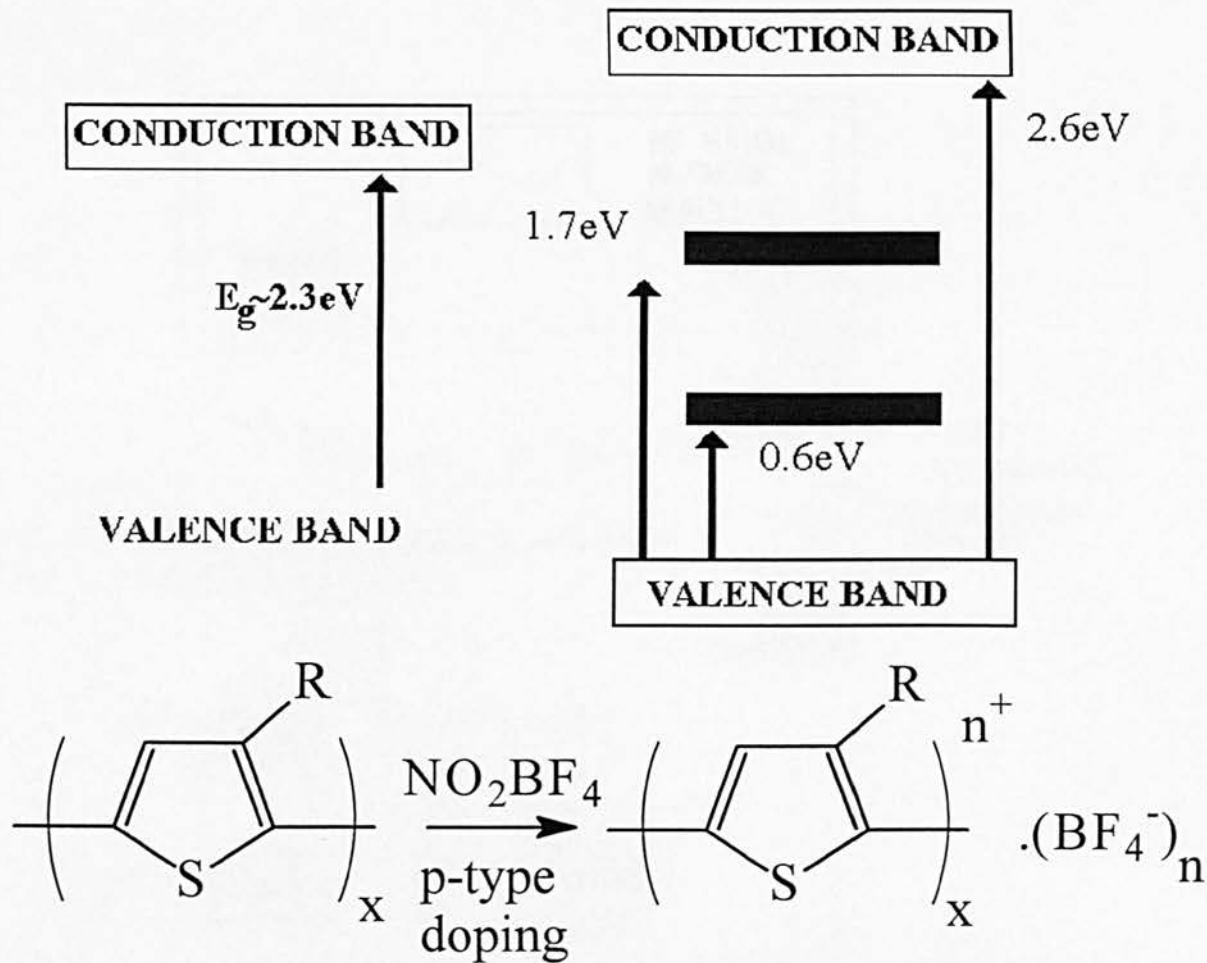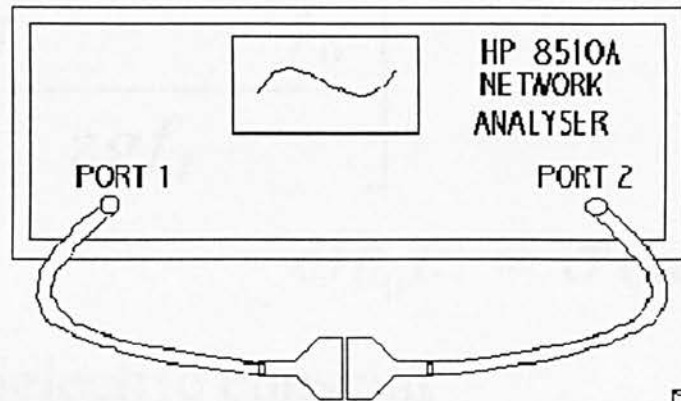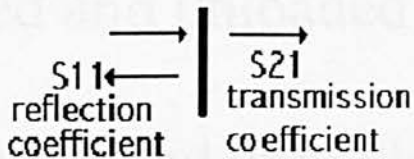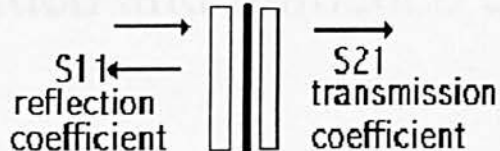
1. Teflon Matrix dispersed with P3AT
   conducting polymer.

S11
reflection
coefficient

2. S11 ←   S21
    reflection   transmission
    coefficient coefficient

3. S11 ←   S21
    reflection   transmission
    coefficient coefficient
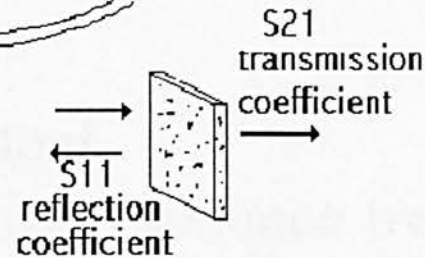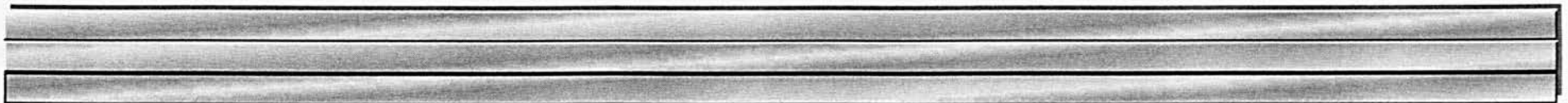
REAL AND IMAGINARY DIELECTRIC CONSTANT FOR FREE-STANDING FILMS

$$\varepsilon' = 1 + \left[\frac{l(f_l - f_0)}{zgf_l} \right] \qquad \varepsilon'' = \frac{l(Q_0 - Q_l)}{2zgQ_lQ_0}$$

$$\omega\varepsilon_0\varepsilon' = \sigma(\omega)_{HF} - \sigma_{dc}$$

ε'=real part of dielectric constant

ε''=imaginary part of dielectric constant

f_l and f_0 are loaded and unloaded cavity resonance frequencies
 respectively

Q_l and Q_0 are loaded and unloaded cavity quality factors
respectively

z=film thickness (m)

g=geometric factor of resonance window

REAL AND IMAGINARY DIELCTRIC CONSTANT FOR TEFLON SAMPLES

$$\varepsilon = \left\{ \frac{\mu}{\left[j/((-1/2\pi d))(\ln(t) + j(\varphi + 2\pi n)) \right]^2} + 21.87^2 \right\} \lambda_0^{\,2}$$

λ_0=waveguide cut-off frequency
t=lumped S parameters
j=phase angle
n=0,1,2,3… the integer of (d/ λ_g)
λ_g=actual wavelength in the sample

$$\sigma = \frac{2\pi f_0 \varepsilon_0 |\varepsilon''|}{100}$$
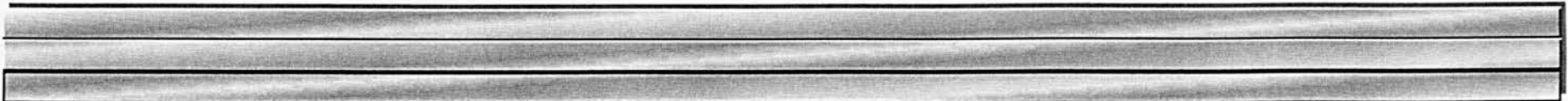
RESULTS

TEFLON SAMPLES

Absorption, Reflection and Transmission for Teflon Matrix Loaded with 10% Poly(3-alkylthiophene)
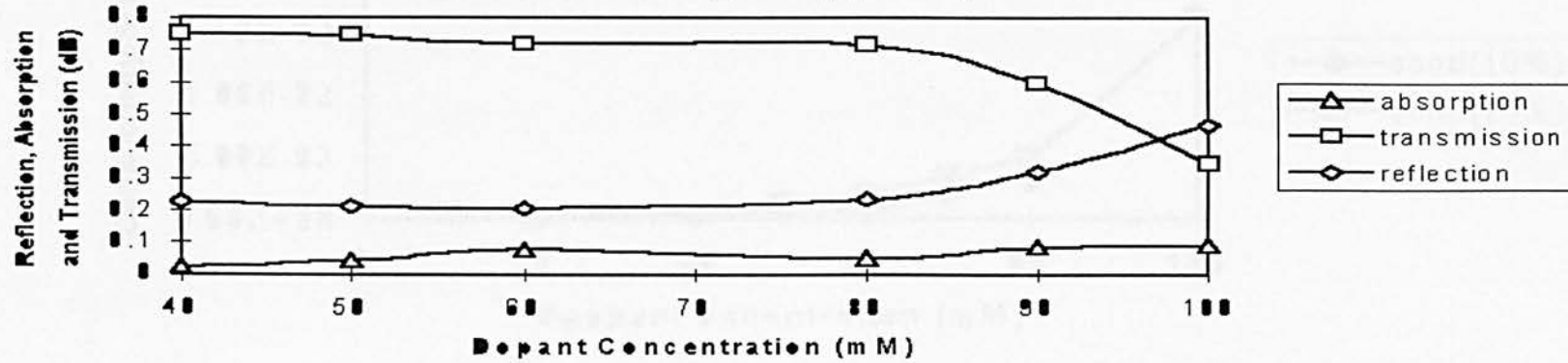
Reflection, Absorption and Transmission for Teflon Matrix loaded with 20% Poly(3-alkylthiophene)
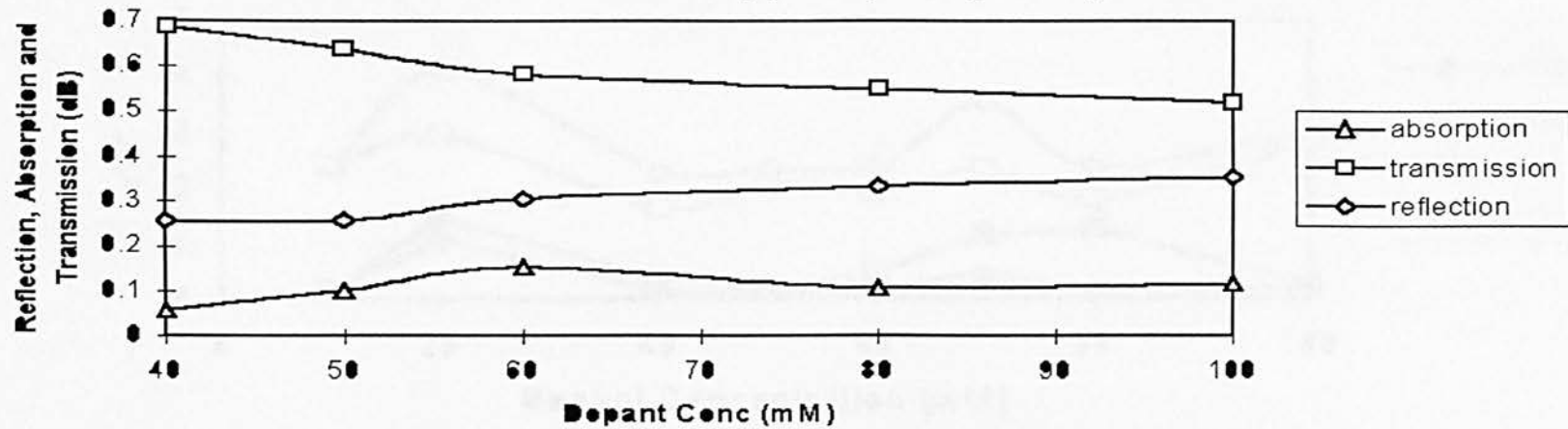
Change in σ(ω) Conductivity with Loading Level for P3HT in Teflon

Legend:
- cond(10%)
- cond(20%)

Y-axis: Conductivity/Scm-1 (2.00E-02, 1.50E-02, 1.00E-02, 5.00E-03, 0.00E+00)
X-axis: Dopant concentration (mM) (0, 20, 40, 60, 80, 100)
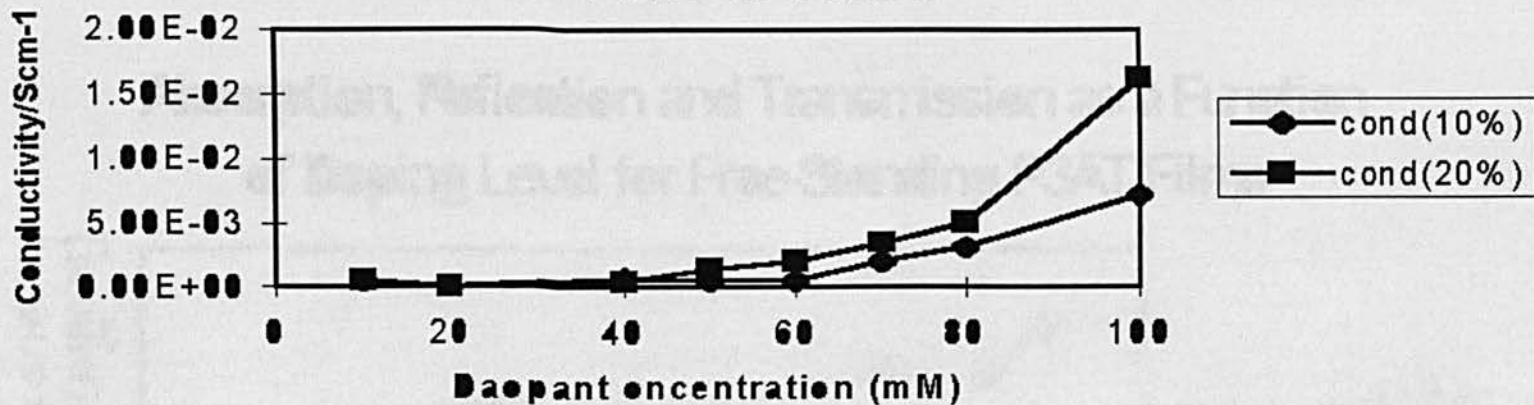
Real and Imaginary Parts of Dielectric Constant Plotted as a Function of Teflon Loading (10 and 20%) for P3HT

Legend:
- e'10%
- e'(20%)
- e'10%
- e'(20%)

Y-axis: ε'/ε" (0, 1, 2, 3, 4, 5)
X-axis: Dopant Concentration (mM) (0, 20, 40, 60, 80, 100)
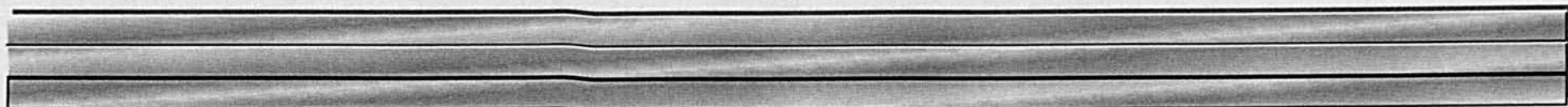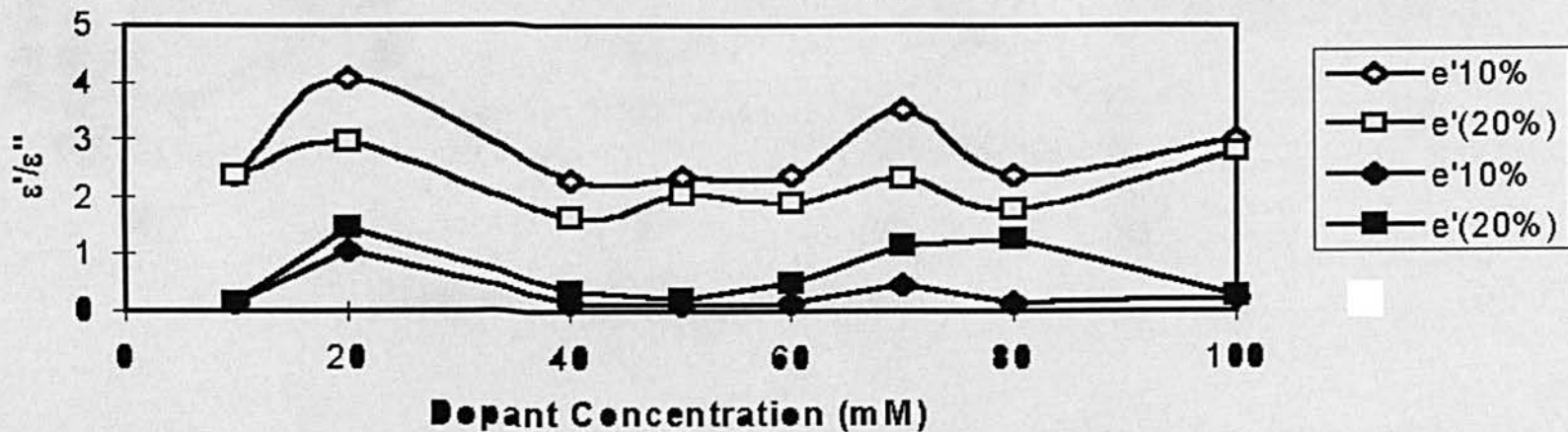
FREE-STANDING FILMS

Absorption, Reflection and Transmission as a Function of Doping Level for Free-Standing P3AT Films
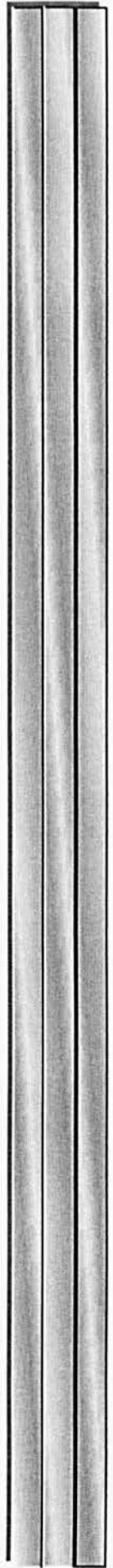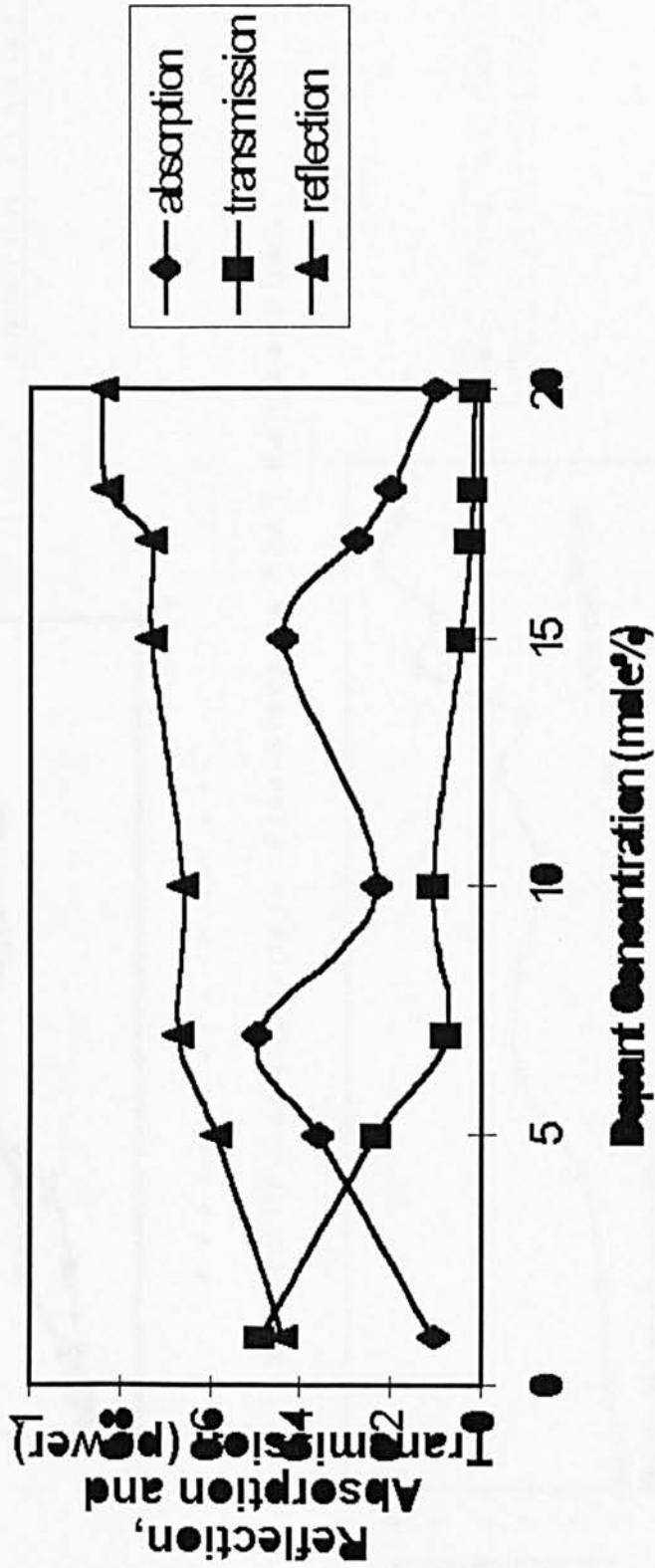
Real and Imaginary Part of Dielectric Constant for Free-Standing P3AT Polymer Films
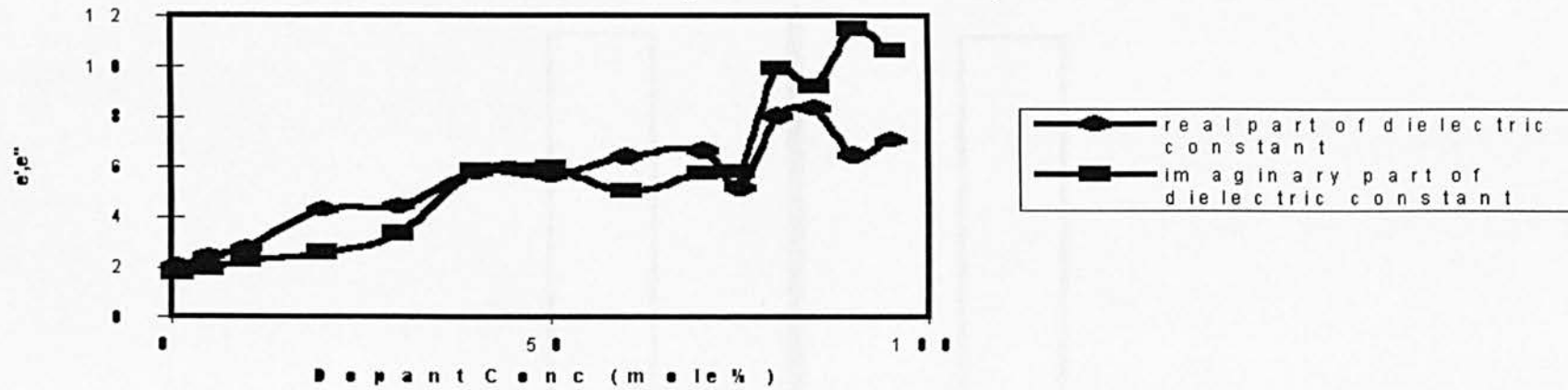
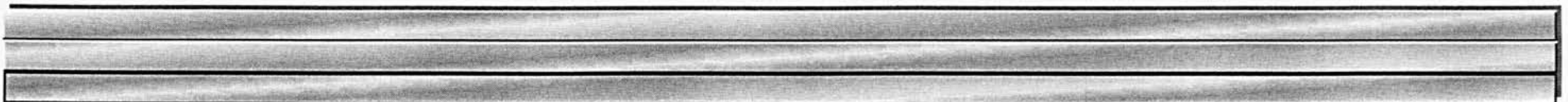# DC and HF Conductivity for Free-Standing P3AT Polymer Films

SANDWICHED FILMS

1 2 3 4 5 6 7
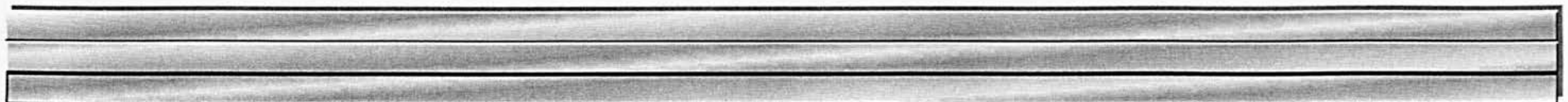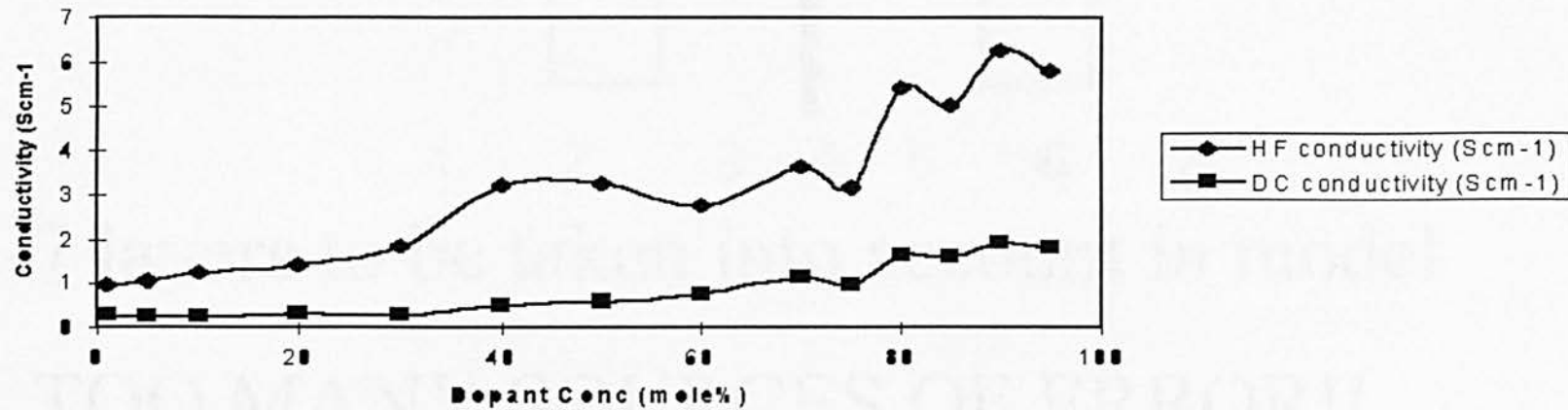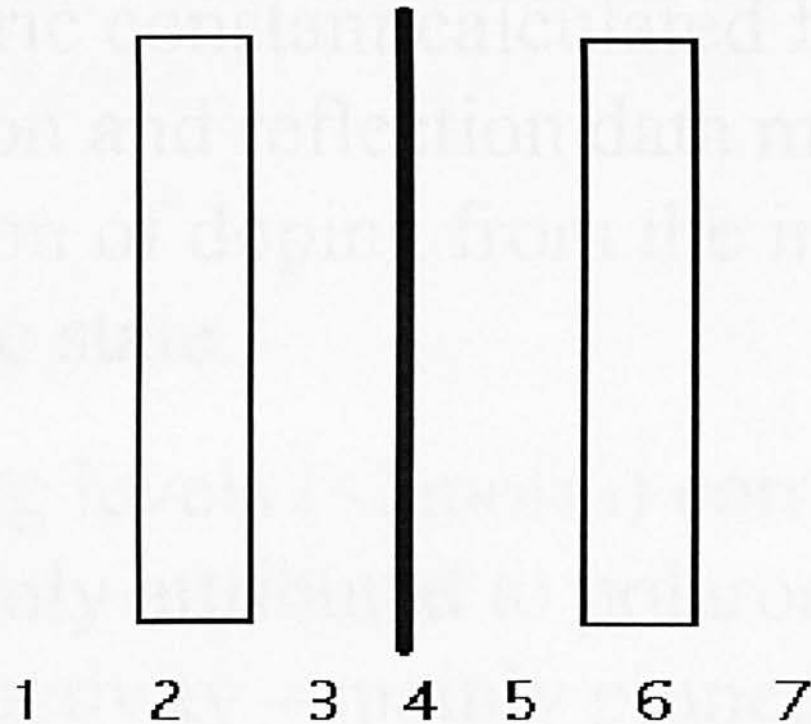
7 layers to be taken into account in model

TOO MANY SOURCES OF ERROR!!

DISCUSSION

1. HF dielectric constant calculated from transmission and reflection data measurements as a function of doping from the insulating to the metallic state.

2. Low doping levels (<3mol%) correspond to events mainly attributed to polaron formation. Low conductivity – mainly pinned carriers.
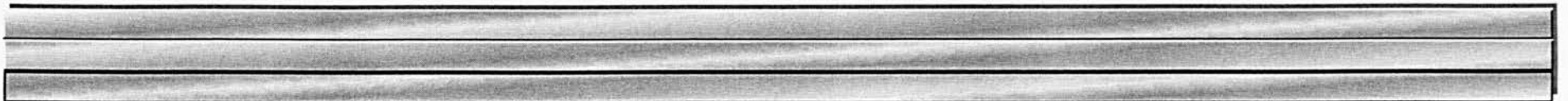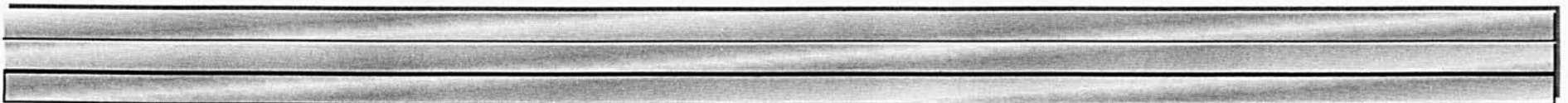
3. (4-5mol%) – Resonant absorption peak, possibly due to polaron-bipolaron transitions.

4. (7-8mol%) – Onset of percolation ?? Appearance of highly mobile charges.

5. (10-20mol%) – Progressive increase in metal – like reflection and free carrier absorption.
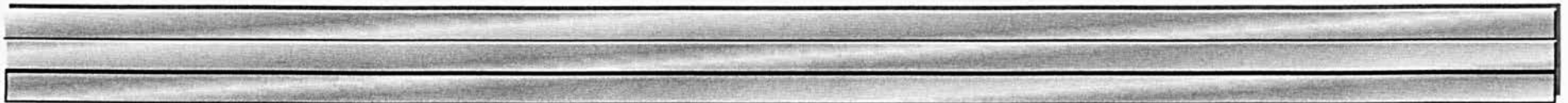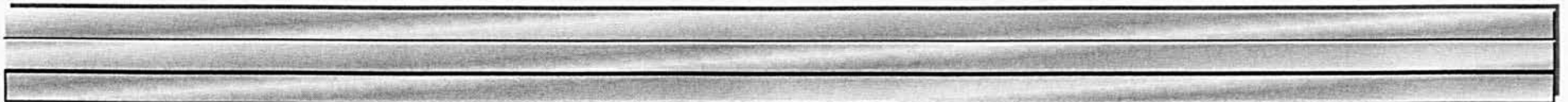
CONCLUSION

- RESULTS COMPARE FAVOURABLY WITH OTHER RESEARCHERS
- MEASUREMENTS MADE ON CHEMICALLY SYNTHESISED CONDUCTING POLYMERS DOPED TO A CONTROLLED LEVEL
- NON-DESTRUCTIVE TECHNIQUE FOR MEASUREMENT OF DIELECTRIC PROPERTIES OF CONDUCTING POLYMERS (~5% ERROR)

ACKNOWLEDGEMENTS